

**Final Report:** “The Influence of Organic-Aerosol Emissions and Aging on Regional and Global Aerosol Size Distributions and the CCN Number Budget” (ER65296-1038624-0017484). The PI attends ASR team meetings and is active in the Aerosol Lifecycle Working Group, focusing on organic-aerosol aging and new-particle formation. As part of our participation in FLAME-IV we have developed a collaboration with the optical properties group at Los Alamos National Laboratory led by M. K. Dubey.

We conducted laboratory experiments and analyzed data on aging of organic aerosol and analysis of field data on volatility and CCN activity. With supplemental ASR funding we participated in the FLAME-IV campaign in Missoula MT in the Fall of 2012, deploying a two-chamber photochemical aging system to enable experimental exploration of photochemical aging of biomass burning emissions. Results from that campaign will lead to numerous publications, including demonstration of photochemical production of Brown Carbon (BrC) from secondary organic aerosol associated with biomass burning emissions as well as extensive characterization of the effect of photochemical aging on the overall concentrations of biomass burning organic aerosol. Excluding publications arising from the FLAME-IV campaign, project research resulted in 8 papers: [11, 5, 3, 10, 12, 4, 8, 7], including one in *Nature Geoscience* addressing the role of organic compounds in nanoparticle growth [11]. The results from FLAME-IV lead to 4 additional publications: [14, 16, 1, 15] including one in *Nature Geoscience* on formation of brown carbon from biomass burning [14].

We made extensive progress in development of the two-dimensional volatility basis set (2D-VBS). We have developed a parameterization giving rate constants for reactions of organics with OH radicals within the 2D-VBS, including representation of heterogeneous aging [3]. In Fig. 1 we show a synopsis of this presented at Faraday Discussion on Atmospheric Chemistry in 2013 [10] showing that the average age of SOA in the Eastern US is roughly 1 day, but that the average lifetime of semivolatile organics associated with organic aerosols is generally much less than 1 day, indicating that organic aerosol will typically be heavily aged under most summertime conditions. We showed that during this organic aerosol aging, condensation of organic compounds to particles throughout the size distribution

A critical input to model calculations of SOA aging is the product distribution (the volatility distribution in VBS jargon) of the initial “fresh” SOA. Furthermore, the interactions of biogenic and anthropogenic SOA remain a topic of great interest. Therefore, we assessed the formation of first-generation SOA from  $\alpha$ -pinene oxidation by different oxidants, finding that oxidation by OH radicals produces somewhat more SOA with on average a lower volatility than oxidation by ozone and suggesting model parameters to describe these different formation pathways [5].

To study organic-aerosol aging in the laboratory, we elected to work with the important toluene secondary organic aerosol system. In an earlier publication we had shown that toluene SOA levels are higher than previously estimated, but also that the degree of oxidation of the toluene SOA correlates with the amount of OH exposure during SOA formation [6]. Because model simulations have shown that aging of anthropogenic SOA can have an important role in both the level and degree of oxidation of simulated ambient organic aerosol, we decided to investigate this further. In collaboration with Thanos Nenes at Georgia Tech we conducted several experiments in which toluene was subjected to varying degrees of oxidation, measur-

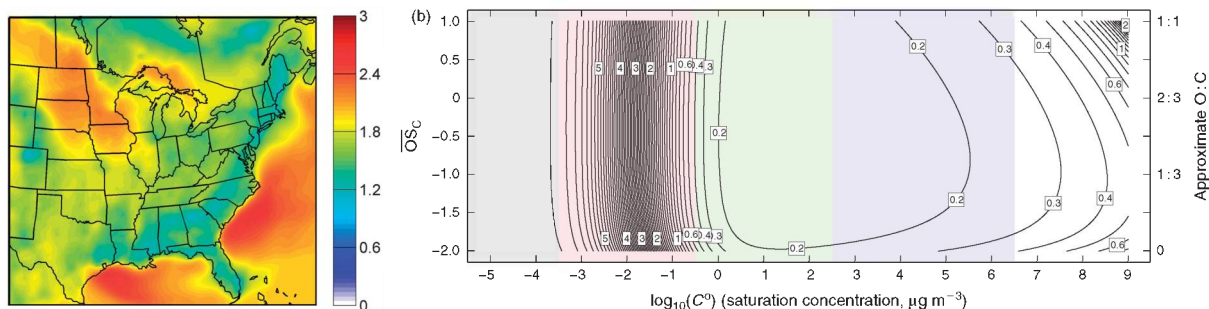


Figure 1: (a) Average age of organic aerosol in the Eastern United States in July using the Volatility Basis Set. (b) Average lifetime of organic species represented in the 2D-VBS in days.

ing the levels and composition of the SOA using a high-resolution Aerosol Mass Spectrometer, volatility using a thermodenuder, and CCN activity using a DMT CCN counter.

We made a significant contribution to the practice of AMS data analysis [2]. The most chemically sound metric for oxidation is the mean oxidation state of carbon:  $\overline{OS}_C = 2O:C - H:C$ , as described by Kroll *et al.* [9].  $\overline{OS}_C$  is a “good” metric for oxidation and thus tends to increase monotonically during oxidation processes. In addition, non-oxidative phenomena such as dehydration (eliminating  $H_2O$ ) will change O:C but not  $\overline{OS}_C$ . This means that  $\overline{OS}_C$  should also be a “better” metric for AMS data analysis because it eliminates the need to accurately estimate the organic contribution to various water signals in the aerosol mass spectrum, which can come from myriad sources. In the process of analyzing data from these campaigns, we realized that the currently accepted data analysis procedures for AMS data did not properly conserve water. Specifically, signal of protons at  $m/z = 1$  was ignored. Some water signal exists at  $m/z = 18$ , but some at  $m/z = 17$  (OH), which should have a companion signal at  $m/z = 1$ . The omission of this signal has a negligible effect on the total organic mass, but a nontrivial effect on the  $\overline{OS}_C$  calculation. In addition, we were able to work out an appropriate way to account for organic nitrates (RONO<sub>2</sub>) by treating the NO<sub>2</sub> moiety as an independent group and ignoring it for calculations of O:C and  $\overline{OS}_C$ .

In a succession of aging experiments on the toluene SOA system we showed that OA produced under more highly oxidizing conditions was significantly more oxidized, less volatile, and more hygroscopic (acting as a better CCN) than OA produced under less highly oxidizing conditions. Significant signals from organic nitrates observed at high NO<sub>x</sub> levels are also relatively volatile, as expected based on volatility predictions [7]. We observed a modest inverse relationship between hygroscopicity and  $\overline{OS}_C$ , as shown in Fig. 2, suggesting that the less volatile, more oxidized material remaining after thermal denuding may well consist of higher molecular weight products (oligomers), which have reduced hygroscopicity [7]. We developed a methodology to better constrain the volatility distribution of organic aerosol before and after aging by combining thermodenuder measurements with dilution experiments [8].

Using data from the FLAME-III campaign at the Missoula Fire Sciences Laboratory, we found that both fresh and aged organics in wood smoke (BBOA) are significantly light absorbing (brown), though the aged (SOA) from BBOA has a lower molar absorptivity (kOA) [12]. These observations were part of the foundation for the FLAME-IV campaign.

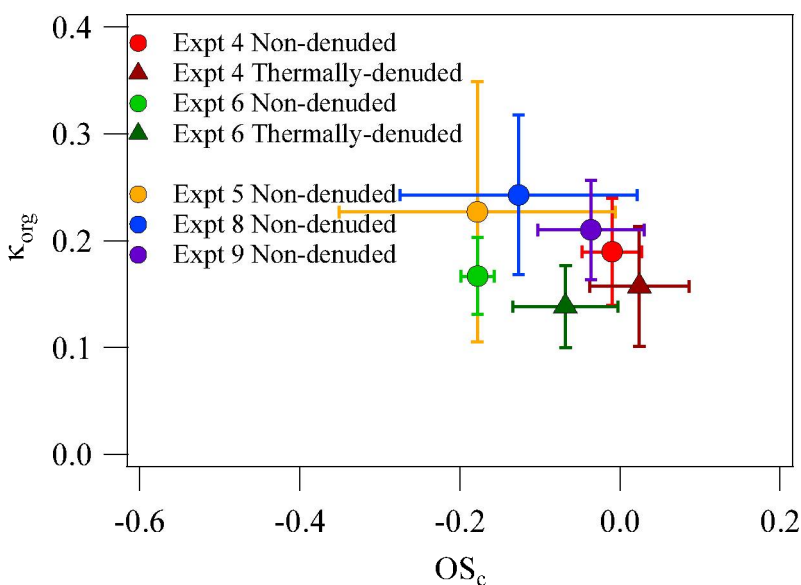


Figure 2: (a) Relationship between hygroscopicity ( $\kappa$ ) and oxidation state of carbon ( $\overline{OS}_C$ ) during aging of SOA formed from toluene photooxidation.

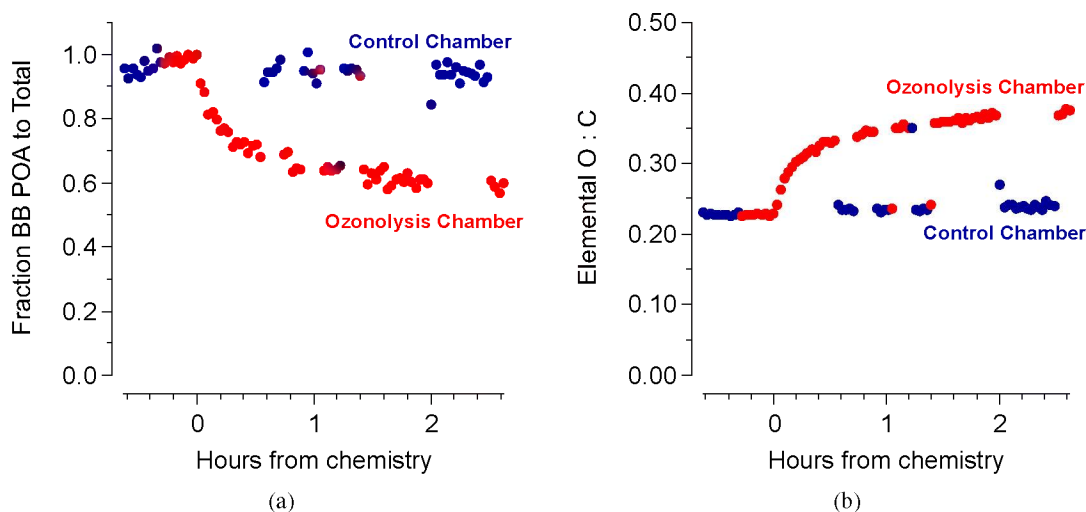


Figure 3: (a) Fraction of POA to total OA as a function of time of oxidation. Control chamber was left unperturbed for the course of the experiment. After 3 hours of oxidation, half of the suspended OA was SOA, the other half POA. (b) Time series of elemental O:C calculated from high-resolution AMS data. Little oxidative change was seen in the POA measured from the control chamber, while oxidation caused a doubling of O:C in the suspended OA.

*FLAME-IV*: The FLAME-IV experiment made use of a dual smog chamber setup [16], which allowed for more precise understanding of biomass burning organic aerosol (BBOA) composition changes, mass enhancements, and other physical properties than the single-chamber design used in FLAME-III (also with CMU participation) [12]. During FLAME-IV we developed a significant collaboration with Los Alamos National Lab (Manvendra Dubey) focused on experimental constraints of biomass burning optical properties. When using one chamber as a control and the other as a photochemical reactor, we can more accurately characterize chemical evolution of the primary smoke emissions, and constrain any changes in our aerosol due to wall losses. The “control” is sometimes no action and sometimes some form of aging for comparison; we calculate dual-chamber enhancements (DUCE) in each case. This eliminates the burn-to-burn variability of smoke as a source of variability.

*Methods:*

- Aerosol non-refractory chemical composition analysis using the HR-ToF-AMS.
- BC quantification in biomass-burning emissions using the Single- Particle Soot Photometer (SP2)
- Collection efficiency estimation and change with BBOA chemical evolution measured using the light scattering single particle (LSSP) module from the HR-ToF-AMS.

*Results:* For all experiments performed at FLAME-IV, we measured the chemical evolution of the non-refractory aerosol. In the Ponderosa Pine and Black Spruce burning experiments, the BC mass measured by the SP2 was low compared to the organic mass measured by the AMS. Inorganics measured by the AMS were negligible. For a series of fuels selected as potential high emitters of ice nuclei (IN), BC and inorganics comprised a much higher fraction of the total particulate mass, including very high levels of chlorine for two of the fuels. Regardless of the chemical perturbation (UV lights,  $O_3$ , OH from HONO+UV), we see chemical changes in the BBOA in our reaction chamber, indicating that secondary organic aerosol (SOA) formation is important for the fuel types and burn conditions of these experiments. Using a residual method, we have estimated the amount of primary organic aerosol (POA) versus SOA as a function of time from chemical perturbation. Interestingly, even when there is no measured mass enhancement, which was the case for some of the experiments, there is oxidation of the aerosol. Fig. 3a shows this, as the fraction of POA decreases when ozone is added to the reaction chamber in the 121101 Ponderosa Pine experiment. Fig. 3b

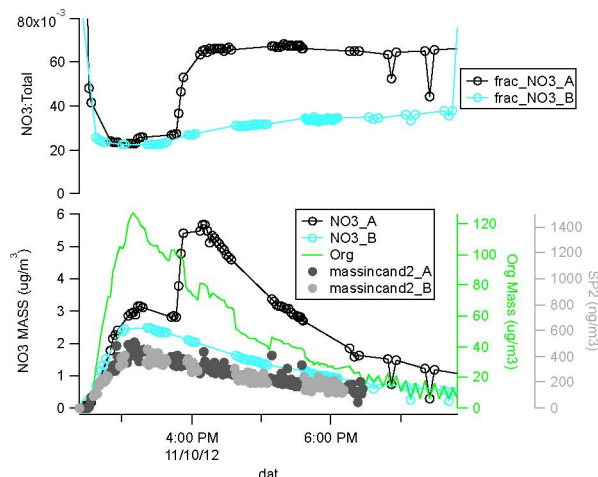


Figure 4: Time series identifying the presence of organonitrates for 121110 Black Spruce burn. Top panel shows the fraction of measured nitrate to total organic mass, with a dramatic increase prior to 4:00PM in the chamber where OH was added from HONO+UV (black markers), and a more gradual increase in the chamber where only UV lights were applied (blue markers). Bottom panel shows measured nitrate and organic masses from the AMS and BC mass from SP2 used for wall corrections.

shows the evolution of oxidation in the particles as a function of time from the ozone injection, as well as the lack of chemical change in the non-perturbed control chamber.

As Fig. 4 shows, we also see indications of the formation of organic nitrates with oxidation. We observe strong signals of  $m/z = 30$  ( $\text{NO}^+$ ) and  $m/z = 46$  ( $\text{NO}_2^+$ ) in the POA for almost all experiments, with an increase (relative to total measured organic mass) after the chemical perturbation. The fragmentation ratio between  $\text{NO}^+$  and  $\text{NO}_2^+$  is of order 10 for all experiments, consistent with organic nitrates.

*Optical Closure:* In collaboration with LANL, we perform optical closure analysis to determine the imaginary part of the refractive indices (absorptivity) of organic aerosol (OA) in fresh and aged biomass burning emissions. The derived imaginary part of the refractive indices (kOA) can be used in chemical transport models employing Mie-theory to predict light absorption for different atmospheric conditions. Optical closure combines Mie theory model calculations with light absorption and aerosol size distribution measurements to determine optical properties of the aerosol [12]. The procedure includes the following steps:

1. Measure black carbon (BC) and total size distributions using a Single Particle Soot Photometer (SP2) and a Scanning Mobility Particle Sizer (SMPS), respectively.
2. Infer the mixing state of BC and OA from the SP2 and SMPS measurements [12].
3. Measure absorption coefficients as a function of wavelength of the aerosol ensemble using a 7-wavelength Aethalometer and a 3-wavelength Photo Acoustic Soot Spectrometer (PASS-3, LANL).
4. Optimize the Mie-theory model using BC and OA size distributions as inputs in order to match the observed absorption coefficients, with the free parameter being the wavelength-dependent kOA.

Fig. 5a shows an example of optical closure analysis, for fresh black spruce emissions. The red symbols are the absorption coefficient data points used to constrain the Mie theory model (black solid line). The Aethalometer measurements are prone to artifacts related to organic loadings on the filter, which can lead to bias in the magnitude of the absorption coefficients; however, the Aethalometer is reliable in determining the wavelength-dependence of the absorption curve [12]. PASS-3 provides more accurate absorption coefficient measurements. In this work, we use the PASS-3 data to scale the Aethalometer data, and then the data points from the two instruments are used in the optical closure analysis, as shown in Fig. 5a. The advantage of

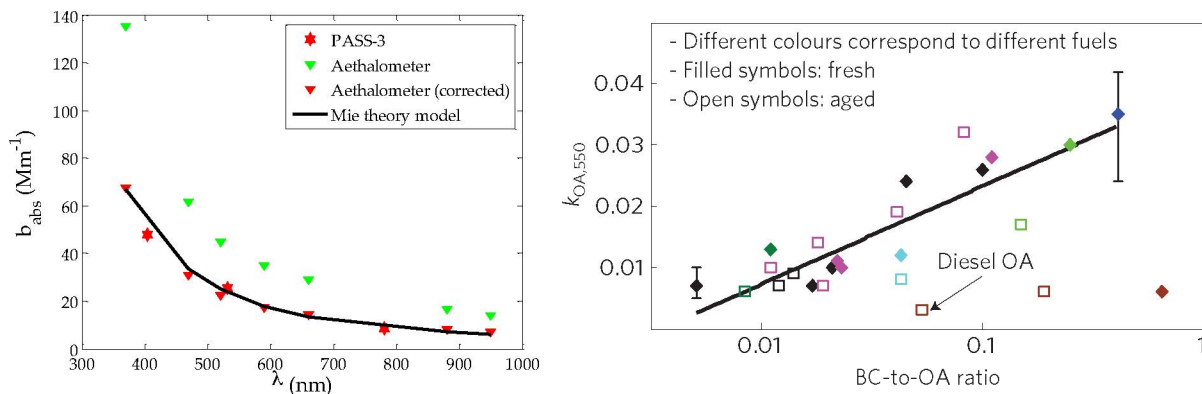


Figure 5: (a) Optical closure analysis for fresh black spruce emissions to obtain molecular absorption coefficient ( $k_{\text{OA}}$ ) for one burn condition. (b) Overall relationship between absorptivity (brownness) of BrC and black-carbon content (BC:OA) of the emissions.

this over relying solely on PASS-3, is to obtain more data points over a wider range of wavelengths, which constitutes a better constraint.

Analyzing the optical properties of the complete set of burns, with and without aging chemistry, we observed a relationship between the molecular absorptivity ( $k_{\text{OA}}$ ) of the brown carbon and the amount of black carbon in the BBOA (BC:OA). This relationship is mechanistically plausible, as it suggests that the chromophores in BBOA brown carbon are “frustrated black carbon” formed by the same pyrolysis mechanism in fuel rich combustion conditions. These findings do not suggest that the overall absorptivity ( $b_{\text{abs}}$ ) of high-BC biomass-burning emissions is higher than smoky high-OA emissions, because the mildly absorbing BrC in emissions with high OA content can still lead to more overall absorption. It does show, however, that on a molecule by molecule basis the high BC brown carbon is far more efficient at absorbing light.

The implications of this finding are substantial, and thus we were able to publish the work in *Nature Geoscience* [14]. First, the relatively refractory brown carbon does not evaporate in most thermodenuders, and it exists both as a coating on BC cores as well as independently in an external mixture (as part of “tarballs”). This means that analysis of optical properties – specifically lensing – in experiments where thermodenuders are used to strip OA off of BC cores must be undertaken with great care to consider both the (absorbing and lensing) BrC residual after thermal denuding as well as the externally mixed (absorbing) BrC that remains after thermal denuding. This can significantly affect data interpretation. Second, the findings suggest an easily implementable parameterization that could and does explain variability in absorptivity for various biomass burning environments around the globe. We have in fact developed and implemented such a parameterization in the global model GEOS-Chem and shown that it has high skill in predicting absorptivity in biomass-burning emissions. We also showed that proper treatment of both the mixing state and coupled absorption and refraction in lensing BrC material has a large effect on the predicted optical properties [13].

## References

- [1] A. T. Ahern, D. S. Tkacik, E. S. Robinson, R. Saleh, A. A. Presto, A. L. Robinson, N. M. Donahue, and R. C. Sullivan. Evolution of chemical composition in aging of biomass-burning plumes. *Atmospheric Chemistry and Physics*, in preparation, Apr 16, 2016.
- [2] M.R. Canagaratna, J. L. Jimenez, J. Kroll, Q. Chen, S. Kessler, P. Massoli, L. Hildebrandt Ruiz, E. Fortner, L. Williams, K. Wilson, J. Surratt, N. M. Donahue, J.T. Jayne, and D.R. Worsnop. Elemental ratio measurements of organic compounds using aerosol mass spectrometry: Characterization, improved calibration, and implications. *Atmospheric Chemistry and Physics*, 15:253–272, 2015. URL: <http://www.atmos-chem-phys.net/15/253/2015/>, doi:10.5194/acp-15-253-2015.
- [3] N. M. Donahue, W. K. Chuang, Scott A. Epstein, J. H. Kroll, D. R. Worsnop, A. L. Robinson, P. J. Adams, and S. N. Pandis. Why do organic aerosols exist? Understanding aerosol lifetimes using the two-dimensional volatility basis set. *Environmental Chemistry*, 10:151–157, 2013. URL: <http://dx.doi.org/10.1071/EN13022>, doi:10.1071/EN13022.
- [4] N. M. Donahue, A. L. Robinson, E. R. Trump, I. Riipinen, and J. H. Kroll. *Atmospheric and Aerosol Chemistry*, volume 339 of *Topics in Current Chemistry*, chapter Volatility and Aging of Atmospheric Organic Aerosols, pages 97–144. Springer, 2014. URL: <http://www.springerlink.com/content/n53082n87324462r/>, doi:10.1007/128\\_2012\\_355.
- [5] K. M. Henry and N. M. Donahue. Organic aerosol yields from  $\alpha$ -pinene oxidation: Bridging the gap between first-generation yields and aging chemistry. *Environmental Science & Technology*, 46:12347–12354, 2012. URL: <http://pubs.acs.org/doi/abs/10.1021/es302060y>, doi:10.1021/es302060y.
- [6] L. Hildebrandt, K. M. Henry, J. H. Kroll, D. R. Worsnop, S. N. Pandis, and N. M. Donahue. Evaluating the mixing of organic aerosol components using high-resolution aerosol mass spectrometry. *Environmental Science & Technology*, 45:6329–6335, 2011. URL: <http://dx.doi.org/10.1021/es200825g>, doi:10.1021/es200825g.
- [7] L. Hildebrandt Ruiz, A. Paciga, K. Cerully, A. Nenes, N. M. Donahue, and S. N. Pandis. Aging of secondary organic aerosol from small aromatic VOCs: changes in chemical composition, mass yield, volatility and hygroscopicity. *Atmospheric Chemistry and Physics*, 15:8301–8313, 2015. URL: <http://www.atmos-chem-phys.net/15/8301/2015/>, doi:10.5194/acp-15-8301-2015.
- [8] E. Karnezi, I. Riipinen, and S. N. Pandis. Measuring the atmospheric organic aerosol volatility distribution: a theoretical analysis. *Atmospheric Measurement Techniques*, 7(9):2953–2965, 2014. URL: <http://www.atmos-meas-tech.net/7/2953/2014/>, doi:10.5194/amt-7-2953-2014.
- [9] J. H. Kroll, N. M. Donahue, J. L. Jimenez, S. Kessler, M. R. Canagaratna, K. Wilson, K. E. Alteri, L. R. Mazzoleni, A. S. Wozniak, H. Bluhm, E. R. Mysak, J. D. Smith, C. E. Kolb, and D. R. Worsnop. Carbon oxidation state as a metric for describing the chemistry of atmospheric organic aerosol. *Nature Chemistry*, 3:133–139, 2011. URL: <http://www.nature.com/nchem/journal/vaop/ncurrent/full/nchem.948.html>, doi:10.1038/nchem.948.
- [10] Spyros N. Pandis, Neil M. Donahue, Benjamin N. Murphy, Ilona Riipinen, Christos Fountoukis, Eleni Karnezi, David Patoulias, and Ksakousti Skyllakou. Atmospheric organic aerosols: Insights from the combination of measurements and chemical transport models. *Faraday Discussions*, 165:9–24, 2013. URL: <http://pubs.rsc.org/en/content/articlelanding/2013/fd/c3fd00108c>, doi:10.1039/c3fd00108c.

- [11] I Riipinen, T Yli-Juuti, J. R. Pierce, T. Petäjä, D. R. Worsnop, M. Kulmala, and N. M. Donahue. Contribution of organics to atmospheric nanoparticle growth. *Nature Geoscience*, 5:453–458, 2012. URL: <http://www.nature.com/ngeo/journal/v5/n7/full/ngeo1499.html>, doi: 10.1038/Ngeo1499.
- [12] R. Saleh, C. J. Hennign, G. R. McMeeking, W. K. Chuang, H. Coe, N. M. Donahue, and A. L. Robinson. Light absorption properties of brown carbon from fresh and photo-chemically aged biomass burning emissions. *Atmospheric Chemistry and Physics*, 13:7683–7693, 2013. URL: <http://www.atmos-chem-phys.net/13/7683/2013/>, doi:10.5194/acp-13-7683-2013.
- [13] R. Saleh, M. Marks, J. Heo, P. J. Adams, N. M. Donahue, and A. L. Robinson. Contribution of brown carbon and lensing to the direct radiative effect of carbonaceous aerosols in biomass and biofuel burning emissions. *Journal of Geophysical Research Atmospheres*, 120:10285–10296, 2015. URL: <http://onlinelibrary.wiley.com/doi/10.1002/2015JD023697/abstract>, doi:10.1002/2015JD023697.
- [14] R. Saleh, E. S. Robinson, D. S. Tkacik, A. T. Ahern, S. Liu, A. Aiken, R. C. Sullivan, A. A. Presto, M. K. Dubey, R. J. Yokelson, N. M. Donahue, and A. L. Robinson. Brownness of organics in aerosols from biomass burning linked to their black carbon content. *Nature Geoscience*, 7:647–650, 2014. URL: <http://www.nature.com/ngeo/journal/vaop/ncurrent/full/ngeo2220.html>, doi:10.1038/ngeo2220.
- [15] A. Sinha, R. Saleh, E. S. Robinson, D. S. Tkacik, A. T. Ahern, A. A. Presto, R. C. Sullivan, N. M. Donahue, and A. L. Robinson. Volatility and partitioning kinetics of organic aerosol in biomass burning emissions. *Aerosol Science and Technology*, in preparation, Feb 16, 2016.
- [16] D. S. Tkacik, E. S. Robinson, R. Saleh, A. T. Ahern, E. M. Lipsky, A. A. Presto, R. C. Sullivan, N. M. Donahue, and A. L. Robinson. A dual chamber enhancement method to quantify aerosol formation: Biomass burning secondary organic aerosol. *Aerosol Science and Technology*, in preparation, Dec 15, 2016.

# The contribution of organics to atmospheric nanoparticle growth

Ilona Riipinen<sup>1,5\*</sup>, Taina Yli-Juuti<sup>2</sup>, Jeffrey R. Pierce<sup>3</sup>, Tuukka Petäjä<sup>2</sup>, Douglas R. Worsnop<sup>2,4</sup>, Markku Kulmala<sup>2</sup> and Neil M. Donahue<sup>5</sup>

**Aerosols have a strong, yet poorly quantified, effect on climate. The growth of the smallest atmospheric particles from diameters in the nanometre range to sizes at which they may act as seeds for cloud droplets is a key step linking aerosols to clouds and climate. In many environments, atmospheric nanoparticles grow by taking up organic compounds that are derived from biogenic hydrocarbon emissions. Several mechanisms may control this uptake. Condensation of low-volatility vapours and formation of organic salts probably dominate the very first steps of growth in particles close to 1 nm in diameter. As the particles grow further, formation of organic polymers and effects related to the phase of the particle probably become increasingly important. We suggest that dependence of particle growth mechanisms on particle size needs to be investigated more systematically.**

According to the Intergovernmental Panel on Climate Change, the impacts of aerosol particles on clouds are the largest individual source of uncertainty in estimates of the Earth's energy balance<sup>1</sup>. Most atmospheric cloud droplets are formed from aerosol particles (cloud condensation nuclei, CCN). CCN concentrations control cloud droplet numbers, influencing precipitation and the amount of sunlight reflected to space. We must understand the processes controlling the concentration of atmospheric CCN to understand the climate effects of aerosols.

Atmospheric aerosol particles range from nanometres ( $10^{-9}$  m) to hundreds of micrometers ( $10^{-4}$  m) in diameter, but only particles larger than 30–100 nm can act as CCN (ref. 2; Fig. 1). Anthropogenic combustion processes emit many particles that are initially smaller than 100 nm, and the clustering of vapours is a major source of new particles around 1 nm in diameter in the planetary boundary layer (see Fig. 2 for an example of a particle formation event observed at the Hyytiälä research station in boreal forest)<sup>3,4</sup>. These small particles must grow in size to influence clouds, and this growth happens primarily through the uptake of vapours. Growth from 1 nm to 50 nm in diameter corresponds to more than a 100,000-fold increase in particle mass. The condensing vapours thus determine the composition of the CCN that form through this uptake. Furthermore, growth needs to be fast enough to compete with scavenging by larger particles<sup>5</sup> (Fig. 1). Observed diameter growth rates of new atmospheric particles range from about 0.1 to tens of nanometres per hour<sup>3,6</sup>, depending on the environment. Measurements extending down to 1 nm indicate that growth rates typically increase with particle size during intense particle formation<sup>6,7</sup>.

Organic compounds constitute 20–90% of the submicron aerosol mass, depending on location. Most of this contribution is secondary — that is, these submicron organic particles form in the atmosphere through the oxidation of volatile organic compounds (VOCs) by  $O_3$ , OH and  $NO_3$ , followed by the conversion of the gaseous oxidation products to particles<sup>8</sup>. The VOCs emitted by plants are probably the dominant source of secondary organic aerosol

(SOA)<sup>9</sup>, although recent studies also indicate a strong anthropogenic influence on SOA formation<sup>10</sup>.

SOA comprises thousands of compounds, complicating our understanding of its behaviour. Although sulphuric acid<sup>11,12</sup>, water and basic compounds (such as ammonia and amines)<sup>13–15</sup> drive the very first steps of atmospheric particle formation, their condensation typically explains only a small fraction of atmospheric nanoparticle growth<sup>5,12</sup> — with the exception of some sulphur-rich environments<sup>16,17</sup>. Instead, oxidation products of VOCs — most importantly, biogenic monoterpenes — are the main drivers of atmospheric new particle formation in many rural<sup>6,12,18–21</sup> and urban sites<sup>12,20,21</sup>. In Hyytiälä, for example, nanoparticle growth shows a clear correlation with monoterpene concentrations<sup>6</sup> and the mass flux of organics to the aerosol phase<sup>22</sup>. Of the atmospheric oxidants, OH seems to be of importance in the initial steps of aerosol formation. When aerosols exceed a diameter of 5 nm, a stronger connection with ozonolysis has been reported<sup>23</sup>.

Whether a molecule will reside in atmospheric nanoparticles depends on its volatility — that is, its tendency to evaporate compared with the rate at which it is added to the particles. The latter is driven by condensation and/or chemical reactions. Most state-of-the-art global aerosol models are split in their assumptions regarding the volatility of secondary organics. Some models assume that secondary organics are completely non-volatile, in which case the uptake of SOA components is governed solely by the gas phase<sup>18,24</sup>, and the only mechanism removing SOA from the atmosphere is deposition. Other models assume that SOA is semi-volatile and thus able to evaporate, but in constant thermodynamic equilibrium with the gas phase<sup>25</sup>. Neither of these approaches adequately describe atmospheric aerosol populations<sup>5,26</sup> — the former neglects SOA evaporation and the latter cannot capture the growth of atmospheric nanoparticles. The two approaches result in considerably different aerosol size distributions and CCN concentrations<sup>5</sup>.

The role of biogenic organic compounds in nanoparticle growth initiates a coupling between biosphere and climate: emissions from plants influence aerosol concentrations and clouds, whereas climate

<sup>1</sup>Department of Applied Environmental Science & Bert Bolin Center for Climate Research, Stockholm University, SE-10691, Stockholm, Sweden,

<sup>2</sup>Department of Physics, University of Helsinki, FI-00014, Helsinki, Finland, <sup>3</sup>Department of Physics and Atmospheric Science, Dalhousie University, B3H 3J5, Halifax, Nova Scotia, Canada, <sup>4</sup>Aerodyne Research Inc., 01821, Billerica, Massachusetts, USA, <sup>5</sup>Center for Atmospheric Particle Studies, Carnegie Mellon University, 15213, Pittsburgh, Pennsylvania, USA. \*e-mail: ilona.riipinen@itm.su.se

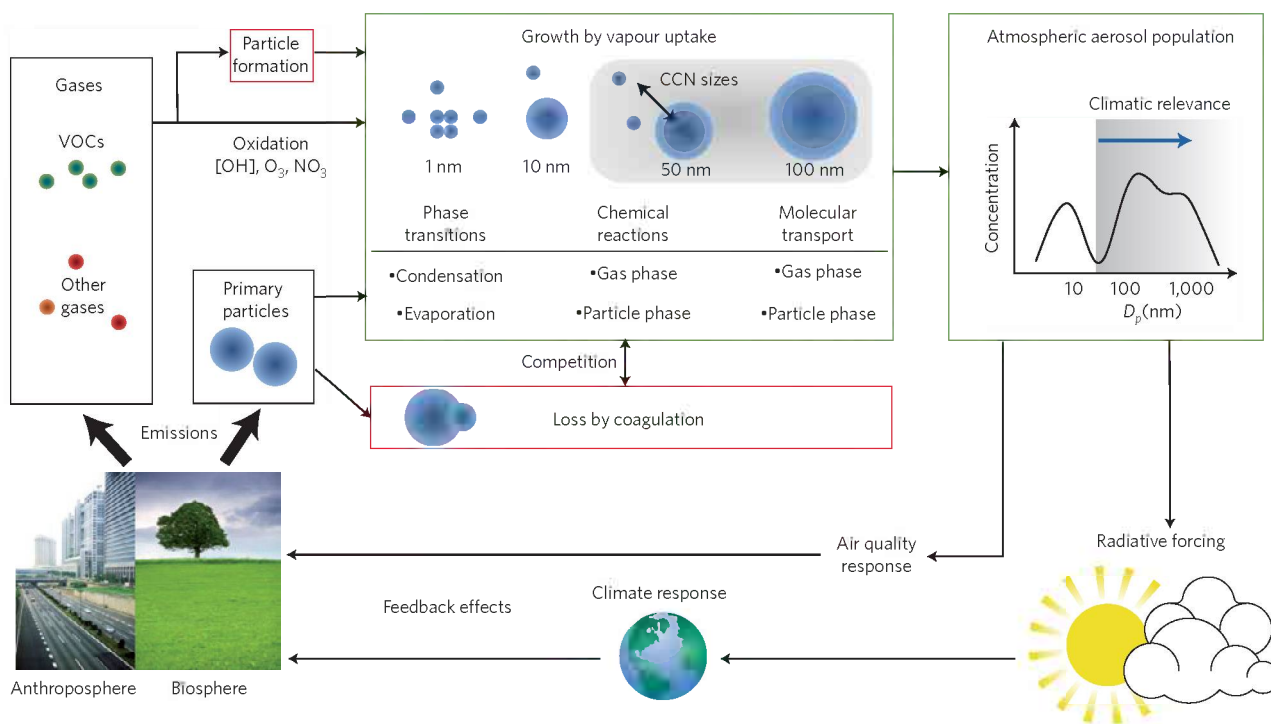


**Figure 1 | Connections between volatile organic compound (VOC) emissions, nanoparticle growth, climate and air quality.** VOCs are oxidized by  $\text{O}_3$ , OH and  $\text{NO}_3$ , and the vapours formed in these reactions condense on to particles. Freshly formed particles must grow from  $\sim 1$  nm to 30–100 nm before colliding with larger particles to have an impact on climate. Uptake of organic vapours is a major source of the growth of these small particles. Because the biosphere is a major source of VOCs, a feedback loop exists between the biosphere, aerosols and climate. This study focuses on the impact of organics on nanoparticle growth.  $D_p$ , particle diameter.

affects vegetation growth and VOC emissions<sup>27</sup> (Fig. 1). Understanding this cycle is a prerequisite for reconstructing historical aerosol loadings and predicting future climate. Resolving the processes driving the uptake of organic compounds by atmospheric nanoparticles is a key requirement for this task. Here we summarize the potential mechanisms governing atmospheric nanoparticle growth by organic vapour uptake, discuss the importance of these mechanisms for varying particle sizes and review the remaining questions, with a particular focus on particles smaller than 50 nm in diameter. We also highlight recent findings relating to the larger submicron SOA particles, which have potential relevance for nanoparticle growth.

### Organic vapour uptake mechanisms

The most commonly proposed mechanisms for organic uptake by nanoparticles include production of low-volatility vapours by gas-phase oxidation of organic precursors and their reversible partitioning (condensation and evaporation)<sup>28</sup>; formation of organic salts through chemical reactions in the particulate phase<sup>21,29</sup>; and formation of organic oligomers and polymers<sup>30,31</sup> (Fig. 3).

The composition of atmospheric nanoparticles is difficult to measure directly, and constraints from multiple instruments are needed for a balanced picture of their growth. Size-resolved composition measurements with mass spectrometers indicate that organic compounds are present in particles greater than 8 nm in diameter (thermal desorption mass spectrometry (TD-CIMS)<sup>21</sup> data), and that they dominate the growth of particles greater than 20 nm in diameter in the boreal environment (aerosol mass spectrometer (AMS)<sup>32</sup> data; Fig. 2d). These organic-containing particles are water-soluble<sup>33</sup>, although less so than pure sulphate. Reduced solubility of nucleated particles indicates that organics may even be present in particles smaller than 3 nm (ref. 34). Oxidized organics have also been detected in growing nanoparticles around 20 nm in size in a more anthropogenically influenced environment<sup>35</sup>, using the nano aerosol mass spectrometer.

However, despite convincing evidence of their presence, the exact identities of the organic molecules driving the growth of atmospheric sub-50-nm particles are largely unresolved.

The net uptake of a compound  $i$  by a nanoparticle is driven by the difference of the condensational and/or chemical flux (governed by gas-phase concentration of  $i$  and/or its precursors) and the evaporational flux (governed by volatility of  $i$ )<sup>22</sup> to/from the particle (Fig. 3). If the particle is well mixed, the volatility of  $i$  is directly related to its equilibrium vapour pressure over the particle surface,  $p_{eq,i}$ , which is determined by the pure component saturation vapour pressure, particle curvature (through the Kelvin effect)<sup>15</sup> and bulk composition. Box model calculations of the condensation and evaporation of organics indicate that equilibrium vapour pressures as low as  $10^{-8}$  to  $10^{-7}$  Pa (concentrations below  $10^{-3}$  to  $10^{-2}$   $\mu\text{g m}^{-3}$  or  $10^6$  to  $10^7$   $\text{cm}^{-3}$ ) are needed to explain the growth of sub-50-nm particles in continental forest environments<sup>22</sup>. These low-volatility compounds are produced either by gas-phase reactions or particulate-phase processing. The abundance and chemical reactivity of the precursor molecules define the pathways for the formation of such material.

Gas-phase formation of condensable vapours through VOC oxidation is the major mechanism creating SOA mass. Unfortunately, there are no direct and comprehensive gas-phase measurements of the products of these reactions. It is therefore not clear if they generate compounds with saturation vapour pressures low enough to grow atmospheric nanoparticles without chemical processing in the condensed phase. The saturation vapour pressures inferred from observations of atmospheric aerosol growth and evaporation<sup>22,36</sup> are generally lower than those measured for identified monoterpene oxidation products<sup>17,37</sup>. Using the properties of organics inferred from smog chamber data, it can be estimated that the net condensation of gas-phase oxidation products of monoterpenes can potentially explain a significant fraction of nanoparticle growth in boreal forests, but not necessarily all of it<sup>28</sup>.

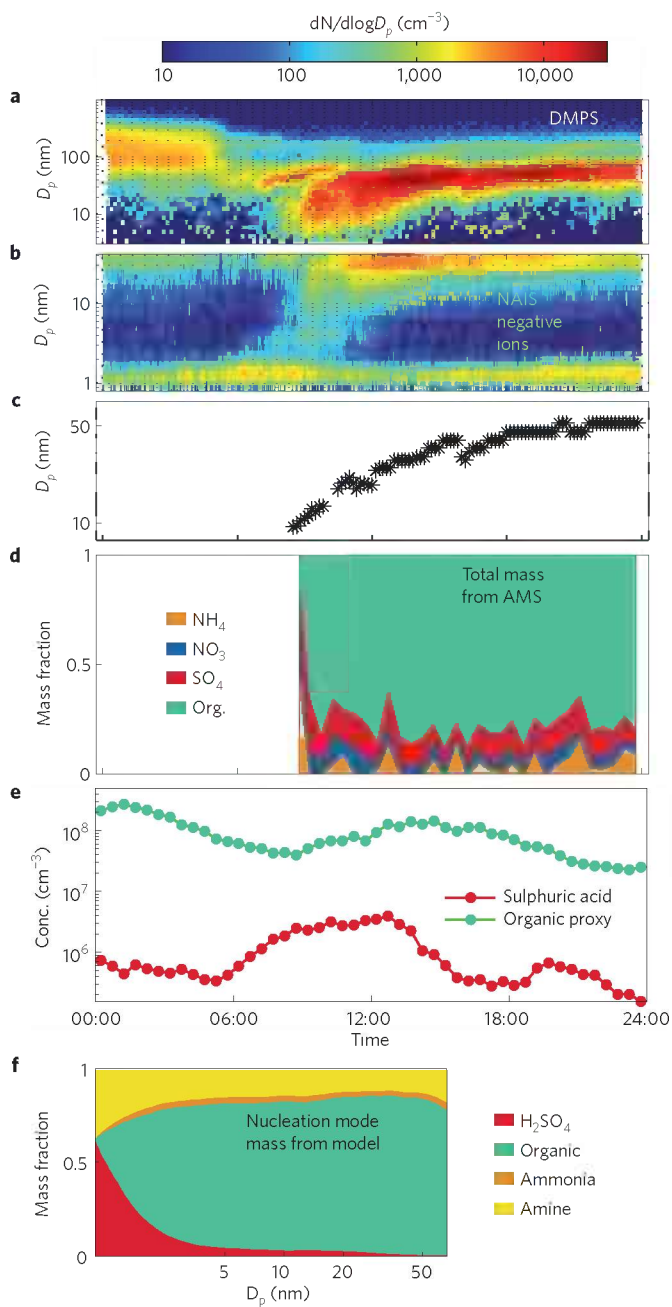


**Figure 2 | Particle formation event on 23 July 2010 in Hyytiälä, Finland<sup>4</sup>.** **a, b**, Aerosol size distribution measured with a differential mobility particle sizer (DMPS) and a neutral cluster and air ion spectrometer (NAIS). **c**, Median diameter of the growing particles.  $D_p$ , particle diameter. **d**, >20 nm particle composition measured with the aerosol mass spectrometer (AMS). **e**, Concentrations of gas-phase sulphuric acid from the chemical ionization mass spectrometer (CIMS)<sup>11</sup> and organic acid proxy, whose diurnal profile was constrained by measured malonic acid concentration and level by organic flux to the aerosols. **f**, Modelled composition of particles growing by uptake of sulphuric acid, organic acid, trimethylamine ( $5 \times 10^7 \text{ cm}^{-3}$ ) and ammonia ( $2 \times 10^{10} \text{ cm}^{-3}$ ), where the initial cluster contains sulphuric acid and trimethylamine<sup>13</sup>, saturation vapour pressure of the organic acid is 10 times higher than sulphuric acid, and the stability of aminium salts is 1000-fold higher than ammonium salts<sup>13</sup>.

The formation of organic salts through particulate-phase reactions of organic acids with amines or ammonia is another plausible source of low-volatility organic compounds in growing

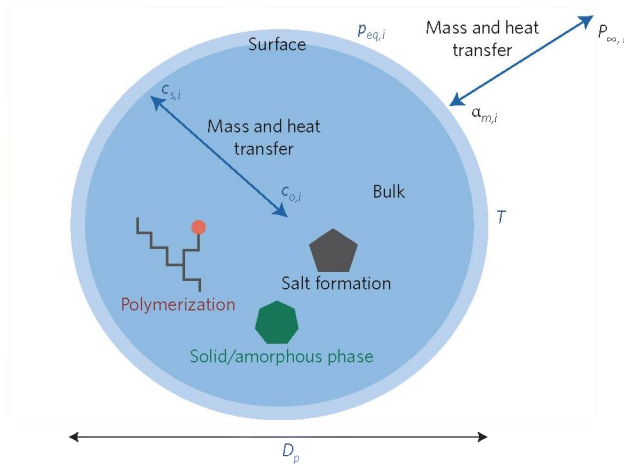


**Figure 3 | The processes influencing organic vapour uptake by atmospheric nanoparticles.**  $c_{s,i}$  is the concentration of compound  $i$  at the particle surface;  $c_{o,i}$  is the concentration of  $i$  in the bulk;  $p_{eq,i}$  is the equilibrium partial pressure of  $i$  at the particle surface and  $p_{\infty,i}$  far away from the surface; and  $\alpha_{m,i}$  is the mass accommodation coefficient of  $i$ .  $T$ , temperature;  $D_p$ , particle diameter. Mass transport is proportional to the vapour pressure or concentration gradients in the gas or particulate phase, and, in practice, coupled with heat transport (due to the latent heat of the phase transition reactions).

nanoparticles. Increased amounts of organic acids and amines have been identified in impactor samples of SOA mass collected from Hyytiälä during particle formation events<sup>38</sup>. Campaign-wise data collected with the TD-CIMS instrument indicate that organic aminium salts can explain, on average, 23% and 47% of the growth of 10 nm particles in Hyytiälä and Tecamac, Mexico, respectively<sup>21</sup>. However, the presence of amines in atmospheric particles smaller than 50 nm in diameter in Hyytiälä has not yet been verified by other mass spectrometric techniques, such as the AMS (Fig. 2d) or the atmospheric pressure inlet time-of-flight mass spectrometer (for clusters smaller than 2000 amu)<sup>39</sup>, which observe ammonia rather than clear signs of amines.

Polymerization is another potential mechanism for generating low-volatility organic compounds in atmospheric nanoparticles. Although the formation of organic salts involves acid-base chemistry, polymerization is simply the formation of high-molecular-weight molecules from organic monomers. Organic polymerization has been observed in biogenic and anthropogenic SOA (refs 40–42), but it is not clear whether it is fast enough to play a role in atmospheric nanoparticle growth. Potential chemical pathways for generating these high-molecular-weight organics involve the presence of water, acid- or ammonium catalysed reactions, esterification, or the formation of low-volatility organosulphates<sup>40–42</sup>. Although laboratory studies indicate significant growth of 10–20 nm sulphate particles when exposed to glyoxal — one of the main oxidation products of isoprene and aromatics, and a potential source of oligomers — no such indications of oligomer formation have been observed for nanoparticles smaller than 10 nm in diameter<sup>31</sup>.

### The potential importance of particle phase state

Secondary organic aerosols have been observed in solid and amorphous phases in both field and laboratory studies<sup>43,44</sup>, challenging the traditional picture of SOA as a complex liquid mixture. Mixing in solid and amorphous phases could be reduced<sup>45,46</sup> — as molecular diffusion is much slower in solid and amorphous material than in liquids — with potential implications for vapour uptake. Biogenic SOA particles greater than 30 nm in diameter have been observed to bounce when impacted on a plate<sup>43</sup>, implying that their

**Box 1 | Processes governing organic vapour uptake by nanoparticles**

Processes affecting vapour uptake	Particle size			
	1–5 nm	5–20 nm	20–50 nm	>50 nm
Reversible net condensation of gas-phase oxidation products	<b>a</b> Important ?	<b>b</b> Important ?	<b>b</b> Important	<b>b</b> Important
Organic salt formation	<b>c</b> Important	<b>d</b> Important ?	<b>e</b> Potentially important ?	<b>e</b> Potentially important ?
*Polymerization/oligomerization	<b>f</b> Potentially important ??	<b>f</b> Potentially important ??	<b>g</b> Important ?	<b>g</b> Important
*Particulate-phase transport effects	<b>h</b> Not important ?	<b>h</b> Not important ?	<b>i</b> Potentially important ?	<b>i</b> Important

**Figure B1 | Importance of processes affecting organic vapour uptake by atmospheric nanoparticles.** Green, processes that should be considered when modelling nanoparticle growth by organics; yellow, processes that are probably needed for building a complete picture of the growth; and red, processes that are probably not important for the size range in question. The certainty of the conclusion is indicated by the number of question marks: two, very uncertain; one, slightly uncertain; none, likely. \*Polymerization/oligomerization can affect nanoparticle growth through formation of high-molecular-weight and low-volatility compounds, as well as through particulate-phase transport processes by, for example, trapping semi-volatile species.

**a,** Observed growth rates from 1.5–3 nm can exceed possible sulphate condensation by a factor of 5–10 in summer<sup>5–7</sup>. Hygroscopic growth of the smallest particles is also lower than expected from inorganic salts. Although Kelvin effects impede reversible uptake considerably at these small sizes<sup>15,22,28</sup>, it is possible that organics with sufficiently low saturation vapour pressure can condense<sup>28</sup>.

**b,** Above diameters of 5 nm, organic condensation becomes increasingly significant with growing particle size, as the Kelvin effect decreases rapidly with increasing particle size<sup>15,22,26,28</sup>.

**c,** The first steps of atmospheric particle formation are very likely to involve acid-base chemistry<sup>13,14,21</sup>, and there are indications that organics are present already at <3 nm (ref. 34).

**d,** Nanoparticle observations above 5 nm show evidence of acid-base chemistry involving organic acids and, especially, amines<sup>21,29,38</sup>.

**e,** Standard secondary organic aerosol formation experiments show little evidence for condensation enhancement for all but

the most acidic seed particles, and any observed acidity effects have been attributed to oligomerization<sup>10</sup>.

**f,** Oligomerization reactions in the gas phase have been proposed as sources of very low-volatility condensable organics, especially through reactions from Criegee intermediates with organic acids<sup>18,41</sup>, although experimental attribution under ambient conditions remains elusive. Growth of 10–20 nm particles by polymerization has been observed in the laboratory<sup>31</sup>. For particles below 10 nm, no indications of polymerization have been reported<sup>31</sup>.

**g,** Strong evidence shows organic macromolecules in particles of >20 nm diameter<sup>41</sup>.

**h,** Transport effects for particles <20 nm in diameter require extreme diffusion limitations<sup>46</sup>, and observations of glassy behaviour are less evident at the smallest sizes<sup>43</sup>.

**i,** Clear evidence for viscous behaviour has been reported for particles of >30 nm diameter<sup>43</sup>, and estimates on diffusion timescales and observed slow evaporation support potential transport limitations as the particle size increases<sup>44</sup>.

mechanical properties are not liquid-like. Bouncing decreases for 17–30 nm particles, indicating a different phase for smaller particles<sup>44</sup>. Furthermore, 100–200 nm SOA particles tend to evaporate more slowly than expected based on traditional theories, potentially due to the particles being poorly mixed<sup>45,46</sup>.

Quantitative estimates of mixing timescales for 1 nm to CCN-sized particles require knowledge of molecular transport in these particles. Order-of-magnitude estimates of these timescales can be obtained by using the Stokes-Einstein equation, which relates viscosity to ‘self-diffusion coefficient’, and uses the protein bovine serum albumin (BSA) as a proxy for semisolid organic aerosol<sup>47</sup>. The diffusion coefficient of BSA is estimated to vary from 10<sup>-20</sup> to 10<sup>-10</sup> cm<sup>2</sup> s<sup>-1</sup> over a range of ambient relative humidities. This results in a huge range of mixing timescales for 1–50 nm particles — spanning microseconds to days. For a diffusion coefficient of 10<sup>-15</sup> cm<sup>2</sup> s<sup>-1</sup>, the mixing timescales lie on the order of seconds, minutes and hours for 5, 20 and 50 nm particles, respectively. These

mixing timescales correspond roughly to characteristic evaporation timescales of a molecule with  $p_{eq} = 10^{-6}$  Pa (10<sup>-1</sup> μg m<sup>-3</sup>), assuming a mass accommodation coefficient of unity. Based on these rough calculations, it can be concluded that particle-phase diffusivity is expected to have a significant impact on organic uptake at  $\chi$  smaller than 10<sup>-10</sup> to 10<sup>-9</sup> cm<sup>2</sup> s<sup>-1</sup> Pa<sup>-1</sup>, where  $\chi$  is defined as the ratio between diffusivity to equilibrium vapour pressure.

There are several complications regarding these diffusivity calculations. First, the self-diffusion coefficients are defined for BSA, which is an ideal mixture of identical molecules, and the obtained timescales probably represent an upper limit: for small molecules like atmospheric oxidants or water, the timescales are several orders of magnitude shorter<sup>47</sup>. Second, the application of diffusion theory is questionable for nanoscale particles. Third, the diffusivities of atmospheric SOA components are probably strong functions of temperature and relative humidity, whereas most of the measurements of the biogenic SOA phase have been conducted at a single relative

humidity or temperature, dry<sup>45</sup> or in a low pressure environment<sup>43</sup>. Atmospheric nanoparticles show hygroscopic growth<sup>33</sup>, so there is probably some water in all surface-level nanoparticles. Also, one could speculate that nanoparticle growth rates are dependent on relative humidity, if mixing were limiting the growth. Until now, no such correlation has been reported. These uncertainties in the mixing calculations highlight the need for understanding the identities of the mixture of molecules present in atmospheric sub-CCN particles.

### The importance of particle size

Numerous mechanisms affect the contribution of organics to nanoparticle growth (Box 1). No single compound or mechanism generally explains atmospheric nanoparticle growth from clusters to climatically relevant sizes. This complicates the interpretation of observations; for instance, the size-dependence of growth can be reproduced with multiple combinations of mechanisms and condensing vapours<sup>7</sup>.

Acid-base chemistry and the condensation of nucleating vapours, such as sulphuric acid, ammonia and amines, is probably important for the growth of nanoparticles less than 5 nm in diameter. Studies on the growth and composition of 1–5 nm particles indicate<sup>6,7,34</sup> that organic compounds also contribute to growth, even at these small sizes. Although direct composition measurements of very small particles are challenging due to their minuscule masses, building an understanding of particle growth is simplified by the limited number of processes and vapours in play. There are no observations of polymer formation in atmospheric particles 1–5 nm in diameter<sup>31</sup>, and issues related to mixing are of minor importance compared with evaporation of the particle constituents — due to the short mixing timescales.

Besides directly affecting the uptake of organic acids, bases affect the uptake of sulphuric acid by nanoparticles<sup>48</sup>. Sulphate concentration and particle acidity may, in turn, link back to the uptake of organics. Growth calculations with a conceptual model indicate that these interactions are particularly important for the smallest nanoparticles (Fig. 2f). The relative importance of sulphate and organics changes rapidly up to diameters of 5 nm, after which the system relaxes to a steady composition, in which organics dominate particle growth. Below 5 nm, the uptake of sulphate, bases and organics is non-linear, depending on the abundance and properties of all the condensing molecules. We therefore expect that the relative contribution of ammonia, amines, sulphuric acid and organic compounds to the growth of 1–5 nm particles varies greatly with atmospheric conditions.

At diameters between 5 and 50 nm, nanoparticle growth is likely to be driven by a combination of mechanisms, whose relative contributions are poorly constrained. First, observations of the contribution of organic salts at these sizes are not fully consistent<sup>21,38,39</sup>. Second, evidence for polymer formation below 50 nm is limited to laboratory studies<sup>31</sup>. Furthermore, if the SOA particles are solid, it might only affect vapour uptake at particle sizes larger than 30 nm<sup>45</sup> — and the implications of solid-phase formation are poorly constrained theoretically. All of the mechanisms mentioned in this article probably play a role in the growth of nanoparticles over 50 nm in diameter, depending on the environment.

### Future directions and large-scale implications

Techniques to measure the composition of atmospheric nanoparticles in a size-dependent manner are evolving rapidly<sup>14,21,35,39,49</sup>. This development will hopefully help to confirm some of the above-mentioned uncertainties, such as the presence or absence of organic polymers in sub-50-nm particles, and the size at which growing nanoparticles start to resemble the larger background aerosol. Although measurements of atmospheric volatile organic compounds are becoming routine, measurements of their low-volatility oxidation products are in their infancy<sup>39,49,50</sup>. However, these

measurements are needed to bridge the gap between volatile precursors and nanoparticle growth, and secondary organic aerosols in general. Coordinated studies of the atmospheric composition and size distribution and of aerosols, using multiple instruments in varying environments and conditions, would help to constrain the processes limiting the growth of atmospheric nanoparticles.

Measurements of the thermodynamic and kinetic properties of low-volatility organic compounds are also needed to constrain the gas- and particulate-phase transport relevant to nanoparticles. Particularly important in this respect is the detection of saturation vapour pressures, condensed-phase activities, mass accommodation coefficients and condensed-phase transport coefficients of organic vapours. Growth in the sub-20-nm size range is particularly sensitive to the particle surface curvature, and accurate estimates of the surface tension and density of atmospheric particles are needed to predict the size-dependence of nanoparticle growth<sup>15</sup>.

At the global level, predictions of the concentration of cloud condensation nuclei are sensitive to secondary organic volatility and nanoparticle growth in atmospheric models<sup>5,24,26</sup>. Monoterpene emissions have been estimated to double CCN numbers over boreal forests<sup>18</sup>, resulting in a radiative forcing ranging from –1.8 to –6.7 W m<sup>-2</sup>. Uncertainties in the mechanism of secondary organic condensation can yield uncertainties in regional cloud condensation nuclei concentrations that exceed 25%<sup>18,24–26</sup>. This corresponds to an uncertainty in regional radiative forcing of more than 1 W m<sup>-2</sup> (ref. 5). To improve estimates of the climate impacts of organics, atmospheric models need to capture nanoparticle growth without compromising predictions of secondary organic aerosol mass budgets and properties. First attempts have been presented, typically combining a semi-volatile species that can evaporate and a species with negligible volatility<sup>5,26</sup>.

Organic compounds play an important role in the growth of atmospheric nanoparticles to sizes at which they can influence clouds and climate. Although we are advancing quickly in our understanding of the role of organics in nanoparticle growth, the exact molecules and mechanisms driving growth are yet to be resolved. It is evident that the importance of the different uptake mechanisms and chemical processes is highly dependent on the size of the nanoparticle. On the one hand, organic vapours responsible for the first steps of aerosol formation — yielding particles around 1 nm in diameter — cannot explain the growth of nanoparticles to climatically relevant sizes. On the other hand, the behaviour of bulk secondary organic aerosol mass, being typically dominated by particles greater than 50 nm in diameter, also gives an incomplete picture of nanoparticle growth. Systematic studies on organic compound uptake mechanisms in particles ranging from 1 to 50 nm in diameter are needed to bridge the gap between these two extremes. This is an important task, given that accurate predictions of nanoparticle growth are necessary for an integrated assessment of the role of organic compounds in a changing climate.

### References

1. IPCC *Climate Change 2007 – The Physical Science Basis: Contribution of Working Group I* (Cambridge Univ. Press, 2007).
2. Dusek, U. *et al.* Size matters more than chemistry for cloud-nucleating ability of aerosol particles. *Science* **312**, 1375–1378 (2006).
3. Kulmala, M. *et al.* Formation and growth of ultrafine atmospheric particles: A review of observations. *J. Aerosol Sci.* **35**, 143–176 (2004).
4. Williams, J. *et al.* The summertime Boreal forest field measurement intensive (HUMPPA-COPEC-2010): an overview of meteorological and chemical influences. *Atmos. Chem. Phys.* **11**, 10599–10618 (2011).
5. Riipinen, I. *et al.* Organic condensation: a vital link connecting aerosol formation to cloud condensation nuclei (CCN) concentrations. *Atmos. Chem. Phys.* **11**, 3865–3878 (2011).
6. Hirsikko, A. *et al.* Annual and size dependent variation of growth rates and ion concentrations in boreal forest. *Boreal Environ. Res.*, **10**, 357–369, (2005).

7. Kuang, C. *et al.* First size-dependent growth rate measurements of 1 to 5 nm freshly formed atmospheric nuclei. *Atmos. Chem. Phys. Discuss.* **11**, 25427–25471 (2011).
8. Jimenez, J. L. *et al.* Evolution of organic aerosols in the atmosphere. *Science* **326**, 1525–1529 (2009).
9. Guenther, A. *et al.* A global model of natural volatile organic compound emissions. *J. Geophys. Res.* **100**, 8873–8892 (1995).
10. Hoyle, C. R. *et al.* A review of the anthropogenic influence on biogenic secondary organic aerosol. *Atmos. Chem. Phys.* **11**, 321–343 (2011).
11. Sipilä, M. *et al.* Role of sulphuric acid in atmospheric nucleation. *Science* **327**, 1243–1246 (2010).
12. Kuang, C. *et al.* An improved criterion for new particle formation in diverse atmospheric environments. *Atmos. Chem. Phys.* **10**, 8469–8480 (2010).
13. Kurtén, T., Loukonen, V., Vehkamäki, H. & Kulmala, M. Amines are likely to enhance neutral and ion-induced sulfuric acid-water nucleation in the atmosphere more effectively than ammonia. *Atmos. Chem. Phys.* **8**, 4095–4103 (2008).
14. Kirkby, J. *et al.* Role of sulphuric acid, ammonia and galactic cosmic rays in atmospheric aerosol nucleation. *Nature* **476**, 429–433 (2011).
15. Zhang, R., Khalizov, A., Wang, L., Hu, M. & Xu, W. Nucleation and growth of nanoparticles in the atmosphere. *Chem. Rev.* **112**, 1957–2011 (2012).
16. Jung, J., Adams, P. J. & Pandis, S. N. Simulating the size distribution and chemical composition of ultrafine particles during nucleation events. *Atmos. Environ.* **40**, 2248–2259 (2006).
17. Zhang, R. *et al.* Formation of nanoparticles of blue haze enhanced by anthropogenic pollution. *Proc. Natl Acad. Sci.* **106**, 17650–17654 (2009).
18. Spracklen, D. V., Bonn, B. & Carslaw, K. S. Boreal forests, aerosols and the impacts on clouds and climate. *Phil. Trans. R. Soc. A* **366**, 4613–4626 (2008).
19. Tunved, P. *et al.* High natural aerosol loading over boreal forests. *Science* **312**, 261–263 (2006).
20. Laaksonen, A. *et al.* The role of VOC oxidation products in continental new particle formation. *Atmos. Chem. Phys.* **8**, 2657–2665 (2008).
21. Smith, J. N. *et al.* Observations of aminium salts in atmospheric nanoparticles and possible climatic implications. *Proc. Natl Acad. Sci.* **107**, 6634–6639 (2010).
22. Pierce, J. R. *et al.* Quantification of the volatility of secondary organic compounds in ultrafine particles during nucleation events. *Atmos. Chem. Phys.* **11**, 9019–9036 (2011).
23. Hao, L. Q. *et al.* New particle formation from the oxidation of direct emissions of pine seedlings. *Atmos. Chem. Phys.* **9**, 8121–8137 (2009).
24. Makkonen, R. *et al.* Sensitivity of aerosol concentrations and cloud properties to nucleation and secondary organic distribution in ECHAM5-HAM global circulation model. *Atmos. Chem. Phys.* **9**, 1747–1766 (2009).
25. Pye, H. O. T. & Seinfeld, J. H. A global perspective on aerosol from low-volatility organic compounds. *Atmos. Chem. Phys.* **10**, 4377–4401 (2010).
26. Yu, F. A secondary organic aerosol formation model considering successive oxidation aging and kinetic condensation of organic compounds: global scale implications. *Atmos. Chem. Phys.* **11**, 1083–1099 (2011).
27. Kulmala, M. *et al.* A new feedback mechanism linking forests, aerosols and climate. *Atmos. Chem. Phys.* **4**, 557–562 (2004).
28. Donahue, N. M., Trump, E. R., Pierce, J. R. & Riipinen, I. Theoretical constraints on pure vapor-pressure driven condensation of organics to ultrafine particles. *Geophys. Res. Lett.* **38**, L16801 (2011).
29. Barsanti, K. C., McMurry, P. H. & Smith, J. N. The potential contribution of organic salts to new particle growth. *Atmos. Chem. Phys.* **9**, 2949–2957 (2009).
30. Zhang, K. M. & Wexler, A. S. Hypothesis for growth of fresh atmospheric nuclei. *J. Geophys. Res.* **107**, 4577 (2002).
31. Wang, L. *et al.* Atmospheric nanoparticles formed from heterogeneous reactions of organics. *Nature Geosci.* **3**, 238–242 (2010).
32. Allan, J. D. *et al.* Size and composition measurements of background aerosol and new particle growth in a Finnish forest during QUEST 2 using an aerodyne aerosol mass spectrometer. *Atmos. Chem. Phys.* **6**, 315–327 (2006).
33. Ehn, M. *et al.* Hygroscopic properties of ultrafine aerosol particles in the boreal forest: diurnal variation, solubility and the influence of sulfuric acid. *Atmos. Chem. Phys.* **7**, 211–222 (2007).
34. O'Dowd, C. D., Aalto, P., Hämeri, K., Kulmala, M. & Hoffmann, T. Atmospheric particles from organic vapours. *Nature* **416**, 497–498 (2002).
35. Bzdek, B. R., Zordan, C., Luther, G. W. & Johnston, M. V. Nanoparticle Chemical Composition During New Particle Formation. *Aerosol Sci. Technol.* **45**, 1041–1048 (2011).
36. Cappa, C. D. & Jimenez, J. L. Quantitative estimates of the volatility of ambient organic aerosol. *Atmos. Chem. Phys.* **10**, 5409–5424 (2010).
37. Booth, A. M. *et al.* Design and construction of a simple Knudsen Effusion Mass Spectrometer (KEMS) system for vapour pressure measurements of low volatility organics. *Atmos. Meas. Tech.* **2**, 355–361 (2009).
38. Mäkelä, J. M. *et al.* Chemical composition of aerosol during particle formation events in boreal forest. *Tellus B* **53**, 380–393 (2001).
39. Ehn, M. *et al.* Composition and temporal behavior of ambient ions in the boreal forest. *Atmos. Chem. Phys.* **10**, 8513–8530 (2010).
40. Russell, L. M., Bahadur, R. & Ziemann, P. J. Identifying organic aerosol sources by comparing functional group composition in chamber and atmospheric particles. *Proc. Natl Acad. Sci.* **108**, 3516–3521 (2011).
41. Kalberer, M. *et al.* Identification of polymers as major components of atmospheric organic aerosols. *Science* **303**, 1659–1662 (2004).
42. Lim, Y. B. *et al.* Aqueous chemistry and its role in secondary organic aerosol (SOA) formation. *Atmos. Chem. Phys.* **10**, 10521–10539 (2010).
43. Virtanen, A. *et al.* An amorphous solid state of biogenic secondary organic aerosol particles. *Nature* **467**, 824–827 (2010).
44. Virtanen, A. *et al.* Bounce behavior of freshly nucleated biogenic secondary organic aerosol particles. *Atmos. Chem. Phys.* **11**, 8759–8766 (2011).
45. Vaden, T. D., Imre, D., Beránek, J., Shrivastava, M. & Zelenyuk, A. Evaporation kinetics and phase of laboratory and ambient secondary organic aerosol. *Proc. Natl Acad. Sci.* **108**, 2190–2195 (2011).
46. Cappa, C. D. & Wilson, K. R. Evolution of organic aerosol mass spectra upon heating: implications for OA phase and partitioning behavior. *Atmos. Chem. Phys.* **11**, 1895–1911 (2011).
47. Shiraiwa, M., Ammann, M., Koop, T. & Pöschl, U. Gas uptake and chemical aging of semisolid organic aerosol particles. *Proc. Natl Acad. Sci.* **108**, 11003–11008 (2011).
48. Ge, X., Wexler, A. S. & Clegg, S. L. Atmospheric amines — Part II. Thermodynamic properties and gas/particle partitioning. *Atmos. Environ.* **45**, 561–577 (2011).
49. Zhao, J., Eisele, F. L., Titcombe, M., Kuang, C. & McMurry, P. H. Chemical ionization mass spectrometric measurements of atmospheric neutral clusters using the cluster-CIMS. *J. Geophys. Res.* **115**, D08205 (2010).
50. Holzinger, R. *et al.* Aerosol analysis using a thermal-desorption proton-transfer-reaction mass spectrometer (TD-PTR-MS): a new approach to study processing of organic aerosols. *Atmos. Chem. Phys.* **10**, 2257–2267 (2010).

## Acknowledgements

Financial support by European Research Council Grant ATMOGAIN (project no. 278277), Vetenskapsrådet, European FP7 Integrated project PEGASOS (project number 265148), Electric Power Research Institute (EPRI), US Department of Energy (DESC0007075), US National Science Foundation (AGS1136479 and CHE1012293), and Academy of Finland (project numbers 133872 and 139656) are gratefully acknowledged. Antti-Jussi Kieloaho, Theo Kurtén, Ulla Makkonen, Spyros N. Pandis, and Mikko Äijälä are acknowledged for their valuable input in the form of useful discussions and providing experimental data.

## Additional Information

The authors declare no competing financial interests.

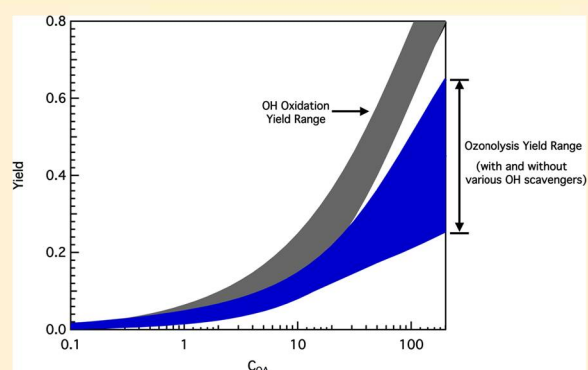
# Organic Aerosol Yields from $\alpha$ -Pinene Oxidation: Bridging the Gap between First-Generation Yields and Aging Chemistry

Kaytlin M. Henry,<sup>†</sup> Theresa Lohaus,<sup>‡</sup> and Neil M. Donahue<sup>†,\*</sup>

<sup>†</sup>Carnegie Mellon University Department of Chemical Engineering, 5000 Forbes Ave Pittsburgh, Pennsylvania 15213, United States

<sup>‡</sup>RWTH Aachen University Department of Chemical Engineering, Templergraben 55, 52056 Aachen, Germany

**ABSTRACT:** Secondary organic aerosol formation from volatile precursors can be thought of as a succession of generations of reaction products. Here, we constrain first-generation SOA formation from the  $\alpha$ -pinene + OH reaction and also study SOA formation from  $\alpha$ -pinene ozonolysis carried out without an OH scavenger. SOA yields from OH oxidation of  $\alpha$ -pinene are significantly higher than SOA yields from ozonolysis including an OH scavenger, and the SOA mass yields for unscavenged ozonolysis generally fall within the range of mass yields for  $\alpha$ -pinene ozonolysis under various conditions. Taken together, first-generation product yields parametrized with a volatility basis set fit provide a starting point for atmospheric models designed to simulate both the production and subsequent aging of SOA from this important terpene.



## 1. INTRODUCTION

Fine particulate matter (PM) causes adverse health effects<sup>1</sup> as well as uncertain climate forcing.<sup>2</sup> Between 20 and 90% of total PM is made up of organic components, and this fraction is still poorly understood.<sup>3</sup> Much organic aerosol (OA) is secondary, produced when volatile organic compounds (VOCs) react in the atmosphere to form less volatile products that can condense to the particle phase. The reactions that form condensable gases are complex, dependent on many reaction conditions, and give wide ranges of secondary OA (SOA) formation.

SOA formation and evolution can be broken down into several stages. It starts with formation of first-generation products from the oxidation of VOC precursors by various oxidants. Product yields are often lumped by volatility via one of several lumping schemes.<sup>4,5</sup> VOCs are also often lumped into emissions categories (anthropogenic, biogenic, biomass burning, etc.) and SOA mass yields are parametrized for these sources.<sup>6</sup> Sometimes these parametrized yields are taken to be first-generation products, whereas sometimes they are taken to represent some form of final SOA formation. Regardless, the yield parametrizations are used in atmospheric chemical transport models (CTMs) to predict OA concentrations.

The second stage of SOA formation is the production of later-generation products via oxidation of first-generation products. This is called aging, which can be represented separately in CTMs.<sup>7</sup> One form of aging is the gas-phase oxidation of first-generation products by OH radicals.<sup>8</sup> Other forms include heterogeneous oxidant uptake to particles, condensed-phase accretion reactions, and photolysis (in either the gas or aerosol phase).<sup>8–11</sup>

To accurately represent the aging process, it is important to constrain the first-generation chemistry for precursor VOCs

driven by each oxidant. Different VOCs and different oxidants present different challenges in this regard. Unsaturated precursors react with several oxidants, including OH, ozone, and NO<sub>3</sub>. Saturated precursors generally only react with OH, but the first-generation products will react with OH as well, sometimes more rapidly than the precursor. Thus, it is difficult to separate the first-generation of chemistry from subsequent oxidation.

$\alpha$ -Pinene is the most abundant monoterpene and is used in atmospheric CTMs as a component of biogenic SOA.<sup>6,12</sup> The oxidation of  $\alpha$ -pinene to form SOA has been studied extensively, characterizing the composition,<sup>13</sup> reaction mechanism,<sup>14</sup> and SOA yields under a variety of experimental conditions.<sup>15–17</sup> The past work has mainly focused on the ozonolysis reaction, which has been thought to be the most efficient at forming SOA because it forms many multifunctional products.<sup>18</sup> However, ozonolysis of  $\alpha$ -pinene produces OH radicals with a stoichiometric yield of roughly 0.8.<sup>19</sup> Consequently, to isolate ozonolysis one must use an OH scavenger to remove the OH. However, because stable first-generation products are formed after a succession of reaction steps involving organic free radicals, the OH scavengers (HO<sub>x</sub>–RO<sub>x</sub> conditioners) invariably perturb the radical chemistry, influence the product distribution, and thus affect SOA mass yields.<sup>20</sup> None-the-less, the first-generation products of  $\alpha$ -pinene + ozone are relatively well constrained under a variety of conditions.

Received: May 23, 2012

Revised: September 10, 2012

Accepted: October 22, 2012

Published: October 22, 2012

OH oxidation reactions as well as photooxidation of  $\alpha$ -pinene have been seen to form significant SOA as well.<sup>21–23</sup> Photooxidation studies can include both OH and ozone, making them difficult to interpret. Thus far, few studies have isolated the oxidation of  $\alpha$ -pinene via OH under low-NO<sub>x</sub> (NO<sub>x</sub> = NO + NO<sub>2</sub>) conditions.<sup>21</sup> Much work has focused on the overall identification of major gas-phase products from this reaction (under both high and low-NO<sub>x</sub> conditions),<sup>24,25</sup> but first-generation SOA formation can be driven by relatively minor products. Eddingsass has determined SOA yields from  $\alpha$ -pinene photooxidation, based on oxidation exposure; however, that work blurs the initial oxidation of  $\alpha$ -pinene and the subsequent aging chemistry.<sup>26</sup> Because direct constraints of first-generation SOA mass yields from OH oxidation are lacking, ozonolysis mass yields have been used as a proxy to calculate SOA formation from low-NO<sub>x</sub>  $\alpha$ -pinene + OH reactions in CTMs.<sup>6</sup>

It is apparent that in addition to first-generation chemistry the OA field must move toward longer time scale experiments (and/or more oxidant exposure) where we can look at the effects of further generations of chemistry. Aging chemistry for  $\alpha$ -pinene SOA systems is driven by OH and/or photolysis, as ozone will only react with the double bond on  $\alpha$ -pinene. In recent work, we have used OH to age the SOA formed from  $\alpha$ -pinene ozonolysis.<sup>8</sup> In theory, this gives a very clean separation between first-generation ozonolysis products and later-generation OH reactions. However, OH scavengers typically used in ozonolysis systems would significantly hinder the aging reactions removing much of the OH desired for aging reactions. Therefore, in most aging experiments the ozone +  $\alpha$ -pinene reaction is carried out without an OH scavenger and as a consequence roughly half of the  $\alpha$ -pinene reacts with ozone and half with OH.<sup>27–30</sup>

SOA mass yields for the unscavenged  $\alpha$ -pinene + ozone system and for first-generation  $\alpha$ -pinene + OH are less well constrained than pure  $\alpha$ -pinene + ozone. Because the unscavenged case involves a mixture of ozone and OH reaction products, we would generally expect SOA mass yields to fall between the mass yields for these two pure systems. Consequently, our objective for this work is to measure SOA production from unscavenged  $\alpha$ -pinene + ozone and from isolated  $\alpha$ -pinene + OH, to better constrain overall first-generation SOA volatility distributions and to test this mixing hypothesis. If the mixing hypothesis is successful, CTMs could then separately describe yields for OH-driven and ozone-driven oxidation of  $\alpha$ -pinene (and presumably other species) and deduce overall mass yields via linear mixing of the two pathways.

## 2. MATERIALS AND METHODS

**2.1. Experimental Setup.** Experiments were performed at the Carnegie Mellon University (CMU) Smog Chamber, a 10m<sup>3</sup> Teflon bag suspended in a temperature controlled room. Prior to experiments the bag was cleaned by flushing with clean, dry air and exposure to high temperatures (~35 °C) and UV irradiation. After cleaning the chamber was maintained at 22 °C ± 1.

All experiments were performed with ammonium sulfate ((NH<sub>4</sub>)<sub>2</sub>SO<sub>4</sub>, Sigma Aldrich, 99.99%) seed particles. The seeds were formed by atomizing a 1 g/L solution of (NH<sub>4</sub>)<sub>2</sub>SO<sub>4</sub> in water, drying and neutralizing the particles before they entered the chamber. Seed concentrations at the time of oxidation were always above 5 × 10<sup>3</sup> cm<sup>-3</sup>, and Tables 1 and 2 list the specific

**Table 1. Ozonolysis Experiment Conditions**

Experiment	Seed Concentration <sup>a</sup> × 10 <sup>3</sup> cm <sup>-3</sup>	[ $\alpha$ -Pinene] <sub>i</sub> (ppb)	[O <sub>3</sub> ] <sub>i</sub> (ppb)
1	6.6	31.8	800
2	8.6	36.9	1000
3	7.4	17.6	800
4	7.8	25.8	1000
5 <sup>a</sup>	12	26.7	460
6 <sup>a</sup>	13	26.7	500
7 <sup>a</sup>	12	22.8	450

<sup>a</sup> $\alpha$ -Pinene injection initiated the reaction.

**Table 2. OH Oxidation Experiment Details**

Experiment	Seed Concentration × 10 <sup>3</sup> cm <sup>-3</sup>	[ $\alpha$ -Pinene] <sub>i</sub> (ppb)	$\Delta$ [ $\alpha$ -Pinene] <sub>i</sub> (ppb)	[OH] × 10 <sup>6</sup> cm <sup>-3</sup>
1	9.9	38.9	19.4	2.6
2	9.5	21.8	16.3	2.0
3	12	27.4	14.9	7.0
4	6.5	32.4	13.3	3.2
5	10	46.5	18.4	2.3
6	5.5	39.3	20.1	7.2
7	14	47.0	20.6	2.4

initial seed concentrations.  $\alpha$ -Pinene was added to the chamber via a septum injector flushed with clean air to volatilize and carry the precursor to the chamber. Typically chemistry was initiated by introducing the oxidant, either ozone or OH (via HOOH photolysis), to the chamber, except in a few ozonolysis experiments where  $\alpha$ -pinene was added after ozone was mixed in the chamber (noted in Table 1). All seed particles were coated with organics during oxidation, which was verified with particle time-of-flight (PToF) aerosol mass spectrometer (AMS) measurements. This has also been shown in previous work with the ozonolysis system.<sup>8</sup> In addition to the seed coating, there was new-particle formation of SOA in some experiments due to the rapid oxidation of the precursor (discussed further below).

We monitored  $\alpha$ -pinene decay with a proton-transfer reaction mass spectrometer (PTR-MS, Ionicon) operated in selected ion mode. The instrument was calibrated to determine  $\alpha$ -pinene's sensitivity (signal/ppb) with a known volume of  $\alpha$ -pinene prior to each experiment.<sup>31</sup> The particle phase was measured by both a scanning mobility particle sizer (SMPS, TSI classifier model 3080, CPC model 3010 or 3772) and a quadrupole aerosol mass spectrometer (Q-AMS, Aerodyne Research Inc.). Particle number concentration and volume were obtained from the SMPS. A unit density was used to convert SMPS volume to a normalized mass to compare to previous  $\alpha$ -pinene literature. The AMS was used to monitor particle mass speciated using the standard fragmentation table.

**2.2. SOA Mass Yields and Wall-Loss Corrections.** When VOCs react with an atmospheric oxidant they form some products of lower volatility that can condense to generate SOA. In smog-chamber experiments we calculate an aerosol mass yield,  $Y$ , as the amount of SOA formed divided by the amount of VOC reacted:

$$Y = \frac{C_{\text{OA}}}{\Delta C_{\text{ROG}}} \quad (1)$$

where  $C_{\text{OA}}$  is the mass concentration of organic aerosol and  $\Delta C_{\text{ROG}}$  is the amount of reacted organic gas. We measured

these concentrations throughout an experiment to get multiple yield points while SOA formation progressed (these are called dynamic yields).<sup>32</sup> To obtain a volatility distribution, we fit our data to the volatility basis set (VBS). The SOA is assumed to be in equilibrium with the vapors, and we use effective saturation concentrations,  $C_i^*$ , spaced logarithmically as in Donahue, et al.<sup>33</sup> Each individual product partitions according to:

$$\xi_i = \left( 1 + \frac{C_i^*}{C_{\text{OA}}} \right)^{-1} \quad (2)$$

where  $\xi_i$  is the fraction of species  $i$  in the condensed phase. When we parametrize the fraction of a species  $i$  that resides in the particle phase, we also then determine the mass residing in the gas phase. For example, if the total OA concentration ( $C_{\text{OA}}$ ) is  $10 \mu\text{g m}^{-3}$ , then a species with a  $C^* = 10 \mu\text{g m}^{-3}$  will reside 50% in the particle phase and 50% in the gas phase. Because of this equilibrium relationship, we can parametrize the product vapors in  $C^*$  bins that are near  $C_{\text{OA}}$  concentrations. Much more volatile  $C^*$  bins must be constrained with a mass balance to track carbon through the lifetime of the OA.

A major challenge in these mass-balance calculations is to properly treat the mass of OA deposited to the chamber walls during an experiment. There are two pathways for organics to reach the walls. The first is deposition of particles onto the walls. Deposition of particle number (and the associated mass) to the walls is relatively straightforward to treat if one can determine the particle wall-loss rate constant.<sup>34,35</sup> The second pathway is condensation of secondary vapors to the walls – either to the particles already present on the walls or to the walls themselves.<sup>36</sup> Here, we consider condensation of vapors to particles deposited to the walls earlier in an experiment. In general, we consider two limiting cases. In the first (designated  $\omega = 0$ ), there is no vapor condensation to the walls (only to suspended particles). In the second (designated  $\omega = 1$ ), condensation to particles on the walls is identical to condensation to suspended particles.<sup>37,38</sup>

### 2.3. Ozonolysis Experiments (With No OH Scavenger).

Typically an OH scavenger is used to isolate the ozonolysis reaction as OH is formed from alkene ozonolysis.<sup>39,40</sup> The scavenger is chosen so that the scavenger–OH reaction does not form products that can condense to form SOA, however the scavenger reactions affect the radical balance in the chamber. It is now known that by adjusting the  $\text{RO}_2/\text{HO}_2$  ratio in the chamber, the product distribution shifts as these radicals play an important role in the complex ozonolysis mechanism. This in turn affects aerosol yields in these systems.<sup>20</sup> As we cannot completely isolate the ozonolysis chemistry without disrupting the radical balance, we have previously suggested that  $\alpha$ -pinene ozonolysis yields be parametrized not only by  $\text{NO}_x$  conditions, but also by the  $\text{RO}_2/\text{HO}_2$  ratio under a low- $\text{NO}_x$  regime.

As we look to expand the system for OH aging after the ozonolysis chemistry, there is one novel OH scavenger that can also be used as an OH radical source: hydrogen peroxide ( $\text{HOOH}$ ). In the dark for ozonolysis  $\text{HOOH}$  acts as an OH scavenger; when UV lights are turned on it becomes an OH source. First-generation SOA yields for this ozonolysis system have been reported previously.<sup>20</sup> In any other case, however, an OH scavenger would severely hinder aging chemistry, as the scavenger would continue to react with OH when OH reactions with ozonolysis product vapors are preferred.

Without a scavenger in the system, any OH produced during ozonolysis reacts with gas-phase compounds in the chamber. Often the dominant compound is the same alkene that reacts with ozone (i.e.,  $\alpha$ -pinene). With molar yields of OH from  $\alpha$ -pinene ozonolysis between 0.8 and 1, just less than half of the  $\alpha$ -pinene in this system will react with OH instead of ozone (over the range of ozone concentrations used here we consider 50:50 ozone versus OH reactions to be the upper bound on OH reactions with  $\alpha$ -pinene).<sup>19</sup> Some of the first generation gas-phase products will react with OH as the  $\alpha$ -pinene concentration nears zero (and all OH reacts rapidly, meaning any aging reactions are completed essentially as soon as all the  $\alpha$ -pinene has reacted). As aging chemistry is minimal in this system we calculate OA yields throughout the entire OA formation (see Table 1 for experiment details).

In the case of ozonolysis (with modestly high ozone concentrations), the chemistry is sufficiently fast ( $\sim 1$  h) and therefore at its completion there are few particles on the chamber walls. In this case the wall-loss correction is of little importance; for simplicity we use the  $\omega = 0$  wall-loss correction assuming that gases only condense onto suspended particles.<sup>15,37</sup> For these experiments we can directly calculate the particle wall-loss rate from the SMPS normalized organic mass after the formation of SOA is complete and the only process occurring in the chamber is wall loss.

Wall loss varies with particle size, and could be of concern when there is a bimodal particle size distribution including a smaller nucleation mode of particles in the smog chamber.<sup>35</sup> To assess the impact of nucleation on the wall-loss correction we divided the total organic mass into the masses of the two distributions and calculated the wall-loss rates for the small particles and larger particles separately. As expected, the smaller particles are lost to the walls much more rapidly than the larger distribution of seed particles coated with organics. When comparing the total organic mass wall-loss rate with separate rates for the two modes, we see that the total wall-loss rate is a linear combination of these two loss rates, weighted by the percent of total organic mass in each mode. The difference in these two corrections is therefore negligible and we can use the total mass wall-loss rate. We note that size-dependent wall-loss rates would be more important for a size distribution that changes throughout an experiment. This is not necessary for these experiments where the distribution does not shift much over the hour of chemistry (coagulation of nucleated particles is not significant and the nucleation mode remains present throughout the experiment). One cannot use the  $\omega = 1$  correction described by Hildebrandt, et al.<sup>37</sup> here with a large nucleation mode of particles which do not have a seed core, and this  $\omega = 1$  correction becomes necessary for longer aging experiments as the percent of total mass on the chamber walls becomes significant.

**2.4. OH Oxidation Experiments.** For OH oxidation experiments, hydrogen peroxide ( $\text{HOOH}$ ) photolysis was used to generate the oxidant. A 50/50 solution of  $\text{HOOH}$  in water (Sigma Aldrich) was bubbled into the chamber for an hour at the start of each OH oxidation experiment. Peroxide was injected before seed addition to minimize the loss of seed particles to the chamber walls. A visual inspection of the bubbler as well as an increase in relative humidity ( $\sim 20\%$ ) verified the injection of  $\text{HOOH}$ . In these experiments  $\alpha$ -pinene was first injected and then the UV lights were turned on to initiate chemistry by the formation of the OH radical.  $\alpha$ -Pinene decay was used to calculate the OH concentration (Table 2)

during the first 10 min of the experiment (at the CMU smog chamber we have typically seen constant OH concentrations from HOOH over the time scales of these experiments).

During OH oxidation experiments, we used excess  $\alpha$ -pinene. This was to ensure that most OH reacted with  $\alpha$ -pinene and not with reaction products of  $\alpha$ -pinene + OH. Therefore, each of these experiments was only carried out for 1 h of OH chemistry. The initial  $\alpha$ -pinene concentration as well as the amount of reacted organic gas ( $\Delta C_{\text{ROG}}$ ) is listed in Table 2.

Finally, ozone was produced during OH oxidation experiments. Consequently,  $\alpha$ -pinene continued to react after the UV lights were turned off and OH production had ceased (OH reacts almost instantaneously upon its formation). Ozone production was also apparent in the UV-absorption ozone monitor (Dasibi 1008 PC); however we could not measure ozone quantitatively via UV absorption because of HOOH interference with the UV absorption signal. Ozone formation has been seen in similar systems and is expected to form from ppt levels of NO in the smog chamber as well as residual material from the chamber walls.<sup>21</sup> The effects of this ozone formation on the OH oxidation yields are discussed further below.

As we only consider the first hour of chemistry in these OH oxidation experiments, there are few particles on the walls and we can assume that gases only condense to suspended particles when performing a wall-loss correction.<sup>15,37</sup> Because of ozone formation, the organic mass grows in the dark chamber after we have stopped the desired OH reactions. Therefore, we must calculate the wall-loss rate of the particles from the ammonium sulfate seeds as measured by the AMS. We did not observe new-particle formation in these experiments, and we observe that all the seed particles are coated with organics via PToF data. The wall-loss rate can then be calculated from the AMS seed mass and applied to the organic decay. The wall-loss rate is calculated from the seed decay after the seed has been coated with organics to avoid collection efficiency problems with uncoated seed particles. The wall-loss constant is used with the SMPS normalized mass (having subtracted out the seed from the total SMPS volume) to calculate the total SOA mass formed through OH oxidation.

**2.5. Interfering Chemistry.** OH radicals will react with first-generation products to age any SOA formed from  $\alpha$ -pinene in both the ozone and OH oxidation experiments. This is unavoidable, yet our objective is to isolate first-generation SOA formation. In both cases the large rate constant for the OH +  $\alpha$ -pinene reaction limits this interference. For ozonolysis, OH is formed from the ozone +  $\alpha$ -pinene reaction and reacts immediately, largely with  $\alpha$ -pinene. However, a straightforward simulation of the kinetics modeling the first-generation products as pinonaldehyde shows that up to 20% of those products may react with OH. For the direct OH +  $\alpha$ -pinene SOA formation experiments, limited to 50%  $\alpha$ -pinene removal, again at most 20% of the first-generation products may react with OH. This corresponds to an OH exposure (using pinonaldehyde as the model) of  $2 \times 10^6$  OH-hr. However, the MUCHACHAS experiments that carefully isolated the effect of OH aging on the  $\alpha$ -pinene SOA system showed that aging could approximately double the SOA mass yields after  $(2-4) \times 10^7$  OH-hr of exposure.<sup>41</sup> On that basis, we estimate that the undesired aging of SOA in these experiments increased the observed mass yields by at most 10–20%.

In the OH-driven SOA formation experiments, some ozone formation was inferred based on residual  $\alpha$ -pinene decay when

the OH source was turned off. However, while direct measurement of ozone via UV absorption was hindered by interference from peroxide absorption, even with a formation efficiency of 2 ozone molecules per  $\alpha$ -pinene removed, at most 40 ppbv of ozone would have been formed in these experiments. The oxidation rate of  $\alpha$ -pinene by ozone at the end of the experiments was thus at most 1/3 of the rate by OH. The integrated  $\alpha$ -pinene oxidation was thus at least 80% by OH.

On the basis of these considerations, we conclude that these experiments successfully isolated the desired reactions (unscavenged ozonolysis and OH oxidation) and their first-generation SOA formation.

### 3. RESULTS AND DISCUSSION

**3.1. Unscavenged Ozonolysis SOA Mass Yields.** A yield curve was obtained using multiple ozonolysis experiments. Because of the high time resolution of the PTR-MS and SMPS we were able to calculate many time-dependent (dynamic) SOA mass-yield points for each experiment. The ozonolysis yields for several experiments are shown in Figure 1. The  $x$  axis,

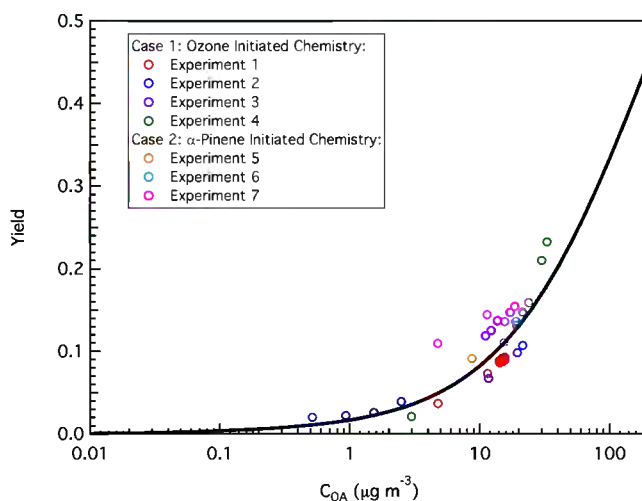


**Figure 1.** Scavenger-free ozonolysis mass yields. SOA mass yields for multiple  $\alpha$ -pinene ozonolysis experiments are shown in the open circles. They are divided into experiments where ozone initiated the chemistry (case 1) and where  $\alpha$ -pinene injection initiated chemistry (case 2). The SOA mass yields are independent of the initiating reactant. The  $\alpha$ -pinene reacts to completion here, with up to 50% reacting with the OH formed through ozonolysis. These yields are obtained at low  $C_{\text{OA}}$  ( $<100 \mu\text{g m}^{-3}$ ) to focus on atmospheric  $C_{\text{OA}}$  levels where subsequent aging chemistry would occur. The black line is a fit to the VBS; parameters are given in Table 3.

which gives the concentration of OA, is shown on a log scale to emphasize the atmospherically relevant range ( $1-100 \mu\text{g m}^{-3}$ ). The ozonolysis experiments were performed over that range as it has been shown that yield extrapolation from higher  $C_{\text{OA}}$  experiments is not accurate.<sup>16</sup>

There are two types of experiments shown in Figure 1 - Case 1: those where chemistry was initiated by ozone injection and Case 2: those where chemistry was initiated by  $\alpha$ -pinene injection. For Case 1, the  $\alpha$ -pinene remained in the chamber, unreacted, for up to ten minutes. This facilitated a steady initial concentration reading for the  $\Delta C_{\text{ROG}}$  calculation. Complete injection of  $\alpha$ -pinene was verified in Case 1 (and no  $\alpha$ -pinene was lost to the walls), therefore for Case 2 the initial

concentration of  $\alpha$ -pinene could be calculated from the injected volume with uncertainty less than that of the instrument precision.

As pointed out in the Materials and Methods section, we use inorganic seed particles as a surface for the oxidized VOCs to condense onto. However, some new particle nucleation occurs specifically in the Case 1 experiments. In general, experiments in the CMU smog chamber observe that less nucleation occurs in Case 2 when we allow the ozone (added in excess) to mix in the chamber before allowing chemistry to proceed. Here we observe nucleation in Case 1 which ranges from modestly 15% of the organic mass up to 75% of the organic mass. This large difference in %OA in the nucleation mode for Case 1 can be attributed to differing reaction speeds for the ozonolysis in different experiments, governed by both the ozone concentration and initial  $\alpha$ -pinene concentration. We see no nucleation in Case 2. However, with either Case 1 or Case 2 we see a yield curve independent of the level of new particle nucleation in Figure 1.

**3.2. OH Oxidation SOA Mass Yields.** Figure 2 shows the SOA mass yields from various OH oxidation experiments. No

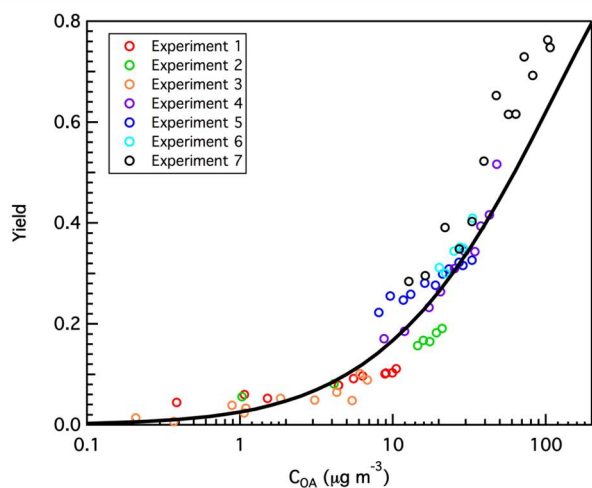


**Figure 2.** OH oxidation mass yields. SOA mass yields for oxidation of  $\alpha$ -pinene by OH are shown in the open circles for multiple experiments.  $\alpha$ -Pinene was only allowed to react with OH (via HOOH photolysis) for 1 h to minimize aging chemistry because CTMs parametrize first-generation yields. The black line is a VBS fit to the data; parameters are given in Table 3.

experiment showed any new-particle formation, and we do not see a yield dependence on seed concentration under these conditions. We have examined the yields from this system, grouping the experiments with similar conditions:  $\alpha$ -pinene starting concentration or amount reacted within 2 ppb, OH concentration of  $\sim 2 \times 10^6$  versus  $7 \times 10^6$  molecules  $\text{cm}^{-3}$  (Table 2). The OH oxidation experiments have more variability than is evident in the ozonolysis experiments. An example of the variability is experiments 1 and 5, which have similar  $\Delta[\alpha\text{-pinene}]$  and OH concentrations. Experiment 5 has a much higher yield than experiment 1.

One potential source of variability is the OH concentration; at higher OH (and more  $\alpha$ -pinene consumption) we might expect more aging chemistry and thus higher yields. Experiments 3 and 6 have an OH concentration of approximately  $7 \times 10^6$  molecules  $\text{cm}^{-3}$ . We would expect that experiment 6 would have a higher yield because more  $\alpha$ -pinene was reacted in that

case, and this is what we observe. However, this trend does not hold for the remaining experiments, all conducted at OH concentrations near  $2 \times 10^6$  molecules  $\text{cm}^{-3}$ . Differing OH concentrations alone cannot describe the amount of variability seen in these experiments.

Another potential source of variability is the ozone production. As we were unable to measure the ozone concentration accurately (due to the interference from HOOH), we cannot directly constrain this, but based on the calculations presented above it is unlikely to be a dominant source of the variability in the SOA mass yields.

SOA formation experiments employing OH oxidation often exhibit more variability in observed SOA mass yields than pure ozonolysis experiments.<sup>37</sup> The reason for this is unknown. We considered chemical composition of aerosol observed with the AMS as a potential clue to the yield variability. There were, however, no systematic differences in the mass spectra to explain the variability in SOA mass yields. In smog-chamber experiments it is difficult to control all variables, and we do not measure the many radical species created during the complex mechanism of OH oxidation. It is possible that variations in the radical balance could be the reason for the more variable SOA yields. However, even with the amount of variability seen, we can still parametrize these yields for the VBS, as will be described below.

**3.3. Volatility Basis Set Parameterization.** The solid lines in Figures 1 and 2 show the VBS fit for each yield data set. In Figure 3, we present the two parametrizations developed

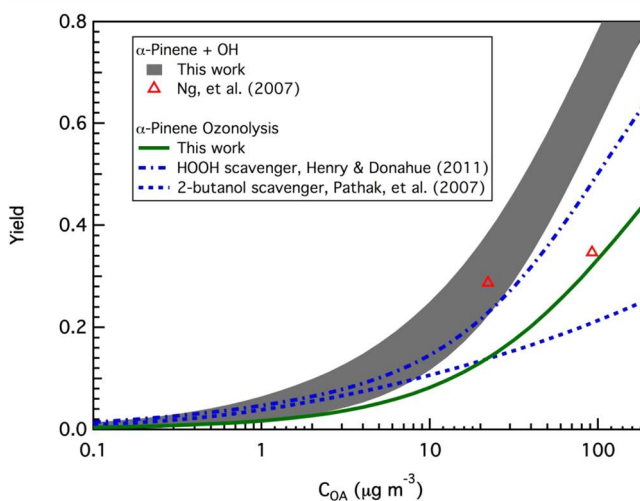


**Figure 3.** Yield Comparison. SOA mass yield curves from this work are compared to previous OH oxidation work as well as two ozonolysis cases with an OH scavenger. The OH oxidation case from this work is shown as the gray area to emphasize the range of the measured mass yields.

from this work along with several other previously published ozonolysis yield curves. The OH oxidation case is shown as a range (shaded gray area) because of the variability in those yields; our best-estimate parametrization falls in the middle of the range. The range is obtained by performing VBS fits of the highest and lowest yield points over the  $C_{\text{OA}}$  range. The parameters in Table 3 are the VBS fit from all of the OH oxidation data and thus represent the average mass yields. We shall focus on the saturation concentration ( $C^*$ ) range constrained by the data ( $C_{\text{OA}} < 100 \mu\text{g m}^{-3}$ ); therefore we

Table 3. Volatility Basis Set Parameters

Saturation Concentration ( $\mu\text{g m}^{-3}$ )	0.1	1	10	100	1000
Ozonolysis, no scavenger	0.0044	0.0063	0.051	0.46	0.51
OH oxidation	0.0001	0.0033	0.16	0.89	0.25

only consider values up to the  $C^* = 1000$  bin (Table 3 for suggested parameters).

Both ozonolysis and OH oxidation of  $\alpha$ -pinene form similar products, (e.g., pinonic acid, pinic acid, and pinonaldehyde),<sup>25,42</sup> so it is not surprising that the SOA mass yields for ozonolysis and OH reactions are similar at low  $C_{\text{OA}}$ . Previous work parametrizing SOA yields from the OH reaction with values from ozonolysis was thus satisfactory from an OA mass standpoint, as atmospherically relevant  $C_{\text{OA}}$  concentrations lie where these yield curves coincide. However, even at  $C_{\text{OA}} = 10 \mu\text{g m}^{-3}$  the mass yields begin to diverge from one another, which in turn means the distributions of vapor-phase products have diverged as well. This is an important distinction for aging these different product sets. Because the yields differ even at modest OA concentrations we must treat them with separate parametrizations. In this way the vapors will be in the proper volatility bins for further chemistry in CTMs.

The most profound conclusion evident in Figure 3 is that the OH SOA mass yields are higher than any of the ozonolysis cases. This is somewhat surprising as ozonolysis was viewed as the main SOA formation pathway for monoterpenes.<sup>18</sup> Because the SOA yields for  $\alpha$ -pinene ozonolysis are lower than those from OH oxidation in general, it is likely that the ozone formation during OH oxidation actually suppressed the SOA yields reported here somewhat. It is possible that some of the variability in yields was due to variability in ozone formation. This could also explain the discrepancy between this work and the OH oxidation work of Ng, et al., which is also shown in Figure 3.<sup>21</sup> Experimental conditions were similar for Ng et al. and this work, including evidence of ozone production (although the magnitude of ozone formation is not known), however, other unmeasured variables, like the radical species concentrations, could also contribute to the differences and variability in the OH oxidation yields. Instrument uncertainty can account for  $\sim 10\%$  error in these measurements. It is unlikely that the wall-loss correction is contributing much to the total error as few particles are on the walls after only 1 h of chemistry.

The radical balance is one reason for the differences in the various ozonolysis yields also shown in Figure 3. We have previously shown that an OH radical scavenger affects the  $\text{HO}_2/\text{RO}_2$  ratio in the chamber, affecting the ozonolysis yield.<sup>20</sup> With the higher  $\text{HO}_2/\text{RO}_2$  in the HOOH scavenger case, the yields are higher than observed with the more common 2-butanol scavenger. In the no-scavenger case presented here, a combination of effects influence the mass yields: the different  $\text{HO}_2/\text{RO}_2$  ratio and the OH reactions occurring (which subsequently change the radical concentrations). Chamber reactions often have artificially high  $\text{RO}_2$  concentrations because of high precursor concentrations.<sup>43</sup> This would likely suppress the ozonolysis yields reported here because we do not have an additional  $\text{HO}_2$  source. However, up to 50% of the  $\alpha$ -pinene reacts with OH and not ozone. As we have shown that OH oxidation can produce more SOA than ozonolysis, we expect that to counterbalance the effect of potentially large  $\text{RO}_2$  concentrations. In Figure 3, we can observe these effects. At low

$C_{\text{OA}}$  all the yields only differ by a few percent. Because we are not measuring the product vapors, we would not know the product distributions (OH oxidation versus ozonolysis without a scavenger) are different by only examining the low  $C_{\text{OA}}$  results. However, as we get to  $C_{\text{OA}}$  above  $10 \mu\text{g m}^{-3}$  we see the scavenger-free ozonolysis yields get closer to the HOOH scavenger case (which we view as an upper bound for the isolated ozonolysis system). This again exposes the need for a wide range of  $C_{\text{OA}}$  measurements because we can only constrain the vapors that are in volatility bins near the  $C_{\text{OA}}$  we have measured.

**3.4. Extension to the Atmosphere and Aging Chemistry.** In some experimental situations (mainly ozonolysis reactions), the first-generation SOA yields are easily isolated. For example,  $\alpha$ -pinene, having one endocyclic double bond, reacts with ozone; ozone destroys the double bond and then cannot react further. SOA is formed, and in a smog chamber the system comes to equilibrium. We can therefore clearly distinguish the SOA formation coming from that first generation of chemistry. In many other experiments, most notably in OH oxidation reactions, the line between different generations of chemistry is blurry. As first-generation gas-phase products rise in concentration (and precursor VOC concentrations become very small), OH is likely to react with these products instead of the precursor. Yield parametrization in these systems can be complicated because it is difficult to determine when aging chemistry begins to play a role in SOA formation. Furthermore, the traditional thermodynamic fits such as the VBS fit described above or the "Odum 2-product model"<sup>44</sup> rely on an implicit assumption that the overall product distribution in a chamber experiment remains unchanged as more precursor is consumed, and that increasing SOA mass is caused only by thermodynamics forcing progressively more product into the condensed phase with increasing concentrations.

As yields are currently parametrized in CTMs, we must try to isolate the first generation chemistry as much as possible for the initial formation of SOA. However, we want to explore aging chemistry because the many processes within aging will bring us to a better understanding of OA transformations through a particle's lifetime. Therefore we examined two systems here that can bridge the gap between first-generation yields and aging, while still isolating the first generation yields for CTM parametrization. As we parametrize these SOA yields we are also distributing the product vapors in the VBS.<sup>33</sup> The volatility of these vapors is very important as we proceed to model the aging chemistry, where gas-phase reactions will dominate the fate of the OA through equilibrium dynamics.<sup>7,41</sup> The results presented here help bridge the gap between first-generation chemistry and aging by giving us an accurate starting point for aging.

In addition, the conditions considered in this work are likely more relevant to the atmosphere (i.e., allowing OH reactions in the ozonolysis system,  $\text{HO}_2/\text{RO}_2$  concentrations). Previous  $\alpha$ -pinene SOA yield work has focused on isolating the ozonolysis system, which requires disrupting the radical balance in the chamber. This was done to parametrize the ozonolysis reaction as it is modeled separately in CTMs. This work examines an ozonolysis system more like the atmospheric conditions. Because  $\alpha$ -pinene reacts rapidly with OH, it will likely react with the OH formed through ozonolysis in the atmosphere. Finally, with typical OH concentrations of  $10^6$  molecules  $\text{cm}^{-3}$  we can expect even more  $\alpha$ -pinene + OH reactions. The results

presented here will allow the ozone and OH channels for SOA production from  $\alpha$ -pinene to be treated separately in model calculations, providing more accurate first-generation SOA and more accurate product volatility distributions for subsequent aging calculations.

## AUTHOR INFORMATION

### Corresponding Author

\*Tel: (412)-268-4415, fax: (412)-268-7139, e-mail: nmd@cmu.edu.

### Notes

The authors declare no competing financial interest.

## REFERENCES

- (1) Pope, C. A.; Ezzati, M.; Dockery, D. W. Fine-Particulate Air Pollution and Life Expectancy in the United States. *N. Engl. J. Med.* **2009**, *360* (4), 376–386.
- (2) IPCC, Climate Change 2007 – The Physical Science Basis. *Contribution of Working Group I to the Fourth Assessment Report of the IPCC*, 2007.
- (3) Zhang, Q.; Jimenez, J. L.; Canagaratna, M. R.; Allan, J. D.; Coe, H.; Ulbrich, I.; Alfarra, M. R.; Takami, A.; Middlebrook, A. M.; Sun, Y. L.; Dzepina, K.; Dunlea, E.; Docherty, K.; DeCarlo, P. F.; Salcedo, D.; Onasch, T.; Jayne, J. T.; Miyoshi, T.; Shimojo, A.; Hatakeyama, S.; Takegawa, N.; Kondo, Y.; Schneider, J.; Drewnick, F.; Borrmann, S.; Weimer, S.; Demerjian, K.; Williams, P.; Bower, K.; Bahreini, R.; Cottrell, L.; Griffin, R. J.; Rautiainen, J.; Sun, J. Y.; Zhang, Y. M.; Worsnop, D. R. Ubiquity and dominance of oxygenated species in organic aerosols in anthropogenically-influenced Northern Hemisphere midlatitudes. *Geophys. Res. Lett.* **2007**, *34* (13), 6.
- (4) Odum, J. R.; Hoffmann, T.; Bowman, F.; Collins, D.; Flagan, R. C.; Seinfeld, J. H. Gas/particle partitioning and secondary organic aerosol yields. *Environ. Sci. Technol.* **1996**, *30* (8), 2580–2585.
- (5) Donahue, N. M.; Robinson, A. L.; Pandis, S. N. Atmospheric organic particulate matter: From smoke to secondary organic aerosol. *Atmos. Environ.* **2009**, *43* (1), 94–106.
- (6) Lane, T. E.; Donahue, N. M.; Pandis, S. N. Simulating secondary organic aerosol formation using the volatility basis-set approach in a chemical transport model. *Atmos. Environ.* **2008**, *42* (32), 7439–7451.
- (7) Murphy, B. N.; Pandis, S. N. Simulating the formation of semivolatile primary and secondary organic aerosol in a regional chemical transport model. *Environ. Sci. Technol.* **2009**, *43* (13), 4722–4728.
- (8) Henry, K. M.; Donahue, N. M. Photochemical aging of  $\alpha$ -pinene secondary organic aerosol: effects of OH radical sources and photolysis. *J. Phys. Chem. A* **2012**, *116* (24), 5932–5940.
- (9) Kroll, J. H.; Smith, J. D.; Che, D. L.; Kessler, S. H.; Worsnop, D. R.; Wilson, K. R. Measurement of fragmentation and functionalization pathways in the heterogeneous oxidation of oxidized organic aerosol. *Phys. Chem. Chem. Phys.* **2009**, *11* (36), 8005–8014.
- (10) Smith, J. D.; Kroll, J. H.; Cappa, C. D.; Che, D. L.; Liu, C. L.; Ahmed, M.; Leone, S. R.; Worsnop, D. R.; Wilson, K. R. The heterogeneous reaction of hydroxyl radicals with sub-micron squalane particles: a model system for understanding the oxidative aging of ambient aerosols. *Atmos. Chem. Phys.* **2009**, *9* (9), 3209–3222.
- (11) Kalberer, M.; Sax, M.; Samburova, V. Molecular size evolution of oligomers in organic aerosols collected in urban atmospheres and generated in a smog chamber. *Environ. Sci. Technol.* **2006**, *40* (19), 5917–5922.
- (12) Guenther, A.; Hewitt, C. N.; Erickson, D.; Fall, R.; Geron, C.; Graedel, T.; Harley, P.; Klinger, L.; Lerdau, M.; McKay, W. A.; Pierce, T.; Scholes, B.; Steinbrecher, R.; Tallamraju, R.; Taylor, J.; Zimmerman, P. A global-model of natural volatile organic-compound emissions. *J. Geophys. Res., [Atmos.]* **1995**, *100* (D5), 8873–8892.
- (13) Shilling, J. E.; Chen, Q.; King, S. M.; Rosenoern, T.; Kroll, J. H.; Worsnop, D. R.; DeCarlo, P. F.; Aiken, A. C.; Sueper, D.; Jimenez, J. L.; Martin, S. T. Loading-dependent elemental composition of alpha-pinene SOA particles. *Atmos. Chem. Phys.* **2009**, *9* (3), 771–782.
- (14) Zhang, D.; Zhang, R. Ozonolysis of alpha-pinene and beta-pinene: Kinetics and mechanism. *J. Chem. Phys.* **2005**, *122* (11), 12.
- (15) Pathak, R. K.; Stanier, C. O.; Donahue, N. M.; Pandis, S. N. Ozonolysis of alpha-pinene at atmospherically relevant concentrations: Temperature dependence of aerosol mass fractions (yields). *J. Geophys. Res., [Atmos.]* **2007**, *112*, (D3).
- (16) Presto, A. A.; Donahue, N. M. Investigation of alpha-pinene plus ozone secondary organic aerosol formation at low total aerosol mass. *Environ. Sci. Technol.* **2006**, *40* (11), 3536–3543.
- (17) Presto, A. A.; Hartz, K. E. H.; Donahue, N. M. Secondary organic aerosol production from terpene ozonolysis. 2. Effect of NO<sub>x</sub> concentration. *Environ. Sci. Technol.* **2005**, *39* (18), 7046–7054.
- (18) Griffin, R. J.; Cocker, D. R.; Flagan, R. C.; Seinfeld, J. H. Organic aerosol formation from the oxidation of biogenic hydrocarbons. *J. Geophys. Res., [Atmos.]* **1999**, *104* (D3), 3555–3567.
- (19) Presto, A. A.; Donahue, N. M. Ozonolysis fragment quenching by nitrate formation: The pressure dependence of prompt OH radical formation. *J. Phys. Chem. A* **2004**, *108* (42), 9096–9104.
- (20) Henry, K. M.; Donahue, N. M. Effect of the OH radical scavenger hydrogen peroxide on secondary organic aerosol formation from alpha-pinene ozonolysis. *Aerosol Sci. Technol.* **2011**, *45* (6), 696–700.
- (21) Ng, N. L.; Chhabra, P. S.; Chan, A. W. H.; Surratt, J. D.; Kroll, J. H.; Kwan, A. J.; McCabe, D. C.; Wennberg, P. O.; Sorooshian, A.; Murphy, S. M.; Dalleska, N. F.; Flagan, R. C.; Seinfeld, J. H. Effect of NO<sub>x</sub> level on secondary organic aerosol (SOA) formation from the photooxidation of terpenes. *Atmos. Chem. Phys.* **2007**, *7* (19), 5159–5174.
- (22) Bonn, B.; Moortgat, G. K. New particle formation during alpha- and beta-pinene oxidation by O<sup>-3</sup>, OH and NO<sub>3</sub>, and the influence of water vapour: Particle size distribution studies. *Atmos. Chem. Phys.* **2002**, *2*, 183–196.
- (23) Noziere, B.; Barnes, I.; Becker, K. H. Product study and mechanisms of the reactions of alpha-pinene and of pinonaldehyde with OH radicals. *J. Geophys. Res., [Atmos.]* **1999**, *104* (D19), 23645–23656.
- (24) Capouet, M.; Peeters, J.; Noziere, B.; Muller, J. F. Alpha-pinene oxidation by OH: simulations of laboratory experiments. *Atmos. Chem. Phys.* **2004**, *4*, 2285–2311.
- (25) Librandi, V.; Tringali, G. Atmospheric fate of OH initiated oxidation of terpenes. Reaction mechanism of alpha-pinene degradation and secondary organic aerosol formation. *J. Environ. Manage.* **2005**, *75* (3), 275–282.
- (26) Eddingsass, N. C.; Loza, C. L.; Yee, L. D.; Chan, M.; Schilling, K. A.; Chhabra, P. S.; Seinfeld, J. H.; Wennberg, P. O.  $\alpha$ -Pinene photooxidation under controlled chemical conditions - Part 2: SOA yield and composition in low- and high-NO<sub>x</sub> environments. *Atmos. Chem. Phys.* **2012**, *12* (16), 7413–7427.
- (27) Salo, K.; Hallquist, M.; Jonsson, A. M.; Saathoff, H.; Naumann, K.-H.; Spindler, C.; Tillmann, R.; Fuchs, H.; Bohn, B.; Rubach, F.; Mentel, T. F.; Muller, L.; Reinnig, M.; Hoffmann, T.; Donahue, N. M. Volatility of secondary organic aerosol during OH radical induced ageing. *Atmos. Chem. Phys.* **2011**, *11* (21), 11055–11067.
- (28) Muller, L.; Reinnig, M. C.; Naumann, K.-H.; Saathoff, H.; Mentel, T. F.; Donahue, N. M.; Hoffmann, T. Formation of 3-methyl-1,2,3-butanetricarboxylic acid via gas phase oxidation of pinonic acid – a mass spectrometric study of SOA aging. *Atmos. Chem. Phys. Discuss.* **2011**, *11* (7), 19443–19476.
- (29) Frosch, M.; Bilde, M.; DeCarlo, P. F.; Juranyi, Z.; Tritscher, T.; Dommen, J.; Donahue, N. M.; Gysel, M.; Weingartner, E.; Baltensperger, U. Relating cloud condensation nuclei activity and oxidation level of alpha-pinene secondary organic aerosols. *J. Geophys. Res., [Atmos.]* **2011**, *116*.
- (30) Tritscher, T.; Dommen, J.; DeCarlo, P. F.; Barmet, P. B.; Praplan, A. P.; Weingartner, E.; Gysel, M.; Prevot, A. S. H.; Riipinen, I.; Donahue, N. M.; Baltensperger, U. Volatility and hygroscopicity of

aging secondary organic aerosol in a smog chamber. *Atmos. Chem. Phys.* **2011**, *11* (22), 11477–11496.

(31) de Gouw, J.; Warneke, C.; Karl, T.; Eerdekens, G.; van der Veen, C.; Fall, R. Sensitivity and specificity of atmospheric trace gas detection by proton-transfer-reaction mass spectrometry. *Int. J. Mass Spectrom.* **2003**, *223* (1–3), 365–382.

(32) Hildebrandt, L.; Henry, K. M.; Kroll, J. H.; Worsnop, D. R.; Pandis, S. N.; Donahue, N. M. Evaluating the mixing of organic aerosol components using high-resolution aerosol mass spectrometry. *Environ. Sci. Technol.* **2011**, *45* (15), 6329–6335.

(33) Donahue, N. M.; Robinson, A. L.; Stanier, C. O.; Pandis, S. N. Coupled partitioning, dilution, and chemical aging of semivolatile organics. *Environ. Sci. Technol.* **2006**, *40* (8), 2635–2643.

(34) Stanier, C. O.; Donahue, N. M.; Pandis, S. N. Parameterization of secondary organic aerosol mass fractions from smog chamber data. *Atmos. Environ.* **2008**, *42*, 2276–2299.

(35) Pierce, J. R.; Engelhart, G. J.; Hildebrandt, L.; Weitkamp, E. A.; Pathak, R. K.; Donahue, N. M.; Robinson, A. L.; Adams, P. J.; Pandis, S. N. Constraining particle evolution from wall losses, coagulation, and condensation-evaporation in smog-chamber experiments: Optimal estimation based on size distribution measurements. *Aerosol Sci. Technol.* **2008**, *42* (12), 1001–1015.

(36) Matsunaga, A.; Ziemann, P. J. Gas-wall partitioning of organic compounds in a teflon film chamber and potential effects on reaction product and aerosol yield measurements. *Aerosol Sci. Technol.* **2010**, *44* (10), 881–892.

(37) Hildebrandt, L.; Donahue, N. M.; Pandis, S. N. High formation of secondary organic aerosol from the photo-oxidation of toluene. *Atmos. Chem. Phys.* **2009**, *9* (9), 2973–2986.

(38) Weitkamp, E. A.; Sage, A. M.; Pierce, J. R.; Donahue, N. M.; Robinson, A. L. Organic aerosol formation from photochemical oxidation of diesel exhaust in a smog chamber. *Environ. Sci. Technol.* **2007**, *41* (20), 6969–6975.

(39) Donahue, N. M.; Kroll, J. H.; Anderson, J. G.; Demerjian, K. L. Direct observation of OH production from the ozonolysis of olefins. *Geophys. Res. Lett.* **1998**, *25* (1), 59–62.

(40) Atkinson, R.; Aschmann, S. M.; Arey, J.; Shorees, B. Formation of OH radicals in the gas-phase reactions of O<sub>3</sub> with a series of terpenes. *J. Geophys. Res., [Atmos.]* **1992**, *97* (D5), 6065–6073.

(41) Donahue, N. M.; Henry, K. M.; Mentel, T. F.; Kiendler-Scharr, A.; Spindler, C.; Bohn, B.; Brauers, T.; Dorn, H. P.; Fuchs, H.; Tillmann, R.; Wahner, A.; Saathoff, H.; Naumann, K.-H.; Mohler, O.; Leisner, T.; Müller, L.; Hoffmann, T.; Salo, K.; Hallquist, M.; Frosch, M.; Bilde, M.; Tritscher, T.; Barmet, P.; Praplan, A. P.; DeCarlo, P. F.; Dommen, J.; Prevot, A. S. H.; Baltensperger, U. Aging of biogenic secondary organic aerosol via gas-phase OH radical reactions. *Proc. Natl. Acad. Sci. U.S.A.* **2012**, *109* (34), 13503–13508.

(42) Hatakeyama, S.; Izumi, K.; Fukuyama, T.; Akimoto, H. Reactions of ozone with  $\alpha$ -pinene and  $\beta$ -pinene in air: yields of gaseous and particulate products. *J. Geophys. Res., [Atmos.]* **1989**, *94* (10), 13013–13024.

(43) Kroll, J. H.; Seinfeld, J. H. Chemistry of secondary organic aerosol: Formation and evolution of low-volatility organics in the atmosphere. *Atmos. Environ.* **2008**, *42* (16), 3593–3624.



# Absorptivity of brown carbon in fresh and photo-chemically aged biomass-burning emissions

R. Saleh<sup>1</sup>, C. J. Hennigan<sup>2</sup>, G. R. McMeeking<sup>3</sup>, W. K. Chuang<sup>1</sup>, E. S. Robinson<sup>1</sup>, H. Coe<sup>4</sup>, N. M. Donahue<sup>1</sup>, and A. L. Robinson<sup>1</sup>

<sup>1</sup>Center for Atmospheric Particle Studies, Carnegie Mellon University, Pittsburgh PA, USA

<sup>2</sup>Chemical, Biochemical, and Environmental Engineering, University of Maryland Baltimore County, Baltimore MD, USA

<sup>3</sup>Droplet Measurement Technologies, Boulder CO, USA

<sup>4</sup>Centre for Atmospheric Science, University of Manchester, Manchester, UK

Correspondence to: A. L. Robinson (alr@andrew.cmu.edu)

Received: 23 April 2013 – Published in Atmos. Chem. Phys. Discuss.: 2 May 2013

Revised: 2 July 2013 – Accepted: 3 July 2013 – Published: 9 August 2013

**Abstract.** Experiments were conducted to investigate light absorption of organic aerosol (OA) in fresh and photo-chemically aged biomass-burning emissions. The experiments considered residential hardwood fuel (oak) and fuels commonly consumed in wild-land and prescribed fires in the United States (pocosin pine and gallberry). Photo-chemical aging was performed in an environmental chamber. We constrained the effective light-absorption properties of the OA using conservative limiting assumptions, and found that both primary organic aerosol (POA) in the fresh emissions and secondary organic aerosol (SOA) produced by photo-chemical aging contain brown carbon, and absorb light to a significant extent. This work presents the first direct evidence that SOA produced in aged biomass-burning emissions is absorptive. For the investigated fuels, SOA is less absorptive than POA in the long visible, but exhibits stronger wavelength-dependence and is more absorptive in the short visible and near-UV. Light absorption by SOA in biomass-burning emissions might be an important contributor to the global radiative forcing budget.

emissions (e.g. Kirchstetter et al., 2004; Sandradewi et al., 2008; Habib et al., 2008; Lewis et al., 2008; Yang et al., 2009; Chen and Bond, 2010; Hecobian et al., 2010), which constitute three quarters of the total primary organic aerosol (POA) globally (Bond et al., 2004). Furthermore, biomass-burning emissions are photo-oxidized in the atmosphere, producing secondary organic aerosol (SOA) at concentrations similar to POA (Lee et al., 2008; Yokelson et al., 2009; Hennigan et al., 2011); to our knowledge, the light-absorption properties of this biomass-burning SOA have not yet been directly investigated.

Absorptivity of particulate matter (PM) is often quantified at a certain wavelength via a mass absorption cross-section (MAC,  $\text{m}^2 \text{g}^{-1}$ ), with its wavelength dependence given by an Absorption Ångström Exponent (AAE) ( $\text{MAC} \sim \lambda^{-\text{AAE}}$ ). Although convenient, these parameters are not fundamental. They depend on the particle size (Bond et al., 2006; Moosmüller et al., 2011), and when used to quantify absorptivity of BC mixed with OA, they represent mass weighted averages of the OA and BC. Thus, MAC and AAE measured for certain emissions cannot be generally applied to aerosols with different size distributions and OA-to-BC ratios.

With recent developments in the ability of global and regional transport models to track PM composition and size (e.g. Chen et al., 2010; Murphy and Pandis, 2010), light absorption can be calculated using Mie-theory if the complex refractive index ( $m = n - ik$ ) of the different PM components is known, assuming that the particles are spherical and homogeneous. While  $m$  of BC and  $n$  of OA and inorganics have

## 1 Introduction

Climate forcing calculations typically treat black carbon (BC) and dust as the only atmospheric particulate light absorbers. However, some organic aerosols (OA), referred to as brown carbon (BrC) (Andreae and Gelencsér, 2006), are also significant light absorbers. BrC occurs in biomass-burning

been extensively studied (e.g. Bond et al., 2006; Bond and Bergstrom, 2005; Hand and Kreidenweis, 2002; Levin et al., 2010), data on  $k$  values of atmospheric OA ( $k_{\text{OA}}$ ) are scarce.

Several methods have been employed to determine  $k_{\text{OA}}$ . One technique involves extracting OA in a solvent and measuring bulk absorption of the extracts (Kirchstetter et al., 2004; Chen and Bond, 2010; Hoffer et al., 2006), with different solvents yielding different  $k_{\text{OA}}$  values because they extract different fractions of the OA (Chen and Bond, 2010). Alexander et al. (2008) used Transmission Electron Microscopy (TEM) to determine the dielectric function, from which refractive indices of individual particles were calculated. While this method has the advantage of probing individual particles rather than an ensemble, it cannot isolate the optical properties of OA if it is internally mixed with BC, as is often the case for biomass-burning PM and aged atmospheric aerosols. A third method employs Mie-theory to obtain optical closure on light absorption and scattering measurements and retrieve refractive indices of the PM (Chakrabarty et al., 2010; Lack et al., 2012). Chakrabarty et al. (2010) applied this method to determine refractive indices of PM in duff-burning emissions. Due to the smoldering burning conditions, the emissions were dominated by OA and contained negligible amounts of BC.

The retrieval of OA optical properties via optical closure becomes more complicated if the OA is internally-mixed with BC. OA, which can form a coating over BC particles, both absorbs and refracts light into the BC core, enhancing its absorption. Light absorption by such particles depends on core size as well as coating thickness, in addition to the refractive indices; thus, detailed optical modeling is required. If the particles are assumed to be spherical, and exhibit core-shell morphology with a homogenous shell, a core-shell Mie-theory model can be employed (Lack et al., 2012). Although the recent study by Cappa et al. (2012) proposed that core-shell morphology is unlikely for aged urban aerosol, BC in biomass-burning emissions is most likely coated by OA. Upon combustion, BC particles form initially at high temperatures, and act as condensation sites for OA. Lack et al. (2012) reported that core-shell morphology was required to explain absorption by particles in biomass-burning plumes over Colorado.

Here, we use optical closure to determine the imaginary part of the refractive indices of OA in fresh and photo-chemically aged biomass-burning emissions. We perform optical closure for two cases. In the first case, OA and BC are assumed to be externally-mixed. In the second case, BC is assumed to be internally-mixed with OA, exhibiting core-shell morphology. While real particle morphologies are almost certainly more complex, these two cases provide conservative limits to the recovered optical properties of the OA. The derived imaginary part of the refractive indices can be used in chemical transport models employing Mie-theory to predict light absorption for different atmospheric conditions.

## 2 Methods

### 2.1 Experimental

Experiments were conducted at Carnegie Mellon University (CMU) and at the US Fire Science Laboratory as part of the Fire Lab at Missoula Experiment campaign (FLAME 3). The CMU experiments featured emissions from wood-burning (oak) in a residential stove, and the FLAME experiments examined small-scale open burns of fuels consumed by wildland and prescribed fires in the US (gallberry, and pocosin pine). In both cases, emissions were diluted and injected into a smog chamber, and then exposed to UV lights to initiate photo-oxidation, generating SOA. Details of the basic experimental set up and procedure are in Hennigan et al. (2010, 2011). For the fresh primary emissions, the analysis was performed on measurements half an hour immediately before turning on the UV lights. For the photo-chemically aged condition, the measurements were taken after one hour of exposure to the UV lights. Although the amount of aging (exposure to UV lights) in the experiments was relatively modest, appreciable amounts of SOA were generated. For gallberry, we present data for the fresh emissions only, because we could not obtain reliable light absorption measurements of the aged emissions due to low particle concentrations.

Aerosol size distributions were measured using a scanning mobility particle sizer (SMPS, TSI). The size distribution of BC was measured using a Single Particle Soot Photometer (SP2, DMT). To calibrate the SP2 incandescence signal, a suspension of aquadag in water was atomized and dried. Monodisperse aquadag particles were then size selected using a differential mobility analyser (DMA). The particle mobility was converted to mass assuming spherical particles and a density of  $1 \text{ g cm}^{-3}$ . The BC mass distributions measured using the SP2 were converted to number distributions assuming spherical particles and a density of  $1.8 \text{ g cm}^{-3}$ .

Mass concentration of non-refractory material was measured using a High Resolution Aerosol Mass Spectrometer (HR-AMS, Aerodyne) and Quadrupole AMS (Q-AMS, Aerodyne) in CMU and FLAME experiments, respectively. For all experiments, non-refractory aerosol mass was dominated by organics ( $> 95\%$ ) as shown in Fig. S1. A 7-wavelength Aethalometer (Magee Scientific, model AE-31) was used to obtain the wavelength-dependence of the absorption coefficients, with data points at wavelengths ( $\lambda$ ) of 370, 470, 520, 590, 660, 880, and 950 nm.

### 2.2 Optical closure

#### 2.2.1 Approach

The imaginary part of the refractive index of OA ( $k_{\text{OA}}$ ) was obtained using combined model calculations and light absorption measurements, as well as measurements of total and BC size distributions.

Model calculations of absorption coefficients ( $b_{\text{abs,model}}$ ) were performed using a size-resolved core-shell Mie-theory model based on the formulation of Bohren and Huffmann (1983) for coated spheres. We extended the computer code for light absorption cross-sections of a single spherical particle by Mätzler (2002) to calculate absorption coefficients of a polydisperse particle distribution, and to account for coating using Eq. (8.2) in Bohren and Huffmann (1983).

Inputs to the Mie-theory model are: (1) BC and OA size distributions, which were determined from SP2 and SMPS measurements as described in section 2.2.3; 2) BC refractive index,  $m_{\text{BC}} = 1.85 - 0.71i$  (Bond and Bergstrom, 2005); and 3) OA real part of the refractive index,  $n_{\text{OA}} = 1.55$  (Bond et al., 2006; Lack and Cappa, 2010; Hand and Kreidenweis, 2002). The shape of the absorption coefficient curve, i.e. the wavelength dependence of  $b_{\text{abs,model}}$  was constrained using Aethalometer measurements as described in Sect. 2.2.2. We assume that  $k_{\text{OA}}$  has a power-law wavelength dependence (Lack and Cappa, 2010; Sun et al., 2007), and express it as  $k_{\text{OA},550} (550/\lambda)^w$ , where  $k_{\text{OA},550}$  is the imaginary part of the refractive index at  $\lambda = 550$  nm.  $k_{\text{OA},550}$  and  $w$  are the free parameters in the model.

The optimization procedure for determination of  $k_{\text{OA},550}$  and  $w$  involves the following steps: (1) BC and OA size distributions are determined from SP2 and SMPS measurements; (2) these size distributions are used in conjunction with Mie-theory to constrain the magnitude of the absorption coefficient; (3) the wavelength dependence of the absorption coefficient (or AAE) is inferred from Aethalometer measurements; (4) Mie-theory calculations are performed to find the best theoretical fit to the measurement-constrained absorption coefficients (determined from steps 2 and 3). These steps are described in details in Sects. 2.2.2 and 2.2.3.

$k_{\text{OA}}$  values of POA were determined from measurements of fresh emissions that were sampled into the smog chamber. To estimate  $k_{\text{OA}}$  of SOA, we assume that the aged OA is well-mixed and that its  $k_{\text{OA}}$  is a mass-weighted average of those of POA and SOA. The concentration of SOA in the aged OA was determined using the method of Hildebrandt et al. (2009) as described in Supplement (SI).

An implicit assumption in the Mie-theory analysis is that BC is spherical. This assumption is reasonable when BC acquires an organic coating since BC agglomerates are compacted upon coating (Bond et al., 2006; Cross et al., 2010; Zhang et al., 2008; Gyawali et al., 2009), and has been employed previously to model absorption of biomass-burning emissions (Lack et al., 2012).

Another implicit assumption is that the BrC size distribution in the emissions is similar to that of OA. This is justified because POA forms by rapid quenching of organic vapors in the cooling plume and subsequent condensation on available seed particles. There is no reason for BrC (or other OA components) to exhibit preferential condensation on certain particles because when the hot vapors are quenched, they are highly supersaturated and will condense on any surface avail-

able. Thus, we expect the POA composition to be fairly uniform among all particle sizes. SOA is also expected to be uniformly distributed among all particles. When SOA forms by oxidation of organic vapors, it condenses on all particles to maintain similar mass fraction (activity) in all particle sizes. Using AMS particle time of flight (pTOF) data, it has been shown that SOA composition is uniform among all particles sizes for both biomass-burning (Grieshop et al., 2009) and diesel (Donahue et al., 2012) emissions.

### 2.2.2 Using Aethalometer measurements to constrain the wavelength dependence of the absorption coefficients

The wavelength-dependent absorption coefficient ( $b_{\text{abs}}$ ) can be determined from Aethalometer measurements as:

$$b_{\text{abs,AET}}(\lambda) = \text{MAC}_{\text{AET}} C_{\text{BC,AET}} \quad (1)$$

Where  $\text{MAC}_{\text{AET}} = 14625/\lambda$  ( $\text{m}^2 \text{g}^{-1}$ ) is the manufacturer's specified mass absorption cross-section, and  $C_{\text{BC,AET}}$  is the BC concentration reported by the instrument. The value of  $b_{\text{abs,AET}}$  requires corrections due to particle loading (Arnott et al., 2005; Kirchstetter and Novakov, 2007) and multiple scattering (Weingartner et al., 2003) as described in the SI.

There are concerns that artifacts associated with organic loading on the Aethalometer filter may bias  $b_{\text{abs,AET}}$  (Lack et al., 2008; Cappa et al., 2008). In particular, the organics can spread on the filter (Subramanian et al., 2007) and enhance scattering in the filter matrix (Lack et al., 2008; Cappa et al., 2008). This enhancement in scattering could be misinterpreted as absorption, and thus lead to overestimation in the magnitude of the absorption coefficients.

To avoid these potential biases, we do not use  $b_{\text{abs,AET}}$  to quantify the magnitude of the absorption coefficient, but only to determine its wavelength dependence (shape of the curve, or AAE):

$$b_{\text{abs,norm}}(\lambda) = \frac{b_{\text{abs,AET}}(\lambda)}{b_{\text{abs,AET}}(950 \text{ nm})} \quad (2)$$

The artifacts associated with OA loading do not have a significant effect on  $b_{\text{abs,norm}}$  (or AAE). Ajtai et al. (2011) compared AAE derived from Aethalometer measurements and a Photo-Acoustic Spectrometer ( $4\lambda$ -PAS). Measurements were performed in a suburban site near Budapest, Hungary during the winter, when the ambient PM was dominated by biomass-burning emissions. They found that  $\text{AAE}_{\text{Aethalometer}}$  and  $\text{AAE}_{4\lambda\text{-PAS}}$  were similar, with  $\text{AAE}_{\text{Aethalometer}}$  being consistently lower than  $\text{AAE}_{4\lambda\text{-PAS}}$  by 10%–15%.  $4\lambda$ -PAS measures the absorption coefficient of an ensemble of aerosol particles at 4 wavelengths (266, 355, 532, and 1064 nm) while suspended. Thus, the agreement between the two instruments indicates that  $b_{\text{abs,norm}}$  (or AAE) derived from aethalometer measurements is not altered due to collection on the filter.

To further evaluate any effect of artifacts due to OA filter loading on the wavelength dependence of  $b_{\text{abs,AET}}$ , we compared  $b_{\text{abs,norm}}$  immediately prior to and following filter-tape advance (Fig. S2). The Aethalometer collects PM on a spot on the filter tape for absorption measurements, and after a certain loading is attained, it advances to a new spot. The measurement made immediately prior to tape advance is the most susceptible to artifacts (has the highest accumulated OA mass loading) while the measurement made immediately following the advance is the least susceptible (has the lowest OA loading). As shown in Fig. S2, the AAE increased by around 10% immediately following the tape advance. This indicates that the OA loading had a small effect on the wavelength dependence of  $b_{\text{abs,AET}}$  in these experiments. Similar, but more pronounced effects were observed by Rizzo et al. (2011) who reported 40% decrease in AAE for biomass-burning emissions in the Amazon Basin due to OA loading.

The data used in the analysis were taken from measurements well before the end of the Aethalometer filter cycle, thus the bias in AAE is considerably less than 10%. Therefore, we ignore the decrease in AAE and assume that  $b_{\text{abs,norm}}$  is not affected by OA loading. We note that this assumption is conservative from the perspective of possible OA absorption, because it minimizes the contribution of OA to total absorption at short wavelengths, and thus minimizes  $k_{\text{OA}}$ .

### 2.2.3 Determination of $k_{\text{OA}}$

As described in the previous section, Aethalometer measurements were used to constrain the wavelength dependence of  $b_{\text{abs}}$ . The magnitude of  $b_{\text{abs}}$  was determined by assuming that OA absorbs negligibly at 950 nm (the longest wavelength of Aethalometer measurements) and using the Mie-theory model combined with PM size distributions obtained from SP2 and SMPS measurements (details can be found in Sect. 3.2) to calculate  $b_{\text{abs}}$  at 950 nm:

$$b_{\text{abs}} = b_{\text{abs,model}}(950 \text{ nm})b_{\text{abs,norm}} \quad (3)$$

The assumption that OA absorbs negligibly at the long visible wavelengths is justified based on numerous findings reported in the literature (e.g. Kirchstetter et al., 2004; Chen and Bond, 2010; Chakrabarty et al., 2010; Lack et al., 2012).

The value of  $b_{\text{abs,model}}(950 \text{ nm})$ , and thus the derived  $k_{\text{OA}}$ , depends on the mixing state of OA and BC (Lack and Cappa 2010; Lack et al., 2012). If BC and OA are externally mixed, OA will have no contribution to  $b_{\text{abs,model}}(950 \text{ nm})$ . However, if BC is coated with organics,  $b_{\text{abs,model}}(950 \text{ nm})$  will be enhanced due to light refraction by the organic shell, with the enhancement being a function of the shell thickness (Bond et al., 2006; Lack and Cappa, 2010; Schnaiter et al., 2005; Zhang et al., 2008). Since the true mixing state of the aerosol is not known, we performed the analysis for the two limiting cases illustrated in Fig. 1.

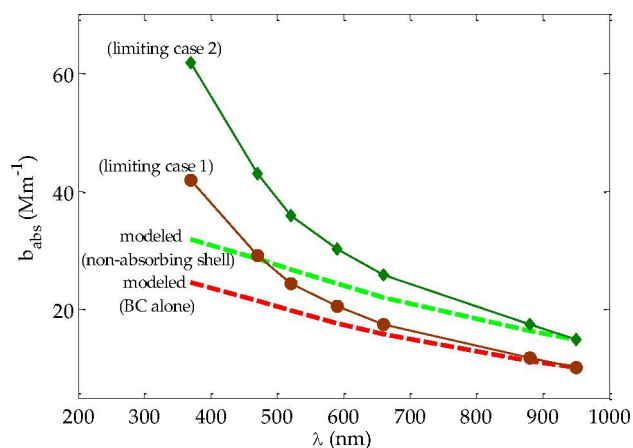


**Fig. 1.** The two limiting cases described in Sect. 2.2.3 to determine measurement-constrained absorption coefficients. Data (symbols) are from the fresh pocosin pine measurements.

In limiting case 1, BC and OA are assumed to be externally-mixed. The dashed red curve in Fig. 1 corresponds to  $b_{\text{abs,model}}$  of BC alone (assuming that OA does not contribute to absorption).  $b_{\text{abs,model}}(950 \text{ nm})$  is estimated using Mie-theory in conjunction with the BC size distribution measured using the SP2. Equations (2) and (3) are then combined to obtain the measurement-constrained  $b_{\text{abs}}$  (brown circles). The difference between the dashed red curve and the brown circles is the contribution of OA to absorption for this limiting case.

In limiting case 2, each BC particle is assumed to have acquired the maximum possible OA coating (see Sect. 3.2). The dashed green curve in Fig. 1 corresponds to  $b_{\text{abs,model}}$  of BC coated with non-absorbing OA, and the dark green diamonds are the measurement-constrained  $b_{\text{abs}}$ . For this limiting case,  $b_{\text{abs,model}}(950 \text{ nm})$  is estimated using core-shell Mie-theory calculations, where the size distribution of the BC cores is obtained using the SP2, and the organic coating thickness is obtained from combining SP2 and SMPS measurements as described in Sect. 3.2. The difference between the dashed green curve and the dark green diamonds is the contribution of OA to absorption.

As evident in Fig. 1, the contribution of OA to absorption in limiting case 2 is larger than limiting case 1. Any other mixing state (varying amount of coating) would yield an OA contribution to absorption within these two limits. Thus, limiting cases 1 and 2 provide a lower and upper bound of  $k_{\text{OA}}$ , respectively.

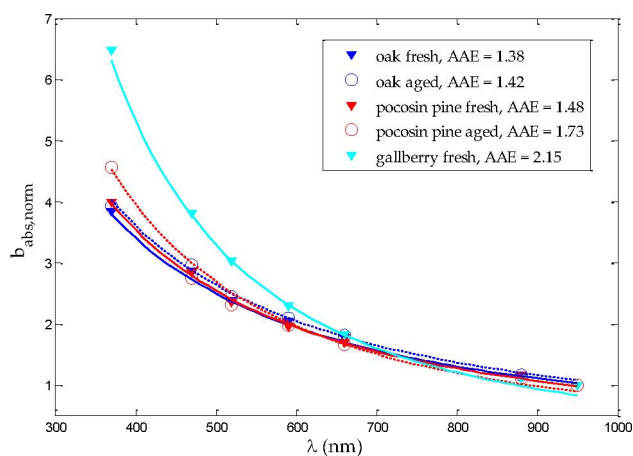


**Fig. 2.** Absorption coefficients of fresh and aged emissions measured using the Aethalometer normalized by absorption coefficient values at 950 nm. Solid lines are power-law fits with AAE values given in the legend.

### 3 Results

#### 3.1 Normalized absorption coefficients and Absorption Ångström Exponents

Figure 2 shows normalized absorption coefficients ( $b_{\text{abs, norm}}$ , Eq. 2) at 7 wavelengths between 370 and 950 nm measured using the Aethalometer for fresh and photo-chemically aged emissions. Also shown in Fig. 2 are power-law fits, from which AAE can be determined. AAE for the investigated fuels are 1.38 for fresh oak, 1.42 for aged oak, 1.48 for fresh pocosin pine, 1.73 for aged pocosin pine, and 2.15 for fresh gallberry. These values are consistent with previous findings reported in the literature for biomass-burning emissions (Sandradewi et al., 2008; Gyawali et al., 2009; Habib et al., 2008).

BC has been shown to have  $\text{AAE} \approx 1$  (Bergstrom et al., 2002; Schnaiter et al., 2005; Kirchstetter et al., 2004), and measured AAE values greater than 1 are interpreted as evidence of BrC (Kirchstetter et al., 2004; Sandradewi et al., 2008; Chen and Bond, 2010; Sun et al., 2007; Clarke et al., 2007; Hecobian et al., 2010; Zhang et al., 2011; Cheng et al., 2011). Thus, the AAE values obtained here indicate that both fresh and photo-chemically aged PM might contain BrC.

One limitation of the analysis presented in Fig. 2 is that AAE does not provide quantitative information on the absorptivity of OA, as it depends on the size distribution and the mixing state of BC and OA. For example, Gyawali et al. (2009) showed that non-absorbing shells over BC cores can lead to AAE greater or less than unity, as the absorption enhancement by lensing can have a direct or inverse wavelength-dependence. Consequently, relying solely on AAE might result in an underestimation or overestimation

of the absorptivity of OA. To obtain quantitative constraints on OA absorptivity, we performed optical closure analysis.

#### 3.2 BC and OA size distributions and mixing state

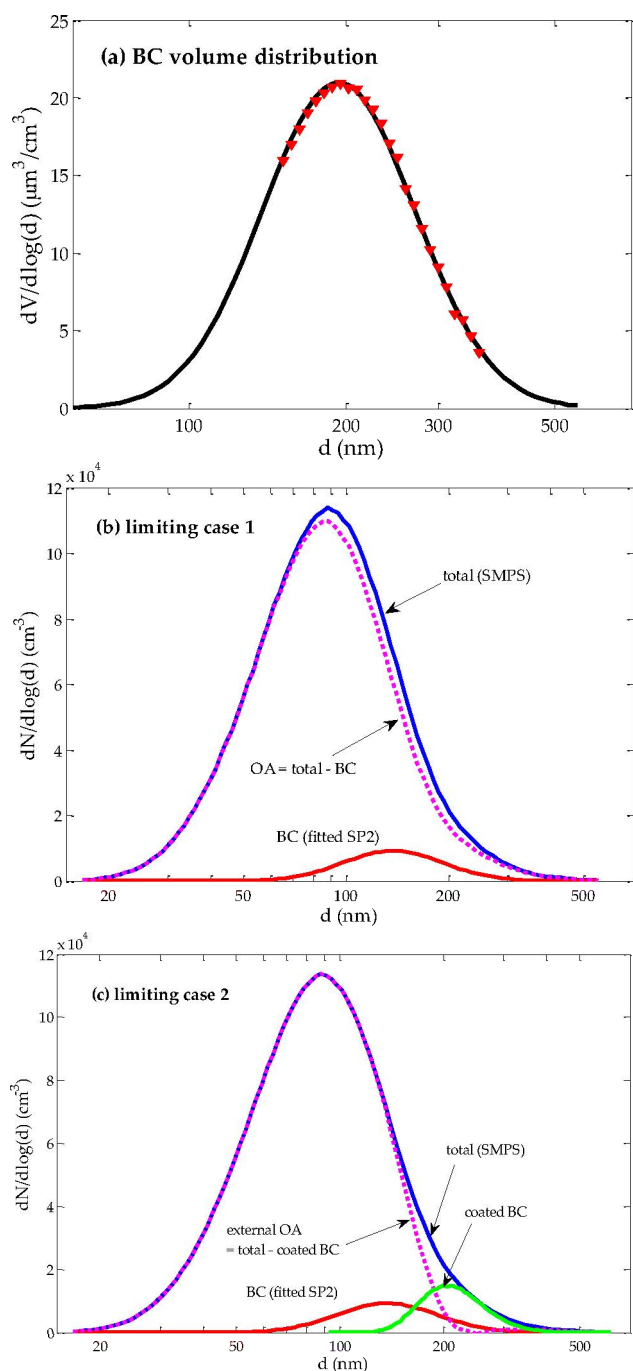
Optical closure using Mie-theory calculations requires the knowledge of BC and OA size distributions and their mixing state. The total (BC + OA) and BC size distributions were measured using an SMPS and SP2, respectively. Due to instrument limitations, reliable BC size distribution measurements were obtained for volume equivalent diameters in the range 150 nm–400 nm. As shown in Fig. 3a, we fit the BC volume distribution with a lognormal function to extend it to smaller and larger sizes. The SP2 captures the peak of the BC volume distribution (around 200 nm), and therefore provides a good constraint on the BC volume distribution if it is mono-modal.

Figure 3b shows the total size distribution measured by the SMPS and the BC size distribution derived from the SP2 measurements. Assuming that BC and OA are externally-mixed (limiting case 1), the OA number distribution can be estimated as the difference between the total and the BC number distributions. It is shown by the dotted magenta curve in Fig. 3b.

Limiting case 2 corresponds to BC being internally-mixed with OA, with BC particles acquiring maximum possible organic coating. To estimate the maximum coating as a function of BC particle size, we hypothesize that BC particles form initially upon combustion, and as the emissions temperature drops, organics start to condense on the BC seeds. Starting with the BC size distribution (derived from SP2 measurements) as the initial condition, we simulated the condensation kinetics assuming that the coated BC size distribution cannot grow beyond the total size distribution measured by the SMPS. The final coated BC size distribution (green curve in Fig. 3c) corresponds to the maximum possible coating. The difference between the total (measured by SMPS) and coated BC (simulated) size distributions corresponds to the externally-mixed OA particle size distribution. We note that the externally-mixed OA constituted 70 %–75 % of the total OA in our experiments by mass, which is in good agreement with the observation (83 %) reported by Lack et al. (2012) in biomass-burning plumes over Colorado.

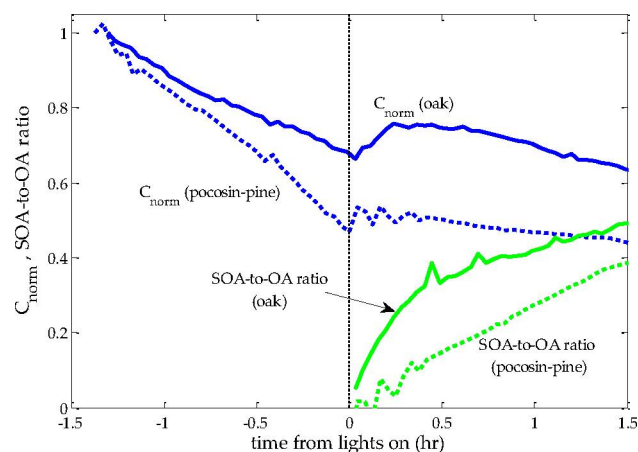
#### 3.3 SOA formation

Figure 4 shows time series of particle mass concentration derived from SMPS measurements and normalized by initial concentration ( $C_{\text{norm}}$ ) for the oak and pocosin-pine experiments.  $C_{\text{norm}}$  decays due to wall-loss in the smog chamber. Time  $t = 0$  indicates when the UV lights were turned on and thus the onset of photo-oxidation. The increase in aerosol concentration due to SOA formation is plainly evident in the “bump” immediately after photo-oxidation is initiated, which is eventually obscured by wall loss. Figure 4



**Fig. 3.** Measured size distributions from fresh oak experiment. **(a)** BC volume distribution inferred from SP2 measurements (red diamonds) and lognormal fit (solid black). **(b)** Total (SMPS), BC (fit to SP2 data), and OA (difference between total and BC) number distributions for limiting case 1 (external-mixing). **(c)** Total, externally-mixed OA, and internally-mixed (BC coated with OA) number distributions for limiting case 2.

also shows SOA-to-OA ratios estimated using the method of Hildebrandt et al. (2009) (see Supplement). In both experiments, significant amounts of SOA were generated, with



**Fig. 4.** Time series of OA concentrations normalized by initial concentrations, and SOA formation rate upon photo-oxidation.

end-of-experiment concentrations in the suspended aerosol similar to those of POA. We note that SOA-to-OA ratios calculated here constitute a lower bound, because in our analysis we assume that POA is conserved upon aging. However, as shown by Hennigan et al. (2011), a fraction of the POA likely evaporates as semi-volatile vapors are oxidized.

### 3.4 Absorptivity of OA

Measurement-constrained absorption coefficients estimated using Eq. (3) are shown in Fig. 5 (black diamonds) for the two limiting cases described in Sect. 2.2.3. Also shown are Mie-theory calculations for different assumptions on OA absorptivity and mixing state. The red curves correspond to OA being non-absorptive ( $k_{\text{OA}} = 0$ ) and externally mixed with BC, thus absorption is due to BC only. The green curves were obtained by assuming that OA is non-absorbing, but coats the BC and thus enhances its absorption. The cyan curves assume that only POA is absorptive in the aged aerosol ( $k_{\text{POA}}$  is obtained from fresh measurements). The blue curves correspond to calculations performed using the optimum value of  $k_{\text{OA}}$  to fit the measurement-constrained absorption coefficients.

For both limiting cases, absorption of BC alone (or BC coated with non-absorbing OA) cannot reproduce the shape of the measurement-constrained absorption coefficients of the fresh emissions. POA must contribute to absorption (i.e. contain BrC) for the model to fit the observations. Furthermore, if SOA in the aged aerosol is assumed to be non-absorbing, the model calculations fall below the measurements at short wavelengths, indicating that SOA is also absorptive. The derived  $k_{\text{OA}}$  values are given in Table 1, and plotted as a function of wavelength in Fig. 6.

Limiting case 2 (core-shell) yields  $k_{\text{OA}}$  values that are on average a factor 4–5 larger than limiting case 1 (external-mixing). Within each limiting case, there is a spread of a

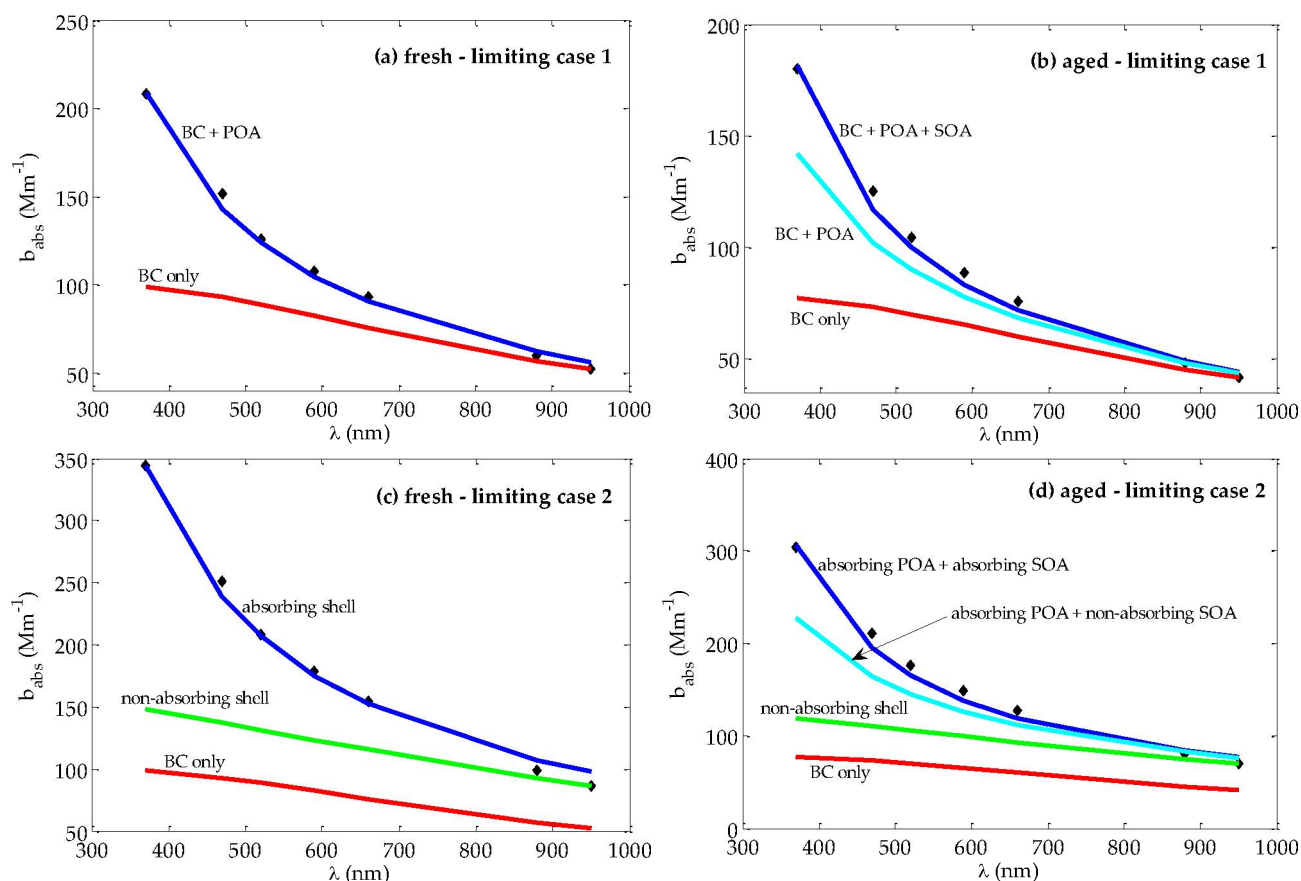


**Fig. 5.** Measurement-constrained absorption coefficients (black diamonds), and model calculations using different assumptions on OA absorptivity (solid lines) for **(a)** fresh oak emissions and assuming external-mixing (limiting case 1), **(b)** aged oak emissions and assuming external-mixing (limiting case 1), **(c)** fresh oak emissions and assuming core-shell morphology (limiting case 2), and **(d)** aged oak emissions and assuming core-shell morphology (limiting case 2). See Sect. 3.4 for description of calculations associated with each curve. The same data are plotted on a log-log scale in Fig. S4.

**Table 1.** Imaginary part of the refractive indices of the organics in the investigated fuels at 550 nm and their wavelength dependence ( $k_{\text{OA}} = k_{\text{OA},550}(550/\lambda)^w$ ). The uncertainty in  $k_{\text{OA}}$  values is approximately  $\pm 50\%$ .

Fuel		Limiting case 1 (external-mixing)		Limiting case 2 (core-shell)	
		$k_{\text{OA},550}$	$w$	$k_{\text{OA},550}$	$w$
Oak	POA	0.02	2.2	0.06	2.1
	SOA	0.014	3	0.05	3
Pocosin Pine	POA	0.015	2.9	0.04	3.2
	SOA	0.01	4	0.03	4.4
Galberry	POA	0.0055	2.4	0.022	2.6

factor of 3 across the three fuel samples investigated fuels. This spread might be due to difference in fuel types as well as burning conditions (Chen and Bond, 2010). This suggests that a more comprehensive dataset investigating a wide range of fuel types and burning conditions is required to constrain  $k_{\text{OA}}$  of biomass-burning emissions.

## 4 Discussion

### 4.1 Uncertainty in the derived $k_{\text{OA}}$ values

In this section, we discuss the potential uncertainty created by the assumptions employed in the optical closure analysis. The largest contributor to uncertainty in  $k_{\text{OA}}$  is mixing state. We explicitly addressed this uncertainty by considering

the two limiting cases described in Sect. 2.2.3. As shown in Fig. 6, limiting case 2 (core-shell) yields  $k_{\text{OA}}$  values that are on average a factor of 4–5 larger than limiting case 1 (external-mixing); both cases show significant absorption by both POA and SOA. We note that for the experiments in this study, where substantial amount of OA are generated (as in biomass-burning emissions in general), limiting case 2 (core-shell) is more likely to resemble the mixing state of BC. OA condenses onto the BC particles when the emissions are cooled, creating a core-shell morphology.

For each of the limiting cases, the assumption that OA absorbs negligibly at 950 nm yields a lower bound on the derived  $k_{\text{OA}}$  values. Finite OA absorptivity at shorter wavelengths is dictated by the shape of the absorption curve obtained from Aethalometer measurements. If, for instance, we assume that OA is non-absorbing at 550 nm (Lack et al., 2012), we would obtain nonphysical negative absorptivity at longer wavelengths, as illustrated in Fig. S3.

As described in Sect. 2.2.3, the magnitude of the measurement-constrained absorption coefficients is constrained by the magnitude of BC absorption at 950 nm, which is dictated by the BC size distribution determined from SP2 measurements. As shown in Sect. 3.2 and Fig. 2, we construct the BC size distributions assuming that they are lognormal, and that there are no other peaks of the volume distribution below the SP2 detection limit. If there were other peaks, our lognormal fits would lead to underestimation of BC concentration, and thus underestimation of BC absorption at 950 nm. This translates into lower bounds on the magnitude of the absorption coefficients, and consequently the derived  $k_{\text{OA}}$  values.

There is minimal uncertainty associated with the Aethalometer measurements since they were used to determine only the wavelength dependency, not the magnitude, of the absorption coefficients. As described in Sect. 2.2.2, measurement biases due to OA loading likely cause a decrease in relative absorption at short wavelengths (decrease in AAE), and can potentially lead to a slight underestimation of  $k_{\text{OA}}$  values.

Other contributors to uncertainty in  $k_{\text{OA}}$  are uncertainties in OA and BC concentrations due to uncertainties in SMPS and SP2 measurements. We consider 20% uncertainty in SMPS (Khlystov et al., 2004) and SP2 measurements. Other minor sources of uncertainty are the assumption on  $m_{\text{BC}}$ , which we assume to have the range (1.75–0.63i, 1.95–0.79i) reported by Bond and Bergstrom (2005), and  $n_{\text{OA}}$ , which we assume to range between 1.41 and 1.61 (Levin et al., 2010). Sensitivity calculations reveal that uncertainties in these parameters yield a maximum combined uncertainty of approximately  $\pm 50\%$  in the derived  $k_{\text{OA}}$  values.

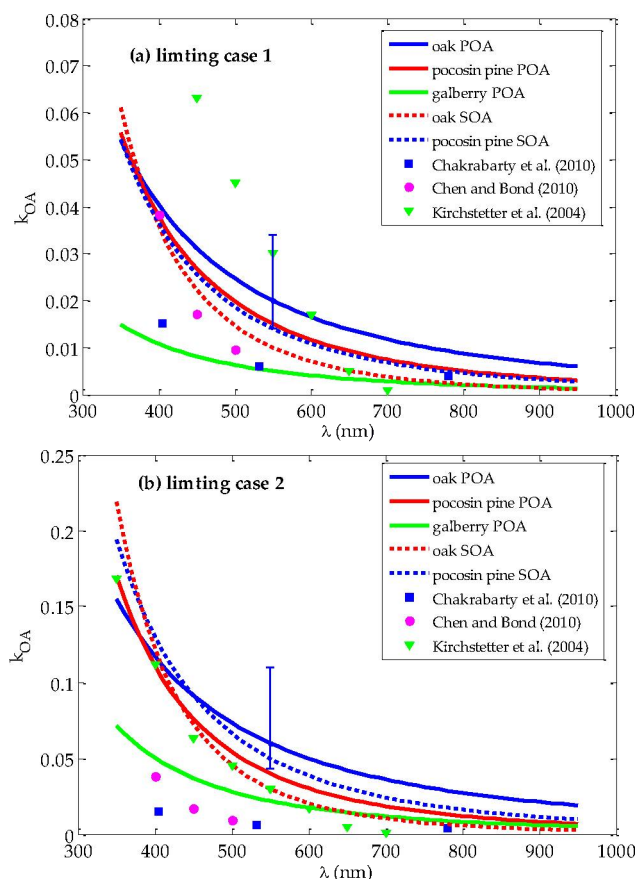


**Fig. 6.** Estimated imaginary part of the refractive indices of POA and SOA for the fuels investigated in this study for (a) limiting case 1 (external-mixing assumption) and (b) limiting case 2 (core-shell assumption). The blue error-bars represent the uncertainty in  $k_{\text{OA}}$  of oak POA at  $\lambda = 550$  nm; other fuels exhibit similar relative uncertainties. Also shown here are  $k_{\text{OA}}$  values of biomass-burning emissions reported by previous studies (see Sect. 4.2 for details).

#### 4.2 Comparison with previous studies

Figure 6 compares our findings with  $k_{\text{OA}}$  of biomass-burning emissions reported in the literature. Chen and Bond (2010) measured the absorptivity of oak pyrolysis emissions extracted in methanol. Chakrabarty et al. (2010) determined  $k_{\text{OA}}$  of BrC in “tar balls” from smoldering duff burning using online absorption and scattering measurements coupled with Mie-theory optical closure. Kirchstetter et al. (2004) estimated  $k_{\text{OA}}$  of emissions from savanna fires and wood burning based on the difference in absorption of samples before and after treatment with acetone.

Our derived  $k_{\text{OA}}$  for limiting case 1 (external-mixing) are bounded by the  $k_{\text{OA}}$  values of Chakrabarty et al. (2010) and Kirchstetter et al. (2004). For limiting case 2 (core-shell), our  $k_{\text{OA}}$  values are larger than the values of Chakrabarty et al. (2010) and Chen and Bond (2010), but are in good agreement with Kirchstetter et al. (2004) at short wavelengths. We

note that the work of Chakrabarty et al. (2010) and Chen and Bond (2010) investigated emissions of low-temperature combustion and pyrolysis which produced only OA (no BC). This form of combustion might produce OA with substantially lower absorptivity than high-temperature combustion (which produces both OA and BC) investigated in this study. On the other hand, the burning conditions in Kirchstetter et al. (2004) were similar to those in our study, which may explain the closer agreement in  $k_{\text{OA}}$ .

### 4.3 Absorption by biomass-burning SOA

It has been shown that SOA from biogenic and anthropogenic precursors absorbs light (Hecobian et al., 2010; Zhang et al., 2011; Cheng et al., 2011; Nakayama et al., 2010; Zhong and Jang 2011; Lambe et al., 2013). However, to our knowledge, this work presents the first direct evidence that SOA formed by photo-oxidation of biomass-burning emissions is light-absorbing. While other studies (e.g. Kirchstetter et al., 2004; Alexander et al., 2008; Lack et al., 2012) have investigated aged biomass-burning emissions in the atmosphere, which potentially contain SOA, the absorptivity of the SOA portion has not been constrained. For both oak and pycosin pine, SOA absorbs light less efficiently than POA in the long visible wavelengths, however it exhibits a stronger wavelength dependence and is more absorptive than POA in the short visible and near-UV. This might be due to differences in chemical composition, namely higher aromaticity in POA, but the true cause is not known. This hypothesis is supported by the recent findings of Lambe et al. (2013) who reported that SOA from aromatic precursors can retain light-absorbing conjugated double bonds, while light-absorption in SOA from non-aromatic precursors is due to carboxylic and carbonyl functional groups. Thus, BrC in POA and SOA in biomass-burning emissions may have overlapping as well as different chromophores. Desyaterik et al. (2013) investigated composition of BrC in cloud water droplets that were heavily affected by biomass-burning. They found that most of BrC absorption is due to aromatic carbonyls, which exist in fresh biomass-burning emissions, and nitrated phenols, which form through gas phase and aqueous chemistry. Nitrated phenols were also observed by Mohr et al. (2013) in biomass-burning plumes over Delting, United Kingdom.

Some field studies have reported significant amounts of SOA formation from photo-oxidation of biomass-burning emissions, with SOA-to-POA ratios up to two (Lee et al., 2008; Yokelson et al., 2009). Light absorption by biomass-burning SOA is thus a potentially important contributor to the global radiative forcing budget. The values of the imaginary part of the refractive indices provided here can be applied in models employing Mie-theory to perform preliminary calculations to assess the extent of SOA light absorption.

**Supplementary material related to this article is available online at:** <http://www.atmos-chem-phys.net/13/7683/2013/acp-13-7683-2013-supplement..zip>.

*Acknowledgements.* The authors acknowledge Sonia M. Kreidenweis, Cyle E. Wold, and Wei Min Hao for organizing the FLAME 3 campaign, and Spyros Pandis and Peter Adams for their valuable comments. This work was supported by the National Park Service and Joint Fire Science Programme and the EPA STAR program through the National Center for Environmental Research (NCER) under grant R833747 and the Department of Energy Atmospheric Sciences Research programme through grant DESC0007075. This paper has not been subject to EPA's required peer and policy review, and therefore does not necessarily reflect the views of the Agency. No official endorsement should be inferred.

Edited by: V. Faye McNeill

### References

- Ajtai, T., Filep, Á., Utry, N., Schnaiter, M., Linke, C., Bozóki, Z., Szabó, G., and Leisner, T.: Inter-comparison of optical absorption coefficients of atmospheric aerosols determined by a multi-wavelength photoacoustic spectrometer and an Aethalometer under sub-urban wintry conditions, *J. Aerosol. Sci.*, 42, 859–866, 2011.
- Andreae, M. O. and Gelencsér, A.: Black carbon or brown carbon? The nature of light-absorbing carbonaceous aerosols, *Atmos. Chem. Phys.*, 6, 3131–3148, doi:10.5194/acp-6-3131-2006, 2006.
- Alexander, D. L. T., Crozier, P. A., and Anderson, J. R.: Brown carbon spheres in East Asian outflow and their optical properties, *Science*, 321, 833–836, doi:10.1126/science.1155296, 2008.
- Arnott, W. P., Hamasha, K., Moosmuller, K., Sheridan, P. J., and Ogren, J. A.: Towards light absorption measurements with a 7-wavelength aethalometer: evaluation with a photoacoustic instrument and a 3-wavelength nephelometer, *Aerosol. Sci. Tech.*, 39, 17–29, 2005.
- Bergstrom, R. W., Russell, P. B., and Hignett, P.: The wavelength dependence of black carbon particles: predictions and results from the Tarfox experiment implications for the aerosol single scattering albedo, *J. Atmos. Sci.*, 59, 567–577, 2002.
- Bohren, C. F. and Huffman, D. R.: *Absorption and Scattering of Light by Small Particles*, John Wiley & Sons, New York, 1983.
- Bond, T. C., Anderson, T. L., and Campbell, D.: Calibration and intercomparison of filter-based measurements of visible light absorption by aerosols, *Aerosol. Sci. Tech.*, 30, 582–600, 1999.
- Bond, T. C., Streets, D. G., Yarber, K. F., Nelson, S. M., Woo, J., and Klimont, Z.: A technologically-based global inventory of black and organic carbon emissions from combustion, *J. Geophys. Res.*, 109, D14203, doi:10.1029/2003JD003697, 2004.
- Bond, T. C. and Bergstrom, R. W.: Light absorption by carbonaceous particles: an investigative review, *Aerosol. Sci. Tech.*, 39, 1–40, 2005.

- Bond, T. C., Habib, G., and Bergstrom, R. W.: Limitations in the enhancement of visible light absorption due to mixing state, *Geophys. Res. Lett.*, 111, D20211, doi:10.1029/2006JD007315, 2006.
- Cappa, C. D., Lack, D. A., Burkholder, J. B., and Ravishankara, A. R.: Bias in filter-based aerosol light absorption measurements due to organic aerosol loading: evidence from laboratory measurements, *Aerosol. Sci. Tech.*, 42, 1022–1032, 2008.
- Cappa, C. D., Onasch, T. B., Massoli, P., Worsnop, D. R., Bates, T. S., Cross, E. S., Davidovits, P., Hakala, J., Hayden, K. L., Jobson, B. T., Kolesar, K. R., Lack, D. A., Lerner, B. M., Li, S.-M., Mellon, D., Nuaaman, I., Olfert, J. S., Petäjä, T., Quinn, P. K., Song, C., Subramanian, R., Williams, E. J., and Zaveri, R. A.: Radiative absorption enhancements due to the mixing state of atmospheric black carbon, *Science*, 337, 1078–1081, 2012.
- Chakrabarty, R. K., Moosmüller, H., Chen, L.-W. A., Lewis, K., Arnott, W. P., Mazzoleni, C., Dubey, M. K., Wold, C. E., Hao, W. M., and Kreidenweis, S. M.: Brown carbon in tar balls from smoldering biomass combustion, *Atmos. Chem. Phys.*, 10, 6363–6370, doi:10.5194/acp-10-6363-2010, 2010.
- Chen, W.-T., Lee, Y. H., Adams, P. J., Nenes, A., and Seinfeld, J. H.: Will black carbon mitigation dampen aerosol indirect forcing?, *Geophys. Res. Lett.*, 37, L09801, doi:10.1029/2010GL042886, 2010.
- Chen, Y. and Bond, T. C.: Light absorption by organic carbon from wood combustion, *Atmos. Chem. Phys.*, 10, 1773–1787, doi:10.5194/acp-10-1773-2010, 2010.
- Cheng, Y., He, K.-B., Zheng, M., Duan, F.-K., Du, Z.-Y., Ma, Y.-L., Tan, J.-H., Yang, F.-M., Liu, J.-M., Zhang, X.-L., Weber, R. J., Bergin, M. H., and Russell, A. G.: Mass absorption efficiency of elemental carbon and water-soluble organic carbon in Beijing, China, *Atmos. Chem. Phys.*, 11, 11497–11510, doi:10.5194/acp-11-11497-2011, 2011.
- Clarke, A., McNaughton, C., Kapustin, V., Shinozuka, Y., Howell, S., Dibb, J., Zhou, J., Anderson, B., Brekhovskikh, V., Turner, H., and Pinkerton, M.: Biomass burning and pollution aerosol over North America: organic components and their influence on spectral optical properties and humidification response, *J. Geophys. Res.*, 112, D12S18, doi:10.1029/2006JD007777, 2007.
- Cross, E. S., Onasch, T. B., Ahern, A., Wrobel, W., Slowik, J. G., Olfert, J., Lack, D. A., Massoli, P., Cappa, C. D., Schwarz, J. P., Spackman, J. R., Fahey, D. W., Sedlacek, A., Trimborn, A., Jayne, J. T., Freedman, A., Williams, L. R., Ng, N. L., Mazzoleni, C., Dubey, M., Brem, B., Kok, G., Subramanian, R., Freitag, S., Clarke, A., Thornhill, D., Marr, L. C., Kolb, C. E., Worsnop, D. R., and Davidovits, P.: Soot particle studies – instrument inter-comparison – project overview, *Aerosol. Sci. Tech.*, 44, 592–611, 2010.
- Desayterik, Y., Sun, Y., Shen, X., Lee, T., Wang, X., Wang, T., and Collet Jr., J. L.: Speciation of “brown” carbon in cloud water impacted by agricultural biomass burning in Eastern China, *J. Geophys. Res.*, 118, 7389–7399, doi:10.1002/jgrd.50561, 2013.
- Donahue, N. M., Robinson, A. L., Trump, E. R., Riipinen, I., and Kroll, J. H.: Volatility and aging of atmospheric organic aerosol, *Top. Curr. Chem.*, doi:10.1007/128, 2012.
- Grieshop, A. P., Miracolo, M. A., Donahue, N. M., and Robinson, A. L.: Constraining the volatility distribution and gas-particle partitioning of combustion aerosols using isothermal dilution and thermodenuder measurements, *Environ. Sci. Technol.*, 43, 4750–4756, 2009.
- Grieshop, A. P., Donahue, N. M., and Robinson, A. L.: Laboratory investigation of photochemical oxidation of organic aerosol from wood fires 2: analysis of aerosol mass spectrometer data, *Atmos. Chem. Phys.*, 9, 2227–2240, doi:10.5194/acp-9-2227-2009, 2009.
- Gyawali, M., Arnott, W. P., Lewis, K., and Moosmüller, H.: In situ aerosol optics in Reno, NV, USA during and after the summer 2008 California wildfires and the influence of absorbing and non-absorbing organic coatings on spectral light absorption, *Atmos. Chem. Phys.*, 9, 8007–8015, doi:10.5194/acp-9-8007-2009, 2009.
- Habib, G., Venkataraman, C., Bond, T. C., and Schauer, J. J.: Chemical, microphysical and optical properties of primary particles from the combustion of biomass fuels, *Environ. Sci. Technol.*, 42, 8829–8834, 2008.
- Hand, L. H. and Kreidenweis, S. M.: A new method for retrieving particle refractive index and effective density from aerosol size distribution data, *Aerosol. Sci. Tech.*, 36, 1012–1026, 2002.
- Hecobian, A., Zhang, X., Zheng, M., Frank, N., Edgerton, E. S., and Weber, R. J.: Water-Soluble Organic Aerosol material and the light-absorption characteristics of aqueous extracts measured over the Southeastern United States, *Atmos. Chem. Phys.*, 10, 5965–5977, doi:10.5194/acp-10-5965-2010, 2010.
- Hennigan, C. J., Sullivan, A. P., Collett, J. L., and Robinson, A. L.: Levoglucosan stability in biomass burning particles exposed to hydroxyl radicals, *Geophys. Res. Lett.*, 37, L09806, doi:10.1029/2010GL043088, 2010.
- Hennigan, C. J., Miracolo, M. A., Engelhart, G. J., May, A. A., Presto, A. A., Lee, T., Sullivan, A. P., McMeeking, G. R., Coe, H., Wold, C. E., Hao, W.-M., Gilman, J. B., Kuster, W. C., de Gouw, J., Schichtel, B. A., J. L. Collett Jr., Kreidenweis, S. M., and Robinson, A. L.: Chemical and physical transformations of organic aerosol from the photo-oxidation of open biomass burning emissions in an environmental chamber, *Atmos. Chem. Phys.*, 11, 7669–7686, doi:10.5194/acp-11-7669-2011, 2011.
- Hildebrandt, L., Donahue, N. M., and Pandis, S. N.: High formation of secondary organic aerosol from the photo-oxidation of toluene, *Atmos. Chem. Phys.*, 9, 2973–2986, doi:10.5194/acp-9-2973-2009, 2009.
- Hoffer, A., Gelencsér, A., Guyon, P., Kiss, G., Schmid, O., Frank, G. P., Artaxo, P., and Andreae, M. O.: Optical properties of humic-like substances (HULIS) in biomass-burning aerosols, *Atmos. Chem. Phys.*, 6, 3563–3570, doi:10.5194/acp-6-3563-2006, 2006.
- Khlystov, A., Stanier, C., and Pandis, S. N.: An algorithm for combining electrical mobility and aerodynamic size distributions data when measuring ambient aerosol, *Aerosol. Sci. Tech.*, 38, 229–238, 2004.
- Kirchstetter, T. W., Novakov, T., and Hobbs, P. V.: Evidence that the spectral dependence of light absorption by aerosols is affected by organic carbon, *J. Geophys. Res.*, 109, D21208, doi:10.1029/2004JD004999, 2004.
- Kirchstetter, T. W. and Novakov, T.: Controlled generation of black carbon particles from a diffusion flame and applications in evaluating black carbon measurement methods, *Atmos. Environ.*, 41, 1874–1888, 2007.
- Lack, D. A., Cappa, C. D., Covert, D. S., Baynard, T., Massoli, P., Sierau, B., Bates, T. S., Quinn, P. K., Lovejoy, E. R., and Ravish-

- hankara, A. R.: Bias in filter-based aerosol light absorption measurements due to organic aerosol loading: Evidence from ambient measurements, *Aerosol. Sci. Tech.*, 42, 1033–1041, 2008.
- Lack, D. A. and Cappa, C. D.: Impact of brown and clear carbon on light absorption enhancement, single scatter albedo and absorption wavelength dependence of black carbon, *Atmos. Chem. Phys.*, 10, 4207–4220, doi:10.5194/acp-10-4207-2010, 2010.
- Lack, D. A., Langridge, J. M., Bahreini, R., Cappa, C. D., Middlebrook, A. M., and Schwarz, J. P.: Brown carbon and internal mixing in biomass burning particles, *P. Natl. Acad. Sci. USA*, 109, 14802–14807, 2012.
- Lambe, E. T., Cappa, C. D., Massoli, P., Onasch, T. B., Forestieri, S. D., Martin, A. T., Cummings, M. J., Croasdale, D. R., Brune, W. H., Worsnop, D. R., and Davidovits, P.: Relationship between oxidation level and optical properties of secondary organic aerosol, *Environ. Sci. Technol.*, 47, 6349–6357, 2013.
- Lee, S., Kim, H. K., Yan, B., Cobb, C. E., Hennigan, C., Nichols, S., Chamber, M., Edgerton, E. S., Jansen, J. J., Hu, Y., Zheng, M., Weber, R. J., and Russell, A. G.: Diagnosis of aged prescribed burning plumes impacting an urban area, *Environ. Sci. Technol.*, 42, 1438–1444, 2008.
- Levin, E. T., McMeeking, G. R., Carrico, C. M., Mack, L. E., Kreidenweis, S. M., Wold, C. E., Moosmüller, H., Arnott, W. P., Hao, W. M., Collett Jr., J. L., and Malm, W. C.: Biomass burning smoke aerosol properties measured during Fire Laboratory at Missoula Experiment (FLAME), *J. Geophys. Res.*, 115, D18210, doi:10.1029/2009JD013601, 2010.
- Lewis, K., Arnott, W. P., Moosmüller, H., and Wold, C. E.: Strong spectral variation of biomass smoke light absorption and single scattering albedo observed with a novel dual-wavelength photoacoustic instrument, *J. Geophys. Res.*, 113, D16203, doi:10.1029/2007JD009699, 2008.
- Mätzler, C.: MATLAB functions for Mie scattering and absorption, Res Rep 2002–08, Inst. Für Angew. Phys., Bern, 2002.
- Mohr, C., Lopez-Hilfiker, F. D., Zotter, P., Prevot, A. S. H., Xu, L., Ng, N. L., Herndon, S. C., Williams, L. R., Franklin, J. P., Zahniser, M. S., Worsnop, D. R., Knighton, W. B., Aiken, A. C., Gorkowski, K. J., Dubey, M. K., Allan, J. D., and Thornton, J. A.: Contribution of nitrated phenols to wood burning brown carbon light absorption in Delting, United Kingdom during winter time, *Environ. Sci. Technol.*, 47, 6316–6324, 2013.
- Moosmüller, H., Chakrabarty, R. K., Ehlers, K. M., and Arnott, W. P.: Absorption Ångström coefficient, brown carbon, and aerosols: basic concepts, bulk matter, and spherical particles, *Atmos. Chem. Phys.*, 11, 1217–1225, doi:10.5194/acp-11-1217-2011, 2011.
- Murphy, B. N. and Pandis, S. N.: Exploring summertime organic aerosol formation in the eastern United States using a regional-scale budget approach and ambient measurements, *J. Geophys. Res.*, 115, D24216, doi:10.1029/2010JD014418, 2010.
- Nakayama, T., Matsumi, Y., Sato, K., Imamura, T., Yamazaki, A., and Uchiyama, A.: Laboratory studies on optical properties of secondary organic aerosols generated during the photooxidation of toluene and the ozonolysis of alpha-pinene, *J. Geophys. Res.*, 115, D24204, doi:10.1029/2010JD014387, 2010.
- Rizzo, L. V., Correia, A. L., Artaxo, P., Procópio, A. S., and Andreae, M. O.: Spectral dependence of aerosol light absorption over the Amazon Basin, *Atmos. Chem. Phys.*, 11, 8899–8912, doi:10.5194/acp-11-8899-2011, 2011.
- Sandradewi, J., Prévôt, A. S. H., Weingartner, E., Schmidhauser, R., Gysel, M., and Baltensperger, U.: A study of wood burning and traffic aerosols in an Alpine valley using a multi-wavelength Aethalometer, *Atmos. Environ.*, 42, 101–112, 2008.
- Schnaiter, M., Linke, C., Möhler, O., Naumann, K.-H., Saathoff, H., Wagner, R., and Schurath, U.: Absorption amplification of black carbon internally mixed with secondary organic aerosol, *J. Geophys. Res.*, 110, D19204, doi:10.1029/2005JD006046, 2005.
- Subramanian, R., Roden, C. A., Boparai, P., and Bond, T. C.: Yellow beads and missing particles: trouble ahead for filter-based absorption measurements, *Aerosol Sci. Tech.*, 41, 630–637, 2007.
- Sun, H., Biedermann, L., and Bond, T. C.: Color of brown carbon: a model for ultraviolet and visible light absorption by organic carbon aerosol, *Geophys. Res. Lett.*, 34, L17813, doi:10.1029/2007GL029797, 2007.
- Weingartner, E., Saathoff, H., Schnaiter, M., Streit, N., Bitnar, B., and Baltensperger, U.: Absorption of light by soot particles: determination of the absorption coefficient by means of aethalometers, *J. Aerosol. Sci.*, 34, 1445–1463, 2003.
- Yang, M., Howell, S. G., Zhuang, J., and Huebert, B. J.: Attribution of aerosol light absorption to black carbon, brown carbon, and dust in China – interpretations of atmospheric measurements during EAST-AIRE, *Atmos. Chem. Phys.*, 9, 2035–2050, doi:10.5194/acp-9-2035-2009, 2009.
- Yokelson, R. J., Crouse, J. D., DeCarlo, P. F., Karl, T., Urbanski, S., Atlas, E., Campos, T., Shinozuka, Y., Kapustin, V., Clarke, A. D., Weinheimer, A., Knapp, D. J., Montzka, D. D., Holloway, J., Weibring, P., Flocke, F., Zheng, W., Toohey, D., Wennberg, P. O., Wiedinmyer, C., Mauldin, L., Fried, A., Richter, D., Walega, J., Jimenez, J. L., Adachi, K., Buseck, P. R., Hall, S. R., and Shetter, R.: Emissions from biomass burning in the Yucatan, *Atmos. Chem. Phys.*, 9, 5785–5812, doi:10.5194/acp-9-5785-2009, 2009.
- Zhang, R., Khalizof, A. F., Pagels, J., Zhang, D., Xue, H., and McMurry, P. H.: Variability in morphology, hygroscopicity, and optical properties of soot aerosols during atmospheric processing, *P. Natl. Acad. Sci. USA*, 105, 10291–10296, 2008.
- Zhang, X., Lin, Y.-H., Surratt, J. D., Zotter, P., Prévôt, A. S. H., and Weber, R. J.: Light-absorbing soluble organic aerosol in Los Angeles and Atlanta: A contrast in secondary organic aerosol, *Geophys. Res. Lett.*, 38, L21810, 2011.
- Zhong, M. and Jang, M.: Light absorption coefficient measurement of SOA using a UV-Visible spectrometer connected with an integrating sphere, *Atmos. Environ.*, 45, 4263–4271, 2011.

# Why do organic aerosols exist? Understanding aerosol lifetimes using the two-dimensional volatility basis set

N. M. Donahue,<sup>A,G</sup> W. Chuang,<sup>A</sup> S. A. Epstein,<sup>A,F</sup> J. H. Kroll,<sup>B</sup>  
D. R. Worsnop,<sup>C,D</sup> A. L. Robinson,<sup>A</sup> P. J. Adams<sup>A</sup> and S. N. Pandis<sup>A,E</sup>

<sup>A</sup>Center for Atmospheric Particle Studies, Carnegie Mellon University, 5000 Forbes Avenue, Pittsburgh, PA 15217, USA.

<sup>B</sup>Department of Civil and Environmental Engineering and Department of Chemical Engineering, Massachusetts Institute of Technology, 77 Massachusetts Avenue, Cambridge, MA 02139, USA.

<sup>C</sup>Aerodyne Research, Inc., 45 Manning Road, Billerica, MA 01821, USA.

<sup>D</sup>University of Helsinki, Department of Physics, FI-00014 Helsinki, Finland.

<sup>E</sup>Department of Chemical Engineering, University of Patras, Patra, GR-26500, Greece.

<sup>F</sup>Present address: Department of Chemistry, 1102 Natural Sciences 2, University of California, Irvine, CA 92697, USA.

<sup>G</sup>Corresponding author. Email: nmd@andrew.cmu.edu

**Environmental context.** Fine particles (aerosols) containing organic compounds are central players in two important environmental issues: aerosol-climate effects and human health effects (including mortality). Although organics constitute half or more of the total fine-particle mass, their chemistry is extremely complex; of critical importance is ongoing oxidation chemistry in both the gas phase and the particle phase. Here we present a method for representing that oxidation chemistry when the actual composition of the organics is not known and show that relatively slow oxidant uptake to particles plays a key role in the very existence of organic aerosols.

**Abstract.** Organic aerosols play a critical role in atmospheric chemistry, human health and climate. Their behaviour is complex. They consist of thousands of organic molecules in a rich, possibly highly viscous mixture that may or may not be in phase equilibrium with organic vapours. Because the aerosol is a mixture, compounds from all sources interact and thus influence each other. Finally, most ambient organic aerosols are highly oxidised, so the molecules are secondary products formed from primary emissions by oxidation chemistry and possibly non-oxidative association reactions in multiple phases, including gas-phase oxidation, aqueous oxidation, condensed (organic) phase reactions and heterogeneous interactions of all these phases. In spite of this complexity, we can make a strong existential statement about organic aerosol: They exist throughout the troposphere because heterogeneous oxidation by OH radicals is more than an order of magnitude slower than comparable gas-phase oxidation.

Received 30 January 2013, accepted 26 April 2013, published online 14 June 2013

## Introduction

Organic aerosols are meta-stable intermediates. Most organic emissions are highly reduced,<sup>[1,2]</sup> and all organics oxidise by complex oxidation pathways in the Earth's atmosphere.<sup>[3–6]</sup> Oxidation would convert all reduced carbon in the atmosphere into CO<sub>2</sub>, given time. Consequently, to first order, the concentration of any given constituent ( $C_i$ ) will be in a pseudo-steady-state at long enough timescales; given a production rate  $P_i$  and a first-order lifetime  $\tau_i$ , the pseudo steady-state concentration  $C_i^{ss}$  will be:

$$C_i^{ss} = P_i \tau_i \quad (1)$$

This means that, for a succession of molecules connected by a simple reaction sequence,  $M_i \rightarrow M_j \rightarrow M_k$  with a shared production rate  $P_i$ , the steady-state concentrations of each will be directly proportional to the lifetime. More generally, the total concentration of species at a given generation number in a

reaction sequence is related to the (properly weighted) average lifetime of the species in that generation. This simple equation governs organic-aerosol levels, and it shows that the atmospheric lifetime is critical.

To apply Eqn 1 we need to know the lifetimes. Unsaturated organic molecules are typically very short lived, and for the most part the double bonds will be eliminated rapidly.<sup>[7]</sup> Our main focus here is on later-generation chemistry of organic compounds, where the dominant oxidant is the OH radical. The chemical lifetime of organic vapours is governed by their rate constant for reaction with OH<sup>•</sup> ( $k_i^{OH}$ ), and the lifetime against oxidation by OH<sup>•</sup> will be  $\tau_i = 1/(k_i^{OH} C_{OH})$ . For the purposes of this discussion we shall consider  $C_{OH} = \sim 2 \times 10^6$  molecules cm<sup>-3</sup>, which is a typical daytime average value.<sup>[8]</sup> If the chemical lifetime is shorter than the deposition timescale, oxidation will in turn dominate the overall atmospheric lifetime. The job of estimating chemical lifetimes thus reduces to estimating OH<sup>•</sup> oxidation rate constants.

Rate constant estimation faces two challenges. First, the most important rate constants in this exercise involve the reaction of  $\text{OH}^\bullet$  with oxygenated organics, especially those containing multiple functional groups. These are generally large molecules by atmospheric standards, with 5–25 carbon atoms. There are very few kinetic data to draw on.<sup>[17]</sup> Second, there are thousands, even millions of specific organic molecules involved in chemistry associated with organic aerosols.<sup>[1,9]</sup> We thus have unmeasured rate constants for unknown molecules.

There are at least two solutions to this problem. One is to take what we do know about the kinetics and mechanisms of organic molecules and train mechanism generators to fill in the rest, connecting precursor molecules to all intermediates and ultimately to  $\text{CO}_2$ .<sup>[10]</sup> Another is to reduce the complexity by lumping the organics into groupings with similar properties. Here we choose the second approach, employing a discretised two-dimensional space consisting of volatility (saturation concentration,  $C^\circ$  in micrograms per cubic metre as the  $x$  coordinate and average carbon oxidation state ( $\overline{\text{OS}}_C \equiv 2\text{O} : \text{C} - \text{H} : \text{C} \approx 3\text{O} : \text{C} - 2$ ) as the  $y$  coordinate. This is known as the two-dimensional volatility basis set (2D-VBS),<sup>[1,11,12]</sup> and it forms the framework for this discussion.

## Methods

The 2D-VBS facilitates consideration of organic oxidation and phase partitioning without requiring specific knowledge of molecular structures, even carbon numbers. The variables themselves are the fundamental quantities describing phase partitioning and oxidation chemistry. Organic aerosol levels are almost always between 1 and  $100 \mu\text{g m}^{-3}$ , and consequently for organics to reside in the aerosol phase they must have a saturation mass concentration,  $C^* < \sim 100 \mu\text{g m}^{-3}$ . Volatility as  $C^*$  is not the pure-component vapour pressure; at a minimum it includes activity coefficients of organics in the aerosol mixture ( $C_i^* = \gamma_i C_i^\circ$ ), and more generally it includes any factors governing the equilibrium phase partitioning.<sup>[11]</sup> The relevant volatility is usually that of any product molecule in the condensed phase (i.e. ammonium oxalate or some other organic salt and not oxalic acid itself).

The equilibrium state says something about organic aerosols; however, the potential for organic aerosols to be out of equilibrium is currently under debate. It is possible that extremely low viscosity (i.e. a glassy state) may inhibit mass transfer within particles.<sup>[13–18]</sup> However, mass exchange between particles and the gas phase remains a critical topic, and particles do grow and shrink.<sup>[19]</sup> Considering uptake and condensational growth, most organic molecules that collide with particles do not stick to them. The property governing which compounds stay in the aerosol phase is volatility, and thus the  $x$ -axis of the 2D-VBS informs which phase the organic material will be in.

The  $y$ -axis of the 2D-VBS concerns oxidation. The oxidation state ( $\overline{\text{OS}}_C$ ) monotonically increases while organics reside in the atmosphere. Gas-phase tropospheric photochemistry is almost exclusively oxidative, with the  $\text{OH}$  radical serving as the dominant oxidant.<sup>[20]</sup> Heterogeneous uptake of  $\text{OH}^\bullet$  to aerosols is also a major cause of particle oxidation.<sup>[21,22]</sup> Ozone can oxidise organics with  $\text{C}=\text{C}$  double bonds, but although ozonolysis is extremely important, the double bonds are oxidised very rapidly and do not substantially affect the aging processes described here. Non-oxidative association reactions leading to high-molecular-weight products (oligomers) clearly occur,<sup>[23,24]</sup> but when the carbon number is followed in

environments where strong oxidative aging occurs, the general tendency is for carbon number to decrease due to fragmentation.<sup>[1,25–28]</sup> The bottom line is that most organic emissions have  $\overline{\text{OS}}_C < \sim -1.5$ , whereas a large majority of the organics (especially organic aerosol), is highly oxidised.<sup>[29]</sup> It follows that oxidation chemistry is a crucial, inevitable, monotonic driver of organic properties in the atmosphere.

Because we use the 2D-VBS framework, in order to assess organic lifetimes we need to estimate the  $\text{OH}^\bullet$  oxidation rate constants of organics in 2D-VBS bins. Fortunately, we do know something about composition (carbon, hydrogen and oxygen numbers,  $n_C, n_H, n_O$ , as well as the more tightly defined  $\text{O} : \text{C}$  and  $\text{H} : \text{C}$  ratios) in the 2D-VBS.<sup>[11]</sup> There is also strong evidence that the oxidised functional groups consist of approximately equal numbers of  $=\text{O}$  and  $-\text{OH}$  groups (the organic compounds appear to be, on average, either hydroxyketones or organic acids or more likely a mixture of both).<sup>[30,31]</sup> This is enough for us to begin to say something about the gas-phase  $\text{OH}^\bullet$  reactivity in the 2D-VBS. To do this we draw upon and simplify structure–activity relations, starting along the lower edge of the 2D-VBS where the organics are simply hydrocarbons.

We do not know the structure of the typical organics in the 2D-VBS, so we rely on a statistical sampling of kinetic data in the (limited) regime of the 2D-VBS where kinetics are available. The kinetics are distilled by the structure–activity relationship (SAR) of Kwok and Atkinson,<sup>[32]</sup> which we sample randomly with 35 000 molecules to maintain the proper  $\text{C} : \text{H} : \text{O}$  relationships (on average) in the 2D-VBS. However, the basis for the SAR consists almost entirely of small molecules, most with either zero or one oxygenated functional group. To extrapolate this over the full range of the 2D-VBS we smooth the resulting rate-constant surface with a functional form based on three simple assumptions: (1)  $\text{OH}^\bullet$  oxidation rate constants typically increase with increasing carbon number; (2) adding oxygenated functional groups for lightly oxygenated molecules typically increases the  $\text{OH}^\bullet$  reactivity and (3) highly oxygenated molecules ultimately become less reactive due simply to a scarcity of abstractable hydrogens. This final assumption is supported by heterogeneous  $\text{OH}^\bullet$  oxidation experiments on highly oxygenated aerosol surrogates, such as citric acid, which show it to be recalcitrant to oxidation.<sup>[33]</sup>

The resulting (vapour-phase) rate-constant ( $k^{\text{vap}}$ ,  $\text{cm}^3 \text{ molecule}^{-1} \text{ s}^{-1}$ ) expression is given by Eqn 2 and plotted in the 2D-VBS in Fig. 1.

$$k^{\text{vap}} = \sim 1.2 \times 10^{-12} (n_C + 9n_O - 10 (\text{O} : \text{C})^2) \quad (2)$$

The first effect (increasing  $k$  with increasing  $n_C$ ) for homologous molecules is very robust.<sup>[32]</sup> The second two effects counteract each other. We express them with one term dependent on  $n_O$  alone and a second one dependent on  $(\text{O} : \text{C})^2$ , which is a measure of the H-atom scarcity. Although the specifics of the functional form in Eqn 2 and the actual rate constants must be regarded as quite uncertain, overall Fig. 1 reveals rate constants that vary only modestly throughout the space. The major feature is that  $k_{\text{OH}}$  increases as  $C^\circ$  decreases, but the overall effect is less than a 1 order of magnitude increase in  $k$  over a 15 decade decrease in  $C^\circ$ . Furthermore, although we include the volatile organic carbon (VOC) region in the 2D-VBS ( $C^\circ > 3 \times 10^6 \mu\text{g m}^{-3}$ ) for completeness, no realistic simulation would actually use it for a numerical simulation in that region – VOC chemistry is represented by a standard chemical mechanism.

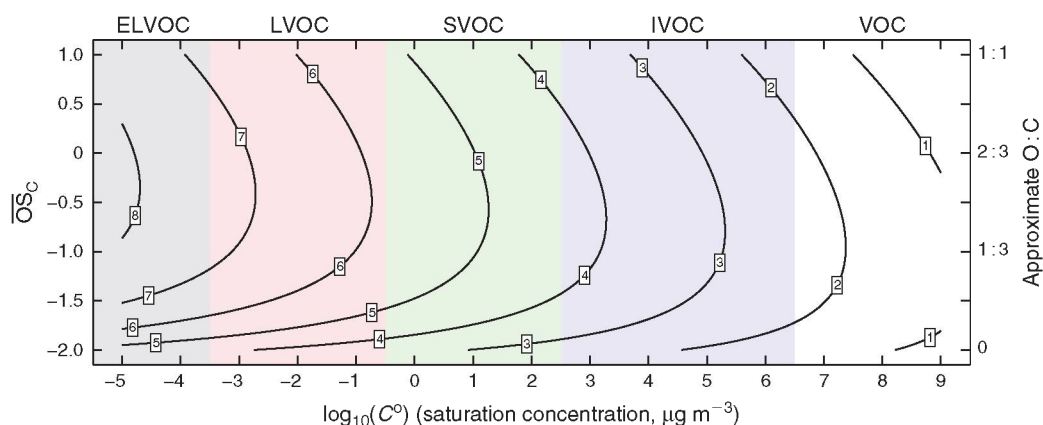


**Fig. 1.** Gas-phase  $\text{OH}^\bullet$  oxidation rate constants for organic species *v.* volatility and oxidation state ( $\overline{\text{OS}}_C$ ) (contours are  $k \times 10^{11} \text{ cm}^3 \text{ molecule}^{-1} \text{ s}^{-1}$ ). Rate constants are estimated based on extrapolated group contribution methods, as described in the text. The  $\text{OH}^\bullet$  oxidation rate constant increases with increasing carbon number, rapidly with increasing oxygen number, but decreases quadratically as O:C increases due to the loss of abstractable hydrogens. (ELVOC, extremely low volatility organic compounds; LVOC, low volatility organic compounds; SVOC, semivolatile organic compounds; IVOC, intermediate volatility organic compounds; VOC, volatile organic compounds.)

## Results and discussion

In Fig. 2a we show the gas-phase chemical lifetime,  $\tau = 1/(kC_{\text{OH}})$ , in days in the 2D-VBS space, assuming  $C_{\text{OH}} = \sim 2 \times 10^6 \text{ molecules cm}^{-3}$ . The semi-volatile range is  $0.3 \leq C^\circ \leq 300 \mu\text{g m}^{-3}$ , organics with lower  $C^\circ$  values will be almost completely in the condensed phase under typical conditions. The critical point is that organic species over the entire range of volatilities representative of aerosols have a gas-phase lifetime of less than 0.2 days. Thus, aerosol species would evolve through upwards of five generations of chemistry in 24 h, if they were in the gas phase. Because the probability of fragmentation and consequent sharp increases in volatility rises rapidly with increasing oxidation state,<sup>[25–27]</sup> this unrestrained oxidation would sweep the system clean of organic aerosols within a day or two. For example, a  $\text{C}_{10}$  backbone, with on average 1.5 oxygen atoms added per generation, will have a simple fragmentation probability (O:C)<sup>1/4</sup> of 0, 0.62, 0.74, 0.82, 0.88 and 0.93 for generations 0–5.

Organic species, however, do not reside solely in the gas phase. The less volatile ones condense to form organic aerosol, and in the condensed phase they are protected from gas-phase  $\text{OH}^\bullet$  by the diffusion rate of  $\text{OH}^\bullet$  to the particles. For the purposes of this work, the heterogeneous uptake of  $\text{OH}^\bullet$  to particles can be converted into an effective gas-phase rate constant, which depends on particle size.<sup>[34,35]</sup> Here we assume that  $\text{OH}^\bullet$  will react with unit efficiency with the first organic species it encounters in a particle, and thus the effective rate constant will be independent of composition.<sup>[36]</sup> For 500-nm diameter particles, the effective rate constant will be  $k_i^{\text{eff}} = 1 \times 10^{-12} \text{ cm}^3 \text{ molecule}^{-1} \text{ s}^{-1}$ , resulting in an oxidation lifetime of 5.8 days, whereas organics in 200-nm diameter particles would have a lifetime of  $\sim 3$  days. This will apply regardless of the condensed-phase composition, provided that the pseudo-ideal solution theory relevant to  $C^\circ$  holds and that the near-surface particle composition is approximately the same as the bulk organic phase composition. This will be true if the particle viscosity is not so high as to significantly limit condensed-phase mass transfer to the particle surface; the timescale for diffusion within the particles must be faster than the timescale for

heterogeneous oxidation (6 days in this example).<sup>[36,37]</sup> Evidence from relative rate experiments of mixtures made by coating primary organic particles with laboratory secondary organic aerosol (SOA) supports this assumption.<sup>[38]</sup>

The condensed-phase lifetime of 6 days is thus much longer than the  $\sim 0.1$ -day gas-phase lifetime of the organic molecules in the low-volatility range. However, it is still comparable to the residence time of particles in the atmosphere, so heterogeneous oxidation *will* play a role even for organics that are more or less homogeneously distributed in the condensed phase. The overall average lifetime of semi-volatile organics will depend on their fraction ( $\xi_i$ ) in the condensed phase:

$$\xi_i = (1 + C_i^*/C_{\text{OA}})^{-1} \quad (3)$$

which gives an overall rate constant ( $k_i^{\text{tot}}$ ) based on the effective heterogeneous rate constant ( $k_i^{\text{eff}}$ ) and the gas-phase rate constant ( $k_i^{\text{vap}}$ ) from Eqn 2.

$$k_i^{\text{tot}} = \xi_i k_i^{\text{eff}} + (1 - \xi_i) k_i^{\text{vap}} \tau_i = 1/(k_i^{\text{tot}} C_{\text{OH}}) \quad (4)$$

The overall lifetimes including the gas-phase diffusion limitations for heterogeneous oxidation are shown in Fig. 2b for a case with concentration of organic aerosol  $C_{\text{OA}} = 1 \mu\text{g m}^{-3}$ . Based on Eqn 1, the steady-state concentration of species sequestered in particles will thus be  $\sim 30$  times higher than it would otherwise be if they were oxidised at the rate given by pure gas-phase oxidation shown in Fig. 2a.

In this work we are considering heterogeneous oxidation by  $\text{OH}$  radical uptake only. Especially at higher relative humidity (and certainly in droplets), aqueous-phase reactions will also contribute to oxidation; it is unclear whether the net effect of these processes will augment or deplete the total organic-aerosol mass, although oxidation of soluble volatile species can clearly contribute to SOA.<sup>[39,40]</sup> For example, levoglucosan can be oxidised in most particles and droplets with lifetimes in the order of days.<sup>[41]</sup> However, with a saturation concentration of the order of  $7 \mu\text{g m}^{-3}$ ,<sup>[42]</sup> levoglucosan will reside principally in the gas phase under many circumstances.<sup>[12]</sup> As Eqn 4 and experimental data show,<sup>[43]</sup> the majority of oxidation is likely to

be by gas-phase  $\text{OH}^\bullet$  reactions. This will apply to other organics even well into the low volatility organic compound region (LVOC) region.

The lifetime contours in Fig. 2b show something profound. The sharp increase in lifetimes with decreasing volatility and thus decreasing gas-phase fractions is the most dramatic feature of the figure (note that the influence of gas-phase oxidation extends to quite low  $C^0$ ). However, just as notable is the broad area of minimum lifetime for semi-volatile organic compounds (SVOC range in green) and intermediate volatility organic compounds (IVOC range in blue). Until recently, many atmospheric models treating SVOCs contained semi-volatile lumped species whose properties ( $C^*$  and molar yields) were based on empirical fits to smog-chamber data. Often these species were effectively immortal in the model, or at most suffered from deposition to the surface. In fact, these SVOCs have a minimum lifetime and thus will have a minimum steady-state concentration of all molecules in a given reaction sequence. Atmospheric chemistry will thus tend to sweep out the SVOC range with progressive aging downwind of a source region, forming either much lower volatility functionalised products or more volatile fragmentation products and thus producing very low volatility, highly oxidised aerosol in the remote atmosphere. This is exactly what is observed.<sup>[29,44]</sup>

The lifetime of individual organic molecules is not the same as the lifetime of the aerosol mass itself. So, in order to test our assertion that without condensed-phase sequestration the atmosphere would be rapidly swept clear of organic aerosol, we simulated the evolution of a SOA plume in a simple box model. The model is initiated by SOA formation by ozonolysis of  $\alpha$ -pinene, assuming 30 ppb of ozone and  $20 \mu\text{g m}^{-3}$  of  $\alpha$ -pinene ( $\sim 2$  ppbv). The initial fresh SOA formation and subsequent aging chemistry follow the yields and chemistry described previously,<sup>[29,45,46]</sup> and the model (including slow heterogeneous oxidation) matches observed aging behaviour well.<sup>[47]</sup> Briefly,  $\text{OH}^\bullet$  reacts with semi-volatile vapours with the rate constants described above. The resulting reaction products are distributed according to two oxidation ‘kernels’, with a ‘functionalisation’ fraction distributed exclusively to lower  $C^*$  values and a ‘fragmentation’ fraction dispersed widely in volatility space. The probability of fragmentation is assumed to vary as  $(\text{O}:\text{C})^{1/4}$ , so as organics become highly oxidised they will inevitably fragment towards  $\text{CO}_2$ , which is required by thermodynamics.

The results of our box-model simulation are shown in Fig. 3. The  $\alpha$ -pinene was allowed to react with ozone in the dark for 12 h, forming  $\sim 1 \mu\text{g m}^{-3}$  of ‘fresh’ SOA with a mass yield of  $\sim 5\%$ . At  $t = 0$  the  $\text{OH}^\bullet$  concentration was suddenly increased

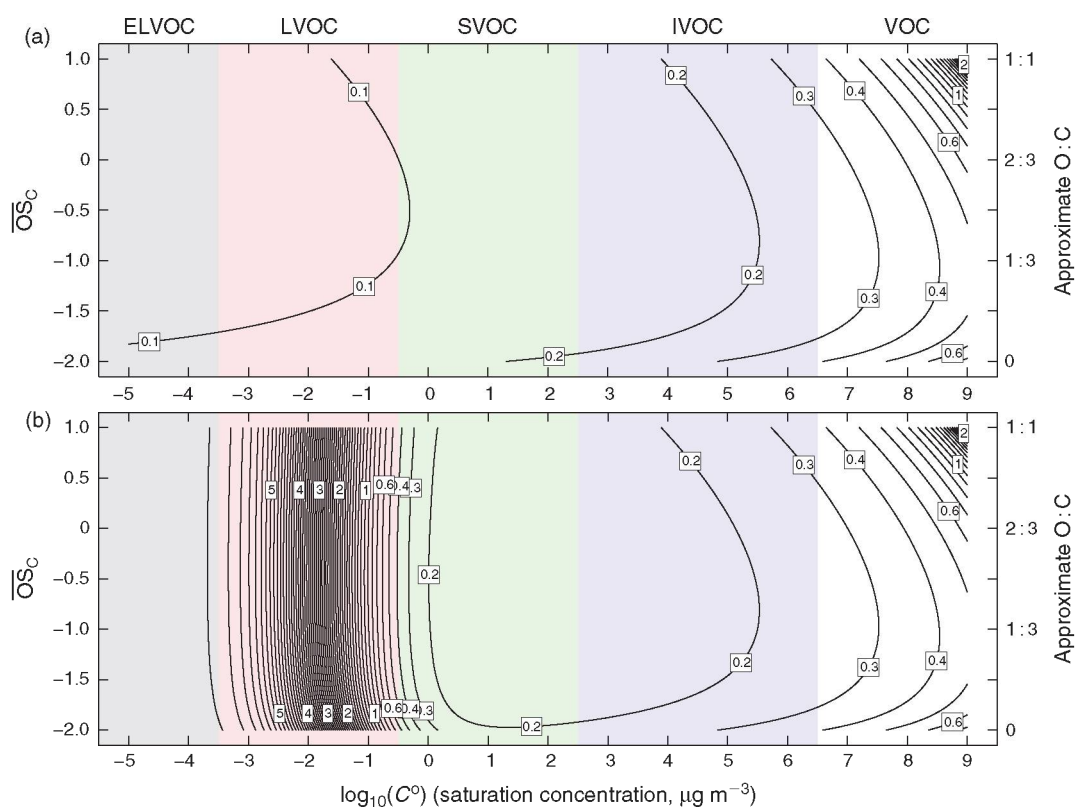


**Fig. 2.**  $\text{OH}^\bullet$  oxidation lifetimes in days of organic compounds in the two-dimensional volatility basis set. Contour intervals are 0.1 day. (a) Gas-phase lifetimes based on the rate constants in Fig. 1 and an assumed  $\text{OH}$  radical concentration of  $2 \times 10^6$  molecules  $\text{cm}^{-3}$ . In the semi-volatile range of  $C^0$  values relevant to organic aerosols (green and blue shading), the gas-phase lifetimes of organic vapours will be less than 0.2 days. (b) Lifetimes including the effect of phase partitioning, where heterogeneous oxidation by  $\text{OH}^\bullet$  uptake to particles is limited by gas-phase diffusion and the heterogeneous oxidation lifetime is 5.6 days (for 500-nm diameter particles). Consequently, semi-volatile organics are the shortest lived species, with a lifetime of  $\sim 0.2$  days. (ELVOC, extremely low volatility organic compounds; LVOC, low volatility organic compound region; SVOC, semivolatile organic compounds; IVOC, intermediate volatility organic compounds; VOC, volatile organic compounds;  $\text{OS}_C$ , oxidation state.)

to  $2 \times 10^6$  molecules  $\text{cm}^{-3}$ . In the base-case simulation the  $\text{OH}^\bullet$  oxidation rate constants are given by Eqn 4. We assume that the mechanism (the product distribution) is not affected by whether the  $\text{OH}^\bullet$  reaction occurs homogeneously in the gas phase or heterogeneously near the particle surface. This is almost certainly an over simplification, but there are insufficient data to describe the chemistry in more detail. The solid curve in Fig. 3 shows the organic aerosol evolution as this aging chemistry progresses. With most of the first-generation ozonolysis products in the vapour phase, the aging causes a dramatic, almost 10-fold, increase in aerosol concentrations over the first half day, but the subsequent aging chemistry is slow because of the slow heterogeneous oxidation. This is broadly consistent with published smog-chamber experiments on SOA aging, although the magnitude of the fractional mass increase is large because of the very low (for a chamber experiment) initial SOA mass loading.<sup>[47]</sup>

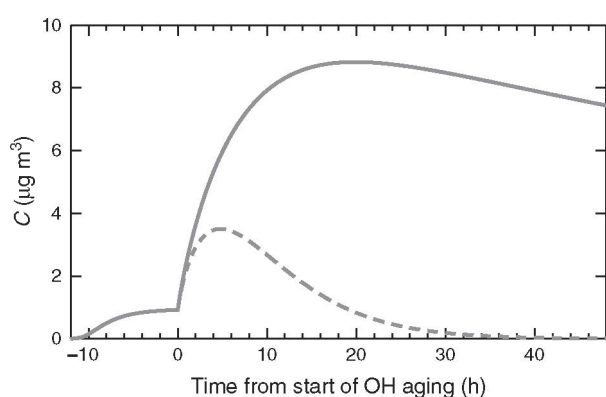


**Fig. 3.** Evolution of organic aerosol concentrations ( $C$ ) in an idealised box model. Secondary organic aerosol is formed by oxidation of  $\alpha$ -pinene by ozone over 12 h ( $t < 0$ ). For  $t \geq 0$ ,  $[\text{OH}^\bullet] = 2 \times 10^6$  molecules  $\text{cm}^{-3}$ . The solid curve is the best model estimate of evolving organic aerosol mass concentrations, with a substantial increase caused by gas-phase oxidation and very little influence from (diffusion limited)  $\text{OH}$  radical uptake to particles. In the simulation shown with a dashed curve all organics are oxidised with their equivalent gas-phase rate constants. The oxidation chemistry rapidly fragments the organics, causing the aerosol to evaporate.

In the second, dashed curve in Fig. 3, the heterogeneous ageing  $k^{\text{eff}}$  is artificially made equal to the gas-phase  $\text{OH}^\bullet$  oxidation rate constant, so the oxidation proceeds unimpeded by diffusion limitations. In this case the organic aerosol rapidly dissipates, vanishing in  $\sim 1$  day. This dramatic difference in behaviour shows that the simple steady-state analysis described by Eqn 1 gives a valid picture for bulk organic-aerosol concentrations as well. A typical average age of aerosols in even an urban setting such as Pittsburgh is greater than 2 days,<sup>[48]</sup> and the ratio in modelled organic aerosol concentrations for  $0 \leq t \leq 48$  h in Fig. 3 is more than a factor of five.

The calculations presented so far have been for ‘typical’ ambient conditions, but in certain times and places the atmosphere can be far more oxidising. One example is the eastern Mediterranean. During the MINOS campaign at the Finokalia research station in Crete in August 2001, ambient  $\text{OH}^\bullet$  levels reached  $2 \times 10^7$  molecules  $\text{cm}^{-3}$ .<sup>[49]</sup> Under these extreme conditions, the gas-phase lifetimes of SVOC within the 2D-VBS are less than 1 h, and even the heterogeneous oxidation timescale is just over 12 h, as shown in Fig. 4 – we show lifetimes for the diurnal maximum  $\text{OH}^\bullet$  levels because under these conditions the oxidation timescales are so fast that the diurnal average is barely meaningful. We thus expect organic aerosols to become completely oxidised very quickly, unless some compounds are able to ‘hide’ in the particles because they are so viscous that they cannot reach the surface to be oxidised.<sup>[14,36]</sup>

Organic-aerosol observations using a unit mass resolution aerosol mass spectrometer (Q-AMS, Aerodyne Inc., Billerica, MA, USA) during the EUCAARI campaigns in May 2008 and February 2009 show that in the late spring organic aerosols arriving at Finokalia were completely oxidised, with no evidence of *any* primary organic aerosol,<sup>[50]</sup> whereas Q-AMS observations at the same site in winter 2009 showed significant levels of primary organic aerosol.<sup>[44]</sup> The highly oxidised aerosols during late spring 2008 were observed even when air-mass back trajectories showed that the sampled air had been in the boundary layer over Athens less than 2 days earlier. The very short lifetimes shown in Fig. 4 confirm this, and the almost complete absence of unoxidised peaks in the mass spectra (even for air recently over Athens) shows that diffusion limitations do not protect extremely

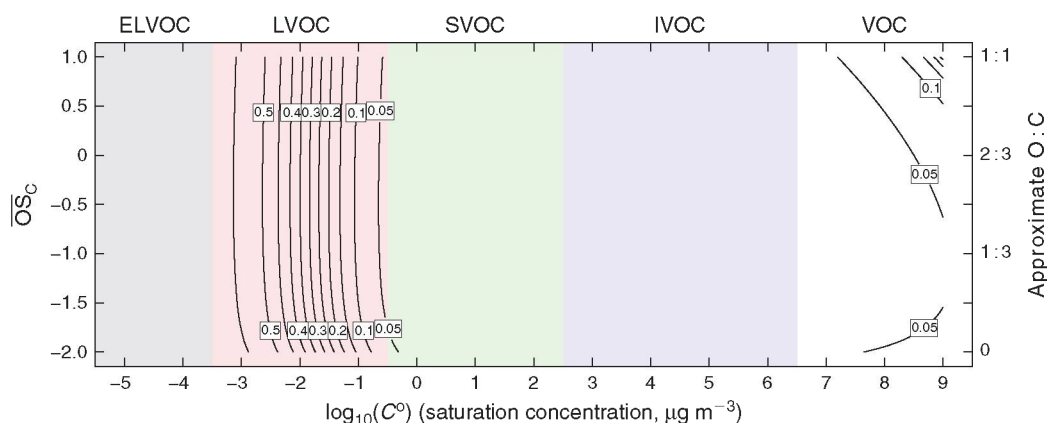


**Fig. 4.**  $\text{OH}^\bullet$  oxidation lifetimes in days of organic compounds in the two-dimensional volatility basis set for conditions observed in the summertime eastern Mediterranean with an assumed  $\text{OH}$  radical concentration of  $2 \times 10^7$  molecules  $\text{cm}^{-3}$ . Contour intervals are 0.05 day. Extreme oxidation conditions will oxidise gas-phase species in less than 1 h; even heterogeneous oxidation will occur during daylight  $t$  of a single day. (ELVOC, extremely low volatility organic compounds; LVOC, low volatility organic compound region; SVOC, semivolatile organic compounds; IVOC, intermediate volatility organic compounds; VOC, volatile organic compounds;  $\overline{\text{OS}}_C$ , oxidation state.)

low volatility primary compounds within the particles under ambient conditions. Given that the heterogeneous oxidation timescale in Fig. 4 is  $\sim 12$  h, this suggests that the diffusional timescales for organics within the aerosols sampled during FAME-08 were faster than this. That in turn suggests a diffusion constant  $D \geq 10^{-14} \text{ cm}^2 \text{ s}^{-1}$ , or a dynamic viscosity  $\eta \leq 3 \times 10^5 \text{ Pa s}$ ,<sup>[15]</sup> even for quite highly oxidised organic aerosol.

### Environmental implications

Oxidation of organic compounds, carried to completion, will form  $\text{CO}_2$ , and consequently oxidation is fundamentally destructive to organic aerosol. However, as Fig. 3 shows, oxidation clearly is a source of organic aerosol as well. Consequently, organic aerosols can only be viewed as metastable intermediates.<sup>[1]</sup> Its concentrations are thus controlled by its lifetime, and as we show the fundamental governor of this lifetime is the delay caused by diffusion of OH radicals to aerosols. Without this, organic aerosol levels would be many times lower than they are, rendering organics virtually irrelevant to aerosol concentrations and properties.

Conversely, although organic compounds can run, they cannot hide. Sequestration into the condensed phase delays oxidation because of diffusion limitations in the gas phase, but heterogeneous oxidation is still important. The near complete oxidation observed in situations where transport occurs within  $\sim 1$  day from intense sources indicates that the diffusion timescale for organics within particles is (in at least some cases relevant to the atmosphere) less than 1 day.

### Acknowledgements

This work was funded by the National Science Foundation, the DOE ASR program and the EPASTAR program.

### References

- [1] J. H. Kroll, N. M. Donahue, J. L. Jimenez, S. Kessler, M. R. Canagaratna, K. Wilson, K. E. Alteri, L. R. Mazzoleni, A. S. Wozniak, H. Bluhm, E. R. Mysak, J. D. Smith, C. E. Kolb, D.R. Worsnop, Carbon oxidation state as a metric for describing the chemistry of atmospheric organic aerosol. *Nat. Chem.* **2011**, *3*, 133. doi:10.1038/NCHEM.948
- [2] A. B. Guenther, X. Jiang, C. L. Heald, T. Sakulyanontvittaya, T. Duhl, L. K. Emmons, X. Wang, The model of emissions of gases and aerosols from nature version 2.1 (MEGAN2.1): an extended and updated framework for modeling biogenic emissions. *Geoscientific Model Development* **2012**, *5*, 1471. doi:10.5194/GMD-5-1471-2012
- [3] R. Kamens, H. Jeffries, M. Gery, R. Wiener, K. Sexton, G. Howe, The impact of  $\alpha$ -pinene on urban smog formation – an outdoor smog chamber study. *Atmos. Environ.* **1981**, *15*, 969. doi:10.1016/0004-6981(81)90097-4
- [4] H. Jeffries, S. Tonnesen, A comparison of 2 photochemical-reaction mechanisms using mass-balance and process analysis. *Atmos. Environ.* **1994**, *28*, 2991. doi:10.1016/1352-2310(94)90345-X
- [5] R. M. Kamens, M. Jaoui, Modeling aerosol formation from  $\alpha$ -pinene +  $\text{NO}_x$  in the presence of natural sunlight using gas-phase kinetics and gas-particle partitioning theory. *Environ. Sci. Technol.* **2001**, *35*, 1394. doi:10.1021/ES001626S
- [6] W. Vizuete, H. E. Jeffries, T. W. Tesche, E. P. Olaguer, E. Couzo, Issues with ozone attainment methodology for Houston, TX. *J. Air Waste Manag. Assoc.* **2011**, *61*, 238. doi:10.3155/1047-3289.61.3.238
- [7] R. Atkinson, Gas phase tropospheric chemistry of organic compounds. *J. Phys. Chem. Ref. Data* **1997**, *26*, 215. doi:10.1063/1.556012
- [8] R. Prinn, J. Huang, R. Weiss, D. Cunnold, P. Fraser, P. Simmonds, A. McCulloch, C. Harth, S. Reimann, P. Salameh, S. O'Doherty, R. Wang, L. Porter, B. Miller, P. Krummel, Evidence for variability of atmospheric hydroxyl radicals over the past quarter century. *Geophys. Res. Lett.* **2005**, *32*, L07809. doi:10.1029/2004GL022228
- [9] A. H. Goldstein, I. E. Galbally, Known and unexplored organic constituents in the Earth's atmosphere. *Environ. Sci. Technol.* **2007**, *41*, 1514. doi:10.1021/ES072476P
- [10] B. Aumont, S. Szopa, S. Madronich, Modelling the evolution of organic carbon during its gas-phase tropospheric oxidation: development of an explicit model based on a self generating approach. *Atmos. Chem. Phys.* **2005**, *5*, 2497. doi:10.5194/ACP-5-2497-2005
- [11] N. M. Donahue, S. A. Epstein, S. N. Pandis, A. L. Robinson, A 2-dimensional volatility basis set: 1. Organic mixing thermodynamics. *Atmos. Chem. Phys.* **2011**, *11*, 3303. doi:10.5194/ACP-11-3303-2011
- [12] N. M. Donahue, J. H. Kroll, A. L. Robinson, S. N. Pandis, A 2-dimensional volatility basis set: 2. Diagnostics of laboratory and ambient organic aerosol. *Atmos. Chem. Phys.* **2012**, *12*, 615. doi:10.5194/ACP-12-615-2012
- [13] B. Zobrist, C. Marcolli, D. A. Pedernera, T. Koop, Do atmospheric aerosols form glasses? *Atmos. Chem. Phys.* **2008**, *8*, 5221. doi:10.5194/ACP-8-5221-2008
- [14] A. Virtanen, J. Joutsensaari, T. Koop, J. Kannosto, P. Yli-Pirila, J. Leskinen, J. M. Makela, J. K. Holopainen, U. Poeschl, M. Kulmala, D. R. Worsnop, A. Laaksonen, An amorphous solid state of biogenic secondary organic aerosol particles. *Nature* **2010**, *467*, 824. doi:10.1038/NATURE09455
- [15] T. Koop, J. Bookhold, M. Shiraiwa, U. Poeschl, Glass transition and phase state of organic compounds: dependency on molecular properties and implications for secondary organic aerosols in the atmosphere. *Phys. Chem. Chem. Phys.* **2011**, *13*, 19238. doi:10.1039/C1CP22617G
- [16] T. D. Vaden, D. Imre, J. Ber'aneek, M. Shrivastava, A. Zelenyuk, Evaporation kinetics and phase of laboratory and ambient secondary organic aerosol. *Proc. Natl. Acad. Sci. USA* **2011**, *108*, 2190. doi:10.1073/PNAS.1013391108
- [17] M. Shiraiwa, M. Ammann, T. Koop, U. Poeschl, Gas uptake and chemical aging of semisolid organic aerosol particles. *Proc. Natl. Acad. Sci. USA* **2011**, *108*, 11003. doi:10.1073/PNAS.1103045108
- [18] V. Perraud, E. A. Bruns, M. J. Ezell, S. N. Johnson, Y. Yu, M. L. Alexander, A. Zelenyuk, D. Imre, W. L. Chang, D. Dabdub, J. F. Pankow, B. J. Finlayson-Pitts, Nonequilibrium atmospheric secondary organic aerosol formation and growth. *Proc. Natl. Acad. Sci. USA* **2012**, *109*, 2836. doi:10.1073/PNAS.1119909109
- [19] A. P. Grieshop, N. M. Donahue, A. L. Robinson, Is the gas-particle partitioning in  $\alpha$ -pinene secondary organic aerosol reversible? *Geophys. Res. Lett.* **2007**, *34*, L14810. doi:10.1029/2007GL029987
- [20] J. A. Logan, M. J. Prather, S. C. Wofsy, M. B. McElroy, Tropospheric chemistry: a global perspective. *J. Geophys. Res. – Atmos.* **1981**, *86*, 7210. doi:10.1029/JC086IC08P07210
- [21] Y. Rudich, Laboratory perspectives on the chemical transformations of organic matter in atmospheric particles. *Chem. Rev.* **2003**, *103*, 5097. doi:10.1021/CR020508F
- [22] Y. Rudich, N. M. Donahue, T. F. Mentel, Aging of organic aerosol: bridging the gap between laboratory and field studies. *Annu. Rev. Phys. Chem.* **2007**, *58*, 321. doi:10.1146/ANNUREV.PHYSCHEM.58.032806.104432
- [23] M. Kalberer, D. Paulsen, M. Sax, M. Steinbacher, J. Dommen, A. S. H. Prévôt, R. Fisseha, E. Weingartner, V. Frankevic, R. Zenobi, U. Baltensperger, Identification of polymers as major components of atmospheric organic aerosols. *Science* **2004**, *303*, 1659. doi:10.1126/SCIENCE.1092185
- [24] M. Tolocka, M. Jang, J. Ginter, F. Cox, R. Kamens, M. Johnston, Formation of oligomers in secondary organic aerosol. *Environ. Sci. Technol.* **2004**, *38*, 1428. doi:10.1021/ES035030R
- [25] J. H. Kroll, J. D. Smith, D. L. Che, S. H. Kessler, D. R. Worsnop, K. R. Wilson, Measurement of fragmentation and functionalization pathways in the heterogeneous oxidation of oxidized organic aerosol. *Phys. Chem. Chem. Phys.* **2009**, *11*, 8005. doi:10.1039/B905289E

- [26] H. J. Chacon-Madrid, A. A. Presto, N. M. Donahue, Functionalization vs fragmentation: *n*-aldehyde oxidation mechanisms and secondary organic aerosol formation. *Phys. Chem. Chem. Phys.* **2010**, *12*, 13 975. doi:10.1039/C0CP00200C
- [27] H. J. Chacon-Madrid, N. M. Donahue, Fragmentation *v.* functionalization: chemical aging and organic aerosol formation. *Atmos. Chem. Phys.* **2011**, *11*, 10 553. doi:10.5194/ACP-11-10553-2011
- [28] A. T. Lambe, T. B. Onasch, D. R. Croasdale, J. P. Wright, A. T. Martin, J. P. Franklin, P. Massoli, J. H. Kroll, M. R. Canagaratna, W. H. Brune, D. R. Worsnop, P. Davidovits, Transitions from functionalization to fragmentation reactions of laboratory secondary organic aerosol (SOA) generated from the OH oxidation of alkane precursors. *Environ. Sci. Technol.* **2012**, *46*, 5430. doi:10.1021/ES300274T
- [29] J. L. Jimenez, M. R. Canagaratna, N. M. Donahue, A. S. H. Prévôt, Q. Zhang, J. H. Kroll, P. F. DeCarlo, J. Allan, H. Coe, N. L. Ng, A. C. Aiken, K. D. Docherty, I. M. Ulbrich, A. P. Grieshop, A. L. Robinson, J. Duplissy, J. D. Smith, K. R. Wilson, V. A. Lanz, C. Hueglin, Y. L. Sun, A. Laaksonen, T. Raatikainen, J. Rautiainen, P. Vaattovaara, M. Ehn, M. Kulmala, J. M. Tomlinson, D. R. Collins, M. J. Cubison, E. J. Dunlea, J. A. Huffman, T. B. Onasch, M. R. Alfarra, P. I. Williams, K. Bower, Y. Kondo, J. Schneider, F. Drewnick, S. Borrmann, S. Weimer, K. Demerjian, D. Salcedo, L. Cottrell, R. Griffin, A. Takami, T. Miyoshi, S. Hatakeyama, A. Shimono, J. Y. Sun, Y. M. Zhang, K. Dzepina, J. R. Kimmel, D. Sueper, J. T. Jayne, S. C. Herndon, A. M. Trimborn, L. R. Williams, E. C. Wood, C. E. Kolb, U. Baltensperger, D. R. Worsnop, Evolution of organic aerosols in the atmosphere: a new framework connecting measurements to models. *Science* **2009**, *326*, 1525. doi:10.1126/SCIENCE.1180353
- [30] C. L. Heald, J. H. Kroll, J. L. Jimenez, K. S. Docherty, P. F. DeCarlo, A. C. Aiken, Q. Chen, S. T. Martin, D. K. Farmer, P. Artaxo, A simplified description of the evolution of organic aerosol composition in the atmosphere. *Geophys. Res. Lett.* **2010**, *37*, L08803. doi:10.1029/2010GL042737
- [31] N. L. Ng, M. R. Canagaratna, J. L. Jimenez, P. S. Chhabra, J. H. Seinfeld, D. R. Worsnop, Changes in organic aerosol composition with aging inferred from aerosol mass spectra. *Atmos. Chem. Phys.* **2011**, *11*, 6465. doi:10.5194/ACP-11-6465-2011
- [32] E. S. C. Kwok, R. Atkinson, Estimation of hydroxyl radical reaction rate constants for gas-phase organic compounds using a structure-reactivity relationship: an update. *Atmos. Environ.* **1995**, *29*, 1685. doi:10.1016/1352-2310(95)00069-B
- [33] S. H. Kessler, T. Nah, K. E. Daumit, J. D. Smith, S. R. Leone, C. E. Kolb, D. R. Worsnop, K. R. Wilson, J. H. Kroll, OH initiated heterogeneous aging of highly oxidized organic aerosol. *J. Phys. Chem. A* **2012**, *116*, 6358. doi:10.1021/JP212131M
- [34] A. T. Lambe, M. A. Miracolo, C. J. Hennigan, A. L. Robinson, N. M. Donahue, Effective rate constants and uptake coefficients for the reactions of organic molecular markers (*n*-alkanes, hopanes and steranes) in motor oil and diesel primary organic aerosols with OH radicals. *Environ. Sci. Technol.* **2009**, *43*, 8794. doi:10.1021/ES901745H
- [35] N. M. Donahue, A. L. Robinson, E. R. Trump, I. Riipinen, J. H. Kroll, Volatility and aging of atmospheric organic aerosols. *Top. Curr. Chem.*, in press. doi:10.1007/128-2012-355
- [36] N. M. Donahue, A. L. Robinson, K. E. Huff Hartz, A. M. Sage, E. A. Weitkamp, Competitive oxidation in atmospheric aerosols: the case for relative kinetics. *Geophys. Res. Lett.* **2005**, *32*, L16805. doi:10.1029/2005GL022893
- [37] A. L. Robinson, N. M. Donahue, W. F. Rogge, Photochemical oxidation and changes in molecular composition of organic aerosol in the regional context. *J. Geophys. Res. – Atmos.* **2006**, *111*, D03302. doi:10.1029/2005JD006265
- [38] E. A. Weitkamp, A. T. Lambe, N. M. Donahue, A. L. Robinson, Laboratory measurements of the heterogeneous oxidation of condensed-phase organic molecular markers for motor vehicle exhaust. *Environ. Sci. Technol.* **2008**, *42*, 7950. doi:10.1021/ES800745X
- [39] B. Ervens, B. J. Turpin, R. J. Weber, Secondary organic aerosol formation in cloud droplets and aqueous particles (aqSOA): a review of laboratory, field and model studies. *Atmos. Chem. Phys.* **2011**, *11*, 11 069. doi:10.5194/ACP-11-11069-2011
- [40] Y. Tan, Y. B. Lim, K. E. Altieri, S. P. Seitzinger, B. J. Turpin, Mechanisms leading to oligomers and SOA through aqueous photo-oxidation: insights from OH radical oxidation of acetic acid and methylglyoxal. *Atmos. Chem. Phys.* **2012**, *12*, 801. doi:10.5194/ACP-12-801-2012
- [41] D. Hoffmann, A. Tilgner, Y. Iinuma, H. Herrmann, Atmospheric stability of levoglucosan: a detailed laboratory and modelling study. *Environ. Sci. Technol.* **2010**, *44*, 694. doi:10.1021/ES902476F
- [42] A. A. May, R. Saleh, C. J. Hennigan, N. M. Donahue, A. L. Robinson, Volatility of organic molecular markers used for source apportionment analysis: measurements and atmospheric implications. *Environ. Sci. Technol.* **2012**, *46*, 12 435. doi:10.1021/ES302276T
- [43] C. J. Hennigan, A. P. Sullivan, J. Jeffrey, L. Collett, A. L. Robinson, Levoglucosan stability in biomass burning particles exposed to hydroxyl radicals. *Geophys. Res. Lett.* **2010**, *37*, L09806. doi:10.1029/2010GL043088
- [44] L. Hildebrandt, E. Kostenidou, V. A. Lanz, A. S. H. Prévôt, U. Baltensperger, N. Mihalopoulos, A. Laaksonen, N. M. Donahue, S. N. Pandis, Sources and atmospheric processing of organic aerosol in the Mediterranean: insights from aerosol mass spectrometer factor analysis. *Atmos. Chem. Phys.* **2011**, *11*, 12 499. doi:10.5194/ACP-11-12499-2011
- [45] A. A. Presto, N. M. Donahue, Investigation of  $\alpha$ -pinene + ozone secondary organic aerosol formation at low total aerosol mass. *Environ. Sci. Technol.* **2006**, *40*, 3536. doi:10.1021/ES052203Z
- [46] B. N. Murphy, N. M. Donahue, C. Fountoukis, M. Dall'Osto, C. O'Dowd, A. Kiendler-Scharr, S. N. Pandis, Functionalization and fragmentation during ambient organic aerosol aging: application of the 2-D volatility basis set to field studies. *Atmos. Chem. Phys.* **2012**, *12*, 10 797. doi:10.5194/ACP-12-10797-2012
- [47] N. M. Donahue, K. M. Henry, T. F. Mentel, A. K. Scharr, C. Spindler, B. Bohn, T. Brauers, H. P. Dorn, H. Fuchs, R. Tillmann, A. Wahner, H. Saathoff, K. H. Naumann, O. Möhler, T. Leisner, L. Müller, M.-C. Reinnig, T. Hoffmann, K. Salow, M. Hallquist, M. Frosch, M. Bilde, T. Tritscher, P. Barmet, A. P. Praplan, P. F. DeCarlo, J. Dommen, A. S. H. Prévôt, U. Baltensperger, Aging of biogenic secondary organic aerosol via gas-phase OH radical reactions. *Proc. Natl. Acad. Sci. USA* **2012**, *109*, 13 503. doi:10.1073/PNAS.1115186109
- [48] K. M. Wagstrom, S. N. Pandis, Determination of the age distribution of primary and secondary aerosol species using a chemical transport model. *J. Geophys. Res. – Atmos.* **2009**, *114*, D14303. doi:10.1029/2009JD011784
- [49] H. Berresheim, C. Plass-Dulmer, T. Elste, N. Mihalopoulos, F. Rohrer, OH in the coastal boundary layer of Crete during MINOS: measurements and relationship with ozone photolysis. *Atmos. Chem. Phys.* **2003**, *3*, 639. doi:10.5194/ACP-3-639-2003
- [50] L. Hildebrandt, E. Kostenidou, B. H. Lee, N. Mihalopoulos, D. R. Worsnop, N. M. Donahue, S. N. Pandis, Formation of low-volatility oxygenated organic aerosol in the atmosphere: insights from the Finokalia Aerosol Measurement Experiments. *Geophys. Res. Lett.* **2010**, *37*, L23801. doi:10.1029/2010GL045193

# Introductory lecture: Atmospheric organic aerosols: insights from the combination of measurements and chemical transport models

Spyros N. Pandis,<sup>\*a</sup> Neil M. Donahue,<sup>b</sup> Benjamin N. Murphy,<sup>b</sup> Ilona Riipinen,<sup>c</sup> Christos Fountoukis,<sup>d</sup> Eleni Karnezi,<sup>b</sup> David Patoulias<sup>a</sup> and Ksakousti Skyllakou<sup>a</sup>

Received 24th August 2013, Accepted 28th August 2013

DOI: 10.1039/c3fd00108c

The formation, atmospheric evolution, properties, and removal of organic particulate matter remain some of the least understood aspects of atmospheric chemistry despite the importance of organic aerosol (OA) for both human health and climate change. Here, we summarize our recent efforts to deal with the chemical complexity of the tens of thousands of organic compounds in the atmosphere using the volatility–oxygen content framework (often called the 2D-Volatility Basis Set, 2D-VBS). Our current ability to measure the ambient OA concentration as a function of its volatility and oxygen to carbon (O : C) ratio is evaluated. The combination of a thermodenuder, isothermal dilution and Aerosol Mass Spectrometry (AMS) together with a mathematical aerosol dynamics model is a promising approach. The development of computational modules based on the 2D-VBS that can be used in chemical transport models (CTMs) is described. Approaches of different complexity are tested against ambient observations, showing the challenge of simulating the complex chemical evolution of atmospheric OA. The results of the simplest approach describing the net change due to functionalization and fragmentation are quite encouraging, reproducing both the observed OA levels and O : C in a variety of conditions. The same CTM coupled with source-apportionment algorithms can be used to gain insights into the travel distances and age of atmospheric OA. We estimate that the average age of OA near the ground in continental locations is 1–2 days and most of it was emitted (either as precursor vapors or particles) hundreds of kilometers away. Condensation of organic vapors on fresh particles is critical for the growth of these new particles to larger sizes and eventually to cloud condensation nuclei (CCN) sizes. The semivolatile organics currently simulated by CTMs are too volatile to condense on these tiny particles with high curvature. We show that chemical aging reactions converting these semivolatile

<sup>a</sup>Department of Chemical Engineering, University of Patras, Patra, Greece. E-mail: [spyros@chemeng.upatras.gr](mailto:spyros@chemeng.upatras.gr); Tel: +30-2610-969510

<sup>b</sup>Carnegie Mellon University, Pittsburgh, Pennsylvania, USA

<sup>c</sup>Stockholm University, Stockholm, Sweden

<sup>d</sup>FORTH, Patra, Greece

compounds to extremely low volatility compounds can explain the observed growth rates of new particles in rural environments.

## 1 Introduction

In the past 20 years ambient air pollution, most notably particulate matter (PM), has come to be recognized as a risk factor contributing to declines in respiratory and cardiovascular health<sup>1,2</sup> and increased risk of acute morbidity and mortality.<sup>3–5</sup> At the same time, atmospheric aerosol particles influence the Earth's radiation balance directly by scattering and absorbing solar radiation, and indirectly by acting as CCN. The role of these particles in the energy balance of our planet is one of the major uncertainties in the global change problem.<sup>6</sup>

Organic compounds are important components of atmospheric fine particles (PM<sub>2.5</sub>, particles < 2.5 μm in diameter). Throughout the troposphere they constitute roughly half of the PM<sub>2.5</sub> mass, residing mostly on accumulation mode particles.<sup>7</sup> However, while the inorganic fraction of PM<sub>2.5</sub> is relatively well understood, significant uncertainty limits our understanding of almost all aspects of OA, including its sources, atmospheric transformation, and fate.

OA has been traditionally viewed as a relatively inert, non-volatile mixture of compounds from numerous primary sources (primary organic aerosol, POA), coated by secondary compounds derived from gas-phase oxidation of volatile precursors (secondary organic aerosol, SOA).<sup>8</sup> The chemical complexity of the OA (there are thousands or even tens of thousands of complex large organic compounds in typical ambient aerosol),<sup>9</sup> its unknown chemical composition (less than 20% of the OA mass has been quantified even by the best studies),<sup>10</sup> the unknown physical and chemical properties of the majority of the known OA components, and the difficulty of describing mathematically such a complex system in atmospheric CTMs have seriously limited scientific progress in both the air quality and climate change areas. CTMs in both regional and global scales are often not able to reproduce the observed OA levels, their chemical characteristics (degree of oxidation), their diurnal variation, *etc.*<sup>11,12</sup> As a result, we are currently unable to accurately evaluate the effects of different strategies of reduction of OA concentrations in polluted areas and to quantify the effect of OA on the energy balance of the planet.

Recent work<sup>13</sup> has changed the above picture of OA. Most of the emitted organic particulate matter from combustion sources like transportation, biomass burning, *etc.* evaporates after emission. The resulting semi-volatile organic vapors can then react in the gas phase with the hydroxyl radical, OH, and other atmospheric oxidants forming low volatility oxidation products that can recondense to the particulate phase in timescales of several hours or even days. This evaporation/reaction/condensation process causes significant changes to the chemical nature of primary OA (it becomes highly oxygenated), its size distribution, its distribution in space and its physical and chemical properties. The resulting products will probably have quite different health effects than the original compounds. This theory can explain why the aerosol in large urban centers is dominated by oxygenated compounds (Oxygenated Organic Aerosol, OOA) and not hydrocarbon-like OA (HOA).<sup>14</sup>

Similar challenges exist in our efforts to understand secondary OA. Initially the SOA precursors were assumed to form practically non-volatile SOA with a constant yield.<sup>15</sup> This description is actually still used in most climate models.<sup>12</sup> The next step was to assume the production of two surrogate products that form a pseudo-ideal solution (Odum *et al.*, 1996).<sup>16</sup> This approach is used currently by the majority of the available regional CTMs. However, the resulting models fail to reproduce observed OA concentrations in the US, Europe, Asia, *etc.*, especially in periods (warm sunny summer days) when SOA is expected to be the dominant OA component. Potential gaps in understanding include homogeneous reactions of the SOA vapors,<sup>17</sup> heterogeneous reactions (oxidation of the organics in the particulate phase,<sup>18</sup> oligomerization,<sup>19</sup> the role of NO<sub>x</sub> and UV levels in the formation of SOA, *etc.* These processes are not well understood and are not included explicitly in most CTMs.

Our existing mental model of OA (primary and secondary) is insufficient to describe the thousands of semivolatile organic compounds, moving between the gas and particulate phases, continuously reacting, generating even more organic products, and interacting with each other and the inorganic compounds, including water, in the particulate phase. This results in problems with source apportionment (quantification of the OA sources) and also predicting the response of OA during potential changes in emissions of anthropogenic pollutants. Significant uncertainties in the role of the organics in the formation and growth of new particles to cloud condensation nuclei remain. Efforts to approach the problem at the individual compound level have had limited success. Each organic compound has its own complex behavior that is difficult to extrapolate and the study of each one of them requires a few person-years.

It is clear that we need a robust framework on which to place past and future measurements in both the lab and the field so that we can then use these results in CTMs. Our efforts to develop and apply this framework are summarized in the following sections of this paper.

## 2 The 2-D volatility–oxygen content framework

Describing the chemical complexity of ambient OA in chemical transport models requires the simplification of the system to its most important dimensions. One of the promising ways to map this chemical space with tens of thousands of dimensions to a manageable space is using as dimensions the volatility and oxygen content of the OA (expressed as the O : C ratio)<sup>20</sup> (Fig. 1). The volatility determines the partitioning of the OA compounds between the gas and particulate phases and also the ability of a molecule to participate in the formation of new particles. The oxygen content of organic particles is directly connected to their ability to absorb water and act as cloud condensation nuclei (CCN). Our hypothesis is that we can capture the most essential elements of the OA system using these two dimensions. The corresponding challenges are to find ways to easily experimentally characterize OA in these two dimensions, describe the corresponding processes in this coordinate system, and then translate all of this into computational modules that can be used in the existing CTMs. Obviously, OA will have a distribution of volatilities and distribution of O : C ratios so we will need to work with these distributions and not just the average values.

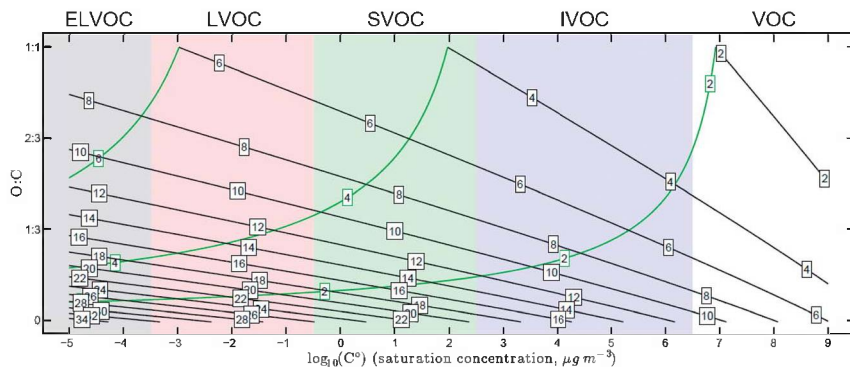


**Fig. 1** The 2D Volatility Basis Set space with the volatility (expressed as the logarithm of the saturation concentration) as the x-axis and the O : C ratio as the y-axis (based on Fig. 4 of Donahue *et al.*<sup>21</sup>). The black isopleths are the number of carbon atoms and the green isopleths the number of oxygen atoms.

The organic compounds can be separated in five groups by volatility (Fig. 1):

(i) *Extremely Low Volatility Organic Compounds* (ELVOCs with  $C^* < 3.2 \times 10^{-4} \mu\text{g m}^{-3}$ , volatility bins  $10^{-4} \mu\text{g m}^{-3}$ ,  $10^{-5} \mu\text{g m}^{-3}$ , *etc.*). These compounds, if created by gas-to-particle conversion processes, can be very important for the formation and growth of new particles created *in situ* in the atmosphere by nucleation.

(ii) *Low Volatility Organic Compounds* (LVOCs, with  $3.2 \times 10^{-4} \mu\text{g m}^{-3} < C^* < 3.2 \times 10^{-1} \mu\text{g m}^{-3}$ , volatility bins  $10^{-3}$ ,  $10^{-2}$  and  $10^{-1} \mu\text{g m}^{-3}$ ). These compounds are in the particulate phase in typical atmospheric concentration levels.

(iii) *Semi Volatile Organic Compounds* (SVOCs, with  $3.2 \times 10^{-1} \mu\text{g m}^{-3} < C^* < 3.2 \times 10^2 \mu\text{g m}^{-3}$ , volatility bins 1, 10 and  $100 \mu\text{g m}^{-3}$ ). The corresponding compounds exist in both the gas and particulate phases under typical ambient conditions.

(iv) *Intermediate Volatility Organic Compounds* (IVOCs, with  $3.2 \times 10^2 \mu\text{g m}^{-3} < C^* < 3.2 \times 10^6 \mu\text{g m}^{-3}$ , volatility bins  $10^3$ ,  $10^4$ ,  $10^5$  and  $10^6 \mu\text{g m}^{-3}$ ). These exist in the gas phase in the atmosphere but can be easily converted to condensible compounds producing secondary organic aerosol.

(v) *Volatile Organic Compounds* (VOCs, with  $C^* > 3.2 \times 10^6 \mu\text{g m}^{-3}$ ). Most of the emissions of gas-phase organics fall in this traditional category.

This grouping facilitates discussion of the vast array of atmospheric organic compounds.

The O : C of atmospheric organic compounds varies from 0 (for hydrocarbons) to 2 (for carbon dioxide, oxalic acid, *etc.*). However, there are few organic compounds with O : C exceeding unity. Donahue *et al.*<sup>21</sup> used group contribution methods to determine the mean chemical properties of the compounds in this 2-D VBS showed in Fig. 1. They argued that the compounds in the space shown have 0–8 oxygens.

Donahue *et al.*<sup>22</sup> and Kroll *et al.*<sup>23</sup> have suggested that the average oxidation state of carbon, OSc, may be used as the principal y-axis of the 2D-VBS. In practice, the O : C and OSc are highly correlated allowing their use almost interchangeably. In this work we will use the O : C as the preferred axis.

### 3 Measurement of OA in the 2D-VBS

Measurement of the OA in this framework requires the measurement of the OA concentration distribution as a function of volatility and O : C content. Measuring the OA volatility distribution or the OA O : C content distributions on their own is challenging. Some recent efforts are described in the following sections.

#### 3.1 Measurement of the volatility distribution

The most commonly used technique for the measurement of the OA volatility is the use of a thermodenuder (TD) together with a technique for the measurement of the OA concentration. Thermodenuders heat the aerosol sample to a fixed temperature, allow the particles to evaporate, remove the organic vapors from the sample stream and cool the sample back to ambient temperature.<sup>24–26</sup> Their result is the mass fraction remaining (MFR) of the OA as a function of temperature (Fig. 2). While the MFR provides some qualitative information about the volatility of the OA (the further the MFR curve is to the right the lower the volatility of the OA), it generally depends not only on the volatility of the OA and the characteristics of the TD but also on the mass concentration of the OA, its size distribution, the enthalpies of evaporation of the OA components and any mass transfer delays in the evaporation of the particles.<sup>27</sup>

Estimation of the volatility distribution of the OA requires combination of the thermodenuder MFR with a model describing the OA evaporation. Fitting of the model predictions to the MFR measurements allows estimation of the OA volatility distribution and the other unknown parameters (enthalpies, resistances in mass transfer other than gas-phase diffusion). Given the nature of the MFR curve (a monotonically decreasing curve going from one to zero, almost always with a roughly sigmoidal shape) and the multiple unknown parameters there can be multiple “good” solutions to the problem. For example, Fig. 2 shows the predicted thermograms (MFR *versus* temperature) for two organic aerosols with very

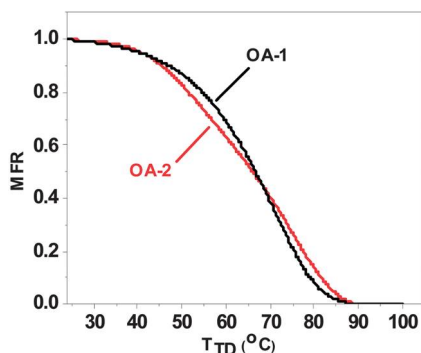


**Fig. 2** Predicted thermograms (MFR *versus*  $T_{TD}$ ) for OA with different properties. A single component aerosol OA-1 (effective saturation concentration  $C^* = 1 \mu\text{g m}^{-3}$ , enthalpy of vaporization  $\Delta H_{vap} = 80 \text{ kJ mol}^{-1}$  and effective mass accommodation coefficient  $a_m = 1$ ) gives practically the same thermogram as one with a multi component aerosol OA-2 (consisting of 50%  $C^* = 0.1 \mu\text{g m}^{-3}$ , 25%  $1 \mu\text{g m}^{-3}$ , 25%  $10 \mu\text{g m}^{-3}$ ,  $\Delta H_{vap} = 150 \text{ kJ mol}^{-1}$  and  $a_m = 0.05$ ).

different properties. Any reasonable experimental error in the measurements will make them practically indistinguishable.

Karnezi *et al.*<sup>28</sup> proposed an algorithm for the estimation of the volatility distribution from the TD measurements and the corresponding uncertainty. They argued that in a lot of cases the uncertainty of the estimated volatility distributions is quite high. Fig. 3a depicts a theoretically predicted thermogram and pseudo-measurements constructed by the addition of random experimental error to these predictions. The results of the parameter estimation using just these measurements are shown in Fig. 3b, together with the correct volatility distribution. The estimated volatility distribution is quite uncertain and the best guess has the wrong shape.

Karnezi *et al.*<sup>28</sup> investigated a number of ways to improve the accuracy of the volatility distribution. These included additional measurements, measurements at multiple residence times, *etc.* The best approach, based on their analysis, was the performance of isothermal dilution measurements (Fig. 3c) in a small smog chamber together with the thermodenuder measurements. Isothermal dilution has the advantage that it produces results that do not depend on the enthalpy of evaporation, while the use of a small chamber allows access to much longer

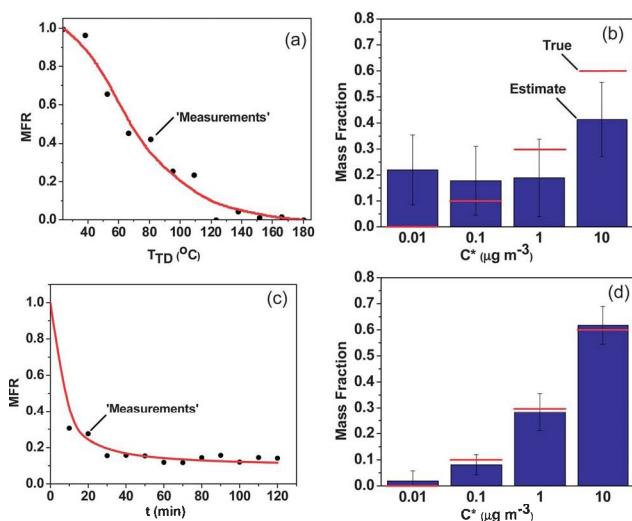


**Fig. 3** (a) The red line is the thermogram corresponding to the true properties of the aerosol (consisting of 10%  $C^* = 0.1 \mu\text{g m}^{-3}$ , 30%  $1 \mu\text{g m}^{-3}$ , 60%  $10 \mu\text{g m}^{-3}$ ,  $\Delta H_{\text{vap}} = 50 \text{ kJ mol}^{-1}$  and  $a_m = 1$ ) and the black dots correspond to the 'measured' MFR versus  $T_{\text{TD}}$  for the aerosol. (b) Estimated and true volatility distribution, using TD measurements, for an OA (consisting of 10%  $C^* = 0.1 \mu\text{g m}^{-3}$ , 30%  $1 \mu\text{g m}^{-3}$ , 60%  $10 \mu\text{g m}^{-3}$ ,  $\Delta H_{\text{vap}} = 50 \text{ kJ mol}^{-1}$  and  $a_m = 1$ ). The error bars represent the uncertainty of the estimated value. The vaporization enthalpy was estimated with a value equal to  $91 \text{ kJ mol}^{-1}$  and the accommodation coefficient with a value equal to 0.44. (c) Isothermal dilution measurements (MFR as function of time). The red line corresponds to the aerosol consisting of 10%  $C^* = 0.1 \mu\text{g m}^{-3}$ , 30%  $1 \mu\text{g m}^{-3}$ , 60%  $10 \mu\text{g m}^{-3}$ ,  $\Delta H_{\text{vap}} = 50 \text{ kJ mol}^{-1}$  and  $a_m = 1$  and the black dots correspond to the 'measured' MFR versus time. (d) Estimated and true volatility distribution, combining TD and isothermal dilution measurements, for an OA (consisting of 10%  $C^* = 0.1 \mu\text{g m}^{-3}$ , 30%  $1 \mu\text{g m}^{-3}$ , 60%  $10 \mu\text{g m}^{-3}$ ,  $\Delta H_{\text{vap}} = 50 \text{ kJ mol}^{-1}$  and  $a_m = 1$ ). The error bars represent the uncertainty of the estimated value. The vaporization enthalpy was estimated to be equal to  $50 \text{ kJ mol}^{-1}$  and the accommodation coefficient with a value equal to 0.88.

timescales than a thermodenuder. Combination of the information of the two methods produced in most cases an accurate volatility distribution with modest uncertainty (Fig. 3d).

One of the major potential problems in thermodenuder-based estimates of the OA volatility distribution is the potential for chemical changes to the organic aerosol compounds during their heating to high temperatures. Comparisons of the AMS spectra of the remaining OA at the same MFR with that of isothermal dilution experiments can provide a valuable test of the validity of the thermodenuder measurements. Based on our existing measurements, problems may start to arise at temperatures over 150 °C in thermodenuders.

### 3.2 Measurement of the O : C

The OA O : C can be measured with a High Resolution AMS (HR-AMS) using the detailed mapping of the AMS spectrum to fragments of organic molecules. However, the AMS provides on its own only the average O : C of the OA and not a distribution. There may be compounds with much higher and much lower O : C compared to the average in the sampled aerosol. Some information about the O : C distribution, but not the actual distribution, can be obtained by combination of the AMS with a thermodenuder.<sup>29</sup> This can allow the estimation of the average O : C of each volatility bin in the VBS framework.

Despite the high-resolution of the mass spectra and the corresponding information there are uncertainties in the measured O : C due to the uncertainty introduced by the need to separate the water from the dehydration of the organic molecules from the water vapor from the ambient air, *etc.*

### 3.3 Combination of physical and chemical characteristics

The combination of the rich dataset that the AMS spectra provide with a factor analysis technique (Positive Matrix Factorization or PMF)<sup>30</sup> can provide additional insights into the sources and processing of ambient OA that can be mapped onto the 2D-VBS. PMF can separate the fresh primary organic aerosol from hydrocarbon combustion sources like transportation (Hydrocarbon-like OA or HOA), the relatively oxygenated OA from biomass combustion (BBOA), and the oxygenated OA (OOA) (Fig. 4).

PMF often results in two OOA types, one of moderate oxygen content that correlates with semivolatile inorganic PM components and has been named semivolatile-OOA (SV-OOA) and one of higher oxygen content that correlates with low volatile components like sulfates (LV-OOA). The significance of these OOA types is still under debate. They could represent different aerosol types (*e.g.*, from different precursors or chemical pathways) or they could be the two extremes of the oxidation of OA observed in the corresponding study.

PMF can be performed in measurements of a thermodenuder-AMS combination, providing in this way thermograms of the corresponding aerosol types. These thermograms can then be used (as discussed in Section 3.1) together with a thermodenuder model to estimate the volatility distribution of each aerosol type and place them in the 2D-VBS space (Fig. 4). While this still does not provide a full 2D-VBS distribution due to our inability to measure the O : C distribution, it does provide a rich characterization of the ambient OA in the corresponding space. These measurements can be used both to provide insights about the sources and

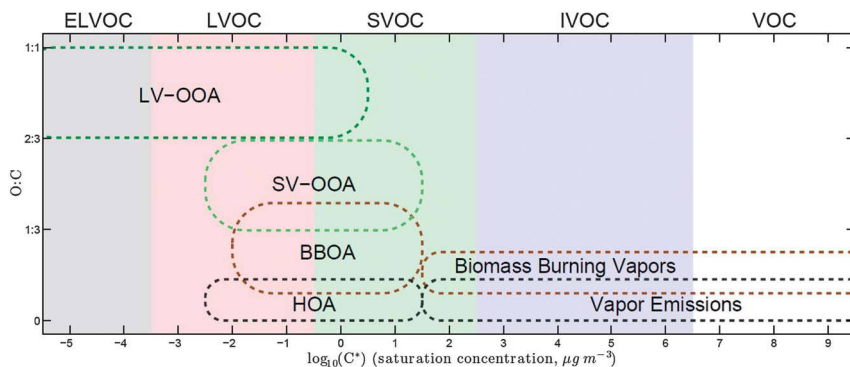


**Fig. 4** Volatility and O : C ratio for atmospheric organic compounds. The volatility ranges discussed in the text (ELVOC, LVOC, SVOC, IVOC and VOC) are indicated by colour bands. Also shown are the approximate locations of factors (HOA, BBOA, SV-OOA, and LV-OOA) estimated from the PMF analysis of ambient OA mass spectra together with the locations of primary emissions of biomass burning vapors and other organic vapour emissions.

processing of ambient OA and also to test our understanding during the evaluation of chemical transport models.

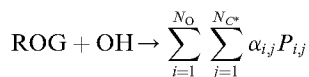
## 4 Simulation of OA in the 2D-VBS

Application of the 2D-VBS in CTMs requires discretization of the volatility–oxygen content space into bins. Murphy *et al.*<sup>31</sup> used 12 logarithmically spaced bins along the axis of effective saturation concentration ( $C^* = 10^{-5}$  to  $10^6 \mu\text{g m}^{-3}$  at 300 K). They included, therefore, ELVOCs, LVOCs, SVOCs and IVOCs in the system while they simulated the VOCs explicitly using the SAPRC gas-phase chemistry mechanism. The 0.0 to 1.2 O : C range was simulated using 13 bins spaced by 0.1. The 2D-VBS was therefore discretized using 156 bins.

Emissions of primary organic aerosol (LVOCs, SVOCs and IVOCs) were assumed to have an O : C of 0.1 and to have a volatility distribution based on the available measurements.<sup>32</sup> The first generation products of anthropogenic and biogenic VOCs were assumed to have volatility distributions consistent with the available smog chamber studies and a volatility dependent O : C ratio based on the literature.<sup>33–36,29</sup> More details can be found in Murphy *et al.*<sup>37,31</sup>

### 4.1 Combining functionalization and fragmentation

One of the major features of the 2D-VBS is its ability to describe the multiple generations of reactions of the first generation products of the VOCs as well as the SVOCs and IVOCs. Murphy *et al.*<sup>31</sup> focused on the gas-phase oxidation of these compounds by the hydroxyl radical, OH. After the unique first-generation step, we hypothesize that aging by reaction with OH can be written as follows:



where ROG is a specific reactive organic gas and  $\alpha_{i,j}$  is the stoichiometric yield of the product,  $P_{i,j}$  with  $i$  oxygen atoms added relative to the organic gas parent and

experiences a change in volatility by  $j$  volatility bins relative to the parent.  $N_{C^*}$  is the total number of volatility intervals. The number of oxygen atoms added per generation of oxidation,  $i$ , will vary depending on the particular chemical pathway followed. Murphy *et al.*<sup>31</sup> following the analysis of Donahue *et al.*<sup>21</sup> adopted the functionalization scheme shown in Fig. 5. The transformation must be mapped from the kernel, which describes the number of added oxygens, to the y-axis of the 2D-VBS, which is O : C. Each point in the 2D-VBS has a different average carbon number<sup>21</sup> and thus will inform the translation from number of added oxygen atoms to change in O : C.<sup>37</sup> In this scheme all OA components (anthropogenic and biogenic) were allowed to age chemically.

Fragmentation takes place at the same time as functionalization. Murphy *et al.*,<sup>31</sup> following the analysis of Donahue *et al.*,<sup>21</sup> assumed that the O : C of the larger fragments will be similar to the O : C of the reactant compounds. As a result these fragments will move directly to the right in the 2D-VBS space, increasing in volatility but not in O : C. The smallest fragments will have a much larger O : C than the reactant. Murphy *et al.*<sup>31</sup> assigned mass in all of the volatility bins to the right of the midpoint (from the reactant volatility bin to the highest modeled bin) O : C values that move diagonally towards the highest modeled O : C. The fragmentation branching ratio was parameterized following Donahue *et al.*<sup>22</sup> as:  $\beta_{\text{frag}} = (\text{O} : \text{C})^{(1/6)}$ . Based on this dependence on O : C, compounds with O : C exceeding 0.4 will most likely fragment.

This scheme was tested in a Lagrangian CTM against measurements collected during the EUCAARI campaigns using AMS measurements from Finokalia (Greece), Cabauw (Netherlands) and Mace Head (Ireland) during the summer of 2008 and winter of 2009. The resulting model tended to underpredict the OA during the summer (average fractional bias = -0.13 and average fractional error = 0.17) in all sites while during the winter it overpredicted OA concentration in Cabauw and Mace Head (average fractional bias = 0.59 and average fractional error = 0.61) and underpredicted in Finokalia (average fractional bias = -0.34 and average fractional error = 0.34). While this performance for OA mass concentration is encouraging the scheme seriously underpredicted the O : C in all locations in both seasons (average fractional bias = -0.56 and average fractional error = 0.56). The scheme drives the OA components to much lower volatility rapidly, after one or may be two oxidation steps (Fig. 5) and the corresponding

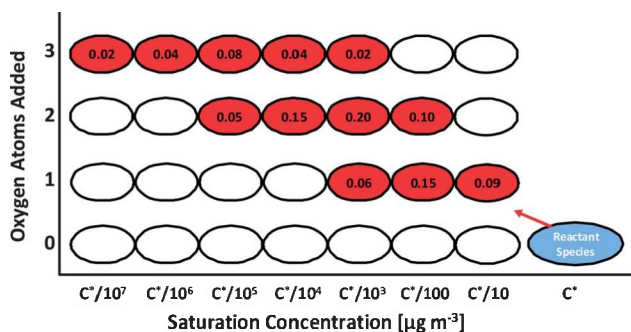


**Fig. 5** Functionalization scheme in the 2D-VBS proposed by Murphy *et al.*<sup>31</sup> The numbers in the red circles are the yields of the corresponding products.

compounds move almost completely to the particulate phase. While in the particulate phase they are protected to a large extent from attacks by  $\text{OH}^{38}$  and additional oxidation and therefore their O : C does not increase further. Fragmentation reduces the OA concentration, balancing to some extent the significant increases caused by this relatively aggressive functionalization scheme, but it does not increase the corresponding O : C.

This detailed functionalization/fragmentation scheme of Murphy *et al.*<sup>31</sup> had encouraging performance but additional improvements are needed so that it can capture the evolution of OA.

## 4.2 A simple scheme

Murphy *et al.*,<sup>31,37</sup> recognizing the challenges of capturing the complexities of fragmentation and functionalization, proposed a simple aging scheme for the 2D-VBS to capture the net change of the aging OA volatility–O : C distribution. This scheme outlined in Fig. 6 assumes that the net change caused by the various processes is a reduction of the average volatility by a factor of 10 and the addition of one oxygen atom for half the products and two for the other half. This scheme is an extension of the 1D-VBS having the same volatility reduction rate during the gas-phase reactions with OH (a rate constant of  $1 \times 10^{-11} \text{ cm}^3 \text{ molec}^{-1} \text{ s}^{-1}$  for anthropogenic SOA and  $4 \times 10^{-11} \text{ cm}^3 \text{ molec}^{-1} \text{ s}^{-1}$  for the products of anthropogenic IVOCs and SVOCs). Murphy *et al.*<sup>31,37</sup> assumed that for biogenic SOA the aging resulted in an increase in O : C but no net change in volatility.

The evaluation of this simple scheme against the EUCAARI measurements was surprisingly good. The model reproduced the summer OA concentration measurements in all sites well (average fractional bias = 0.33 and average fractional error = 0.25) and had a tendency towards overprediction in the winter (average fractional bias = 0.47 and average fractional error = 0.52). It did quite well in reproducing the O : C observations in all sites during both seasons (average fractional bias = 0.01 and average fraction error = 0.18). This suggests that this simple scheme appears to capture the net impact of chemical aging on the OA concentration and O : C ratio, at least for the specific conditions of the EUCAARI dataset. It clearly represents an oversimplification of what is actually taking place, but it can still provide useful guidance for the development of future 2D-VBS aging schemes.

## 4.3 The road forward

The above examples illustrate the efforts to translate our limited understanding of the OA evolution to practical computational schemes for the simulation of atmospheric OA. Even if these schemes are at their infancy, they already provide

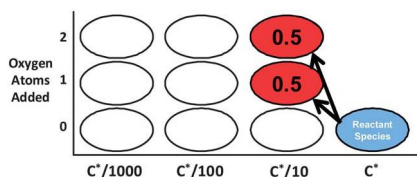


Fig. 6 Simple aging parameterization proposed by Murphy *et al.*<sup>37</sup>

encouraging results. Future steps should involve more detailed evaluation and constraining of these schemes with ambient observations not only of the OA concentration and the O : C but also the OA volatility distribution, laboratory studies of the chemical aging of anthropogenic and biogenic SVOCs, IVOCs, and subsequent analysis of the results using this modeling framework, and finally efforts to project detailed reaction schemes onto the 2D-VBS.

## 5 The age of OA

The OA in the atmosphere appears to reach a highly oxidized state (LV-OOA in Fig. 4). However, the time required for the transition from fresh POA, VOCs, or IVOCs to LV-OOA is uncertain. It is for sure less than the lifetime of particles in the atmosphere (estimated to be of the order of week). Wagstrom and Pandis<sup>39</sup> proposed an algorithm for the calculation of the age distribution of the different pollutants at a given place including OA and its components. The algorithm is based on the Particle Source Apportionment Technology (PSAT), a technique to follow material emitted from different sources inside a CTM.<sup>40</sup> The age of pollutants is calculated by defining as a “source” the emissions during specified time intervals (instead of the traditional use of source types or source areas). The simulation period is then discretized (say in periods of six hours) and PSAT calculates the contribution of the different temporal sources to the concentration of a pollutant in a given place and time. From these, the age distribution of the pollutant is calculated.

The average age of the OA at the ground level during a summertime period in the Eastern US is depicted in Fig. 7.

The age is based on the time of emission of either the corresponding particles or the precursor vapors. So the age includes the period required for the formation of secondary particulate matter. The average age varies from approximately a day in areas with significant emissions of VOCs to approximately three days in more

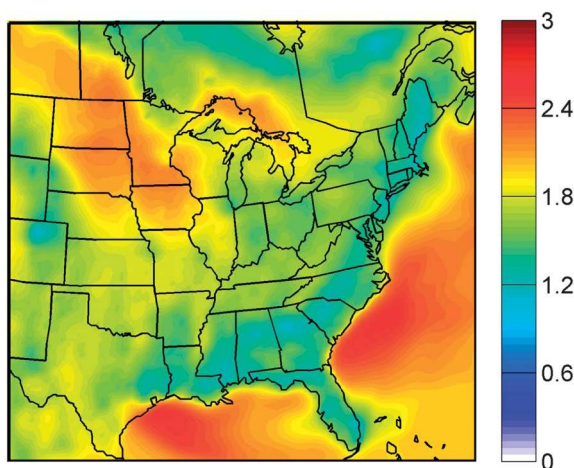


**Fig. 7** Estimated average age (days) of OA at the ground level during July. The estimates were made using PSAT and PMCAMx following the approach of Wagstrom and Pandis.<sup>39</sup> The OA was simulated using the VBS approach.

remote areas (e.g., over the ocean). It is significantly less than the average lifetime of particles as one would expect. These results strongly suggest that the conversion of material to OOA requires 1–2 days during the summertime.

### 5.1 Source–receptor relationships

The fact that a lot of the OA around us (even in major urban areas) has been in the atmosphere for a significant period of time suggests that a significant fraction of this PM has been emitted elsewhere. As an example, Skyllakou *et al.*<sup>41</sup> examined the contribution of different source areas to the OA in Paris, a megacity, during the summer. They classified the OA into three categories based on its origin: local sources referred to the contributions from the urban agglomeration (an area of around 50 km around the city center), mid-range those coming from distances between 50 and 500 km, and long range those coming from more than 500 km from Paris. Using PSAT they estimated the contributions shown in Fig. 8. While more than half of the fresh POA was local, both the anthropogenic and biogenic SOA came mostly from midrange sources, with significant contributions from long-range transport. For total OA, the local contribution was estimated to be quite small (around 10%), with half of the remaining OA coming from mid-range and the other half from long-range sources. These estimates were consistent with the highly oxygenated nature of OA measured during that period in the MEGA-POLI project<sup>42</sup> and estimates based on the small differences of OA concentrations in sites inside and around Paris.<sup>43</sup>

## 6 OA and ultrafine particles

Studies during the last decade have revealed that sulfuric acid plays a dominant role in the formation of new particles in the atmosphere by nucleation.<sup>44</sup> However, the growth of the fresh ultrafine particles to larger sizes in the boundary layer

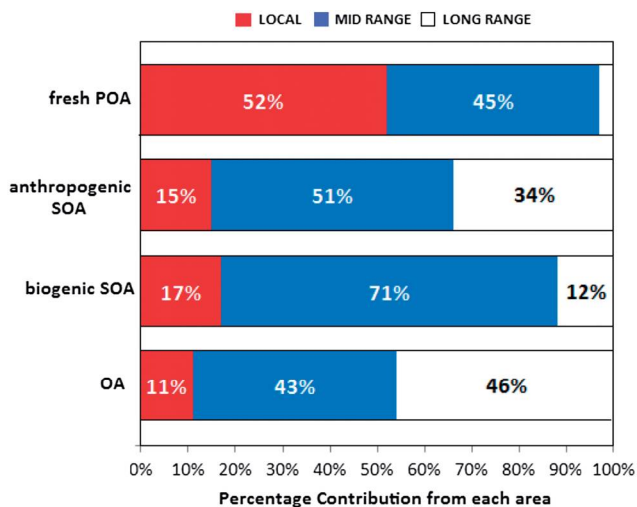


**Fig. 8** Percent contributions from each transport category (local, mid-range and long range) for different types of organic aerosol in Paris during the summer.

cannot be explained in most cases by condensation of sulfuric acid monomers alone.<sup>45</sup> Low volatility organics appear to be involved and to actually dominate the growth in periods of high biogenic activity. Exceptions to this are areas with high sulfur dioxide concentrations, like parts of the northeastern US.<sup>46</sup> However, the gas-phase organics simulated by current CTMs are in the SVOC volatility range. The curvature of the fresh particles (they are a few nanometers in diameter) together with the corresponding Kelvin effect makes condensation of these vapors on these fresh particles negligible and cannot explain the corresponding growth.

There have been a number of efforts to explain how organic vapors can help these nanometer size particles grow. Riipinen *et al.*<sup>45</sup> estimated that a significant fraction of the SOA produced (around 50%) should behave as if it were non-volatile. Something like that is, however, not compatible with the first-generation yields of SOA from biogenic precursors observed in the lab. The yields are quite low for low SOA concentrations. One potential explanation is that these ELVOCs are produced as second-generation products from the oxidation for SVOCs in the gas phase by OH.<sup>38</sup> To test this hypothesis we coupled the VBS approach with the DMAN particle dynamics model of Jung *et al.*<sup>47</sup> and evaluated it under typical nucleation conditions in Europe. We found, after a number of tests that a reaction converting the gas-phase fraction of the  $C^* = 1 \mu\text{g m}^{-3}$  to ELVOCs with  $C^* = 10^{-3} \mu\text{g m}^{-3}$  with a reasonable rate constant of  $1 \times 10^{-11} \text{ cm}^3 \text{ molec}^{-1} \text{ s}^{-1}$  (currently used in the VBS for secondary OA components) can explain the observations. The predicted growth of new particles for a typical nucleation event is shown in Fig. 9. The new particles grow to approximately 50 nm with an average growth rate of  $5 \text{ nm h}^{-1}$ .

The composition of the growing particles is shown in Fig. 10. In the beginning they consist mostly of ammonium sulfate and bisulfate as sulfuric acid and ammonia were the nucleating vapors in the simulation. However, the system soon runs out of sulfuric acid (most of the available sulfur dioxide has reacted) and organics are responsible for the growth of the particles to larger sizes. By the end of the day these new particles consist mostly of organic particulate matter. The organic material that is required for the corresponding growth is quite small, just  $30 \text{ ng m}^{-3}$ . Of course at the same time there is considerable condensation of

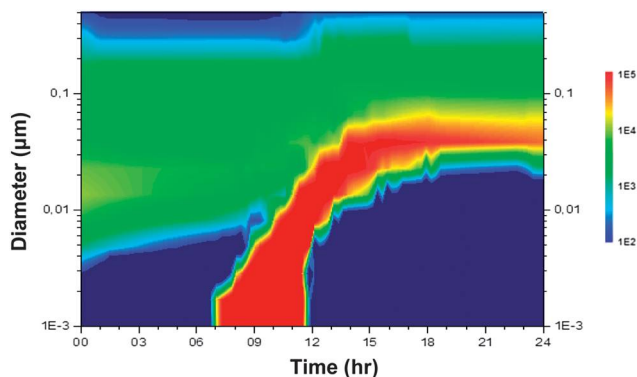


**Fig. 9** Predicted evolution of the aerosol number distribution (particles  $\text{cm}^{-3}$ ) for a typical nucleation event in Northern Europe.

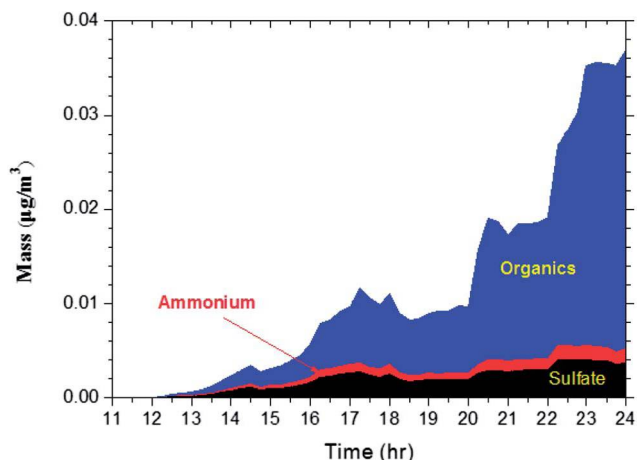


Fig. 10 Predicted chemical composition of the new particles formed during a nucleation event.

organic PM to the larger particles in the accumulation mode. The volatility distribution of the material condensing on the growing fresh particles is interesting. Less than half of this material is the ELVOCs produced from the assumed aging reaction. The other material is SVOCs that mix with these ELVOCs, accelerating in this way the overall growth rate.

## 7 Conclusions

Most of the OA that we are breathing, even in urban areas, has started its atmospheric life (as organic vapors or particles) a day or two ago in an area probably a few hundred kilometers away. Coupling of the available CTMs with source apportionment algorithms like PSAT used in this work suggest that the average age of the OA that we are breathing is 1–2 days and that its average transport distance is 300–1000 km depending on the conditions. This allows the OA to chemically age, become quite oxygenated and to have different properties from its original form.

The two dimensional volatility–oxygen content space can be a useful tool for the description of the behavior of atmospheric OA. Measurement of the OA distribution in this space is challenging, but there has been significant progress during the last decade. The combination of thermodenuder with isothermal volatility measurements, the AMS and the corresponding aerosol evaporation models is a promising approach for this measurement. The PMF analysis of the corresponding AMS measurements of the evaporating OA can also provide valuable information about the characterization of the OA in this two-dimensional space.

The evolution of the OA in the 2D-VBS can be included in the available CTMs. The existing first efforts are encouraging, showing the potential of these models to reproduce the observed OA concentrations and O:C levels. However, the best performing approach is still the simplest one, simulating only the net effect of functionalization and fragmentation processes. Additional studies of these

processes in the laboratory and mapping of the corresponding results in the 2D-VBS space is required to improve the corresponding models.

The low volatility and semivolatile components of ambient OA (LVOCs and SVOCs) are the most important for its mass concentration. However, the extremely low volatility components (ELVOCs) can be critical for the growth of new particles formed by nucleation and therefore for the CCN concentration. Ambient observations strongly indicate that the growth of new particles by organics is indeed taking place and can dominate the growth in environments with modest or low sulfur dioxide concentrations. Chemical aging reactions converting the SVOCs to ELVOCs through reactions with OH can explain the observed growth and are consistent with the available observations.

## Acknowledgements

This research was supported by the US Department of Energy and the FP7 IDEAS project ATMOPACS.

## References

- 1 C. A. Pope, *J. Aerosol Med.*, 2000, **13**, 335–354.
- 2 S. F. van Eeden, A. Yeung, K. Quinlam and J. C. Hogg, *Proc. Am. Thorac. Soc.*, 2005, **2**, 61–67.
- 3 D. W. Dockery, *Environ Health Perspect*, 2001, **109**(Suppl. 4), 483–486.
- 4 R. D. Brook, *et al.*, *Circulation*, 2004, **109**, 2655–2671.
- 5 K. A. Miller, *et al.*, *N. Engl. J. Med.*, 2007, **356**, 447–458.
- 6 IPCC, Intergovernmental Panel on Climate Change, *Climate Change 2007: The Scientific Basis*, Cambridge University Press, Cambridge, 2007.
- 7 J. H. Seinfeld and S. N. Pandis, *Atmospheric Chemistry and Physics: From Air Pollution to Climate Change*, J. Wiley, New York, 2nd edn, 2006.
- 8 N. M. Donahue, A. L. Robinson and S. N. Pandis, *Atmos. Environ.*, 2009, **43**, 97–109.
- 9 A. H. Goldstein and I. E. Galbally, *Environ. Sci. Technol.*, 2007, **41**, 1514–1521.
- 10 M. Hallquist, *et al.*, *Atmos. Chem. Phys.*, 2009, **9**, 5155–5236.
- 11 P. H. McMurry, M. F. Shepherd, and J. S. Vickery, *Particulate Matter Science for Policy Makers*, Cambridge University Press, Cambridge, 2004.
- 12 M. Kanakidou, *et al.*, *Atmos. Chem. Phys.*, 2005, **5**, 1053–1123.
- 13 A. L. Robinson, *et al.*, *Science*, 2007, **315**, 1259–1262.
- 14 Q. Zhang, *et al.*, *Geophys. Res. Lett.*, 2007, **34**, L13801.
- 15 S. N. Pandis, *et al.*, *Atmos. Environ.*, 1992, **26**, 2266–2282.
- 16 J. R. Odum, *et al.*, *Environ. Sci. Technol.*, 1996, **30**, 2580–2595.
- 17 M. Claeys, *et al.*, *Science*, 2004, **303**, 1173–1176.
- 18 Y. Rudich, *et al.*, *Annu. Rev. Phys. Chem.*, 2007, **58**, 321–352.
- 19 M. Kalberer, *et al.*, *Science*, 2004, **303**, 1659–1662.
- 20 J. L. Jimenez, *et al.*, *Science*, 2009, **326**, 1525–1529.
- 21 N. M. Donahue, *et al.*, *Atmos. Chem. Phys.*, 2011, **11**, 3303–3318.
- 22 N. M. Donahue, *et al.*, *Atmos. Chem. Phys.*, 2012, **12**, 615–634.
- 23 J. H. Kroll, *et al.*, *Nat. Chem.*, 2011, **3**, 133–139.
- 24 H. Burtscher, *et al.*, *J. Aerosol Sci.*, 2001, **32**, 427–442.
- 25 B. Wehner, *et al.*, *J. Aerosol Sci.*, 2002, **33**, 1087–1093.
- 26 W. J. An, R. K. Pathak, B. H. Lee and S. N. Pandis, *J. Aerosol Sci.*, 2007, **38**, 305–314.
- 27 I. Riipinen, *et al.*, *Atmos. Environ.*, 2010, **44**, 597–607.
- 28 E. Karnezi, I. Riipinen and S. N. Pandis, *Atmos. Meas. Tech.*, 2013, submitted for publication.
- 29 E. Kostenidou, *et al.*, *Environ. Sci. Technol.*, 2009, **43**, 4884–4889.
- 30 V. A. Lanz, *et al.*, *Atmos. Chem. Phys.*, 2007, **7**, 1503–1522.
- 31 B. N. Murphy, *et al.*, *Atmos. Chem. Phys.*, 2012, **12**, 10797–10816.
- 32 A. P. Tsimpidi, *et al.*, *Atmos. Chem. Phys.*, 2010, **10**, 525–546.
- 33 J. A. Huffman, *et al.*, *Environ. Sci. Technol.*, 2009, **43**, 5351–5357.
- 34 J. E. Shilling, *et al.*, *Atmos. Chem. Phys.*, 2009, **9**, 771–782.
- 35 N. L. Ng, *et al.*, *Atmos. Chem. Phys.*, 2010, **10**, 4625–4641.

- 36 Q. Chen, *et al.*, *Environ. Sci. Technol.*, 2011, **45**, 4763–4770.
- 37 B. N. Murphy, *et al.*, *Atmos. Chem. Phys.*, 2011, **11**, 7859–7873.
- 38 N. M. Donahue, *et al.*, *Environ. Chem.*, 2013, **10**, 151–157.
- 39 K. M. Wagstrom and S. N. Pandis, *J. Geophys. Res.*, 2009, **114**, D14303.
- 40 K. M. Wagstrom, *et al.*, *Atmos. Environ.*, 2008, **42**, 5650–5659.
- 41 K. Skyllakou, *et al.*, *Atmos. Chem. Phys.*, 2013, submitted for publication.
- 42 F. Freutel, *et al.*, *Atmos. Chem. Phys.*, 2013, **13**, 933–959.
- 43 M. Beekmann, *et al.*, *Atmos. Chem. Phys.*, 2013, submitted for publication.
- 44 M. Sipilä, *et al.*, *Science*, 2010, **327**, 1243–1246.
- 45 I. Riipinen, *et al.*, *Atmos. Chem. Phys.*, 2011, **11**, 3865–3878.
- 46 J. G. Jung, P. J. Adams and S. N. Pandis, *Aerosol Sci. Technol.*, 2008, **42**, 495–504.
- 47 J. G. Jung, P. J. Adams and S. N. Pandis, *Atmos. Environ.*, 2006, **40**, 2248–2259.



# Measuring the atmospheric organic aerosol volatility distribution: a theoretical analysis

E. Karnezí<sup>1</sup>, I. Riipinen<sup>2</sup>, and S. N. Pandis<sup>1,3,4</sup>

<sup>1</sup>Department of Chemical Engineering, Carnegie Mellon University, Pittsburgh, USA

<sup>2</sup>Department of Applied Environmental Studies, Stockholm University, Stockholm, Sweden

<sup>3</sup>Department of Chemical Engineering, University of Patras, Patra, Greece

<sup>4</sup>Inst. of Chemical Engineering Sciences, FORTH/ICEHT, Patra, Greece

Correspondence to: S. N. Pandis (spyros@chemeng.upatras.gr)

Received: 7 October 2013 – Published in Atmos. Meas. Tech. Discuss.: 28 January 2014

Revised: 20 July 2014 – Accepted: 22 July 2014 – Published: 16 September 2014

**Abstract.** Organic compounds represent a significant fraction of submicrometer atmospheric aerosol mass. Even if most of these compounds are semi-volatile in atmospheric concentrations, the ambient organic aerosol volatility is quite uncertain. The most common volatility measurement method relies on the use of a thermodenuder (TD). The aerosol passes through a heated tube where its more volatile components evaporate, leaving the less volatile components behind in the particulate phase. The typical result of a thermodenuder measurement is the mass fraction remaining (MFR), which depends, among other factors, on the organic aerosol (OA) vaporization enthalpy and the accommodation coefficient. We use a new method combining forward modeling, introduction of “experimental” error, and inverse modeling with error minimization for the interpretation of TD measurements. The OA volatility distribution, its effective vaporization enthalpy, the mass accommodation coefficient and the corresponding uncertainty ranges are calculated. Our results indicate that existing TD-based approaches quite often cannot estimate reliably the OA volatility distribution, leading to large uncertainties, since there are many different combinations of the three properties that can lead to similar thermograms. We propose an improved experimental approach combining TD and isothermal dilution measurements. We evaluate this experimental approach using the same model, and show that it is suitable for studies of OA volatility in the lab and the field.

## 1 Introduction

Atmospheric aerosol particles play an important role in the Earth’s energy balance by absorbing and scattering solar radiation (direct effect) and influencing the properties and lifetime of clouds (indirect effects) (IPCC, 2007). They have significant negative effects on human health, including premature death, increases in respiratory illnesses, and cardiopulmonary mortality (Nel, 2005; Pope and Dockery, 2006).

Aerosols contain a wide variety of inorganic and organic compounds, with organics representing about 50% of the fine (< 1 μm) aerosol mass (Zhang et al., 2007). Organic aerosol (OA) originates from many different natural and anthropogenic sources and processes. It can be emitted directly, e.g., from fossil fuels and biomass combustion (so-called primary organic aerosol), or formed by atmospheric oxidation of volatile organic compounds (VOCs) (secondary organic aerosol, SOA). Since the oxidation pathways for VOCs are complex and the reactions lead to hundreds or thousands of oxygenated products, our understanding of organic aerosol formation mechanisms and the OA chemical and physical properties is still incomplete.

The volatility of atmospheric OA is one of its most important physical properties. It determines the partitioning of these organic compounds between the gas and particulate phases, and the organic aerosol concentration, and influences the rate of reactions and the atmospheric fate of the corresponding compounds. Measurement of the OA volatility distribution has been recognized as one of the major challenges in our efforts to quantify the rates of formation of secondary organic particulate matter (Donahue et al., 2012).

OA consists of thousands of compounds, too few of which have been identified. The volatility basis set framework (Donahue et al., 2006) was developed to describe absorptive partitioning by lumping all these compounds into surrogates along an axis of volatility. This approach typically employs species with effective saturation concentrations at 298 K separated by one order of magnitude (bin), with values ranging from, say, 0.01 to  $10^6 \mu\text{g m}^{-3}$ . By quantifying the volatility distributions of primary and secondary OA, a physically reasonable description of semi-volatile organics that is still suitable for large-scale chemical transport models can be obtained (Pathak et al., 2007; Stanier et al., 2008).

Thermodenuders (TD) have been developed to measure the volatility of ambient aerosol (Burtscher et al., 2001; Wehner et al., 2002, 2004; Kalberer et al., 2004; An et al., 2007). A TD consists of two basic parts: a heated tube where the more volatile particle components evaporate, leaving less volatile species behind, and the denuder tube containing usually activated carbon where the evaporated material is adsorbed, avoiding potential re-condensation when the sample is cooled to room temperature. The aerosol mass fraction remaining (MFR) at a given temperature, after passing through the TD, is the most common way of reporting the TD measurements.

The measurement of the volatility of OA has received considerable attention recently, and has been carried out both in the field (Engler et al., 2007; Huffman et al., 2009; Lee et al., 2010; Cappa and Jimenez, 2010) and in the laboratory (An et al., 2007; Jonsson et al., 2007; Saleh et al., 2008; Faulhaber et al., 2009). One of the main issues related to the use of thermodenuders is whether equilibrium is reached in the heating section of the instrument. Saleh et al. (2008) used high organic aerosol concentrations, allowing the model organic aerosol in their experiments to reach equilibrium in their TD. Using their integrated volume method, they were then able to determine the saturation concentration of the corresponding organic particles. Riipinen et al. (2010) showed that equilibration times in TDs depend on many factors, such as the organic aerosol loading and the accommodation coefficient. These authors argued that OA practically never reaches equilibrium in a TD at ambient concentration levels. For laboratory measurements, equilibrium can be reached with the use of high organic aerosol loadings (larger than  $200 \mu\text{g m}^{-3}$ ), and when the residence time in the heated section of the TD exceeds 30 s (Riipinen et al., 2010; Saleh et al., 2011). An et al. (2007) introduced an improved TD allowing for larger residence times. Lee et al. (2010, 2011) performed thermodenuder experiments at two residence times, and argued that multiple residence times are needed in order to decouple mass transfer effects from thermodynamics. Similar conclusions were reached by Riipinen et al. (2010) and Cappa (2010). Saleh et al. (2012) used a particle concentrator before passing the ambient aerosol through the thermodenuder to increase the aerosol concentration levels and to reduce the equilibration timescale. Volatility measurements on

longer timescales, where equilibrium of the system can be reached, have been performed by Grieshop et al. (2009).

Dynamic aerosol evaporation models (Riipinen et al., 2010; Cappa, 2010; Fuentes and McFiggans, 2012) are needed in most cases for the interpretation of TD measurements and the estimation of OA volatility. However, the MFR of OA in a TD depends not only on its volatility distribution, but also on the vaporization enthalpy and potential mass transfer resistances as the particles evaporate. The inversion of the TD measurements to calculate the OA volatility distribution has proven to be challenging because of the many parameters affecting the resulting MFR.

Previous studies have assumed a priori values for the effective vaporization enthalpy and the mass accommodation coefficient in order to estimate the OA volatility. Lee et al. (2010) tried to measure the volatility of ambient OA assuming values for the vaporization enthalpy and the accommodation coefficient equal to  $80 \text{ kJ mol}^{-1}$  and 0.05, respectively. They used the time-dependent evaporation model by Riipinen et al. (2010), with least-squares minimization, to reproduce ambient measurements collected in the eastern Mediterranean. For most measurements, it was difficult to estimate the volatility distribution, especially for the less volatile components. Moreover, a change in the accommodation coefficient from 0.05 to 1 resulted in a shifting of the estimated volatility distribution by one order of magnitude. Lee et al. (2011) used the same mass transfer model in order to reproduce experimental measurements from different precursors, assuming values for the vaporization enthalpy and the accommodation coefficient. Cappa (2010) developed a new model of evaporation in a TD accounting for the cooling section and the velocity profile across the TD tube. They demonstrated the importance of the vaporization enthalpy, especially for values less than  $100 \text{ kJ mol}^{-1}$ . They also underlined the importance of constraining the value of accommodation coefficient in order to quantify the volatility distribution of OA. Cappa and Jimenez (2010) used the model of Cappa (2010) to quantify the volatility distribution of ambient OA in Mexico City using measurements from the MILAGRO (Megacity Initiative: Local And Global Research Observations) campaign. Assuming several values for the vaporization enthalpy, either using the relationship from Epstein et al. (2010) or assuming that the vaporization enthalpy depended linearly on temperature or that it had constant values from 50 to  $150 \text{ kJ mol}^{-1}$ , they estimated different volatility distributions. Changing the value of the accommodation coefficient from 1 to 0.1, the estimated volatility distribution was shifted to higher values by approximately one order of magnitude. Fuentes and McFiggans (2012) used a dynamic aerosol evaporation model and the Epstein et al. (2010) relationship for the vaporization enthalpy, to calculate the volatility distribution for a-pinene SOA together with a small value of the accommodation coefficient. The estimation of the accommodation coefficient during the evaporation of atmospheric OA has been the focus of a number of studies.

Saleh et al. (2012) developed a method combining a particle concentrator (in order to achieve high mass loadings) and a thermodenuder. Using the thermodenuder model by Saleh et al. (2011), they measured the effective evaporation coefficient of ambient aerosol. Their results suggested accommodation coefficients with values around 0.3 for the ambient particles that they examined. Cappa and Wilson (2011) focused on the evolution of organic aerosol mass spectra from lubricating oil and secondary aerosol from  $\alpha$ -pinene oxidation upon heating, using the Cappa (2010) model. They adopted volatility distributions from previous studies (Pathak et al., 2007; Grieshop et al., 2009), and a vaporization enthalpy based on the Epstein et al. (2010) relationship. One of their major conclusions was that there were high mass transfer resistances (estimated accommodation coefficients on the order of  $10^{-4}$ ) during the evaporation of the  $\alpha$ -pinene SOA.

The sensitivity of TD results to several additional parameters has also been investigated in past studies. Lee et al. (2010) concluded that a monodisperse approximation using one effective value for the diameter of the particles instead of the full distribution resulted in changes in the thermograms of less than 2%. Lee et al. (2011) explored the effect of the cooling section and the role of surface free energy, and Cappa (2010) the role of the assumed value for the diffusion coefficient or the average effective diameter of the particles. Once again, the conclusion was that these parameters were not as important as the vaporization enthalpy and the accommodation coefficient for the estimation of the volatility distribution. Recondensation in the cooling section has been investigated in a number of studies (Cappa, 2010; Saleh et al., 2011; Fuentes and McFiggans, 2012). Fuentes and McFiggans (2012), through a parametric analysis, concluded that recondensation depends on a combination of factors, such as the mass loading, the particle size and the kinetic coefficient for re-condensation. Cappa (2010) showed that recondensation becomes significant for large aerosol loadings (larger than  $200 \mu\text{g m}^{-3}$ ); thus, it is a problem mostly for laboratory experiments. Saleh et al. (2011) showed that a configuration with a small diameter for the cooling section can lead to negligible recondensation, even for higher aerosol loadings.

In this study, we explore methods for estimating the OA volatility distribution, together with the effective vaporization enthalpy and mass accommodation coefficient. We develop a method combining forward modeling with known values for the three properties that we will try to estimate, introduction of random “experimental” error and, finally, inverse modeling with least-squares error minimization for the estimation of the OA volatility distribution, its effective vaporization enthalpy and the mass accommodation coefficient. We show that the best fit does not correspond to the most accurate estimate, due to the multiple local minima occurring in this problem. We propose an approach of estimating an ensemble of solutions, and use them to derive a best guess and corresponding uncertainties for each of the three

properties. Experimental approaches to improve these estimates and to reduce the corresponding uncertainties are explored. We examine the utility of using two residence times, using isothermal dilution instead of thermodenuder measurements (Grieshop et al., 2009), and finally combining TD and isothermal dilution measurements.

## 2 Thermodenuder model

We use the mass transfer model of Riipinen et al. (2010) modeling the time-dependent evaporation of multicomponent aerosol particles by solving the mass transfer equations for a monodisperse population of particles suspended in air. We assume a monodisperse population of particles. Lee et al. (2010) showed with the use of the same mass transfer model that this simplification resulted in errors of only a few percent (2%), and it reduced the computational time considerably. The mass flux of compound  $i$  from the gas phase to the particles,  $I_i$ , is calculated by (Seinfeld and Pandis, 2006)

$$I_i = \frac{2\pi d_p M_i \beta_{mi} D_i}{RT_{\text{TD}}} (p_i - p_i^0), \quad (1)$$

where  $d_p$  is the particle diameter,  $R$  the ideal gas constant,  $M_i$  and  $D_i$  the molecular weight and diffusion coefficient of compound  $i$  in the gas phase at temperature  $T_{\text{TD}}$  (the temperature in the heated part of the TD), and  $p_i^0$  and  $p_i$  are the partial vapor pressures of  $i$  at the particle surface and far away from the particle, respectively. In our simulations, we assume a particle diameter of 200 nm, a molecular weight of  $0.2 \text{ kg mol}^{-1}$  and a diffusion coefficient of  $10^{-5} \text{ m}^2 \text{ s}^{-1}$ .

The mass flux is corrected for kinetic and transition regime effects with the factor  $\beta_{mi}$  (Fuchs and Sutugin, 1970):

$$\beta_{mi} = \frac{1 + Kn_i}{1 + \left(\frac{4}{3a_{mi}} + 0.377\right) Kn_i + \frac{4}{3a_{mi}} Kn_i^2}, \quad (2)$$

where  $Kn_i$  is the Knudsen number, that is, the ratio of the mean free path of vapor  $i$  and the particle radius, and  $a_{mi}$  the mass accommodation coefficient of  $i$  on the particles. The mean free path is estimated by

$$\lambda_i = \frac{3 \cdot D_i}{\bar{c}}, \quad (3)$$

where  $\bar{c}$  is the mean velocity of the gas molecules, given by

$$\bar{c} = \sqrt{\frac{8 \cdot R \cdot T_{\text{TD}}}{\pi \cdot M_i}}. \quad (4)$$

The partial vapor pressure of  $i$  at the particle surface,  $p_i^0$ , is given by

$$\begin{aligned} p_i^0 &= x_i \gamma_i p_{\text{sat},i} \exp\left(\frac{4M_i\sigma}{RT_p \rho d_p}\right) \\ &= x_{mi} \frac{C_i^* RT_{\text{TD}}}{M_i} \exp\left(\frac{4M_i\sigma}{RT_p \rho d_p}\right), \end{aligned} \quad (5)$$

where  $x_i$  is the mole fraction and  $\gamma_i$  the activity coefficient of  $i$  in the particle phase,  $p_{\text{sat},i}$  the pure-component vapor pressure of  $i$  over a flat surface,  $T_p$  the particle temperature,  $C_i^*$  represents the effective saturation concentration of  $i$  in the volatility basis set (Donahue et al., 2006), and  $x_{mi}$  is the mass fraction of  $i$  in the particle. In this study, we will be using a fixed basis set with four volatility bins, with effective saturation concentrations of 0.01, 0.1, 1 and  $10 \mu\text{g m}^{-3}$  for each volatility bin. We assume a surface tension of  $0.05 \text{ N m}^{-1}$  as a median of the range used in Riipinen et al. (2010). We repeated our simulations with values of  $0.05\text{--}0.2 \text{ N m}^{-1}$  for the surface energy, but this choice had practically no effect on the results, since the particles examined are too big and the Kelvin effect is not important. We also use a density of the surrogate compounds of  $1500 \text{ kg m}^{-3}$ .

The saturation concentrations of the evaporating species at  $T_{\text{TD}}$  are estimated using the integrated form of the Clausius–Clapeyron equation:

$$C_i^*(T_{\text{TD}}) = C_i^*(298\text{K}) \exp\left[\frac{\Delta H_{\text{vap},i}}{R} \left(\frac{1}{298} - \frac{1}{T_{\text{TD}}}\right)\right] \left(\frac{298}{T_{\text{TD}}}\right), \quad (6)$$

where  $\Delta H_{\text{vap},i}$  is the vaporization enthalpy of species  $i$ . The temperature dependence of the diffusion coefficients of the evaporating species is taken into account by using

$$D_i(T_{\text{TD}}) = D_i(298) \left(\frac{T_{\text{TD}}}{298}\right)^\mu, \quad (7)$$

where  $\mu$  is a constant usually ranging from 1.5 to 2.0 (Chen and Othmer, 1962). We used the value of 1.75 for all the studied compounds.

The time-dependent evaporation of the organic aerosol is simulated by solving the differential equations for total particle mass  $m_p$  and gas phase concentrations  $C_i$  of the evaporating species:

$$\frac{dm_p}{dt} = - \sum_{i=1}^n I_i \quad \frac{dC_i}{dt} = I_i \cdot N_{\text{tot}}, \quad (8)$$

where  $N_{\text{tot}}$  is the total number concentration of the particles (assuming a monodisperse particle population). The MFR is then calculated from the ratio of the particle mass at  $t = t_{\text{res}}$  (where  $t_{\text{res}}$  is the residence time through the heating tube) to the initial mass of the particles. In this work, we study the evaporation of particles in a TD independently of the TD design and geometry: the only variables representing the instrument are the particle residence time and the temperature of the thermodenuder. We neglect the velocity and potential temperature gradients in the radial direction and thus focus on the particles moving along the centerline of the TD and at the corresponding centerline temperature. Saleh et al. (2011) showed that a similar model neglecting the radial dependence of the system reproduced well the behavior of model particles consisting of dicarboxylic acids.

We use, as inputs, values for the geometry of the TD (the length and the residence time in the heated tube), the temperature inside the TD ( $T_{\text{TD}}$ ), the initial mass concentration of the organic aerosol ( $C_{\text{aer}}$ ), and the properties of the organic compounds (such as the volatility distribution, vaporization enthalpy, accommodation coefficient, etc.). For the description of the geometry of the TD, we used the values for the Carnegie Mellon TD of Lee et al. (2010). Specifically for the heated tube, we used a length of 55 cm and a centerline residence time of 17 s.

Using the mass transfer model of Riipinen et al. (2010), modeling the time-dependent evaporation of multicomponent aerosol particles, we constructed theoretical thermograms (MFR versus  $T_{\text{TD}}$ ). Previous studies have often assumed that thermograms can be directly connected to the volatility of OA. Figure 1 indicates that we can have very similar thermograms for organic aerosols with very different volatilities (orders of magnitude different). In this example, the reduction in the saturation concentration is balanced by changes in the accommodation coefficient and the vaporization enthalpy. The similarity of these suggests that the inversion of the thermograms in order to calculate the OA volatility will be very challenging.

## 2.1 Pseudo-experimental data

In order to evaluate how well we can estimate the volatility distribution, we used “pseudo-experiments” corrupting the output of the TD model, for systems with known volatility distributions and properties, with randomly generated “experimental” errors. In this way, we could take into account the measurement uncertainty due to the variability of measurement conditions, and produce relatively realistic “experimental results” for systems with known volatility distributions and properties. We “corrupted” the TD model predictions with random errors assuming a normal distribution, based on the variability of laboratory measurements with the same TD conducted by Paciga and Pandis (2014), with a standard deviation given by

$$\sigma = 0.51 \cdot \text{MFR}_{\text{true}} - 0.5 \cdot \text{MFR}_{\text{true}}^2, \quad (9)$$

where  $\text{MFR}_{\text{true}}$  are the correct MFR values. A typical example is shown in Fig. 2.

In the rest of the inversion approaches, pseudo-experimental data were used. In this way, the experimental uncertainty was always taken into account, and an overestimation/underestimation of the corresponding algorithm is avoided.

## 2.2 Optimum OA volatility distribution

The MATLAB least-squares fitting algorithm *lsqcurvefit* was used in order to obtain the best possible fit between the “measured” and modeled MFRs. Four lognormally equally spaced volatility bins were used, with volatilities from  $10^{-2}$

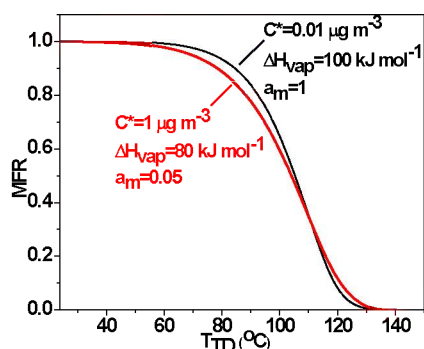


**Figure 1.** Predicted thermograms (MFR versus  $T_{TD}$ ) for OA with different properties. A single-component aerosol ( $C^* = 1 \mu\text{g m}^{-3}$ ,  $\Delta H_{\text{vap}} = 80 \text{ kJ mol}^{-1}$  and  $a_m = 0.05$ ) gives practically the same thermogram as one with a much lower volatility ( $C^* = 0.01 \mu\text{g m}^{-3}$ ,  $\Delta H_{\text{vap}} = 100 \text{ kJ mol}^{-1}$  and  $a_m = 1$ ).

to  $10 \mu\text{g m}^{-3}$ . The corresponding volatility distribution, vaporization enthalpy and mass accommodation coefficient were estimated by the algorithm minimizing the sum of the squared differences between the MFR model predictions and the pseudo-measurements. In the least-squares optimization, a total of 12 pseudo-measurements was used in all cases.

A wide variety of compositions was tested during the simulations, including one-component, two-component or multi-component aerosols with various volatility distributions and with different values for the vaporization enthalpy and the accommodation coefficient. The results for three of these tests that are used as illustrative examples are shown in Table 1. For Test 1 corresponding to OA consisting of very low and high volatility material (60 %  $0.01 \mu\text{g m}^{-3}$  and 40 %  $10 \mu\text{g m}^{-3}$ ), the optimization resulted in an absolute volatility error of less than 10 % for all bins. The vaporization enthalpy was well estimated (relative error equal to 8 %), and the mass accommodation coefficient was estimated within a factor of 2 (0.97 instead of 0.5). For Test 2 corresponding to multicomponent OA (10 %  $0.1 \mu\text{g m}^{-3}$ , 30 %  $1 \mu\text{g m}^{-3}$  and 60 %  $10 \mu\text{g m}^{-3}$ ), the estimated volatility distribution had a different shape than the true one, with more material predicted for the bin of  $1 \mu\text{g m}^{-3}$  (predicted mass fraction equal to 0.49 instead of 0.3), and less for the  $10 \mu\text{g m}^{-3}$  bin (predicted mass fraction equal to 0.31 instead of 0.6). Also, some very low volatility material was estimated (predicted mass fraction equal to 0.07 while none was present). The vaporization enthalpy was estimated with a relative error equal to 40 %, and the accommodation coefficient was well estimated (0.72 instead of unity). For Test 3 with the case of one-component OA with a volatility of  $1 \mu\text{g m}^{-3}$ , the estimates of all properties were far from the truth. Most of the material (88 %) was estimated to be in the  $0.1 \mu\text{g m}^{-3}$  bin instead of  $1 \mu\text{g m}^{-3}$ , and some material (12 %) was predicted in the highest volatility bin of  $10 \mu\text{g m}^{-3}$ . The estimated vaporization enthalpy was more than a factor of 2 higher than

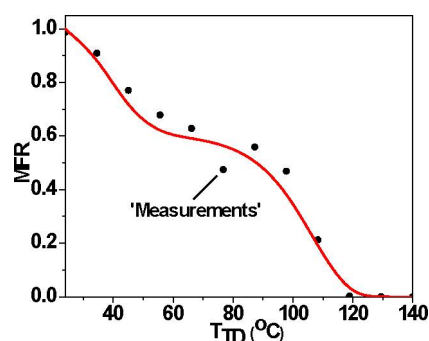


**Figure 2.** Typical example of “construction” of TD pseudo-data. The red line is the thermogram corresponding to the true properties of the aerosol, and the black dots correspond to the “measured” MFR versus  $T_{TD}$  for an aerosol consisting of two components: very low volatility material (60 %  $C^* = 0.01 \mu\text{g m}^{-3}$ ) and relatively high volatility material (40 %  $C^* = 10 \mu\text{g m}^{-3}$ ), with a vaporization enthalpy and a mass accommodation coefficient equal to  $100 \text{ kJ mol}^{-1}$  and 1, respectively. Twelve “measurements” were constructed for equally spaced temperatures between 24 and  $140 \text{ }^\circ\text{C}$  by corrupting the correct values with random experimental errors.

the true value, and the estimated accommodation coefficient was a factor of 25 lower than it should be.

The results, using different initial guesses for the case of multiple-component OA (Test 2), are shown in Fig. 3. For an initial guess of [0 0 0.3 0.7] for the mass fractions of the volatility bins ( $C^* = [0.01 \ 0.1 \ 1 \ 10] \mu\text{g m}^{-3}$ ),  $50 \text{ kJ mol}^{-1}$  for the vaporization enthalpy and 0.5 for the accommodation coefficient, the shape of the volatility distribution was estimated correctly, but with significant errors of 0.1–0.2 in the 0.1, 1 and  $10 \mu\text{g m}^{-3}$  bins. The vaporization enthalpy estimation error was 24 % and the estimated accommodation coefficient was 0.9, close to the true value of unity. This is however a local minimum of the objective function. The global minimum (minimum error) was found when we used an initial guess of [0.1 0.1 0.3 0.5] for the mass fractions,  $80 \text{ kJ mol}^{-1}$  for  $\Delta H_{\text{vap}}$ , and 0.2 for  $a_m$ . The estimated OA volatility distribution, in this case, is shown in Fig. 3b. In this case, the shape of the volatility distribution is not correct, and there are errors in the mass fractions of the volatility bins as large as 0.3. The estimated vaporization enthalpy and accommodation coefficient were similar to those of the previous guess, with a relative error of 35 % for  $\Delta H_{\text{vap}}$ . Due to the experimental error, the global minimum can correspond to volatility distributions that are far from the true values. We conclude that the optimization method may not be appropriate for the estimation of the volatility distribution, the vaporization enthalpy and the mass accommodation coefficient. It is also clear that we need an approach for estimating the corresponding uncertainties.

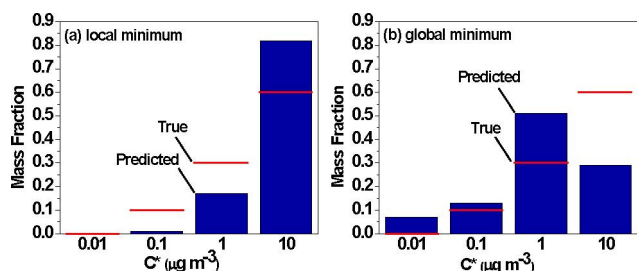


**Figure 3.** Estimated (bars) and true (red lines) volatility distribution for OA consisting of 10 %  $C^* = 0.1 \mu\text{g m}^{-3}$ , 30 %  $1 \mu\text{g m}^{-3}$ , 60 %  $10 \mu\text{g m}^{-3}$ ,  $\Delta H_{\text{vap}} = 50 \text{ kJ mol}^{-1}$  and  $a_m = 1$ , based on TD pseudo-data. **(a)** Solution corresponding to a local minimum of the objective function. The estimated vaporization enthalpy and accommodation coefficient are  $\Delta H_{\text{vap}} = 38 \text{ kJ mol}^{-1}$  and  $a_m = 0.9$ . **(b)** Solution for the global minimum. The estimated  $\Delta H_{\text{vap}}$  and  $a_m$  are  $68 \text{ kJ mol}^{-1}$  and 0.84, respectively.

### 2.3 Estimation of uncertainty

In an effort to explore in more detail the solution space for the problem, we discretized the parameter space and simulated all combinations of volatilities,  $\Delta H_{\text{vap}}$  and  $a_m$ . We used once more four bins for volatilities from  $10^{-2}$  to  $10 \mu\text{g m}^{-3}$ , and varied the mass fraction of each bin from 0 to 1 with a step of 0.1. The values used for  $\Delta H_{\text{vap}}$  were from 20 to 200, with discrete values of 20, 50, 80, 100, 150 and  $200 \text{ kJ mol}^{-1}$ , and for  $a_m$ , the values were from 0.01 (large mass resistance) to 1 (no mass resistance), with discrete values of 0.01, 0.05, 0.1, 0.2, 0.5 and 1. We also tried in our simulations other discretizations for the values of the vaporization enthalpy and the mass accommodation coefficient, and they did not affect the results. In the rest of the paper, the discretizations for the  $\Delta H_{\text{vap}}$  and the  $a_m$  described above will be used for all of the simulations. For each simulation, the percentage error was estimated from

$$E_i = \frac{100}{n} \sqrt{\sum_i^n (\text{MFR}_{i,\text{guess}} - \text{MFR}_i)^2}, \quad (10)$$

where  $\text{MFR}_{i,\text{guess}}$  is the MFR for a certain combination of parameters for data point  $i$  (corresponding to a specific temperature),  $\text{MFR}_i$  is the “measured” MFR, and  $n$  is the number of the different temperatures  $T_{\text{TD}}$  used in our “measurements”.

After performing simulations for all combinations of all properties, we identified the combinations that led to small errors (less than 2 %). From these values, we then calculated a “best estimate” using the inverse error as a weighting factor:

$$\bar{x} = \frac{\sum_i^N \left[ (x_i) \cdot \left( \frac{1}{E_i} \right) \right]}{\sum_i^N \left[ \frac{1}{E_i} \right]}, \quad (11)$$

where  $x_i$  is the value of property  $i$  (the mass fractions of the volatility bin  $i$  or the vaporization enthalpy  $\Delta H_{\text{vap}}$  or the accommodation coefficient  $\log(a_m)$ ).

We also calculated the uncertainty range for all three properties by calculating the standard deviation ( $\sigma$ ) of the corresponding values:

$$\sigma = \sqrt{\frac{\sum_i^N \left[ \left( (x_i - \bar{x})^2 \cdot \left( \frac{1}{E_i} \right) \right) \right]}{\sum_i^N \left[ \frac{1}{E_i} \right]}}. \quad (12)$$

The logarithms of the accommodation coefficient values were used in order to avoid negative accommodation coefficient values inside the uncertainty range. We report one standard deviation as the uncertainty range in the rest of the paper.

## 3 Results

The first parameter of the thermodenuder experiments explored was the number of measurements at different temperatures in the thermogram under consideration. In previous studies, thermodenuder measurements vary between 6 (An et al., 2007) and 12 measurements (Faulhaber et al., 2009).

A wide variety of cases of OA were tested during the simulations once more. The results for a multicomponent OA with mostly nonvolatile material (80 %  $0.01 \mu\text{g m}^{-3}$ , 5 %  $0.1 \mu\text{g m}^{-3}$ , 10 %  $1 \mu\text{g m}^{-3}$  and 5 %  $10 \mu\text{g m}^{-3}$ ), for the cases of 6 and 12 measurements, are given in Fig. 4 as a representative example. For the first experiment, with a small number of measurements (6 points), there is large uncertainty in the two least volatile bins (with a standard deviation up to 0.25). The uncertainty range in the least and most volatile bins ( $0.01$  and  $10 \mu\text{g m}^{-3}$ ) does not include the correct values for the distribution. In the second experiment, twice as many measurements were used (12 points), the estimated uncertainty range is smaller (the standard deviation of all the predicted mass fractions is less than 0.08), and it contains the correct volatility distribution. The relative error of the estimated  $\Delta H_{\text{vap}}$  is 13 %, in both experiments. Finally, the  $a_m$  is underestimated for both experiments, but with the second experiment (using 12 measurements), the uncertainty range includes the correct value.

For cases of OA with more uniform volatility distributions (e.g., cases where the mass fraction varies less than 0.2 between the bins), the use of 12 measurements instead of 6 gave similar estimates for the three properties (volatility distribution, vaporization enthalpy and mass accommodation coefficient) and the same uncertainty ranges. In cases of extreme volatility distributions, where most material is in one or two volatility bins, as in the case of the example in Fig. 4, using more measurements resulted in better estimates and smaller

**Table 1.** Values of the true and estimated properties (volatility distribution, vaporization enthalpy, accommodation coefficient) for three OA examples.

	Test 1 OA with very low and high volatility material	Test 2 Multiple-component OA	Test 3 One-component OA
True values	$C_i^* = [0.01 \ 0.1 \ 1 \ 10]$ $X_i = [0.6 \ 0 \ 0 \ 0.4]$ $\Delta H_{\text{vap}} = 100 \text{ kJ mol}^{-1}$ $a_m = 0.5$	$C_i^* = [0.01 \ 0.1 \ 1 \ 10]$ $X_i = [0 \ 0.1 \ 0.3 \ 0.6]$ $\Delta H_{\text{vap}} = 50 \text{ kJ mol}^{-1}$ $a_m = 1$	$C_i^* = [0.01 \ 0.1 \ 1 \ 10]$ $X_i = [0 \ 0 \ 1 \ 0]$ $\Delta H_{\text{vap}} = 80 \text{ kJ mol}^{-1}$ $a_m = 1$
Optimization results	$C_i^* = [0.01 \ 0.1 \ 1 \ 10]$ $X_i = [0.63 \ 0 \ 0 \ 0.37]$ $\Delta H_{\text{vap}} = 92 \text{ kJ mol}^{-1}$ $a_m = 0.97$ $E_i = 1.09^a$	$C_i^* = [0.01 \ 0.1 \ 1 \ 10]$ $X_i = [0.07 \ 0.13 \ 0.49 \ 0.31]$ $\Delta H_{\text{vap}} = 70 \text{ kJ mol}^{-1}$ $a_m = 0.72$ $E_i = 0.3$	$C_i^* = [0.01 \ 0.1 \ 1 \ 10]$ $X_i = [0 \ 0.88 \ 0 \ 0.12]$ $\Delta H_{\text{vap}} = 181 \text{ kJ mol}^{-1}$ $a_m = 0.04$ $E_i = 0.81$

<sup>a</sup> The error, given by Eq. (10), describes the quality of the fit.

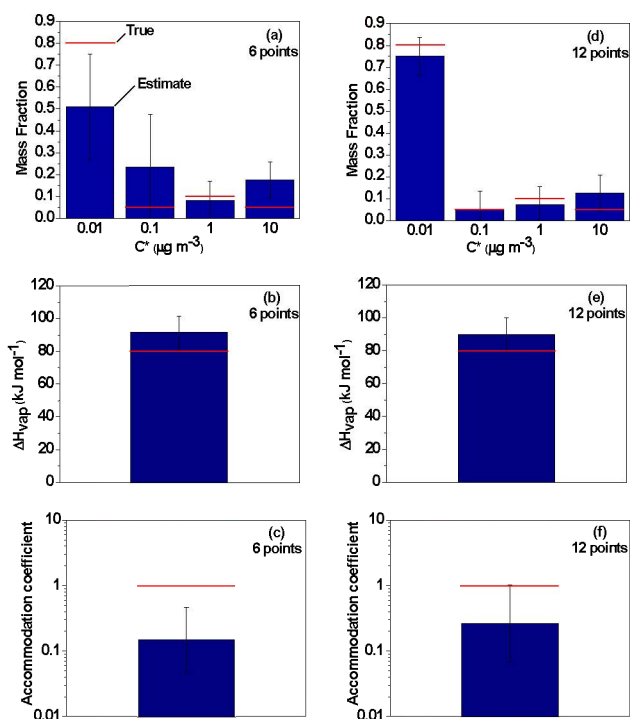


**Figure 4.** Estimated (bars) and true (red lines) parameter values for an OA with 80 %  $0.01 \mu\text{g m}^{-3}$ , 5 %  $0.1 \mu\text{g m}^{-3}$ , 10 %  $1 \mu\text{g m}^{-3}$ , and 5 %  $10 \mu\text{g m}^{-3}$ ,  $\Delta H_{\text{vap}} = 80 \text{ kJ mol}^{-1}$  and  $a_m = 1$  for 6 measurements, (a) volatility distribution, (b)  $\Delta H_{\text{vap}}$ , and (c)  $a_m$ , and using 12 measurements for (d) volatility distribution, (e)  $\Delta H_{\text{vap}}$ , and (f)  $a_m$ . The error bars represent the uncertainty of the estimated value.

uncertainty ranges than using only a small number of measurements.

In Fig. 5, we examine two more cases of OA with extreme volatility distributions using 12 pseudo-measurements. In the first test, which is the same OA as in Test 1 discussed

in Sect. 2.2, the OA consists of two components: very low volatility material (60 %  $0.01 \mu\text{g m}^{-3}$ ) and high volatility material (40 %  $10 \mu\text{g m}^{-3}$ ). The estimated uncertainty range is large, especially for the two least volatile bins (with an uncertainty equal to 0.2), but it includes the actual volatility distribution. Also, the estimated volatility distribution has the correct shape. The estimated vaporization enthalpy has an error of 5 %, while the accommodation coefficient error is around 20 %.

In the second test, we assume that the OA consists of very low volatility material (50 %  $0.01 \mu\text{g m}^{-3}$ ) and relatively high volatility material (50 %  $1 \mu\text{g m}^{-3}$ ). The shape of the volatility distribution of the OA is not captured by the inversion results, the estimated uncertainty range is large (the uncertainty of all the predicted mass fractions is around 0.2), and the uncertainty range does not contain the actual volatility distribution. The error of the estimated  $\Delta H_{\text{vap}}$  is 8 %. The accommodation coefficient is underpredicted by one order of magnitude (value equal to 0.15 instead of unity). The TD measurements are not sufficient in this case for the accurate estimation of the OA volatility distribution.

In order to evaluate how general the above results of the proposed volatility estimation method are, we performed additional tests using ten randomly generated volatility distributions. The sets of parameters used are shown in Table 2. The ten first parameter sets have random OA volatility distributions, a vaporization enthalpy equal to  $90 \text{ kJ mol}^{-1}$  (chosen as a reasonable intermediate value between 20 and  $200 \text{ kJ mol}^{-1}$ ), and an accommodation coefficient of 0.1 (chosen as a medium mass resistance). Additional cases with either low (sets 11–13) or high mass transfer resistance (sets 14–16) and cases with low (sets 11 and 13) or higher vaporization enthalpies (sets 12, 15 and 16) were also examined.

The inversion results are shown in Table 3. They include the average absolute errors for the VBS bins, the relative error (%) for the vaporization enthalpy, and the errors for  $a_m$  (in

**Table 2.** Sets of random volatility distributions used for the evaluation of different inversion approaches.

OA parameter set	Mass fraction				$\Delta H_{\text{vap}}$ (kJ mol <sup>-1</sup> )	$a_m$
	0.01 $\mu\text{g m}^{-3}$	0.1 $\mu\text{g m}^{-3}$	1 $\mu\text{g m}^{-3}$	10 $\mu\text{g m}^{-3}$		
1	0.135	0.06	0.14	0.665	90	0.1
2	0.45	0.04	0.315	0.195	90	0.1
3	0.255	0.115	0.47	0.16	90	0.1
4	0.235	0.045	0.025	0.695	90	0.1
5	0.565	0.23	0.175	0.03	90	0.1
6	0.105	0.21	0.59	0.095	90	0.1
7	0.375	0.405	0.15	0.07	90	0.1
8	0.375	0.095	0.07	0.46	90	0.1
9	0.145	0.435	0.25	0.17	90	0.1
10	0.245	0.085	0.08	0.59	90	0.1
11	0.565	0.23	0.175	0.03	70	1
12	0.565	0.23	0.175	0.03	140	1
13	0.245	0.085	0.08	0.59	60	1
14	0.245	0.085	0.08	0.59	120	0.01
15	0.135	0.06	0.14	0.665	120	0.01
16	0.105	0.21	0.59	0.095	140	0.01

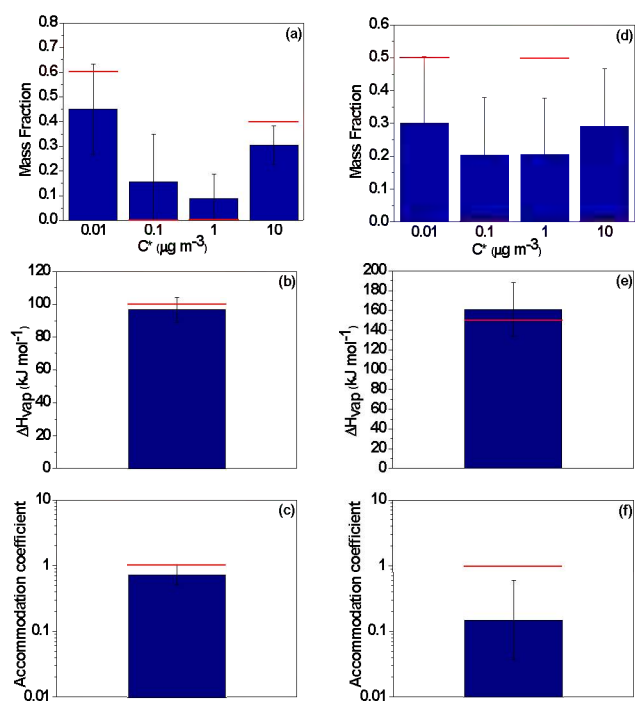


**Figure 5.** Estimated (bars) and true property values (red lines) using 12 TD measurements, for two types of OA. **(a)** Volatility distribution, **(b)**  $\Delta H_{\text{vap}}$ , **(c)**  $a_m$  for OA, with 60 % 0.01  $\mu\text{g m}^{-3}$  and 40 % 10  $\mu\text{g m}^{-3}$ ,  $\Delta H_{\text{vap}} = 100 \text{ kJ mol}^{-1}$  and  $a_m = 1$ , and **(d)** volatility distribution, **(e)**  $\Delta H_{\text{vap}}$ , and **(f)**  $a_m$  for OA, with 50 % 0.01  $\mu\text{g m}^{-3}$  and 50 % 1  $\mu\text{g m}^{-3}$ ,  $\Delta H_{\text{vap}} = 150 \text{ kJ mol}^{-1}$  and  $a_m = 1$ . The error bars represent the uncertainty of the estimated value.

orders of magnitude). These results indicate that an accurate estimation of the OA volatility distribution is challenging in most cases. The volatility distribution was estimated with average absolute errors less than 0.1 for six out of the sixteen cases tested (sets 1, 4, 8, 9, 10 and 13), and for the rest of the cases, the errors were up to 0.22. The average relative error of the estimated  $\Delta H_{\text{vap}}$  was roughly 10 %. The error for the estimated accommodation coefficient varied from half to almost one and a half order of magnitude. Concerning the uncertainties (not shown), the uncertainty range of the volatility distribution in most of the cases was large (around 0.2). Exceptions are the cases with most material in the lowest and highest volatility bins, where the uncertainty range is 0.05–0.15. The uncertainty in the estimated  $\Delta H_{\text{vap}}$  for most of the cases was around 20 %. The uncertainty in the estimated accommodation coefficient varied from less than one order of magnitude to two orders of magnitude.

Based on the above results, it is evident that it is very difficult to estimate the three properties accurately and with a small uncertainty range, since there are many combinations of properties that can lead to a thermogram quite similar to the one from the pseudo-experiment. So, even if the uncertainty estimation method proposed here is a step forward, the TD inversion results are either too uncertain or sometimes erroneous. The TD measurements using one residence time (17 s) are not sufficient to constrain the three properties, since equilibrium is not reached in most cases. It is clear that improvements in the volatility measurement approach itself are needed. A number of ideas are explored in the next section. These include using more than one TD residence time or using measurements on much longer timescales (e.g., isothermal dilution measurements).

## 4 Improvements in the volatility measurement method

### 4.1 Use of two residence times

In order to improve the method for the estimation of the OA volatility distribution,  $\Delta H_{\text{vap}}$  and  $a_m$ , we simulated “measurements” using two residence times (Lee et al., 2010), but with half the data points for each measurement (6 points for each residence time). We used two residence times of 17 and 34 s. The estimation of the volatility distributions was improved, but the improvement in most cases was small to modest. For example, for the case of OA consisting of very low volatility material (50 %  $0.01 \mu\text{g m}^{-3}$ ) and relatively high volatility material (50 %  $1 \mu\text{g m}^{-3}$ ), the correct volatility distribution was still not retrieved, the uncertainty range once again was large (equal to 0.2), and it did not contain the actual volatility distribution. The relative error of the estimated  $\Delta H_{\text{vap}}$  was 6 %. The accommodation coefficient was under-predicted by one order of magnitude (value equal to 0.12 instead of unity).

We performed a number of tests with different OA systems. The use of two residence times resulted in improved estimates in some cases (e.g., single-component systems), but in the majority of the cases, the improvement was marginal. The results were often quite similar to those of the one residence time discussed above (with twice the data points). This was due to the fact that in most cases, the system is still far from equilibrium. We concluded that just doubling the residence time was not sufficient and that the residence time should increase to tens of minutes in most of the cases. This is very difficult though for continuous flow systems, so the next step was the exploration of the utility of evaporation measurements at much longer timescales than those that can be reached with a TD.

### 4.2 Isothermal dilution experiments

We tested the effectiveness of performing only isothermal dilution measurements instead of TD measurements. The isothermal evaporation of OA can take place in a smog chamber, and allows residence times of a few hours (Grieshop et al., 2009). The isothermal evaporation results at room temperature do not depend on  $\Delta H_{\text{vap}}$ , but only on  $C^*$  and  $a_m$ . We assume that we dilute our OA samples during the injection in the chamber with a 10-fold volume of clean air, so in this way, the initial gas and particle concentrations are lowered by a factor of 10, and the system is out of equilibrium. We allow the aerosol to evaporate in the chamber for 2 h and assume that its concentration is measured every 10 min. The error distribution used for the isothermal dilution is also based on the variability of the corresponding laboratory data. We “corrupted” the time-dependent mass transfer model predictions with a random error, assuming a uniform distribution with a standard deviation given by

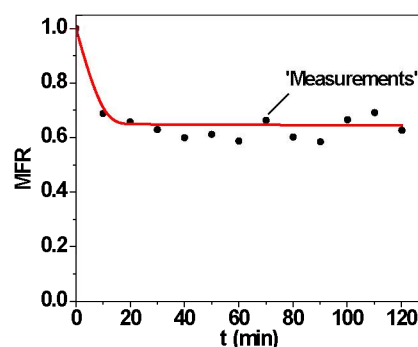


**Figure 6.** Isothermal dilution measurements (MFR as a function of time) for an aerosol with 60 %  $0.01 \mu\text{g m}^{-3}$  and 40 %  $10 \mu\text{g m}^{-3}$ ,  $\Delta H_{\text{vap}} = 100 \text{ kJ mol}^{-1}$  and  $a_m = 1$ . The red line corresponds to the true properties of the aerosol, and the black dots are the “measured” MFR values.

$$\sigma = 0.05 \cdot \text{MFR}_{\text{true}} + 0.03, \quad (13)$$

where  $\text{MFR}_{\text{true}}$  are the correct MFR values.

A typical set of isothermal dilution “measurements” is shown in Fig. 6. The organic particles reach equilibrium with the gas phase after approximately thirty minutes in this pseudo-experiment. The inversion results for the case of OA consisting of very low volatility material (60 %  $0.01 \mu\text{g m}^{-3}$ ) and high volatility material (40 %  $10 \mu\text{g m}^{-3}$ ), are shown in Fig. 7. The estimated volatility distribution had significant error, and the uncertainty was large (equal to 0.2). The accommodation coefficient was estimated within 20 %.

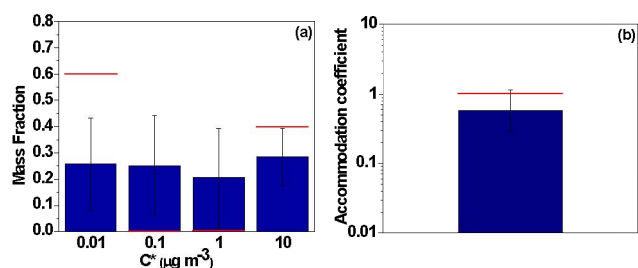
The dilution method was also used for the random sets of volatility distributions shown in Table 2, and the results are shown in Table 3. The average absolute errors for the VBS bins were around 0.2, and the errors for the accommodation coefficient in all cases were up to one order of magnitude. Isothermal dilution did not consistently improve the estimated volatility distributions and the accommodation coefficient compared to the use of TD measurements. The uncertainty remains large, since there are still many combinations of the two properties that can lead to similar dilution curves.

### 4.3 Combination of TD and isothermal dilution measurements

We continued with the test of effectiveness of combining TD and isothermal dilution “measurements” using the same method as in Sect. 2.3. We used the same discretization for the values of the volatility distribution, the vaporization enthalpy and the accommodation coefficient, and constructed, using the evaporation model, the theoretical thermograms. Using random numbers based on a normal distribution (for the case of thermogravimetric measurements) and uniform distribution (for the case of isothermal dilution

**Table 3.** Results for the sets of random volatility distributions using different inversion approaches.

OA parameter set	TD measurements			Dilution measurements		TD and dilution measurements		
	Average absolute error for VBS bins	Relative error (%) for $\Delta H_{\text{vap}}$	Error for $a_m$ (orders of magnitude)	Average absolute error for VBS bins	Error for $a_m$ (orders of magnitude)	Average absolute error for VBS bins	Relative error (%) for $\Delta H_{\text{vap}}$	Error for $a_m$ (orders of magnitude)
1	0.05	6	0.43	0.13	0.39	0.02	11	0
2	0.13	3	0.06	0.11	0.17	0.02	2	0.16
3	0.1	8	0.1	0.51	0.19	0.07	2	0.02
4	0.08	10	0.45	0.19	0.36	0.02	4	0.1
5	0.14	4	0.28	0.12	0.44	0.14	0.7	0.46
6	0.1	10	0.02	0.15	0.02	0.07	10	0.04
7	0.14	7	0.13	0.06	0.19	0.07	2	0.05
8	0.07	4	0.17	0.18	0.34	0.04	0.9	0.06
9	0.09	3	0.04	0.07	0.21	0.09	0.1	0.34
10	0.06	11	0.45	0.16	0.46	0.06	11	0.37
11	0.14	14	1.17	0.12	1.06	0.1	14	0.77
12	0.11	14	0.95	0.12	1.06	0.06	23	0.96
13	0.06	2	0.3	0.07	0.17	0.08	0.04	0.24
14	0.18	25	1.22	0.2	0.75	0.33	17	1
15	0.22	14	1.12	0.21	0.83	0.3	8	1.22
16	0.11	11	0.63	0.18	0.50	0.17	4	0.32

**Figure 7.** Estimated (bars) volatility distribution and accommodation coefficient and true (red lines) values using isothermal dilution “measurements”, for an OA with 60 %  $0.01 \mu\text{g m}^{-3}$  and 40 %  $10 \mu\text{g m}^{-3}$ ;  $\Delta H_{\text{vap}} = 100 \text{ kJ mol}^{-1}$  and  $a_m = 1$ . (a) Volatility distribution and (b)  $a_m$ .

measurements), we produced pseudo-measurements for the different experiments. For the resulting 24 measurements (12 for each TD and dilution pseudo-experiment), we then performed the error minimization with the percentage error given by Eq. (10), treating equally the TD and isothermal dilution measurements. In the case of Test 1 (Table 1) shown in Fig. 8, the estimated volatility distribution has the correct shape, and the corresponding uncertainty range is small (uncertainty less than or equal to 0.1). The  $\Delta H_{\text{vap}}$  and the  $a_m$  were estimated within a few percent. In another challenging test (Fig. 9), the shape of the volatility distribution is again predicted correctly. The estimated value of the vaporization enthalpy has an error of only 7 %, and the estimated accommodation coefficient is 0.4 instead of unity.

We also repeated all the tests of Table 2. The results are shown in Table 3. In 70 % of the cases, the volatility distribution was reproduced with absolute errors less than 0.1. The average relative error of the estimated

$\Delta H_{\text{vap}}$  was roughly 7 %. The error for the estimated accommodation coefficient for the cases of OA varied from less than half an order of magnitude up to one order of magnitude. The uncertainties (not shown) for the volatility distribution in 70 % of the cases were not higher than 0.05–0.1. The uncertainties for the vaporization enthalpy were around 10 %. The accommodation coefficient, for the cases of OA with a value equal to 0.1, had an uncertainty of half an order of magnitude. For cases where the accommodation coefficient was equal to unity, it was underpredicted, with an uncertainty varying from half an order of magnitude (set 13), to one order of magnitude (set 11), to two orders of magnitude (set 12). For the cases of OA (sets 14 to 16) where the accommodation coefficient is equal to 0.01, it was overestimated by up to one order of magnitude.

Problems appeared in the three cases (sets 5, 9, and 13) in which less than 20 % of the OA evaporated, and in the three cases where equilibrium was not reached (sets 14, 15, and 16). Using a higher initial dilution (100 times dilution), the actual volatility distribution was captured in sets 9 and 13, with uncertainties equal to 0.2 and 0.1, respectively. Results for set 5 improved marginally, because further evaporation could not be achieved due to the large amount of nonvolatile material in the OA. The longer residence times improved the accuracy of the estimated volatility distributions (errors less than 0.1). The errors in  $\Delta H_{\text{vap}}$  and the accommodation coefficient were also reduced in all cases.

Summarizing, using both TD and dilution experiments reproduced volatility distributions with average uncertainties between 0.05 and 0.1 for most cases, provided that more than 20 % or so of the aerosol evaporated during dilution and that the system had enough time to come close to equilibrium. The vaporization enthalpy was estimated with average errors

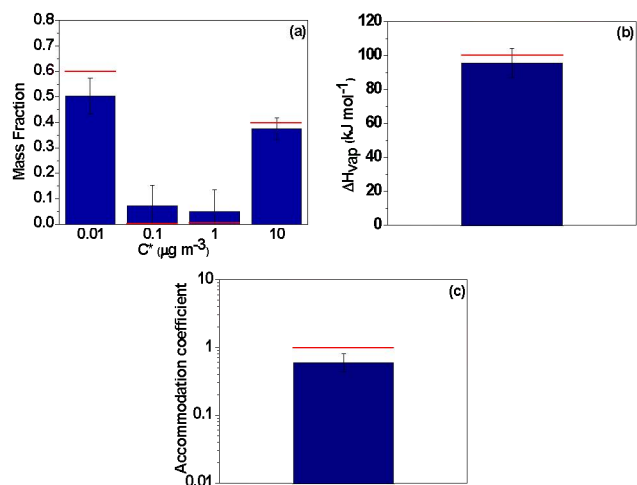


**Figure 8.** Estimated (bars) and true (red lines) parameter values combining TD and isothermal dilution measurements, for an OA with 60 % 0.01  $\mu\text{g m}^{-3}$  and 40 % 10  $\mu\text{g m}^{-3}$ ,  $\Delta H_{\text{vap}} = 100 \text{ kJ mol}^{-1}$  and  $a_m = 1$  for (a) volatility distribution, (b)  $\Delta H_{\text{vap}}$ , and (c)  $a_m$ .

less than 10 % in most cases. Estimation of the accommodation coefficient was more challenging than the other parameters. Problems occur mostly when evaporation in dilution experiments is less than 20 %, or when equilibrium is not reached.

## 5 Conclusions

Multiple combinations of parameters ( $C^*$ ,  $\Delta H_{\text{vap}}$ ,  $a_m$ ) can lead to practically indistinguishable thermograms during TD measurements. The estimated volatility distribution, based on the minimum error, can be wrong by several orders of magnitude due to the multiple solutions that exist, leading to multiple local minima of the objective function. We introduce a new method combining forward modeling, introduction of experimental error and inverse modeling with error minimization for the interpretation of existing TD measurements. With this method, using an ensemble of “best solutions”, we were able to calculate a best estimate and an uncertainty range for the estimated volatility distribution, the vaporization enthalpy and the accommodation coefficient. We show that this uncertainty range is often large and sometimes does not even include the true value of the properties, with the exception in the estimation of the vaporization enthalpy, where the errors are around 5–20 % in most cases tested.

Experimental approaches that would improve the method were explored. The performance of TD measurements under multiple residence times results in a small to modest improvement in the results, since equilibrium is still not reached. The idea of using experiments on a totally longer timescale in order to achieve equilibrium was then examined

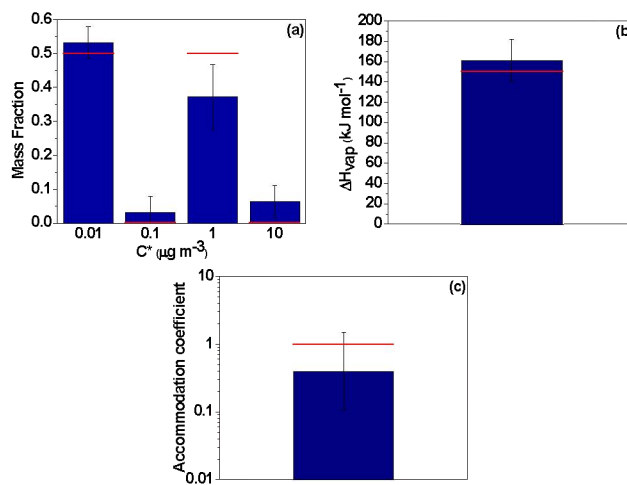


**Figure 9.** Estimated (bars) and true (red lines) parameter values combining TD and isothermal dilution measurements, for an OA with 50 % 0.01  $\mu\text{g m}^{-3}$  and 50 % 1  $\mu\text{g m}^{-3}$ ,  $\Delta H_{\text{vap}} = 150 \text{ kJ mol}^{-1}$  and  $a_m = 1$  for (a) volatility distribution, (b)  $\Delta H_{\text{vap}}$ , and (c)  $a_m$ .

with the use of dilution measurements. Use of isothermal dilution on its own instead of TD measurements usually leads to worse estimates of the volatility distribution compared to the TD. However, combining both TD and isothermal dilution measurements leads to promising results in the majority of the cases. Cases for which problems remain include those in which the OA does not come close to equilibrium after dilution, or when the corresponding evaporated fraction is less than 20 %. Increased dilution and longer residence times can help in these cases. The approach combining TD and isothermal dilution measurements is recommended for future studies of OA volatility in both the lab and the field.

*Acknowledgements.* This research was supported by the ESF-NRSF ARISTEIA grant ROMANDE, the US Department of Energy, and the FP7 IDEAS ATMOPACS project.

Edited by: J. Schneider

## References

- An, W. J., Pathak, R. K., Lee, B. H., and Pandis, S. N.: Aerosol volatility measurement using an improved thermodenuder: Application to secondary organic aerosol, *J. Aerosol. Sci.*, 38, 305–314, doi:10.1016/j.jaerosci.2006.12.002, 2007.
- Burtcher, H., Baltensperger, U., Bukowiecki, N., Cohn, P., Hüglin, C., Mohr, M., Matter, U., Nyeki, S., Schmatloch, V., Streit, N., and Weingartner, E.: Separation of volatile and non-volatile aerosol fractions by thermodesorption: instrumental development and applications, *J. Aerosol Sci.*, 32, 427–442, 2001.
- Cappa, C. D.: A model of aerosol evaporation kinetics in a thermodenuder, *Atmos. Meas. Tech.*, 3, 579–592, doi:10.5194/amt-3-579-2010, 2010.

- Cappa, C. D. and Jimenez, J. L.: Quantitative estimates of the volatility of ambient organic aerosol, *Atmos. Chem. Phys.*, 10, 5409–5424, doi:10.5194/acp-10-5409-2010, 2010.
- Cappa, C. D. and Wilson, K. R.: Evolution of organic aerosol mass spectra upon heating: implications for OA phase and partitioning behavior, *Atmos. Chem. Phys.*, 11, 1895–1911, doi:10.5194/acp-11-1895-2011, 2011.
- Chen, N. H. and Othmer, D. F.: New generalized equation for gas diffusion coefficient, *J. Chem. Eng. Data*, 7, 37–41, 1962.
- Donahue, N. M., Robinson, A. L., Stanier, C. O., and Pandis, S. N.: Coupled partitioning, dilution, and chemical aging of semivolatile organics, *Environ. Sci. Technol.*, 40, 2635–2643, 2006.
- Donahue, N. M., Kroll, J. H., Pandis, S. N., and Robinson, A. L.: A two-dimensional volatility basis set – Part 2: Diagnostics of organic-aerosol evolution, *Atmos. Chem. Phys.*, 12, 615–634, doi:10.5194/acp-12-615-2012, 2012.
- Engler, C., Rose, D., Wehner, B., Wiedensohler, A., Brüggemann, E., Gnauk, T., Spindler, G., Tuch, T., and Birmili, W.: Size distributions of non-volatile particle residuals ( $D_p < 800$  nm) at a rural site in Germany and relation to air mass origin, *Atmos. Chem. Phys.*, 7, 5785–5802, doi:10.5194/acp-7-5785-2007, 2007.
- Epstein, S. A., Riipinen, I., and Donahue, N. M.: A semiempirical correlation between enthalpy of vaporization and saturation concentration for organic aerosol, *Environ. Sci. Technol.*, 44, 743–748, 2010.
- Faulhaber, A. E., Thomas, B. M., Jimenez, J. L., Jayne, J. T., Worsnop, D. R., and Ziemann, P. J.: Characterization of a thermodenuder-particle beam mass spectrometer system for the study of organic aerosol volatility and composition, *Atmos. Meas. Tech.*, 2, 15–31, doi:10.5194/amt-2-15-2009, 2009.
- Fuchs, N. A. and Sutugin, A. G.: *Highly Dispersed Aerosols*, Ann Arbor Science Publishers, Ann Arbor, London, 1970.
- Fuentes, E. and McFiggans, G.: A modeling approach to evaluate the uncertainty in estimating the evaporation behaviour and volatility of organic aerosols, *Atmos. Meas. Tech.*, 5, 735–757, doi:10.5194/amt-5-735-2012, 2012.
- Grieshop, A. P., Miracolo, M. A., Donahue, N. M., and Robinson, A. L.: Constraining the volatility distribution and gas-particle partitioning of combustion aerosols using isothermal dilution and thermodenuder measurements, *Environ. Sci. Technol.*, 43, 4750–4756, doi:10.1021/es8032378, 2009.
- Huffman, J. A., Docherty, K. S., Mohr, C., Cubison, M. J., Ulbrich, I. M., Ziemann, P. J., Onasch, T. B., and Jimenez, J. L.: Chemically-resolved volatility measurements of organic aerosol from different source, *Environ. Sci. Technol.*, 43, 5351–5357, 2009.
- IPCC: *Climate Change: The Physical Science Basis – Contribution of Working Group I to the Fourth Assessment Report of the Intergovernmental Panel on Climate Change*, edited by: Solomon, S., Qin, D., and Manning, M., Cambridge University Press, Cambridge, 996 pp., 2007.
- Jonsson, A. M., Hallquist, M., and Saathoff, H.: Volatility of secondary organic aerosols from the ozone initiated oxidation of  $\alpha$ -pinene and limonene, *J. Aerosol Sci.*, 38, 843–852, 2007.
- Kalberer, M., Paulsen, D., Sax, M., Steinbacher, M., Dommen, J., Prevot, A. S. H., Fisseha, R., Weingartner, E., Frankevich, V., Zenobi, R., and Baltensperger, U.: Identification of polymers as major components of atmospheric organic aerosols, *Science*, 303, 1659–1662, 2004.
- Lee, B. H., Kostenidou, E., Hildebrandt, L., Riipinen, I., Engelhart, G. J., Mohr, C., DeCarlo, P. F., Mihalopoulos, N., Prevot, A. S. H., Baltensperger, U., and Pandis, S. N.: Measurement of the ambient organic aerosol volatility distribution: application during the Finokalia Aerosol Measurement Experiment (FAME-2008), *Atmos. Chem. Phys.*, 10, 12149–12160, doi:10.5194/acp-10-12149-2010, 2010.
- Lee, B. H., Pierce, J. R., Engelhart, G. J., and Pandis, S. N.: Volatility of secondary organic aerosol from the ozonolysis of monoterpenes, *Atmos. Environ.*, 45, 2443–2452, 2011.
- Nel, A.: Air pollution-related illness: Effects of particles, *Science*, 308, 804–806, doi:10.1126/science.1108752, 2005.
- Paciga, A. and Pandis, S. N.: Reduction of the volatility of atmospheric diacids due to their reactions with ammonia, submitted, 2014.
- Pathak, R. K., Presto, A. A., Lane, T. E., Stanier, C. O., Donahue, N. M., and Pandis, S. N.: Ozonolysis of  $\alpha$ -pinene: parameterization of secondary organic aerosol mass fraction, *Atmos. Chem. Phys.*, 7, 3811–3821, doi:10.5194/acp-7-3811-2007, 2007.
- Pope, C. A. and Dockery, D. W.: Health effects of fine particulate air pollution: Lines that connect, *J. Air Waste Manage. Assoc.*, 56, 709–742, 2006.
- Riipinen, I., Pierce, J. R., Donahue, N. M., and Pandis, S. N.: Equilibration time scales of organic aerosol inside thermodenuders: Kinetics versus equilibrium thermodynamics, *Atmos. Environ.*, 44, 597–607, 2010.
- Saleh, R., Walker, J., and Khlystov, A.: Determination of saturation pressure and enthalpy of vaporization of semi-volatile aerosols: The integrated volume method, *J. Aerosol. Sci.*, 39, 876–887, doi:10.1016/j.jaerosci.2008.06.004, 2008.
- Saleh, R., Shihadeh, A., and Khlystov, A.: On transport phenomena and equilibration time scales in thermodenuders, *Atmos. Meas. Tech.*, 4, 571–581, doi:10.5194/amt-4-571-2011, 2011.
- Saleh, R., Khlystov, A., and Shihadeh, A.: Determination of evaporation coefficients of ambient and laboratory-generated semivolatile organic aerosols from phase equilibration kinetics in a thermodenuder, *Aerosol Sci. Technol.*, 46, 22–30, 2012.
- Seinfeld, J. H. and Pandis, S. N.: *Atmospheric Chemistry and Physics*, 2nd Edn., John Wiley and Sons, Hoboken, New Jersey, USA, 2006.
- Stanier, C. O., Donahue, N., Pandis, S. N.: Parameterization of secondary organic aerosol mass fractions from smog chamber data, *Atmos. Environ.*, 42, 2276–2299, 2008.
- Wehner, B., Philippin, S., and Wiedensohler, A.: Design and calibration of a thermodenuder with an improved heating unit to measure the size-dependent volatile fraction of aerosol particles, *J. Aerosol Sci.*, 33, 1087–1093, 2002.
- Wehner, B., Philippin, S., Wiedensohler, A., Scheer, V., and Vogt, R.: Variability of non-volatile fractions of atmospheric aerosol particles with traffic influence, *Atmos. Environ.*, 38, 6081–6090, 2004.

Zhang, Q., Jimenez, J. L., Canagaratna, M. R., Allan, J. D., Coe, H., Ulbrich, I., Alfarra, M. R., Takami, A., Middlebrook, A. M., Sun, Y. L., Dzepina, K., Dunlea, E., Docherty, K., DeCarlo, P. F., Salcedo, D., Onasch, T., Jayne, J. T., Miyoshi, T., Shimojo, A., Hatakeyama, S., Takegawa, N., Kondo, Y., Schneider, J., Drewnick, F., Borrmann, S., Weimer, S., Demerjian, K., Williams, P., Bower, K., Bahreini, R., Cottrell, L.,

Griffin, R. J., Rautiainen, J., Sun, J. Y., Zhang, Y. M., and Worsnop, D. R.: Ubiquity and dominance of oxygenated species in organic aerosols in anthropogenically-influenced Northern Hemisphere midlatitudes, *Geophys. Res. Lett.*, 34, L13801, doi:10.1029/2007GL029979, 2007.

# Volatility and Aging of Atmospheric Organic Aerosol

Neil M. Donahue, Allen L. Robinson, Erica R. Trump, Ilona Riipinen,  
and Jesse H. Kroll

**Abstract** Organic-aerosol phase partitioning (volatility) and oxidative aging are inextricably linked in the atmosphere because partitioning largely controls the rates and mechanisms of aging reactions as well as the actual amount of organic aerosol. Here we discuss those linkages, describing the basic theory of partitioning thermodynamics as well as the dynamics that may limit the approach to equilibrium under some conditions. We then discuss oxidative aging in three forms: homogeneous gas-phase oxidation, heterogeneous oxidation via uptake of gas-phase oxidants, and aqueous-phase oxidation. We present general scaling arguments to constrain the relative importance of these processes in the atmosphere, compared to each other and compared to the characteristic residence time of particles in the atmosphere.

**Keywords** Aerosols · Atmospheric Chemistry · Multiphase Chemistry

---

N.M. Donahue (✉), A.L. Robinson and E.R. Trump  
Carnegie Mellon University Center for Atmospheric Particle Studies, Pittsburgh, PA, USA  
e-mail: [nmd@andrew.cmu.edu](mailto:nmd@andrew.cmu.edu)

I. Riipinen  
Department of Applied Environmental Science and Bert Bolin Centre for Climate Research,  
Stockholm University, Stockholm, Sweden

Carnegie Mellon University Center for Atmospheric Particle Studies, Pittsburgh, PA, USA

J.H. Kroll  
Department of Civil and Environmental Engineering, Massachusetts Institute of Technology,  
Cambridge, MA, USA

Department of Chemical Engineering, Massachusetts Institute of Technology,  
Cambridge, MA, USA

## Contents

1	Introduction .....	98
2	Background .....	99
	2.1 Phase Partitioning Thermodynamics .....	100
	2.2 Dynamics of Condensation and Evaporation .....	107
3	Evidence for Volatility in Atmospheric Aerosol .....	110
	3.1 Volatility of Primary Organic Aerosol .....	110
	3.2 Volatility of Secondary Organic Aerosol .....	112
4	Aging .....	121
	4.1 Gas-Phase Oxidation .....	121
	4.2 Heterogeneous Aging .....	126
	4.3 Aqueous-Phase Aging .....	129
5	Conclusions .....	132
	References .....	133

## 1 Introduction

Until very recently organic aerosol (OA) was commonly regarded as a mixture of non-volatile, non-reactive, primary organic aerosol (POA) [1, 2] augmented with a coating of secondary organic aerosol (SOA). POA particles were regarded as relatively non-volatile composites of organic compounds emitted by individual sources, such as biomass burning [3–5], gasoline [6–8] and diesel [1, 9] vehicles, food preparation [10–13], smoking [14], and numerous other small sources. SOA was regarded as an additional coating of secondary organic compounds formed via gas-phase oxidation of volatile organic carbon (VOC) precursors. Some of these reaction products evidently had a sufficiently low vapor pressure to condense onto pre-existing particles [15, 16]. Through a decade or so of research it became clear that SOA consisted of a mixture containing a large fraction of semi-volatile organic compounds that partitioned between the vapor and condensed phases based on well-established solution thermodynamics [17, 18].

This basic picture of organic aerosol was relatively well developed by the end of the 1990s. Chemical transport models were fed by inventories for POA emissions from a wide array of sources, and those emissions were treated in a variety of microphysics modules as effectively non-volatile and often chemically inert particles [19, 20]. SOA models evolved from relatively primitive treatments that simply converted a fixed fraction of VOC emissions into equally non-volatile secondary material (for example 12% of monoterpene emissions) to more sophisticated “two-product” representations that treated the equilibrium partitioning of surrogate species based on smog-chamber experiments [21–23]. Even today some global-scale models represent SOA as a fixed non-volatile fraction of VOC emissions [24, 25].

In most model representations of OA behavior, there was little if any consideration of long-term OA aging. With the realization that some OA could serve as relatively efficient cloud condensation nuclei [26–28] and also that soluble salts

such as ammonium sulfate would condense onto even the most hydrophobic organic cores, many models added some form of ad hoc aging timescale, typically converting a “hydrophobic” organic mode into a “hydrophilic” organic mode with a fixed timescale (usually of order 2 days).

Recently this picture has been more or less turned upside down. We now recognize that most POA emissions are actually fairly volatile, while SOA (at least in the form found in the atmosphere) is not very volatile at all [29, 30]. There is some debate over the effective volatility of even “traditional” SOA formed in smog-chamber experiments (called “chamber SOA” hereafter) [31], but it is also clear that chamber SOA is often a poor match for the SOA observed in the atmosphere. At the same time, recent papers have raised questions about the physical state of OA particles. There is considerable evidence that some OA particles may exist in a glassy or semi-solid state [32–34], and there is some confusion about whether this glassy state invalidates the solution thermodynamics treatments that have been developed to date (it does not) and debate over whether the mixtures actually reach equilibrium (they may not).

Work in our groups over the past decade has focused on the hypothesis that the coupling of gas-particle partitioning and gas-phase oxidation chemistry plays a central role in the properties and evolution of organic aerosol in the atmosphere, and that a very large fraction of all organic carbon atoms found in ambient particles has been involved in gas-phase chemical reactions at some point during their stay in the atmosphere. Volatility, in other words, plays a central role in the aging of organic aerosol in the atmosphere.

This chapter will focus on the interplay between volatility and chemical aging as it relates to organic aerosol. We shall emphasize the role of gas-phase oxidation chemistry but address other mechanisms as well. That emphasis is not meant to suggest that other aging mechanisms are unimportant, but rather that this one is important. Many of those other processes are ably covered by other articles in this volume.

## 2 Background

Of a total flux of non-methane reduced organic compounds into the atmosphere of about  $1,350 \text{ Tg year}^{-1}$  [35, 36], only 10% or so leads to organic aerosol [25, 37]. However, less than 1% of the primary organic emissions into the atmosphere have a sufficiently low volatility to remain in the condensed phase under ambient conditions, so SOA formation must be a huge part (90% or more) of the OA story [38]. The straightforward fact is that only a small fraction of all organic compounds (by mass) in the atmosphere have what it takes to stay on or in a particle. That special property is low volatility, and most compounds acquire that low volatility via chemical transformation in the atmosphere.

It is important to develop a sense of scale for volatility. A typical OA concentration is of the order  $1 \mu\text{g m}^{-3}$  (a mass fraction of 1 ppbm) and, if the molar weight of the SOA molecules averages  $200 \text{ g mole}^{-1}$ , the mole fraction of OA is roughly 100 ppt. If OA consisted of a single, pure organic compound and it had a saturation vapor pressure of  $10^{-7}$  Torr ( $1.3 \times 10^{-5}$  Pa), that compound would be 50% in the gas phase and 50% in the condensed phase at equilibrium under ambient conditions. That is a good definition of a semi-volatile constituent. Compounds with this saturation vapor pressure (over a sub-cooled liquid state) include pentacosane ( $\text{C}_{25}\text{H}_{52}$ , the canonical paraffin) and glucose. Those are not molecules one normally considers “semi volatile”; it is thus reasonable to expect standard intuition to be off target when considering organic aerosol. Of course, OA particles are *not* pure but rather contain thousands of different molecules, so mixing thermodynamics plays an important role as well. Furthermore, paraffin and glucose are notably viscous, so it is not necessarily surprising that viscosity effects may be important to OA behavior.

## 2.1 Phase Partitioning Thermodynamics

The thermodynamics of semi-volatile phase partitioning for atmospheric OA mixtures has been extensively treated in the literature [17, 18, 39, 40] and will only briefly be reviewed here. We express the effective saturation concentration ( $C_i^*$ ) of an organic compound by converting its saturation vapor pressure into mass concentration units and multiplying by the appropriate activity coefficient for the organic mixture (this is the inverse of the partitioning coefficient used in some formulations:  $K_{p,i} = 1/C_i^*$ ). The general effect of a solution is to lower the equilibrium partial pressure of a species from the equilibrium vapor pressure of the pure species; if the fractional reduction in the partial pressure (the activity) is equal to the fraction in the condensed phase, the solution is ideal and Raoult’s law applies. One simplifying assumption is to treat the system as a “pseudo-ideal” solution [23] in which the activity coefficients of individual compounds remain more or less constant over ambient conditions, in which case  $C_i^*$  for a given compound will remain constant as well.

The fundamental property of interest is the equilibrium fraction  $\xi_i$  of a compound in the condensed phase (vs the total in the condensed and vapor phases). With a total concentration of condensed-phase solute (often assumed to be the total concentration of organic aerosol,  $C_{\text{OA}}$ ), this is given very simply by

$$\xi_i = (1 + C_i^*/C_{\text{OA}})^{-1}. \quad (1)$$

This is a straightforward equation. It is evident that when the total OA concentration equals the saturation concentration of a constituent ( $C_i^* = C_{\text{OA}}$ ), that constituent will be 50% in the condensed phase at equilibrium ( $\xi_i = 0.5$ ).

Furthermore, a constituent with  $C_i^* = 0.1 C_{OA}$  will be ~90% in the condensed phase while a constituent with  $C_i^* = 10 C_{OA}$  will be only ~10% in the condensed phase. There is thus a fairly narrow range of (extremely low) volatilities spanning approximately a factor of 100 in  $C_i^*$ , centered around  $C_{OA}$ , where a compound will be “semi volatile.” Furthermore, this range varies with the aerosol loading – at high  $C_{OA}$  of perhaps  $100 \mu\text{g m}^{-3}$  found in very polluted cities (or source-dominated locations such as highway tunnels), the whole range of semi-volatiles will be shifted by a factor of 100 toward higher volatility. Also, experiments with significantly higher aerosol concentrations may not have phase partitioning consistent with the atmosphere. Until quite recently aerosol chamber experiments were performed with hundreds to thousands of micrograms per cubic meter of aerosol, resulting in phase partitioning very different from ambient conditions. Emissions measurements are still routinely performed at these unrealistic conditions.

There are at least three separate ways of treating partitioning for practical application to atmospheric aerosol. One is to run a full thermodynamic model containing an ensemble of specific molecules, while the other two are empirical.

### 2.1.1 Explicit Methods

Explicit methods seek to treat chemistry and thermodynamics with molecular detail, either including as complete a set of compounds as possible [41] or employing a reduced set of surrogate compounds to represent the full array of atmospheric compounds [21]. In either case the thermodynamics for this model system are treated as fully as possible, with individual vapor pressures and activity coefficients for the mixture calculated using one of several thermodynamic schemes [42–45]. A major challenge for this approach is the fact that the molecular composition of the vast majority of the OA mass is not known. However, when OA composition is known or if it can be predicted, they do allow one to assess as completely as possible the consistency of available data.

Recent studies on SOA derived from  $\alpha$ -pinene are a good illustration of the explicit methods. Simulations of  $\alpha$ -pinene ozonolysis using detailed chemistry from the Master Chemical Mechanism reproduce both SOA mass yields and the volatility distribution derived from chamber studies with good fidelity [46], though an earlier simulation using similar MCM chemistry but different vapor pressure estimation methods under-predicted SOA mass yields at low loading ( $C_{OA} < 10 \mu\text{g m}^{-3}$ ) [47]. A tailored  $\alpha$ -pinene oxidation mechanism also performs well in comparison with chamber experiments [48]. A generative mechanism (GECKO-A) applied to  $\alpha$ -pinene photo-oxidation generally over-predicts SOA formation, especially under low- $\text{NO}_x$  conditions [49]. None of those simulations modeled additional condensed-phase oligomerization chemistry. While the model-measurement intercomparisons were in general good, the dual uncertainties of the chemical mechanisms and vapor pressure estimation greatly complicated

substantive intercomparisons, even when additional measurements such as oxidation state of the SOA were included [46, 49].

### 2.1.2 Empirical Methods

Empirical methods are based on fits of partitioning data (generally chamber observations) to identify a set of pseudo-compounds with different abundances, which can then be used to simulate the gas-particle partitioning of OA. A major challenge with this approach is whether the properties of these pseudo-compounds are constant as one extrapolates away from the conditions under which the experiment was conducted. To help minimize these errors, it is critical to condition the partitioning experiments over as much atmospherically relevant space as possible.

#### N-Product Models

The most widely used empirical method is the “Odum two-product model” used to interpret many chamber experiments and implemented widely in air-quality models [23, 50]. When chamber SOA formation data are fitted to a two-product model, the output parameters are two mass yield parameters and two partitioning coefficients ( $K_{p,i} = 1/C_i^*$ ), giving a total of four free parameters. The two pseudo-species are not typically associated with any particular molecular products but rather regarded as completely empirical objects. In general they split into a “low-volatility” and a “high-volatility” product. One issue is that the recovered  $C^*$  values are highly dependent on the experimental dataset. The  $C^*$  values recovered from data fitting often coincide approximately with the range of measured  $C_{OA}$  values in the data, so the volatility of the two pseudo products depends on the concentration range of the experiments [51]. As an example, the  $C^*$  value commonly used for isoprene SOA is approximately  $1 \mu\text{g m}^{-3}$  [52], while the “low-volatility”  $C^*$  value used until recently for  $\alpha$ -pinene SOA was higher, at  $15 \mu\text{g m}^{-3}$  [53, 54]. It would be surprising if SOA derived from isoprene (with five carbons) were less volatile than SOA derived from  $\alpha$ -pinene (with ten carbons); however, because isoprene SOA experiments produce much less SOA than  $\alpha$ -pinene SOA experiments, the empirically derived product volatilities are skewed. This can have unexpected consequences when the two systems are mixed in a model simulation, where the presence of isoprene SOA will “seed” more volatile  $\alpha$ -pinene SOA formation. Reality is more likely to be the opposite of this.

Some of the deficiencies of the empirical two-product model can be eliminated by adding information to a multiple product model. One solution is to map products from chamber experiments onto a “carbon-number–polarity grid” based not only on the empirically observed SOA mass but also expected product properties [55]. Chemical evolution could be described on the grid, enabling a sensible description of aging.

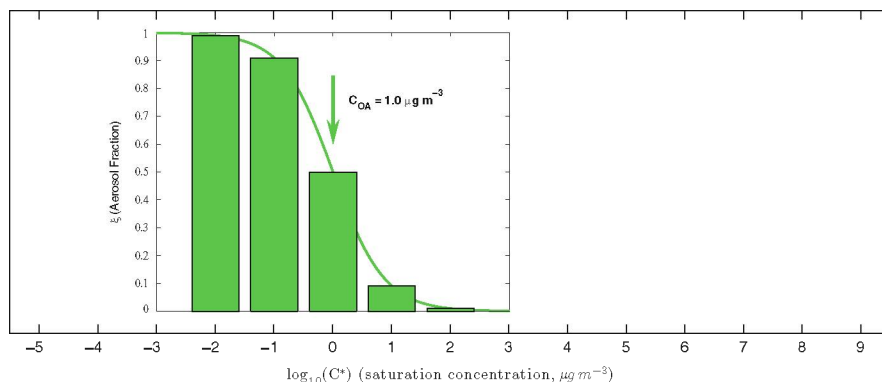


**Fig. 1** Partitioning behavior of organics for  $1 \mu\text{g m}^{-3}$  of total organic aerosol ( $C_{OA}$ ), shown as the fraction in the condensed phase ( $\xi$ , height of bars and curve) vs saturation concentration ( $C^*$ )

### Volatility Basis Set

Another empirical approach is known as the “Volatility Basis Set” (VBS). Like the two-product model, the VBS is empirical. However, the pseudo-product volatilities are fixed over a wide range, with  $C^*$  values typically separated by a single order of magnitude at 300 K [40]. An example is shown in Fig. 1. In a VBS fit the free parameters correspond to the different total concentrations (in any phase) in each volatility “bin” (each pseudo product). Thus, a VBS fit to SOA data with  $C^*$  bins at 1, 10, 100, and  $1,000 \mu\text{g m}^{-3}$  has the same number of formal degrees of freedom as a two-product model, but there is a crucial difference. Because the VBS  $C^*$  values are fixed, the overall partitioning function (Eq. 1) is only sensitive to the volatility of a given bin when  $C_{OA}$  is within about a single order of magnitude of the  $C^*$  value for that bin. The VBS parameters are thus relatively robust and independent of each other (there is covariance among adjacent bins, however, and so data can often have many equally good fits where material is divided differently among neighboring bins [56]). VBS parameters can only be fitted to data over slightly more than the range of  $C_{OA}$  values in a dataset – the extremes at lower or higher volatility must be constrained by other means, such as an overall carbon balance. With those constraints, a nine-bin VBS is often employed with  $C^*$  ranging from  $0.01 \mu\text{g m}^{-3}$  to  $10^6 \mu\text{g m}^{-3}$  [38]. This spans the full range of fully condensed organics, semi-volatile vapors, and “intermediate volatility” species and permits a good carbon mass balance. Though this requires nine species for transport in a model, if all organics form a pseudo-ideal solution the VBS fits from different OA sources can easily be combined to predict overall partitioning for a mixture without the unexpected consequences sometimes emerging from the two-product model.

## Non-ideality

A downside of the empirical approaches is they give little insight into non-ideal behavior of complex mixtures, including mixing effects of different organics (their activity coefficients), interaction with water, and interaction with inorganic constituents including salts and elemental carbon. These latter two types of interactions typically involve significant extrapolation away from the conditions of the experiments used to derive the fits. Unfortunately, there are very few direct measurements of activity coefficients for relevant organic molecules over relevant organic mixtures. It seems reasonable to expect seemingly similar OA, such as SOA derived from different precursors, to interact in a more or less ideal fashion, and indeed isotopic labeling experiments have confirmed this [57, 58]. However, mixing of less similar organics, such as relatively non-polar POA and more polar SOA, is less clear. Some experiments using non-polar organic “seeds” show little enhancement in SOA formation over experiments employing inorganic seeds [59], while other experiments directly observing mixing of SOA and POA by tracking the evolution of different size modes using size-resolved mass spectrometry show more nuanced behavior, with rapid mixing of semi-volatile POA into SOA seeds in some cases but not in others [60].

While methods based on explicit surrogate molecules (or complete enumeration of the organic mixture) can rely on calculated activity coefficients, the empirical methods must rely on approximations. In two-product SOA schemes one approach is to assume that generally similar classes of species mix with each other ideally (for example all SOA pseudo-products), but to permit either ideal mixing or complete phase separation of less similar constituents (for example SOA with POA) [23]. More generally, the empirical methods contain very little information about the molecular structure of OA constituents as they are based only on observed gas-particle partitioning and total mass concentrations. This complicates calculations not only of activity coefficients but also of important properties like the organic mass to organic carbon ratio (OM:OC) or the closely related oxygen to carbon ratio (O:C). Of course, composition information can be added based on additional observations, as with the carbon-number–polarity grid described above [61]. However, with the one-dimensional VBS there is an intrinsic problem: compounds with similar volatility can be very different chemically. For example, two compounds with a (sub-cooled liquid) saturation concentration near  $10 \mu\text{g m}^{-3}$  are tricosane ( $\text{C}_{23}\text{H}_{48}$ ) and levoglucosan ( $\text{C}_6\text{H}_{10}\text{O}_5$ ). Each are important in the atmosphere – tricosane is a constituent of lubricating oil [9] while levoglucosan is an important tracer for wood burning because it is a cellulose pyrolysis product [62] – but it is not surprising that lumping both into an identical bin in the 1D-VBS could obscure critical differences in their behavior.

An important issue to consider is the consequence of non-ideality. Interactions that enhance partitioning to the particle phase are important because they increase

aerosol concentrations and also often shield organics from the gas-phase oxidation discussed below. However, interactions that increase volatility will drive compounds into the gas phase where they will likely be oxidized quickly. In many cases the reaction products will return to the condensed phase, though on different particles and in a higher oxidation state. It is thus essential that one considers phase partitioning and aging together, and also that the coupled issues be considered jointly when developing simplified parameterizations for complex chemical transport models.

## Two-Dimensional Volatility Space

A two-dimensional version of the VBS addresses the issues just described, including non-ideality and the substantial differences in species contained in a single bin of the 1D-VBS [63, 64]. In addition, the two-dimensional volatility space (2D-VBS) enables more realistic treatment of aging chemistry and important properties such as hygroscopicity. The second dimension is formally the average oxidation state of carbon ( $OS_C$ ) described in Kroll et al. [65], which is related to the oxygen to carbon ratio (for “normally” bonded molecules,  $OS_C = 2 \text{ O:C} - \text{H:C}$ ). Figure 2a shows the average molecular composition (carbon number,  $n_C$ ; hydrogen number  $n_H$ ; oxygen number  $n_O$ ) in this space and also the approximate O:C for typical ambient aerosol composition [66]. Also shown are the measured saturation concentrations and  $OS_C$  for tricosane and levoglucosan. This shows that the approximate formulae given by the contours are not far off from observations, that these seemingly non-volatile species are in fact quite volatile by atmospheric standards, and that in the 2D space these quite different species are well separated even though their volatilities are nearly identical.

The  $x$  axis in the 2D-VBS is formally the pure-component saturation concentration  $C^\circ$  rather than the effective saturation concentration  $C^*$ , which includes the activity coefficient:  $C^* = \gamma C^\circ$ . A simplifying assumption in the 2D-VBS is that the activity coefficient is a function of the average O:C of the OA as well as the properties of the individual organic solute [63]. Figure 2b shows  $\gamma$  as an example for a case where the O:C of the bulk OA is 0.5 (typical of fairly fresh oxidized organic aerosol (OOA) in an urban setting [67]). In this case the contours are for different pseudo species (or bins) in the 2D-VBS. For example, a species with a  $C^\circ$  of  $1 \mu\text{g m}^{-3}$  and an O:C of 0.1 would have  $\gamma = 10$  (the last contour shown), meaning  $C^* = 10 \mu\text{g m}^{-3}$  for that particular mixture. The notable thing in Fig. 2b is that the predicted activity coefficients are mostly very close to 1, with the exception of very reduced material in the paraffin range typically associated with POA emissions. This confirms that most SOA species (with elevated O:C) will tend to form a nearly ideal solution with each other and only the semi-volatile POA species will tend to either phase separate into a distinct condensed phase or else have a *higher* partial pressure and thus partition toward the gas phase.

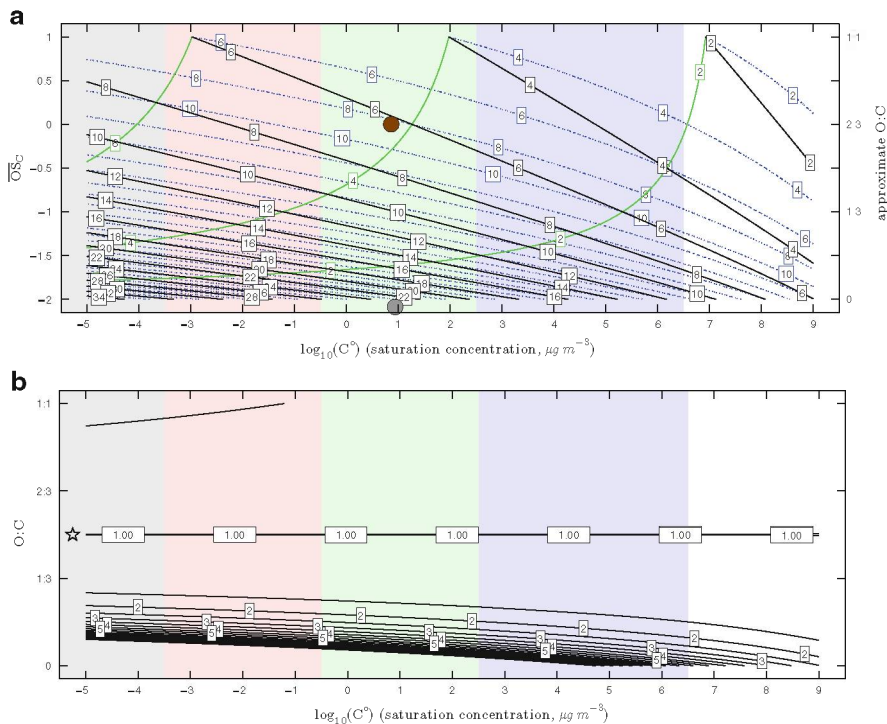


**Fig. 2** (a) Organic aerosol composition in 2D space defined by pure component saturation concentration ( $C^o$ ) and average carbon oxidation state ( $OS_C$ ). Solid black lines extending from lower left to upper right are average carbon number ( $n_C$ ). Solid green curves bending from top to lower left are average oxygen number ( $n_O$ ). Dashed blue curves bending from bottom to upper left are average hydrogen number ( $n_H$ ). Measured saturation concentrations for tricosane ( $C_{23}H_{48}$ , gray circle) and levoglucosan ( $C_6H_{10}O_5$ , brown circle) are shown as well. Both are semi volatile under ambient conditions. (b) Activity coefficients of organics in an organic solution with an average O:C = 0.5 (typical of fresh SOA or urban conditions). Contours are spaced by 0.5 and extend to 10.0. Values in the lower left of the space (occupied by compounds typically constituting POA) are much larger than 10.0

### Temperature Dependence

The temperature dependence of saturation concentrations can be approximated to first order by an Arrhenius type equation resembling the Clausius Clapeyron equation [40, 68]:

$$C^o(T) = C^o(300) \exp\left[\frac{\Delta H_{\text{vap}}}{R(1/300 - 1/T)}\right]. \quad (2)$$

In the VBS formalism the effect of changing temperature is to shift the  $C^*$  (or  $C^o$ ) values of the bins. The bins themselves shift with temperature – one does not

repartition material from one bin to another. This is straightforward [40, 69]. The exact  $\Delta H_{\text{vap}}$  for organic compounds remain a topic of some debate, but for a  $\Delta H_{\text{vap}}$  near  $100 \text{ kJ mole}^{-1}$ , a temperature change of 20 K results in a one-decade shift in a volatility bin.

## 2.2 Dynamics of Condensation and Evaporation

The equilibrium thermodynamics described above applies to all systems, but a key question is whether atmospheric systems actually reach that equilibrium. Furthermore, equilibrium phase partitioning says little about what size particles organic compounds end up on. The dynamics of organic condensation and evaporation have recently gained renewed attention for several reasons. First, it is clear that in many environments organic condensation plays a critical role in the growth of freshly nucleated particles up to diameters of 100 nm or so [70–75], where they can influence cloud physics by acting as cloud condensation nuclei. Because the timescale for growth of these ultrafine particles is similar to the production and loss timescales of the condensable vapors, a dynamic treatment is required. Second, there is also growing evidence that many particles containing OA may be in a highly viscous (glassy) state [32–34]. For particle growth, the *net* condensation rate of organics to particles is critical because that controls the growth rate. For glassy particles, diffusion limitations within particles may be rate limiting in condensation and growth, potentially preventing semi-volatile organics from reaching equilibrium on atmospherically relevant timescales [31]. In-particle diffusion limitations could cause apparent mass accommodation coefficients well below unity.

The VBS provides a convenient framework for organic dynamics in addition to equilibrium partitioning because equilibrium is a balance between condensation (the molecular flux from the gas to the particle phase) and evaporation (the molecular flux from the particle phase to the gas). The difference between the vapor concentrations at the particle surface and far away from it serves as a driving force for *net* condensation or evaporation. Because the particle surface is usually assumed to be in equilibrium with the gas phase adjacent to it, evaporation depends explicitly on volatility. Condensation on the other hand depends only on the collision rate of molecules with the surface and so it is first order independent of volatility. The volatility of organic compounds thus affects the aerosol growth dynamics specifically through its influence on the evaporation term in the driving force for mass transport.

It can be shown that the intrinsic growth or evaporation rate associated with a given organic volatility is given by  $v_D C_1^*$  where the characteristic velocity  $v_D$  is  $226 \text{ nm h}^{-1}/(\mu\text{g m}^{-3})$  [75]. This is modified by three important terms – the mass accommodation coefficient,  $\alpha$ , the surface-energy (Kelvin) term for particles smaller than 50 nm or so, and the Fuchs term for gas-phase diffusion limitations in the boundary layer around a particle for particles *larger* than 50 nm or so (with Knudsen

numbers  $Kn \leq 1$ ). Barring other limitations, the evaporation rate (in nanometers per hour) for a pure particle with a gas-phase concentration  $C_i^{\text{vap}}$  held at 0 is thus given by

$$dd_p/dt = F(d_p)K(d_p)C_i^* \alpha_i \nu_D. \quad (3)$$

This corresponds to a volume evaporation rate from a spherical particle of

$$dV/dt = 1/2\pi d_p^2 F(d_p)K(d_p)C_i^* \alpha_i \nu_D. \quad (4)$$

Given a volume  $V = 1/6\pi d_p^3$ , we can define a timescale for mass transfer via condensation or evaporation from a particle as  $\tau_e = V/(dV/dt)$ , or

$$\tau_e = (3F(d_p)K(d_p)C_i^* \alpha_i \nu_D)^{-1} d_p. \quad (5)$$

This timescale for a given species is independent of the fraction of that species present in an ideal organic mixture, but it is based on the limit of little net diameter change (evaporation of a pure particle will be quicker because the expression must be integrated down to zero volume). The timescale as a function of  $d_0$  is shown in Fig. 3 for unit mass accommodation and pure particles made up of constituents with different  $C^*$  values. The central bold curve is for  $C^* = 1 \mu\text{g m}^{-3}$ . Actual equilibration timescales will differ from this characteristic evaporation timescale; the exact timescale for equilibration of compounds in particles containing organic mixtures will depend on the extent of growth or evaporation required for a mixed particle to reach equilibrium. This in turn depends on the number concentration of particles because that dictates the total mass exchange between condensed and vapor phases, and for low volatility species equilibration timescales are often controlled by the condensational timescale, which can be faster than the evaporation timescale [76, 77]. Regardless, the intrinsic evaporation timescale for  $C^* = 1 \mu\text{g m}^{-3}$  organics in 200 nm diameter particles is very nearly 1 h. Timescales for more or less volatile compounds can be found simply by multiplying these values by  $C^*$  in  $\mu\text{g m}^{-3}$ , as shown by the parallel curves for different  $C^*$  bins. For example, in a typical SOA formation experiment from  $\alpha$ -pinene in which 100–1,000  $\mu\text{g m}^{-3}$  of SOA is formed, both VBS and two-product fits of product volatilities suggest that much of the SOA consists of species with volatilities also in the 100–1,000  $\mu\text{g m}^{-3}$  range. One would thus expect these SOA particles to evaporate substantially in 30 s to 6 min if the gas phase were forced to remain free of vapors.

There are at least three reasons why an evaporation timescale could be *longer* than the intrinsic value shown in Fig. 3. First, the actual mass accommodation coefficient  $\alpha$  for the compound could be less than 1 [78, 79]. Mass accommodation is defined as the fraction of vapor collisions with the surface of a particle that wind up adsorbed onto that surface as opposed to more or less immediately rebounding from the surface. There is some debate for light molecules such as water as to whether  $\alpha$  must be unity or whether it may be as low as 0.04 [80–84], and the average  $\alpha$  for  $\text{CO}_2$  from perfluorinated polyether (PFPE) is also approximately 0.5 [85]. Values of

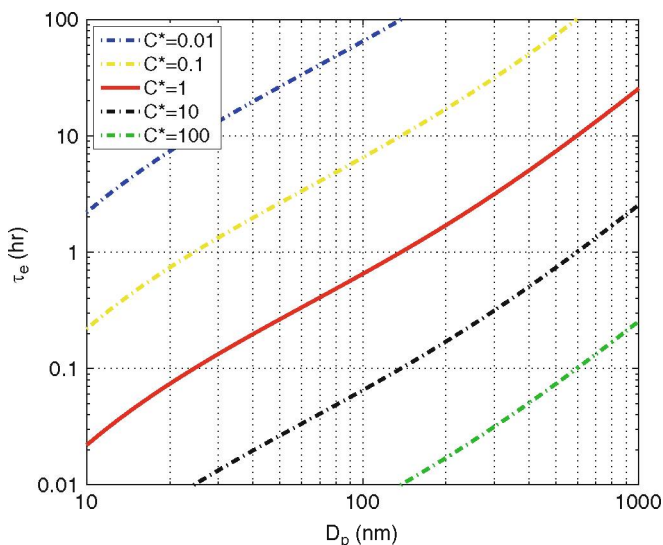


**Fig. 3** Characteristic evaporation timescales for organics vs particle diameter for a series of volatilities ( $C^*$ ) defined by contours. Organics with  $C^* = 1 \mu\text{g m}^{-3}$  in a 200-nm particle will evaporate in approximately 1 h if mass accommodation is perfect and diffusion within the particle is more rapid than 1 h

$0.1 \leq \alpha \leq 1$  seem plausible and have been reported for pure systems [86]. Lower values seem unlikely. However, even the meaning of  $\alpha$  at a molecular level is not firmly established and so non-unit accommodation coefficients must remain under consideration. Regardless of the exact value, at any given time the accommodation and evaporation coefficients for a molecule must be the same, or else the physical process responsible for changing  $\alpha$  would instead really be changing the  $C^*$  value itself.

The second possibility for slower evaporation is diffusion limitations within the particle itself, or possibly slow annealing of a particle to its equilibrium morphology (as in Ostwald's ripening). In this case the surface composition would not reflect the average composition of the particle. Glassy particles typify this possibility. The timescale for diffusive mixing of a constituent in a spherical particle is  $\tau_m = d_p^2 / (4\pi^2 \times 3,600 D)$  [87], where  $D$  in  $\text{cm}^2 \text{s}^{-1}$  is the diffusion constant of that constituent in the particle, and  $\tau_m$  is again expressed in h. Just as we use  $1 \mu\text{g m}^{-3}$  as a characteristic volatility, we shall use 200 nm as a characteristic diameter ( $200 \text{ nm}^2$  is  $4 \times 10^{-10} \text{ cm}^2$ ). Given these constraints, a 1-h or greater mixing timescale in a 200 nm diameter particle requires a diffusion constant (for the diffusing constituent in the mixture) of  $D \leq 10^{-14} \text{ cm}^2 \text{s}^{-1}$ . Alternately, it has been suggested that a thin coating of very viscous material on particles may inhibit organic mass transfer of higher volatility molecules to the particle surface, thus slowing or preventing evaporation [31]. Assuming a coating thickness of 10 nm, the diffusion coefficient of the evaporating molecules in this crust would have to be  $D \leq 3 \times 10^{-16} \text{ cm}^2 \text{s}^{-1}$

for the timescale to exceed 1 h. These are very low numbers, and no direct measurements of molecules/mixtures with such low binary diffusivities exist. Koop et al. [34] report that the primary predictor for the glass transition temperature in organics (indicative of  $D \leq 10^{-20} \text{ cm}^2 \text{ s}^{-1}$ ) is the molecular weight, followed by the degree of oxygenation (i.e., molecular polarity). Compounds with glass transition temperatures of 300 K are tricarboxylic acids with molecular weights of order 200 g/mole. Extension to  $D(T)$  for mixtures containing much less polar constituents remains unclear.

A third factor potentially influencing evaporation timescales of organic compounds is the presence of weakly bound oligomeric species or organic salts with dissociation lifetimes greater than the evaporation timescale. Even a weakly bound species, with a binding energy of 100 kJ mole<sup>-1</sup> and a unimolecular dissociation A factor of 10<sup>14</sup> s<sup>-1</sup>, would have a 1-h dissociation timescale at 300 K. Alone among these confounding factors, thermal decomposition can easily lead to an evaporation timescale that is independent of particle size; if the decomposition itself is the rate-limiting step for particle evaporation, the timescale will be fixed by the chemistry and not a mass-transfer limitation.

### 3 Evidence for Volatility in Atmospheric Aerosol

There is compelling evidence that a significant fraction of OA constituents are semi-volatile, with dynamic gas-particle partitioning under atmospheric conditions. However, the evidence also suggests that volatility is greatest near source regions, where aerosol is “fresh” [69, 88]. This is consistent with the hypothesis that chemical aging generally reduces, or really “resolves” volatility, driving semi-volatile species either toward relatively stable lower volatility products or toward highly volatile, highly oxidized small organic molecules (and ultimately CO<sub>2</sub>).

#### 3.1 Volatility of Primary Organic Aerosol

Despite the historical tendency of models to represent POA as a non-volatile mixture, there is longstanding and compelling evidence that POA emissions are substantially semi-volatile. The evidence comes in two major forms. First, both volatility-based chromatography and molecular elucidation of emissions profiles for various sources show clearly that most POA emissions span a wide range of  $C^*$  values and that most of those are  $\gg 1 \mu\text{g m}^{-3}$  [89, 90]. This is often simply a consequence of the properties of the parent materials for the emissions, such as lubricating oil. Second, when the gas-particle equilibrium is perturbed, either via isothermal dilution or via heating, POA particles shrink.

The second characteristic of primary organic emissions is that they tend to be relatively reduced. Using the average carbon oxidation state as a measure [65], most

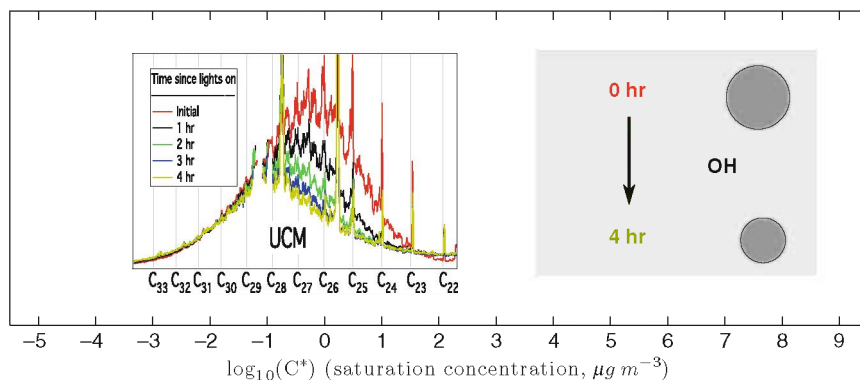


**Fig. 4** Oxidation of a motor oil mixture by OH radicals in a smog chamber, followed by thermal desorption gas chromatograms (TAG) taken every hour. Carbon numbers in the chromatogram are registered to typical saturation concentrations. More volatile organics ( $n_C < 28$ ) are removed more rapidly, indicating that gas-phase oxidation dominates the removal

but not all primary organic emissions have an  $OS_C \leq -1.5$ . This has significant consequences for aging chemistry, but in practical terms it also means that the emissions are relatively nonpolar and thus relatively easy to elute from standard gas-chromatograph columns.

As just one example of volatility separation, in Fig. 4 we show chromatograms of nebulized motor oil particles from an experiment in the CMU smog chamber using a thermal-desorption aerosol gas-chromatography (TAG) system [91], registered in the 1D-VBS. The figure shows two things. First, the red trace shows the initial chromatogram from oil droplets at  $C_{OA} \sim 10 \mu\text{g m}^{-3}$ . Only hydrocarbons with  $n_C \geq 23$  appear in the condensed phase because the more volatile constituents evaporate once the droplets are diluted to low concentrations in the chamber. Second, the experiment involved subsequent exposure to OH radicals, and the series of colored traces show chromatograms of non-polar material for each hour [92, 93]. Clearly, the more volatile fraction of the motor oil decayed much more rapidly than the less volatile fraction. The experiments showed simultaneous buildup of secondary oxidized organics on the particles [93]. This is consistent with gas-phase oxidation of vapors from that volatile fraction causing evaporation to compensate for the gas-phase loss, while heterogeneous oxidation of the less volatile constituents via OH uptake is evidently much slower [92].

Isothermal dilution consistently reveals that POA particles are semi-volatile [90]. Specifically, when POA samples are diluted, the particles shrink. They shrink because the gas-phase dilution lowers the partial pressure of vapors over the particles, and the particles respond to this perturbation by evaporating to raise the partial pressure of those vapors back to equilibrium. Analyses of POA dilution data suggest that a large fraction of the POA mass falls in the  $1\text{--}1,000 \mu\text{g m}^{-3}$  range [56, 94].

Evaporation upon heating can complement isothermal dilution. Most POA species are saturated and so are relatively inert and thermally stable; heating is thus unlikely to induce chemistry. Consequently, shrinking on heating in a thermodenuder is unambiguous evidence that the condensed-phase species in a POA particle are semi-volatile. An extra uncertainty associated with thermodenuders is the vaporization enthalpy of the organics [68]; however, as discussed above, a temperature change of 20 K corresponds roughly to an order of magnitude change in  $C^*$  (also a change in  $n_C$  of 2 corresponds to an order of magnitude change in  $C^*$ ). Most POA emissions evaporate quite readily in a thermodenuder [56]. For example, lubricating oil such as that shown in Fig. 4 evaporates almost completely when heated by 40 K, and one can see that a shift in the (unreacted) mode from  $n_C = 26.5$  to 30.5 should indeed correspond by substantial evaporation.

Several studies of primary particles near sources such as roadways [95] and fires [96] have also established that primary particles tend to shrink as they are isothermally diluted during dispersion downwind of a concentrated source [97, 98].

The bottom line is that emissions from (typically high-temperature) POA sources such as internal combustion engines, wood burning, and food preparation are all characterized by constituents with a broad range of volatilities, a large fraction of which have  $C^* > 1 \mu\text{g m}^{-3}$  [90]. Consequently, most of these emissions, even those with vapor pressures many orders of magnitude lower than traditional “volatile organic carbon,” will be in the gas phase very soon after emission (in seconds to minutes). The subsequent gas-phase chemistry of those vapors is thus one form of aging to consider in organic-aerosol evolution.

### 3.2 Volatility of Secondary Organic Aerosol

Somewhat ironically given the history of SOA and POA, SOA volatility is a more complicated topic than POA volatility. The principal reason is that SOA species are by definition products of reactions in the atmosphere, and many product compounds are themselves highly reactive. In addition, more oxidized organic species tend to be more polar than their reduced precursors and thus more difficult to sample using separation techniques. Furthermore, the added functionality associated with oxygenation opens up a vast space of potential chemical species, rendering complete speciation of a sample practically impossible [65]. In spite of this, there is every reason to believe that most SOA (especially “fresh” SOA) has a significant amount of semi-volatile mass.

Because of their comparatively large flux to the atmosphere [99], terpenes have long been a major focus of SOA-formation experiments [15]. Significant effort has been expended on speciating SOA, and while the complete mass has not been elucidated, many important product species have been identified [100, 101]. For example, with  $\alpha$ -pinene SOA many  $C_{10}$  products have been identified, and their  $C^*$  values range from roughly 1 to  $> 1,000 \mu\text{g m}^{-3}$  [46, 49]. Recently,

two-dimensional chromatography has been employed to combine volatility and polarity separation in a manner highly complementary to the 2D-VBS described above. 2D-GC can be mapped onto the 2D-VBS and, for example, a substantial amount of the eluted material from SOA formed via the longifolene + ozone reaction falls in the  $0.1\text{--}10\ \mu\text{g m}^{-3}$  range, with O:C varying systematically from about 0.25 at the low  $C^*$  end to about 0.1 at the high  $C^*$  end [102]. Longifolene is a sesquiterpene ( $\text{C}_{15}\text{H}_{24}$ ), and the observed  $C^*\text{--O:C}$  range is consistent with the range expected for product molecules with 12–15 carbons seen in Fig. 1a.

Less volatile compounds have been observed from terpene-ozone SOA as well, including  $\text{C}_{20}$  and larger “oligomers” [103–105] and very low volatility organosulfates [106]. It remains unclear what fraction of the SOA mass is comprised of these less volatile species, but estimates range from 1/3 to 1/2 [105]. It is also not clear whether the majority of oligomers are formed irreversibly or whether they are in equilibrium with monomer species [107]. What is clear is that a substantial fraction of the SOA mass consists of semi-volatile monomeric species, and one thus expects phase partitioning to play a major role in their behavior.

Indeed, absorptive partitioning theory [18] played a critical role in the interpretation of SOA chamber data, making sense of a confusing disarray of mass yield data [17]. Specifically, partitioning theory explains the general tendency for mass yields to increase with increasing total OA concentrations. In Fig. 5 we show mass yield data for the  $\alpha$ -pinene + ozone reaction along with a representation of the rising yields with increasing  $C_{\text{OA}}$ . In this figure  $C_{\text{OA}}$  (in micrograms per cubic meter) is plotted on the same axis as  $C^*$  (also in micrograms per cubic meter). The concentration range over which mass yields rise sharply is the concentration range where the bulk of the products lie – in this case  $C^* \geq 1\ \mu\text{g m}^{-3}$ . An extremely important caveat is that this partitioning analysis is only valid if the overall product distribution (including the condensed and vapor phases) remains constant during a chamber experiment, so that only thermodynamics and not chemical aging governs the amount of material that partitions into the particle phase (in other words,  $C_{\text{OA}}$  responds to the amount of identical products being produced and not to changes in the product and volatility distribution over the course of a reaction). The very small mass yields at very low  $C_{\text{OA}}$  pose a challenge to quantitative treatment of the oligomerization reactions described above, as even at fairly low  $C_{\text{OA}}$  particles in chamber experiments are quite stable, maintaining a constant diameter over many hours [101] and thus showing no clear evidence (no increase of SOA mass) of any slow chemical reactions that might slowly alter the volatility distribution.

To be truly consistent with partitioning theory, particles must also shrink upon dilution, much like POA described above. Different experiments have confirmed that  $\alpha$ -pinene + ozone SOA particles do evaporate upon dilution, but not in the minute or so suggested by the volatility distribution in Fig. 5 and the timescales in Fig. 3. Rather, particles relax back to equilibrium after dilution over hours [31, 108], though they do eventually reach the size predicted from equilibrium partitioning theory [108]. This delay is consistent with some phenomenon slowing evaporation by at least a factor of 100. Potential causes for this delay include dissociation of weakly bound oligomers [108] or slowed diffusion in the particles themselves

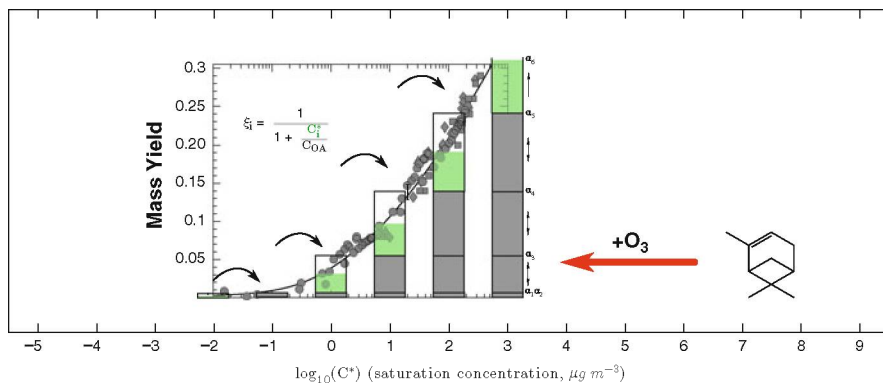


**Fig. 5** SOA mass yields from  $\alpha$ -pinene ozonolysis vs total SOA mass ( $C_{OA}$ ). Increasing mass fractions with increasing  $C_{OA}$  are consistent with progressive partitioning of more volatile products at higher loadings, as shown

[31, 108]. A recent study [31] reports that size selected  $\alpha$ -pinene + ozone SOA particles at  $d_p = 160$  and  $250$  nm showed nearly identical evaporation behavior, whereas the timescales in Fig. 3 are a factor of 2 different. That is consistent with a dissociation timescale being rate limiting as opposed to pure evaporation.

A final element in the evidence supporting a substantially semi-volatile nature for most “fresh” SOA comes from thermodenuders. As with POA, SOA formed in smog chambers evaporates quite readily in thermodenuders [109–113]. Quantitative analysis (inverting thermodenuder data to find a volatility distribution) is difficult because of several confounding factors. These include uncertainties in  $\Delta H^{vap}$  as well as the mass accommodation coefficient [69, 77]. An extra cause of concern with SOA, unlike POA, is the potential for the SOA to change chemically when it is heated [68]. However, with significant evaporation of chamber-derived “fresh” SOA mass after only 40 K of heating, thermodenuder data are certainly consistent with a substantial fraction of the SOA mass from chamber experiments being semi volatile [110, 114].

Ambient SOA, or at least the highly-oxygenated OOA, generally loses much less mass in thermodenuders [29, 69, 115] than fresh SOA, suggesting that it is much less volatile. Inversions using a VBS framework find a very broad distribution of  $C^*$  values for OOA constituents, suggesting (along with the high degree of oxidation) that OOA has undergone substantial oxidative aging in the atmosphere [64, 69].

### 3.2.1 Do OA Particles Form Mixtures?

In order for mixing thermodynamics to apply, an OA particle must actually be mixed. There are compelling reasons to believe this is so but also some reasons to question whether the mixing is complete. This question really splits into two questions: is the *equilibrium* for OA constituents a uniform mixture and, if so, do

ambient particles relax to that equilibrium more rapidly than they are transported or lost?

There is little doubt that most organic compounds in ambient particles exist in some form of mixture, simply because the particles are composed of an enormous number of different molecules. In the most extreme cases a single constituent can make up as much as 10% of some ambient particles (for example levoglucosan near some fire plumes or certain isoprene oligoesters in very isoprene-rich environments) [116, 117]. However, in most cases the most abundant identified constituent in OA samples comprises less than 1% of the total OA mass. Consequently most organic molecules in most particles are far more likely to be solvated by and interacting with many different molecules with a variety of carbon chain lengths, branching structures, and numbers and types of functional groups. This is one reason why crystallization seems highly unlikely for most particles and consequently why the mixing thermodynamics are developed for amorphous mixtures (thus employing the sub-cooled liquid vapor pressure as the starting point for partial-pressure calculations) [18]. This also provides information on experimental design, especially relating to organic “seeds” for SOA formation that might promote condensation via absorptive partitioning. High fractions of any individual seed species will enhance the probability that a separate (potentially crystalline) “seed phase” will form in an experiment, while more realistic seed mixtures will be less vulnerable to such phase separation.

A second factor favoring mixtures is that most OA constituents arrive in a particle via condensation. The organic condensation rate in the boundary layer under many conditions is roughly  $1\text{--}10\text{ nm h}^{-1}$  [73]. Near sources there will be (sometimes concurrent) evaporation and condensation of POA species, and both near and far from sources there will be condensation of oxidized secondary molecules as well as uptake of oxidants. Furthermore, in many cases important inorganic species such as sulfuric acid, nitric acid, and ammonia are condensing (and in the latter two cases evaporating) from particles simultaneously. Perhaps most importantly, as relative humidity (RH) varies, the activity of water in a particle will vary as well. Above about 90% RH, more than half of the volume of most particles will be water, and this water will form an extremely high ionic strength aqueous phase incorporating at least some of the more soluble organic molecules (and even the “hydrophobic” residual organic phase may include significant water). Under many circumstances air parcels move vertically through the boundary layer in minutes, and consequently they cycle through a wide RH range (often including saturation if a cloud layer is present) [118].

If the organic mixture does indeed form a single phase at equilibrium, then the conditions for complete equilibration require equal composition in each particle. Actually attaining this equilibrium requires mass exchange, which in turn can occur only through coagulation (which is not really an exchange mechanism) or inter-particle mass transfer (condensation–evaporation) [39]. Strict equilibration would require that all species be present in (the organic fraction of) all particles in equal abundances; however, we can also define a “volatility equilibrium” in which particles are neither growing nor shrinking because their “volatility composition”

is equilibrated even though their exact composition is not. Specifically, within the VBS the mass fraction of each VBS bin represented in each particle would be the same, so the fraction of semi-volatiles in each particle would be the same. A trivial example of this is a suspension of single-component particles in which some particles have an isotopic label. The particles would be at all times in volatility equilibrium and there would be no driving force for a net mass change, and yet to reach full equilibrium the isotopic composition of each particle would need to become identical, driven by the entropy of mixing.

The concept of volatility equilibration is important when considering very low volatility constituents in particles. The timescale for equilibration of extremely low volatility molecules via net condensation approaches infinity; the molecules will simply never leave their initial particles. However, the more volatile molecules in a mixture can still attain volatility equilibrium by independently establishing equal activity over all particles long before the less volatile constituents have been able to equilibrate. The overall timescale for this process may be complex as different constituents evolve simultaneously.

### Condensation, Aging, and Mixing

Mixing for atmospheric aerosol essentially always involves some form of condensational uptake to particles. A unique characteristic of condensational uptake is that it is proportional to the (modified) surface area of particles and not their volume (“modified” refers to the Fuchs correction for gas-phase diffusion for larger particles with  $Kn \lesssim 1$ , which reduces the effective surface area for condensation). Because the surface area to volume ratio of particles increases as their diameter decreases, condensation tends to have a larger effect on smaller particles, when measured on a mass (or volume) basis. The concept of “surface limited” vs “volume limited” aging has been used before to diagnose different processes in aerosol evolution [119]. However, condensation also tends to drive mixtures out of equilibrium, as the volume fraction of condensing vapors will grow more rapidly for smaller particles than for larger particles. This can be a very useful diagnostic of mixing effects in particles. As an example of “pure condensation” we shall discuss condensation of SOA from the  $\alpha$ -pinene + ozone reaction onto pre-existing ammonium sulfate “seed” particles, and then we shall discuss two other cases with more interesting mixing effects.

The condensation rate of organics to a particle surface is given by Eq. 3, multiplied by the saturation ratio of the organic vapors ( $S = C_i(\text{gas})/C_i^*$ ) [75]. In Fig. 6 we show the theoretical condensation of organic vapors to inert seeds with an initial lognormal mass mode centered at 300 nm and a Gaussian width of 0.2. The vapors condense onto the inert seeds in proportion to the diffusion-modified seed surface area. The figure shows the initial and final total aerosol size distributions (dashed curves) as well as the final mass distribution of condensed organics and inert seeds (labeled “sulfate” because we tend to use ammonium sulfate for seeds). In the final distribution the condensed organics strongly favor the smaller particles.

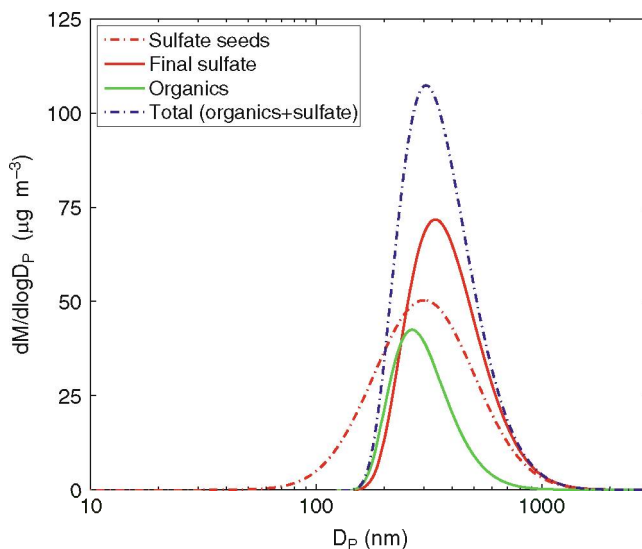


**Fig. 6** Calculated condensational growth of organics onto inert (sulfate) seeds, shown as mass distributions vs log of particle diameter. Initial seeds are shown as a *dashed red* Gaussian centered at 300 nm. The final total size distribution is shown as a dashed blue curve. The final sulfate mass distribution is shown as a *solid red* curve, shifted to a 370-nm mode because of organic condensation. The final organic mass distribution is shown as a solid green curve. The organic mass mode after condensation is at 270 nm because condensation (of organics in this case) strongly favors smaller particles with larger surface area to volume and less inhibition from gas-phase diffusion. Because the organics and sulfate do not form a mixture, the final composition (organic:sulfate) is a strong function of particle diameter

This weighting toward smaller sizes of a purely condensational process is characteristic of the interaction between condensing vapors and an inert seed (or of completely non-volatile condensation). It is what drives “condensational narrowing” [120] which is evident in the distorted final distributions in the simulation. In either case the composition of the particles is a strong function of size: in Fig. 6 the 200-nm particles are more than 80% organic, while the 500-nm particles are less than 20% organic; if the particles comprised a single condensed phase they would be far out of equilibrium.

Many SOA formation experiments use inorganic seed particles to encourage condensation onto suspended particles instead of chamber walls [121]. Often the assumption in these experiments is that the inorganic seeds do not influence the SOA mass yields, and mass-yield data confirm this assumption [122]. In Fig. 7 we show size-resolved mass spectra obtained using an aerosol mass spectrometer in particle time of flight (pToF) mode for SOA formed from the toluene + OH reaction and condensed onto dried ammonium sulfate seeds at 15% RH from experiments reported in Hildebrandt et al. [123]. The pToF data show exactly the features expected for condensation onto inert seeds. Very similar data are shown in Prisle et al. [124] for SOA formed from  $\alpha$ -pinene + ozone. It is worth noting that

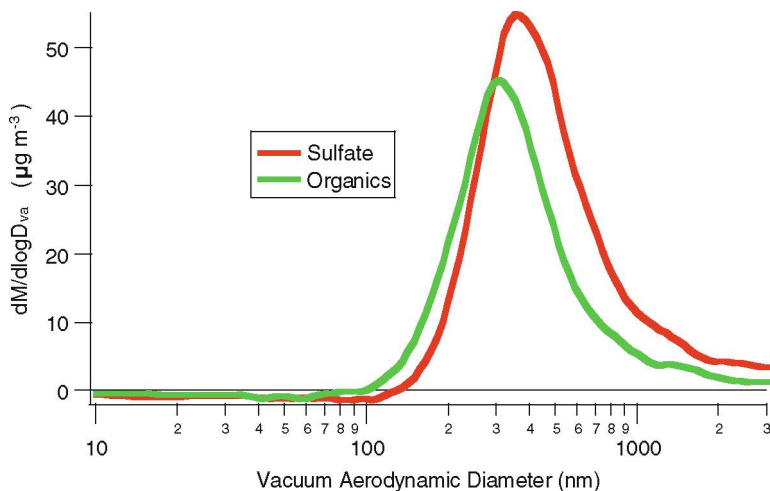


**Fig. 7** Measured organic (*green*) and sulfate (*red*) mass distributions from Aerosol Mass Spectrometer particle time of flight (AMS pToF) data. Data are for SOA from toluene oxidation in the presence of ammonium sulfate seeds. Observations closely follow predictions shown in Fig. 6

ambient particles often do *not* show this displacement between organics and sulfate because *both* the organics and sulfate accumulate via condensation, often more or less simultaneously. How particles anneal to a phase-separated morphology with distinct inorganic and organic phases (if indeed this is the equilibrium state [125, 126]) remains unclear.

The situation is very different when organics mix with each other. In Fig. 8 we show AMS pToF data from a mixing experiment first reported by Asa Awuku et al. [60]. In this case POA from a diesel engine was injected into a chamber containing SOA from  $\alpha$ -pinene + ozone. As shown in the top panel, the POA initially appeared as a distinct mode with ion fragments characteristic of primary emissions and a modal diameter significantly smaller than the SOA particles. Within 5 min the distinct POA mode vanished and the characteristic ion fragments migrated to the SOA mode, as shown in the lower panel. This clearly indicates that relatively volatile POA evaporated and re-condensed into the SOA, with the lower activity of the POA species in the SOA particles acting as a thermodynamic driving force for the mixing. There were, however, strong indications that the mixing was non-ideal. Both composition and concentration influenced these effects. Specifically, an injection of motor-oil droplets similar to the diesel POA remained stable for hours as a distinct mode while the diesel POA quickly mixed with the SOA seeds. The activity coefficients of the oil vapors were thus significantly greater than 1 in the SOA particles, so at some finite concentration of POA species in the SOA (and vice versa, though the mass spectra did not show this directly) the suspension became stable, with two distinct condensed phases present [60]. Also, the rapid (5 min) mixing of a significant quantity of POA into the SOA particles clearly shows that (in this case at least) diffusion of the POA species into the SOA was not a

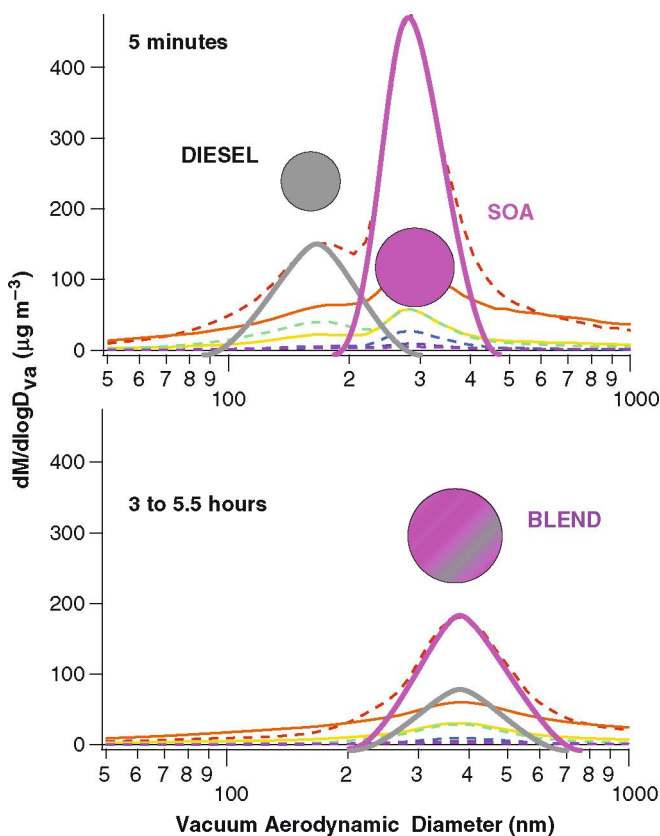


**Fig. 8** Measured AMS pToF distributions for diesel POA particles injected into a smog chamber containing SOA from  $\alpha$ -pinene ozonolysis. POA particles are evident as a distinct mode at 180 nm for only 5 min (*upper panel*) after which they vanish into the SOA seeds (initially at 300 nm, ultimately at 400 nm, *lower panel*). Both the timing and coincident size distributions of the ultimate particle distribution confirm that mixing of POA into SOA occurred via evaporation of fresh POA and subsequent condensation and full (volume) mixing into the SOA seeds

significant impediment; the lack of complete mixing in some cases likely indicates non-ideality as opposed to delayed equilibration.

A final example involves gas-phase aging chemistry. In Fig. 9 we show two pToF spectra from semi-volatile diesel oxidation experiments described elsewhere [127–129]. In these experiments, diesel emissions were diluted to near ambient levels and then exposed to photolytically generated OH radicals [128]. The pToF data are shown for two key ion fragments,  $m/z = 57$  and 44, which are traditionally indicative of reduced (“hydrocarbon like”) POA and oxidized SOA [130]. In these experiments the total OA concentrations more than doubled in 5 h due to SOA formation. The figure reveals that the  $m/z = 44$  marker characteristic of the SOA remained locked into the mode characteristic of the POA defined by  $m/z = 57$ , even as the  $m/z = 44$  abundance increased due to condensation. Data are shown just

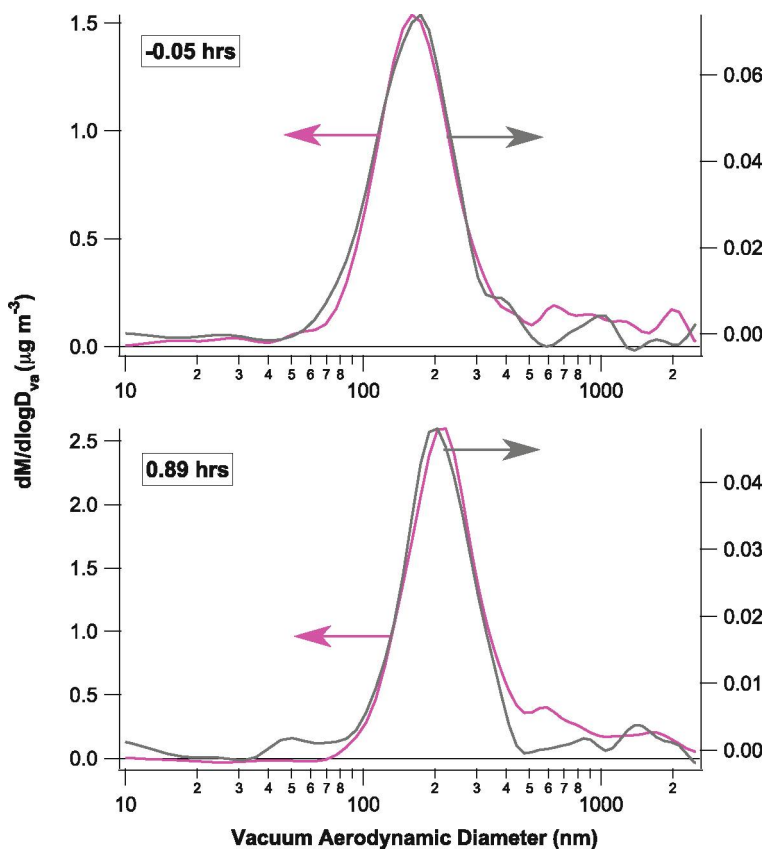


**Fig. 9** SOA production on diesel seed particles. SOA formed from photooxidation of diesel vapors shown by increasing mass fraction of  $m/z = 44$  (largely  $\text{CO}_2^+$ , pink) fragment, left scale vs  $m/z = 57$  (largely  $\text{C}_4\text{H}_9^+$ , gray) fragment, right scale. The horizontal arrows point toward each axis at a constant  $y$  value in the two panels to illustrate the extent of condensation by SOA. Concurrent diameter growth shows that condensation and evaporation maintain equal mass fractions of more reduced and more oxidized organic species in all particles, independent of size

before oxidation and after 1 h of photochemistry, but the OOA mode never lagged behind the POA mode in the manner characteristic of condensation to inert seeds shown in Figs. 6 and 7. The evidence is thus strong that the POA and SOA formed a mixture throughout the diesel oxidation experiment.

To maintain the equal mixing shown in Fig. 9, condensation alone is not sufficient; the only way to keep the volume (mass) distributions of species constant during a period of strong condensational growth is via *net* condensation, meaning that some species also evaporate significantly from relatively enriched particles and re-condense on relatively depleted ones. From these data there is no way to tell whether it was the POA or the SOA species (or both) evaporating and recondensing, only that this surely occurred with more or less complete volume mixing on a timescale faster than the growth (faster than 1 h or so). However, if

the mixing experiment shown in Fig. 6 and the calculations shown in Fig. 3 offer any indication, it is likely that the POA vapors were largely responsible for this equilibration.

## 4 Aging

The previous example brings us to aging. Here “aging” refers to chemical aging – in other words chemical reactions that alter the composition of an organic aerosol. There are at least five modes of aging: gas-phase oxidation of organic vapors, heterogeneous uptake of oxidants, condensed-phase reactions among organics, acid–base reactions involving organics, and aqueous reactions involving organics. As discussed in the introduction, the focus of this work is largely on gas-phase aging.

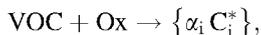
### 4.1 Gas-Phase Oxidation

Gas-phase chemistry is a key player in organic-aerosol evolution. We shall discuss organic oxidation chemistry first because this is a homogenous process. There are no circumstances where it will not happen – no diffusion limitations or other inhibiting phenomena. If an organic compound is oxidized in the gas phase and an oxidation product has a sufficiently low  $C^*$ , that product will condense to a particle when it collides with it. Thus, when we consider gas-phase oxidation we are interested principally in the volatility distribution of the reaction products as well as their composition. All increases in OA mass due to gas-phase chemistry can be called “secondary organic aerosol” (SOA) because the reaction products are secondary molecules and the aerosol mass increases, so the added mass is secondary mass. These topics have been extensively covered in numerous publications and reviews, and so we shall touch only briefly on key issues here. For historical and practical reasons we shall split our discussion between SOA formed from volatile precursors (sometimes called “traditional” SOA) and SOA formed from less volatile precursors (one class of so-called “non-traditional” SOA). Hydrocarbon oxidation is an inexorable process proceeding from a highly reduced primary compound (often relatively volatile) ultimately to  $\text{CO}_2$  (also highly volatile) [65]; however, intermediates in this process can have extremely low vapor pressures.

#### 4.1.1 VOC Secondary Organic Aerosol

SOA from VOCs has a long history [15, 17, 51] and is also discussed elsewhere in this volume. The key finding relevant to a broader aging discussion is that products of gas-phase oxidation reactions can have lower  $C^*$  than the precursor. A recent

focus has been to conserve carbon when parameterizing an SOA formation process, i.e., in a VBS formulation



where  $\{\alpha_i\}$  is a set of carbon mass yields (i.e., micrograms per cubic meter of OC formed for  $1 \mu\text{g m}^{-3}$  of VOC consumed). The total OA mass can then be obtained with some added information – specifically  $\text{OM}:\text{OC}_i$ , the ratio of organic mass to organic carbon within each product bin. This can be estimated from loading-dependent composition (C:H:O) measurements during SOA formation [131] and is directly constrained within a 2D formulation of the VBS that includes composition information as a second dimension [63, 64].

The relevant issue here is that many analyses suggest that much of the SOA mass is semi volatile, as discussed above. In addition, because the SOA mass yields are generally well below 1, it is clear that many other reaction products are lower in volatility than the precursor but too volatile to influence the SOA mass. All of those vapors are in play for subsequent later-generation aging chemistry.

#### 4.1.2 IVOC and SVOC Secondary Organic Aerosol

Intermediate volatility organics (IVOCs) are much less volatile than VOCs but still much more volatile than species that can condense under ambient conditions. Most of the first-generation SOA products shown in the VBS fits in Fig. 10, with  $300 < C^* < 3 \times 10^6 \mu\text{g m}^{-3}$ , are considered IVOCs. In addition, a substantial fraction of primary emissions from high-temperature combustion, including wood burning, food preparation, internal combustion engines, and turbine engines, consists of IVOCs and SVOC (with  $0.3 < C^* < 300 \mu\text{g m}^{-3}$ ) [90]. We shall discuss direct formation of SOA from IVOC and primary emissions first because the kinetics and initial mechanisms of these reactions have been studied more widely.

##### SOA from Primary IVOC Emissions

A challenge with the atmospheric chemistry of IVOC is the exponential increase in chemical complexity with increasing carbon number, even for “simple” hydrocarbons containing only carbon and hydrogen [35]. Consequently, studies of SOA formation from IVOCs fall into two categories: study of individual molecules or sequences of molecules as representative model systems and study of undifferentiated “whole” emissions diluted to near ambient conditions to encourage atmospherically relevant partitioning of the primary emissions.

Two broad classes of lower volatility hydrocarbons have been studied extensively: alkanes and polycyclic aromatics. Alkanes have been more systematically treated with regard to their potential for SOA formation, while the chemistry and

phase partitioning of polycyclic aromatics were in many ways the foundation for the ambient partitioning theory described in this chapter because of the significant concerns over PAH health effects.

### *Alkanes*

Alkanes are an excellent model system because they present a homologous sequence in both carbon number (and thus volatility) as well as structure (and thus varying chemical behavior). Alkane SOA formation has been studied systematically by Ziemann and coworkers [132] as well as others. Broadly, the SOA formation potential of *n*-alkanes increases systematically with carbon number [132, 133] as the precursor volatility decreases. Substitution in the form of branching significantly decreases SOA formation at a given carbon number, while cyclization increases SOA formation. In each case the reason is fragmentation of secondary products: branched alkanes are more vulnerable to C–C bond cleavage during oxidation, while cycloalkanes can sustain one C–C bond cleavage event without a decrease in carbon number because of the tethering effect of the cyclic structure [134].

### *Polycyclic Aromatics*

PAHs have been studied for decades because of their high potential for negative health effects [135–137]. Investigators quickly realized that PAH volatility spanned a wide range and thus that important PAH species would be found in both the gas and condensed phases in the atmosphere. Partitioning theory was developed for atmospheric applications in large measure to address these issues. For some time, adsorption to surfaces was considered to be more important than absorption into an organic condensed phase [138]; however, by stages it became evident that the total mass of the condensed phase (TSP) was significant to partitioning [139] and ultimately that absorptive partitioning with the condensed organic phase was often the appropriate framework for partitioning [140]. While that work laid the foundation for the perspective on partitioning described here, consideration of the SOA formation from PAH oxidation is much more recent. Like the alkanes, PAH oxidation has been studied as a potentially important model for SOA formation from IVOCs [141].

### *Evaporated Primary Emissions*

Real primary emissions consist of a complex mixture including linear and branched alkanes, mono aromatics, substituted aromatics (alkyl benzenes), and PAHs, among many other compounds [7, 142]. The most direct evidence that SOA formation is important for typical atmospheric IVOC mixtures thus comes from experiments on vapors from these very mixtures [127, 143–148].

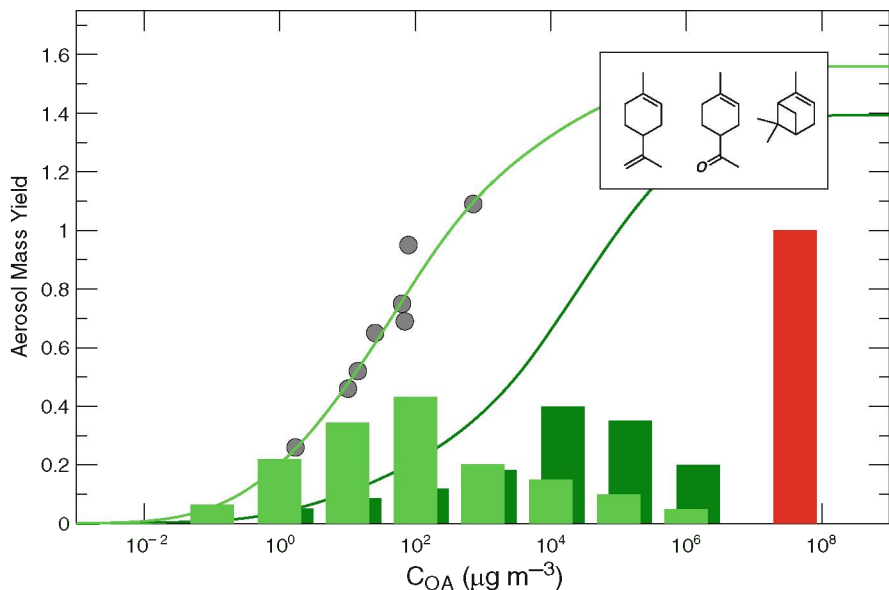


**Fig. 10** SOA product volatility distributions for  $\alpha$ -pinene and limonaketon in *dark green* and mass yields vs  $C_{\text{OA}}$  as *dark green curve*. Precursors with similar volatility, structure, and chemistry have similar yields. Product volatility distribution and yields for *D*-limonene ozonolysis are shown as *light green bars* and a *light green curve* (and *gray data points*). Oxidation of the additional exocyclic double bond in limonene results in substantially less volatile SOA products and correspondingly higher SOA yields

### 4.1.3 Aging of VOC SOA

All of the first-generation vapors from VOC SOA will certainly undergo further gas-phase oxidation, which will in turn influence the phase partitioning thermodynamics of the OA mixture, i.e., gas-phase aging of SOA.

#### Multiple Ozonolysis Generations

Several forms of aging of SOA vapors have been observed. One clear form is oxidation of multiply unsaturated alkenes. Many terpenes have multiple unsaturations, and in some cases different double bonds have very different rate constants for reaction with ozone. Examples include terpinolene, myrcene, limonene,  $\alpha$ -humulene, and  $\beta$ -caryophyllene [149, 150]. In these systems, ozone will react with one double bond in the terpene and produce some SOA. However, after the precursor is completely removed, SOA levels can continue to rise as the first-generation semi-volatile products continue to react with ozone to produce less volatile second-generation products [149].

Limonene is a revealing example. It is similar to  $\alpha$ -pinene in possessing a methyl-substituted endocyclic double bond in a six-member ring, but in addition it has an exocyclic terminal unsaturation. Figure 10 shows SOA mass-yield data and

a corresponding VBS product distribution (in light green) for the limonene + ozone reaction under low-NO<sub>x</sub> conditions [150]. The inset shows structures for limonene, limona ketone, and  $\alpha$ -pinene. The darker green histogram and yield curve is valid for  $\alpha$ -pinene and limona ketone, which generate almost identical SOA mass distributions after ozonolysis [38]. Initial ozonation of limonene also produces SOA much like  $\alpha$ -pinene and limona ketone, but subsequent ozonation of the exocyclic double bond in the first-generation products strongly favors the ketone-oxide over the ketone moiety shown in limona ketone and consequently forms substantially less volatile second-generation products [150–152]. As Fig. 10 shows, the resulting product distribution is two to three orders of magnitude less volatile than typical first-generation terpene ozonolysis products, which is consistent with additional peroxide and carboxylic acid functionality [153] greatly offsetting the loss of one carbon from the terminal methylene.

An interesting wrinkle in the limonene story is that the second ozonolysis reaction can be heterogeneous. The fresh SOA produced when ozone reacts with the endocyclic double bond is unsaturated [153], but under low-NO<sub>x</sub> conditions it reacts much more rapidly than is plausible based on gas-phase kinetics, but at a rate consistent with a heterogeneous ozone uptake coefficient of roughly  $10^{-3}$  [150]. Under high-NO<sub>x</sub> conditions the SOA (which contains organic nitrate functionality) has a much lower heterogeneous reactivity to ozone and consequently species remain in the gas phase that oxidize at a rate consistent with the ozonolysis of terminal double bonds, forming second-generation SOA more slowly, long after the limonene itself has been completely oxidized [150].

### Multi-generation OH Oxidation

Oxidation by OH radicals (or photooxidation in general) is much more difficult to deconvolve than ozonolysis because there is seldom the clear separation in timescales that can appear in the ozonolysis aging just discussed. However, later-generation oxidation by OH is likely to be much more important in the atmosphere because it is ubiquitous. OH will react with essentially all organic molecules, though the kinetics and mechanisms of the highly substituted species typical of first-generation and later-generation oxidation products remain highly uncertain. Nonetheless, there is no doubt that these reactions will occur, and little doubt that they will be quite rapid, in most cases oxidizing semi-volatile vapors within hours [64].

Multiple-generation oxidation has been studied theoretically via mechanism generators that apply structure activity relations for rate constants and product distributions [49]. Several specific tracers of later-generation oxidation have been proposed. One is a C<sub>8</sub> triacid formed via gas-phase oxidation of *cis*-pinonic acid, which is itself a first-generation oxidation product of  $\alpha$ -pinene [154]. The triacid is produced rapidly when gas-phase *cis*-pinonic acid is exposed to OH radicals, but not when the pinonic acid is partitioned into SOA at low temperatures [155]. For bulk SOA characteristics, Chhabra et al. [156] have shown that SOA formation

from oxidized precursors results in SOA whose mass spectrum is higher in the  $f_{44}$ – $f_{43}$  “triangle” space recently proposed as a diagnostic for ambient OA processing [157].

In the recent multiple chamber chemical aerosol aging study (MUCHACHAS), first-generation SOA was produced from  $\alpha$ -pinene + ozone and then exposed to OH radicals in a subsequent, separate step [112, 113, 155, 158–160]. The OH exposure caused a substantial jump in SOA mass concentrations [112, 113, 158] and significant changes in SOA volatility and hygroscopicity [112, 113, 159]. This controlled experiment strongly confirmed that long-term gas-phase aging by OH radicals can substantially alter OA properties.

There is thus compelling evidence that gas-phase OH oxidation will age OA by oxidizing semi-volatile vapors as well as slightly more volatile IVOC intermediate products. This will occur throughout the atmosphere with a rate constant estimated to be of order  $2 \times 10^{-11} \text{ cm}^3 \text{ molec}^{-1} \text{ s}^{-1}$ , giving a lifetime for typical OH concentrations of order 8 h [92, 158]. Other aging mechanisms can be scaled by this ubiquitous value to assess their relative importance.

## 4.2 Heterogeneous Aging

A large body of work addresses aging of organic particulate matter via heterogeneous uptake of oxidants, especially OH and ozone. Just as partitioning theory progressed from a focus on adsorptive to absorptive behavior, heterogeneous uptake has been viewed in terms of uptake of oxidants controlled by Langmuir-Hinshelwood type adsorptive isotherms [79, 161], but diffusion of oxidants into a bulk aerosol has also been considered in various contexts [162]. Heterogeneous formulations can differ depending on whether the principal focus is the loss of an oxidant upon uptake [87] or the loss of condensed-phase constituents due to oxidant uptake [163–166]. The “Pöschl Rudich Ammann” framework was initially presented with a principal focus on gas–surface interactions for multiphase processes, but has recently been extended to resolve diffusion into a spherically symmetric bulk as well [87]. The objective here is not to review even a small portion of the literature on heterogeneous oxidant uptake but to focus on the interplay between heterogeneous oxidation and organic phase partitioning.

Heterogeneous oxidation by OH is intrinsically slower than homogeneous gas-phase oxidation of organic vapors, since most molecules in a given particle are shielded from gas-phase radicals colliding with the surface. A rate constant for the gas-phase reaction of OH radicals with large organic species of  $2 \times 10^{-11} \text{ cm}^3 \text{ molec}^{-1} \text{ s}^{-1}$  is at least ten times larger than that of gas-phase OH with an organic species within a submicron particle [92]. The rate at which a molecule will undergo oxidation in each phase is a function not only of these rate constants but also by its abundance (as measured by mole fraction) in each phase. This is illustrated in Fig. 11 which shows the effective oxidation rate constant in each phase as a function of volatility as well as the total rate constant including

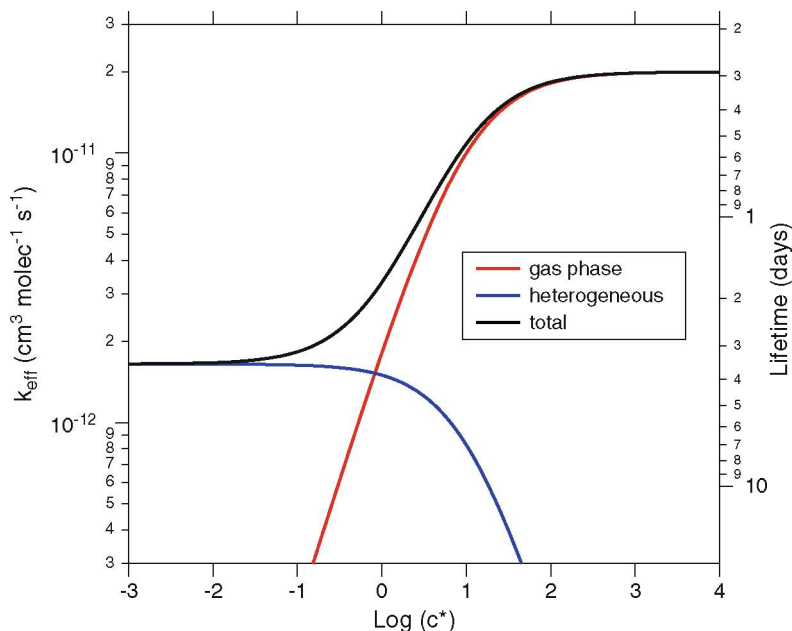


**Fig. 11** Effective OH oxidation rate constants for organics in gas phase (*red curve*) and condensed phase (*blue curve*) for a gas-phase OH rate constant of  $2 \times 10^{-11} \text{ cm}^3 \text{ molec}^{-1} \text{ s}^{-1}$  and a heterogeneous OH uptake coefficient of 1, for 200 nm diameter particles and  $10 \mu\text{g m}^{-3}$  total organic aerosol. Results are given as equivalent gas-phase values, modified by the fraction of organics in each phase and diffusion limitations of gas-phase OH to condensed-phase organics. Oxidation lifetimes (in days) are given on left-hand y axis, for  $2 \times 10^6 \text{ OH cm}^{-3}$

oxidation in either phase. Rates were calculated assuming a gas-phase rate constant of  $2 \times 10^{-11} \text{ cm}^3 \text{ molec}^{-1} \text{ s}^{-1}$ , reactive uptake coefficient ( $\gamma$ ) of 1, particle diameter of 200 nm, and organic aerosol loading ( $C_{OA}$ ) of  $10 \mu\text{g m}^{-3}$ . The figure shows that gas-phase oxidation will almost always dominate over heterogeneous oxidation unless the molecule is very low in volatility ( $C^*$  of  $0.1 \mu\text{g m}^{-3}$  or lower). Molecules almost wholly in the condensed phase of course can only be oxidized there. It is important to note that the heterogeneous timescale of 3–4 days is still shorter than the characteristic atmospheric residence time of submicron particles of 1 week or more [167]. Consequently, heterogeneous oxidation is still clearly an important process for organic compounds contained within aerosol particles.

In addition to providing insight into the kinetics of multiphase aging, studies of heterogeneous oxidation also serve as indirect probes of the mixing effects discussed earlier. Measuring the rate and extent of degradation of individual aerosol components provides information not only on molecular-level reactivity but also on mixing within the particle. This is because the reactive-diffusive length of OH in organic particles is of order 1 nm [168], and so heterogeneous OH reactions will be

confined to the particle surface. For example, in a study of the multigenerational heterogeneous oxidation of squalane ( $C_{30}H_{62}$ ), squalane degradation followed a simple pseudo-first-order kinetics (exponential decay) over multiple oxidation lifetimes, with concentrations eventually falling to zero [169]. Similarly, the first and second generation products reacted away at the same rates. This indicates that, at any given time, a sufficient amount of reactant (squalane and early-generation products) is present at or near the surface of a (pump oil) particle to react with OH; mixing within the particle is thus very fast on the timescale of the experiment (37 s). A similar conclusion can be drawn for heterogeneous oxidation of  $\alpha$ -pinene SOA by OH. Experiments with very high SOA concentrations (which favors the condensed phase and thus heterogeneous oxidation) and very high OH exposure in 37 s found almost complete conversion of fresh SOA into highly aged material. The aged aerosol strongly resembled ambient low-volatility oxidized organic aerosol (LV-OOA) while maintaining almost no correlation with the original fresh SOA mass spectrum [30]. This would not be possible unless essentially all of the organic species within the particles were able to diffuse to the particle surface (or even evaporate) in 30 s or less. On the other hand, in similar experiments on the heterogeneous oxidation of levoglucosan ( $C_6H_{10}O_5$ ) and erythritol ( $C_4H_{10}O_4$ ), the reactants were not totally lost after an initial rapid decay, consistent with the formation of viscous materials with mixing timescales of at least several minutes. This serves as an illustration that generalizations about diffusion limitations within organic particles may be very difficult to draw, as the specific particle composition (including organics, inorganics, and water) as well as temperature may alter constituent diffusivities by many orders of magnitude.

Heterogeneous oxidation experiments also allow for the investigation of the possibility that organic condensation may “coat” existing particles, isolating the core of the particle from the surrounding gas. Such a coating implies a lack of mixing between the condensing vapor (the coating material) and the particle core, but this can be a dangerous assumption if the two are miscible. One example of this is shown in Fig. 12, which is a relative kinetics plot of particle-phase cholestane loss compared to gas-phase oxidation of meta-xylene by OH radicals [143]. For the reasons discussed above, it is reasonable to regard heterogeneous loss of condensed-phase organics as a fairly precise surface probe. Figure 12 shows two things. First, coating of POA particles containing cholestane by a nominally quite thick layer of  $\alpha$ -pinene SOA did nothing to slow down heterogeneous cholestane loss, suggesting that the SOA formed a uniform mixture with the POA. That is consistent with the mixing experiments described above [60]. Second, cholestane loss slowed significantly at high RH ( $\sim 75\%$ ), suggesting that an aqueous surface layer formed, excluding nonpolar compounds such as cholestane. This is consistent with recent findings that two distinct condensed phases form for wet OA particles as long as the O:C of the organics is below approximately 0.7 [125, 126].

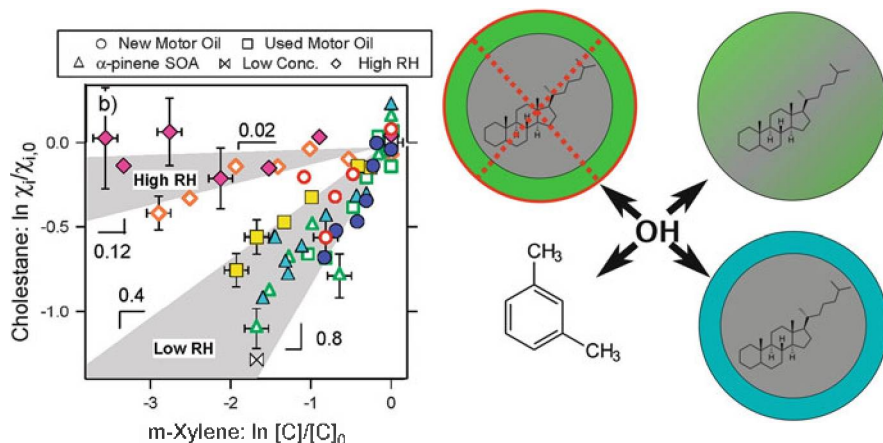


**Fig. 12** Relative oxidation rates by OH radicals of condensed-phase cholestane vs gas-phase *m*-xylene in different organic-aerosol matrices, all of which include a high fraction of motor oil. Cholestane oxidation is independent of OA concentration or the presence of a substantial SOA “coating” consisting of up to half of the total particle mass. However, high relative humidity slows cholestane oxidation by an order of magnitude. This suggests that a thin film of water on oil can significantly retard cholestane oxidation, perhaps by excluding the cholestane from the particle surface; the SOA, on the other hand, does not coat the particle surface but rather mixes with the oil and thus does not impede cholestane oxidation

### 4.3 Aqueous-Phase Aging

In recent years there has been intense interest in the formation and evolution of atmospheric particulate matter within the aqueous phase [170]. Such processes occur by dissolution of organics into a water droplet (deliquesced particle or cloud droplet) followed by oxidation by a dissolved oxidant (most likely OH). Studies of these pathways have been reviewed in detail very recently [118, 171] and so will not be discussed here; instead, as in the previous section, the focus here is on the relationship between partitioning and aging chemistry.

The relative importance of the gas and the aqueous phases as media for the oxidation of organic species depends critically on the fraction of the species present in each phase. This in turn is a function both of the compound’s intrinsic tendency to partition between each (as described by its effective Henry’s Law Constant,  $H^*$ ) and the concentration of liquid water present [118]. Thus partitioning into the aqueous phase is governed by the same general considerations as partitioning into the organic phase (which is governed by saturation vapor pressure and organic aerosol loading). In fact, the Henry’s Law solubility of a compound is really just a measure of the volatility of that compound over water. As with purely organic mixtures, Raoult’s law will apply for ideal solutions, but the activity can be strongly modified by some activity coefficient related to the interaction of that species with water. Accordingly, it is useful to express the Henry’s Law solubility as volatility

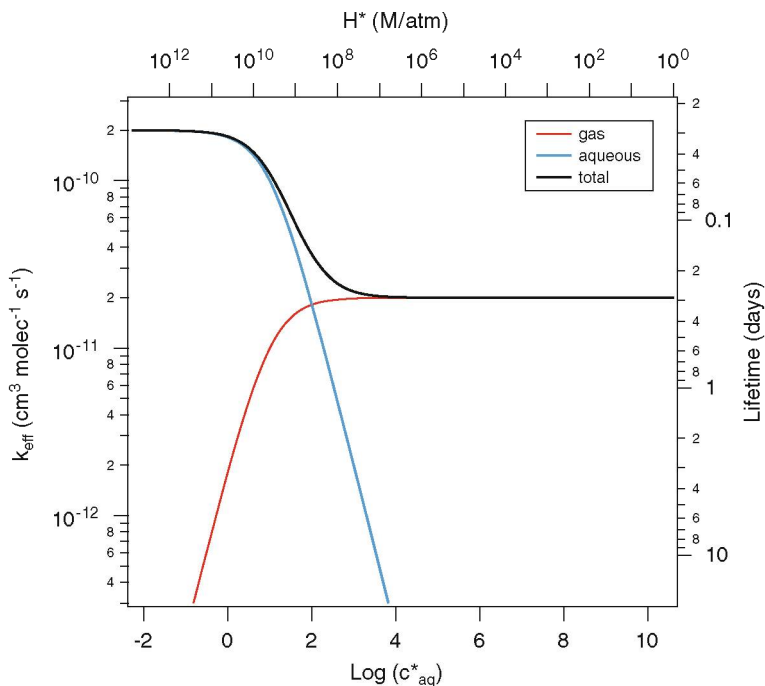


**Fig. 13** Effective OH oxidation rate constants for organics in gas phase (*red curve*) and aqueous phase (*cyan curve*) for a gas-phase rate constant of  $2 \times 10^{-11} \text{ cm}^3 \text{ molec}^{-1} \text{ s}^{-1}$  and an effective aqueous-phase OH rate constant of  $2 \times 10^{-10} \text{ cm}^3 \text{ molec}^{-1} \text{ s}^{-1}$ . The principal abscissa is the effective saturation concentration with respect to dissolution in  $10 \mu\text{g m}^{-3}$  of liquid water. Oxidation lifetimes (in days) are given on the left-hand y axis, for  $2 \times 10^6 \text{ OH cm}^{-3}$  in the gas phase

(micrograms per cubic meter), for comparison with the liquid water content (just as  $C^*$  can be compared to  $C_{\text{OAA}}$ ). Following Ervens et al. [172], this volatility over water is called  $C_{\text{aq}}^*$ , and is equal to  $(R T H^* / \rho_w)^{-1}$ , where  $H^*$  is the effective Henry's Law constant ( $\text{M atm}^{-1}$ ),  $T$  is temperature (K),  $R$  is the gas constant ( $0.08206 \text{ L atm K}^{-1} \text{ mol}^{-1}$ ), and  $\rho_w$  is the density of water ( $10^{12} \mu\text{g m}^{-3}$ ).

Figure 13 shows the effective rate constants for gas-phase and aqueous-phase oxidation as a function of  $C_{\text{aq}}^*$  (and  $H^*$ ), assuming a liquid water content ( $C_w$ ) of  $10 \mu\text{g m}^{-3}$  (a typical ambient value for deliquesced aerosol). This is directly analogous to Fig. 11, which shows the rates of heterogeneous vs gas-phase oxidation as a function of  $C^*$ . As in Fig. 11, the gas-phase OH rate constant is set at  $2 \times 10^{-11} \text{ cm}^3 \text{ molec}^{-1} \text{ s}^{-1}$ . The effective aqueous-phase OH rate constant is chosen to be ten times higher at  $2 \times 10^{-10} \text{ cm}^3 \text{ molec}^{-1} \text{ s}^{-1}$ , reflecting the possibility that aqueous OH concentrations may be higher than in the gas phase [173]. (The actual aqueous-phase rate constants can be quite variable, but are

generally similar to those in the gas phase [173].) Even with this higher rate, aqueous-phase oxidation will dominate only when the molecule of interest is exceedingly water soluble ( $H^* > 7 \times 10^8 \text{ M atm}^{-1}$ ) due to the small amount of liquid water available. Most atmospheric species, even those that are considered to be highly water-soluble (such as glyoxal, glycolaldehyde, and diacids), have  $H^*$  well below this threshold [174], and thus will not partition sufficiently into the aerosol aqueous phase to undergo significant aqueous-phase aging under these conditions.

There are several important caveats to this analysis, however. First, OH concentrations in the aqueous phase are highly uncertain, since there are no measurements of [OH] in deliquesced particles or cloud droplets. If aqueous OH concentrations are still higher than indicated in Fig. 13 (as suggested by some models [173]), the threshold for aqueous-phase oxidation would move to higher values of  $C_{\text{aq}}^*$  (lower values of  $H^*$ ); on the other hand, if aqueous OH concentrations are lower (as suggested by other models [170]), even lower values of  $C_{\text{aq}}^*$  (higher values of  $H^*$ ) would be needed for aqueous oxidation to dominate. This highlights the need for an improved understanding of oxidant concentrations in the atmospheric aqueous phase. Unless there is substantial radical recycling (OH regeneration) in the aqueous phase, aqueous oxidation by OH will be subject to the same diffusion limitations on heterogeneous oxidation.

A second caveat involves the effect of liquid water content  $C_w$ ; the value used ( $10 \mu\text{g m}^{-3}$ ) is reasonable for ambient fine particulate matter but would be orders of magnitude higher for cloud water (with  $C_w$  as high as  $1 \text{ g m}^{-3}$ ). Under such conditions, partitioning into the aqueous phase will happen for much more volatile species ( $H^*$  of  $7 \times 10^4 \text{ M atm}^{-1}$  or higher), including the water-soluble species mentioned above. Third, this analysis assumes that Henry's Law accurately describes partitioning between the gas and aqueous phase, independent of aqueous-phase concentrations. In reality, the high concentrations in the aerosol aqueous phase are likely to introduce substantial deviations from ideality; these substantial activity coefficients could have a dramatic (and uncertain) effect on partitioning. Finally, under some conditions, particles may include multiple phases [125, 175], so that partitioning between at least three phases (gas, organic, aqueous) must be considered. In such cases the simple two-phase picture in Fig. 13 (or Fig. 11) is insufficient to describe the aging chemistry of the entire system, as the relative values of  $C^*$ ,  $C_{\text{aq}}^*$ ,  $C_{\text{OA}}$ , and  $C_w$  must be considered when predicting the equilibrium phase of the organic species.

In spite of all these uncertainties, the description of aqueous oxidation in terms of simple partitioning (Fig. 13) clearly shows that only molecules with very large Henry's Law solubilities can undergo significant oxidation in the aqueous phase. This includes highly water-soluble species such as glyoxal, at least when aqueous [OH] and/or liquid water content is high, but categorically excludes all hydrocarbons as well as most monofunctional organic species that have more

than one carbon [174]. It also points to the need to run laboratory studies of aqueous oxidative processing under atmospherically relevant partitioning conditions, with liquid water contents in the range of  $10 \mu\text{g m}^{-3}$  (for deliquesced particles) to  $1 \text{g m}^{-3}$  (for cloud water). To date, most (though not all [176, 177]) laboratory studies of aqueous oxidation have been carried out in bulk aqueous solution, with liquid water contents that are far higher than this, on the order of  $10^6 \text{g m}^{-3}$  (the density of liquid water). These studies are unlikely to be representative of the gas-droplet partitioning conditions typical of the atmosphere, and thus may not accurately reflect atmospheric aging.

As with heterogeneous oxidation, aqueous-phase oxidation may play an important role in aging water-soluble organics already present in particles, and it can also play a unique role for a small but important set of highly water soluble, low carbon-number organic vapors [172].

## 5 Conclusions

Phase partitioning and aging chemistry are inexorably linked when considering the chemical evolution of organic aerosol, both because the phase defines the aerosol and because absolute rate of aging depends strongly on the phase holding an organic compound. A key observation in ambient organic aerosol is that the aerosol becomes highly oxidized very rapidly [30, 178, 179]. Heterogeneous oxidation mechanisms appear to be incapable of oxidizing OA with sufficient speed, while gas-phase oxidation can do so. However, heterogeneous processes still compete favorably with the residence time of OA in the atmosphere and thus certainly play an important atmospheric role. In addition, processes that might simply retard mass transfer between the particle and gas phases appear unable to provide sufficiently rapid oxidation.

Overall, the coupling among these multiphase processes, including chemistry in all phases and the equilibria and dynamics of mass transfer among the phases, needs to be described in detail before we can resolve with certainty the relative role of each process under atmospheric conditions. The timescales for all three processes discussed here – gas-phase, heterogeneous, and aqueous-phase oxidation – are competitive with the residence time of particles in the atmosphere. Gas-phase oxidation will win out for most organic vapors because it is homogeneous and fast, but condensed-phase processes may have a vital role in the full maturation of organic aerosol over longer timescales during long-range transport.

**Acknowledgments** NMD and ALR are supported by grants from the U.S. National Science Foundation (NSF CHE 1012293 and AGS 1136479) and the Department of Energy (DE-SC0007075). JHK is supported by a grant from the National Science Foundation (AGS 1056225). IR is supported by a grant from the European Research Council (278277) and Vetenskapsrådet. ERT is supported by an NSF doctoral fellowship.

## References

1. Hildemann LM, Mazurek MA, Cass GR, Simoneit BRT (1991) Quantitative characterization of urban sources of organic aerosol by high-resolution gas-chromatography. *Environ Sci Technol* 25(7):1311–1325
2. Schauer JJ, Cass GR (2000) Source apportionment of wintertime gas-phase and particle-phase air pollutants using organic compounds as tracers. *Environ Sci Technol* 34(9):1821–1832
3. Mazurek MA, Cass GR, Simoneit BRT (1991) Biological input to visibility-reducing aerosol-particles in the remote arid southwestern United States. *Environ Sci Technol* 25(4):684–694
4. Rogge WF, Hildemann LM, Mazurek MA, Cass GR, Simoneit BRT (1998) Sources of fine organic aerosol. 9. Pine, oak and synthetic log combustion in residential fireplaces. *Environ Sci Technol* 32(1):13–22
5. Robinson AL, Subramanian R, Donahue NM, Bernardo-Bricker A, Rogge WF (2006) Source apportionment of molecular markers and organic aerosol. 2. Biomass smoke. *Environ Sci Technol* 40:7811–7819
6. Rogge WF, Hildemann LM, Mazurek MA, Cass GR, Simoneit BRT (1993) Sources of fine organic aerosol. 2. Noncatalyst and catalyst-equipped automobiles and heavy-duty diesel trucks. *Environ Sci Technol* 27(4):636–651
7. Schauer JJ, Rogge WF, Hildemann LM, Mazurek MA, Cass GR, Simoneit BRT (1996) Source apportionment of airborne particulate matter using organic compounds as tracers. *Atmos Environ* 30(22):3837–3855
8. Subramanian R, Donahue NM, Bernardo-Bricker A, Rogge WF, Robinson AL (2006) Contribution of motor vehicle emissions to organic carbon and fine particle mass in Pittsburgh. Pennsylvania: effects of varying source profiles and seasonal trends in ambient marker concentrations. *Atmos Environ* 40:8002–8019
9. Schauer JJ, Kleeman MJ, Cass GR, Simoneit BRT (1999) Measurement of emissions from air pollution sources. 2. C-1 through C-30 organic compounds from medium duty diesel trucks. *Environ Sci Technol* 33(10):1578–1587
10. Rogge WF, Hildemann LM, Mazurek MA, Cass GR, Simoneit BRT (1991) Sources of fine organic aerosol. 1. Charbroilers and meat cooking operations. *Environ Sci Technol* 25(6):1112–1125
11. Nolte CG, Schauer JJ, Cass GR, Simoneit BRT (1999) Highly polar organic compounds present in meat smoke. *Environ Sci Technol* 33(19):3313–3316
12. Schauer JJ, Fraser MP, Cass GR, Simoneit BRT (2002) Source reconciliation of atmospheric gas-phase and particle-phase pollutants during a severe photochemical smog episode. *Environ Sci Technol* 36(17):3806–3814
13. Robinson AL, Subramanian R, Donahue NM, Bernardo-Bricker A, Rogge WF (2006) Source apportionment of molecular markers and organic aerosol. 3. Food cooking emissions. *Environ Sci Technol* 40:7820–7827
14. Rogge WF, Hildemann LM, Mazurek MA, Cass GR (1994) Sources of fine organic aerosol. 6. Cigarette-smoke in the urban atmosphere. *Environ Sci Technol* 28(7):1375–1388
15. Paulson SE, Pandis SN, Baltensperger U, Seinfeld JH, Flagan RC, Palen EJ, Allen DT, Schaffner C, Giger W, Portmann A (1990) Characterization of photochemical aerosols from biogenic hydrocarbons. *J Aerosol Sci* 21:S245–S248
16. Kamens R, Jang MS, Hu JX, Coe D, Strommen M (1996) Equilibrium and atmospheric semi-volatiles. *Abstr Pap Am Chem Soc* 211, 121-ANYL
17. Odum JR, Hoffmann T, Bowman F, Collins D, Flagan RC, Seinfeld JH (1996) Gas/particle partitioning and secondary organic aerosol yields. *Environ Sci Technol* 30(8):2580–2585
18. Pankow JF (1994) An absorption-model of gas-particle partitioning of organic-compounds in the atmosphere. *Atmos Environ* 28(2):185–188

19. Liousse C, Penner JE, Chuang C, Walton JJ, Eddleman H, Cachier H (1996) A global three-dimensional model study of carbonaceous aerosols. *J Geophys Res Atmos* 101 (D14):19411–19432
20. Lurmann FW, Wexler AS, Pandis SN, Musarra S, Kumar N, Seinfeld JH (1997) Modelling urban and regional aerosols. 2. Application to California's south coast air basin. *Atmos Environ* 31:2695–2715
21. Griffin RJ, Cocker DR, Seinfeld JH, Dabdub D (1999) Estimate of global atmospheric organic aerosol from oxidation of biogenic hydrocarbons. *Geophys Res Lett* 26 (17):2721–2724
22. Pun BK, Griffin RJ, Seigneur C, Seinfeld JH (2002) Secondary organic aerosol - 2. Thermodynamic model for gas/particle partitioning of molecular constituents. *J Geophys Res Atmos* 107(D17):D4333. doi:10.1029/2001jd000542
23. Koo BY, Ansari AS, Pandis SN (2003) Integrated approaches to modeling the organic and inorganic atmospheric aerosol components. *Atmos Environ* 37:4757–4768
24. Spracklen DV, Carslaw KS, Kulmala M, Kerminen VM, Sihto SL, Riipinen I, Merikanto J, Mann GW, Chipperfield MP, Wiedensohler A, Birmili W, Lihavainen H (2008) Contribution of particle formation to global cloud condensation nuclei concentrations. *Geophys Res Lett* 35(6):L06808. doi:10.1029/2007gl033038
25. Heald CL, Ridley DA, Kreidenweis SM, Drury EE (2010) Satellite observations cap the atmospheric organic aerosol budget. *Geophys Res Lett* 37:L24808. doi:10.1029/2010gl045095
26. Novakov T, Penner JE (1993) Large contribution of organic aerosols to cloud-condensation-nuclei concentrations. *Nature* 365(6449):823–826
27. Cruz CN, Pandis SN (1997) A study of the ability of pure secondary organic aerosol to act as cloud condensation nuclei. *Atmos Environ* 31:2205–2214
28. Huff Hartz KE, Tischuk JE, Chan MN, Chan CK, Donahue NM, Pandis SN (2006) Cloud condensation nuclei activation of limited solubility organic aerosol. *Atmos Environ* 40:605–617
29. Huffman JA, Docherty KS, Aiken AC, Cubison MJ, Ulbrich IM, DeCarlo PF, Sueper D, Jayne JT, Worsnop DR, Zieann PJ, Jimenez JL (2009) Chemically-resolved aerosol volatility measurements from two megacity field studies. *Atmos Chem Phys* 9:7161–7182
30. Jimenez JL, Canagaratna MR, Donahue NM, Prevot ASH, Zhang Q, Kroll JH, DeCarlo PF, Allan JD, Coe H, Ng NL, Aiken AC, Docherty KS, Ulbrich IM, Grieshop AP, Robinson AL, Duplissy J, Smith JD, Wilson KR, Lanz VA, Hueglin C, Sun YL, Tian J, Laaksonen A, Raatikainen T, Rautiainen J, Vaattovaara P, Ehn M, Kulmala M, Tomlinson JM, Collins DR, Cubison MJ, Dunlea EJ, Huffman JA, Onasch TB, Alfarra MR, Williams PI, Bower K, Kondo Y, Schneider J, Drewnick F, Borrmann S, Weimer S, Demerjian K, Salcedo D, Cottrell L, Griffin R, Takami A, Miyoshi T, Hatakeyama S, Shimono A, Sun JY, Zhang YM, Dzepina K, Kimmel JR, Sueper D, Jayne JT, Herndon SC, Trimborn AM, Williams LR, Wood EC, Middlebrook AM, Kolb CE, Baltensperger U, Worsnop DR (2009) Evolution of organic aerosols in the atmosphere. *Science* 326(5959):1525–1529. doi:10.1126/science.1180353
31. Vaden TD, Imre D, Beranek J, Shrivastava M, Zelenyuk A (2011) Evaporation kinetics and phase of laboratory and ambient secondary organic aerosol. *Proc Natl Acad Sci USA* 108 (6):2190–2195
32. Zobrist B, Marcolli C, Pedernera DA, Koop T (2008) Do atmospheric aerosols form glasses? *Atmos Chem Phys* 8(17):5221–5244
33. Virtanen A, Joutsensaari J, Koop T, Kannosto J, Yli-Pirila P, Leskinen J, Makela JM, Holopainen JK, Poschl U, Kulmala M, Worsnop DR, Laaksonen A (2010) An amorphous solid state of biogenic secondary organic aerosol particles. *Nature* 467(7317):824–827
34. Koop T, Bookhold J, Shiraiwa M, Poschl U (2011) Glass transition and phase state of organic compounds: dependency on molecular properties and implications for secondary organic aerosols in the atmosphere. *Phys Chem Chem Phys* 13(43):19238–19255

35. Goldstein AH, Galbally IE (2007) Known and unexplored organic constituents in the Earth's atmosphere. *Environ Sci Technol* 41(5):1514–1521
36. Hallquist M, Wenger JC, Baltensperger U, Rudich Y, Simpson D, Claeys M, Dommen J, Donahue NM, George C, Goldstein AH, Hamilton JF, Herrmann H, Hoffmann T, Iinuma Y, Jang M, Jenkin ME, Jimenez JL, Kiendler-Scharr A, Maenhaut W, McFiggans G, Mentel TF, Monod A, Prevot ASH, Seinfeld JH, Surratt JD, Szmigielski R, Wildt J (2009) The formation, properties and impact of secondary organic aerosol: current and emerging issues. *Atmos Chem Phys* 9(14):5155–5236
37. Spracklen DV, Jimenez JL, Carslaw KS, Worsnop DR, Evans MJ, Mann GW, Zhang Q, Canagaratna MR, Allan J, Coe H, McFiggans G, Rap A, Forster P (2011) Aerosol mass spectrometer constraint on the global secondary organic aerosol budget. *Atmos Chem Phys* 11(23):12109–12136. doi:[10.5194/acp-11-12109-2011](https://doi.org/10.5194/acp-11-12109-2011)
38. Donahue NM, Robinson AL, Pandis SN (2009) Atmospheric organic particulate matter: from smoke to secondary organic aerosol. *Atmos Environ* 43(1):94–106. doi:[10.1016/j.atmosenv.2008.09.055](https://doi.org/10.1016/j.atmosenv.2008.09.055)
39. Marcolli C, Luo BP, Peter T, Wienhold FG (2004) Internal mixing of the organic aerosol by gas phase diffusion of semivolatile organic compounds. *Atmos Chem Phys* 4:2593–2599
40. Donahue NM, Robinson AL, Stanier CO, Pandis SN (2006) Coupled partitioning, dilution, and chemical aging of semivolatile organics. *Environ Sci Technol* 40:2635–2643
41. Aumont B, Szopa S, Madronich S (2005) Modelling the evolution of organic carbon during its gas-phase tropospheric oxidation: development of an explicit model based on a self generating approach. *Atmos Chem Phys* 5:2497–2517
42. Fredenslund A, Jones RL, Prausnitz JM (1975) Group-contribution estimation of activity-coefficients in nonideal liquid-mixtures. *Aiche J* 21(6):1086–1099
43. Clegg SL, Seinfeld JH, Brimblecombe P (2001) Thermodynamic modelling of aqueous aerosols containing electrolytes and dissolved organic compounds. *J Aerosol Sci* 32(6): 713–738
44. Nannoolal Y, Rarey J, Ramjugernath D (2008) Estimation of pure component properties - Part 3. Estimation of the vapor pressure of non-electrolyte organic compounds via group contributions and group interactions. *Fluid Phase Equilib* 269(1–2):117–133
45. Zuend A, Marcolli C, Booth AM, Lienhard DM, Soonsin V, Krieger UK, Topping DO, McFiggans G, Peter T, Seinfeld JH (2011) New and extended parameterization of the thermodynamic model AIOMFAC: calculation of activity coefficients for organic-inorganic mixtures containing carboxyl, hydroxyl, carbonyl, ether, ester, alkenyl, alkyl, and aromatic functional groups. *Atmos Chem Phys* 11(17):9155–9206
46. Chen Q, Liu YJ, Donahue NM, Shilling JE, Martin ST (2011) Particle-phase chemistry of secondary organic material: modeled compared to measured O:C and H:C elemental ratios provide constraints. *Environ Sci Technol* 45(11):4763–4770
47. Xia AG, Michelangeli DV, Makar PA (2008) Box model studies of the secondary organic aerosol formation under different HC/NO(x) conditions using the subset of the Master Chemical Mechanism for alpha-pinene oxidation. *J Geophys Res Atmos* 113:D10
48. Capouet M, Mueller JF, Ceulemans K, Compernelle S, Vereecken L, Peeters J (2008) Modeling aerosol formation in alpha-pinene photo-oxidation experiments. *J Geophys Res Atmos* 113(D2):D02308
49. Valorso R, Aumont B, Camredon M, Raventos-Duran T, Mouchel-Vallon C, Ng NL, Seinfeld JH, Lee-Taylor J, Madronich S (2011) Explicit modelling of SOA formation from alpha-pinene photooxidation: sensitivity to vapour pressure estimation. *Atmos Chem Phys* 11(14):6895–6910
50. Pun BK, Wu SY, Seigneur C, Seinfeld JH, Griffin RJ, Pandis SN (2003) Uncertainties in modeling secondary organic aerosols: three-dimensional modeling studies in Nashville/Western Tennessee. *Environ Sci Technol* 37:3647–3661
51. Kroll JH, Seinfeld JH (2008) Chemistry of secondary organic aerosol: formation and evolution of low-volatility organics in the atmosphere. *Atmos Environ* 42(16):3593–3624

52. Kroll JH, Ng NL, Murphy SM, Flagan RC, Seinfeld JH (2006) Secondary organic aerosol formation from isoprene photooxidation. *Environ Sci Technol* 40(6):1869–1877. doi:[10.1021/Es0524301](https://doi.org/10.1021/Es0524301)
53. Griffin RJ, Cocker DR, Flagan RC, Seinfeld JH (1999) Organic aerosol formation from the oxidation of biogenic hydrocarbons. *J Geophys Res Atmos* 104(D3):3555–3567
54. Presto AA, Huff Hartz KE, Donahue NM (2005) Secondary organic aerosol production from terpene ozonolysis. 2. Effect of NO<sub>x</sub> concentration. *Environ Sci Technol* 39:7046–7054
55. Barsanti KC, Smith JN, Pankow JF (2011) Application of the np plus mP modeling approach for simulating secondary organic particulate matter formation from alpha-pinene oxidation. *Atmos Environ* 45(37):6812–6819
56. Grieshop AP, Miracolo MA, Donahue NM, Robinson AL (2009) Constraining the volatility distribution and gas-particle partitioning of combustion aerosols using isothermal dilution and thermodesorber measurements. *Environ Sci Technol* 43(13):4750–4756. doi:[10.1021/es8032378](https://doi.org/10.1021/es8032378)
57. Dommen J, Hellen H, Saurer M, Jaeggi M, Siegwolf R, Metzger A, Duplissy J, Fierz M, Baltensperger U (2009) Determination of the aerosol yield of isoprene in the presence of an organic seed with carbon isotope analysis. *Environ Sci Technol* 43(17):6697–6702
58. Hildebrandt L, Henry KM, Kroll JH, Worsnop DR, Pandis SN, Donahue NM (2011) Evaluating the mixing of organic aerosol components using high-resolution aerosol mass spectrometry. *Environ Sci Technol* 45(15):6329–6335
59. Song C, Zaveri RA, Alexander ML, Thornton JA, Madronich S, Ortega JV, Zelenyuk A, Yu X-Y, Laskin A, Maughan DA (2007) Effect of hydrophobic primary organic aerosols on secondary organic aerosol formation from ozonolysis of alpha-pinene. *Geophys Res Lett* 34(20):L20803
60. Asa-Awuku A, Miracolo MA, Kroll JH, Robinson AL, Donahue NM (2009) Mixing and phase partitioning of primary and secondary organic aerosols. *Geophys Res Lett* 36:L15827. doi:[10.1029/2009gl039301](https://doi.org/10.1029/2009gl039301)
61. Pankow JF, Barsanti KC (2009) The carbon number-polarity grid: a means to manage the complexity of the mix of organic compounds when modeling atmospheric organic particulate matter. *Atmos Environ* 43(17):2829–2835
62. Simoneit BRT, Schauer JJ, Nolte CG, Oros DR, Elias VO, Fraser MP, Rogge WF, Cass GR (1999) Levoglucosan, a tracer for cellulose in biomass burning and atmospheric particles. *Atmos Environ* 33(2):173–182
63. Donahue NM, Epstein SA, Pandis SN, Robinson AL (2011) A two-dimensional volatility basis set: 1. organic-aerosol mixing thermodynamics. *Atmos Chem Phys* 11(7):3303–3318
64. Donahue NM, Kroll JH, Pandis SN, Robinson AL (2012) A two-dimensional volatility basis set – part 2: diagnostics of organic-aerosol evolution. *Atmos Chem Phys* 12:615–634. doi:[10.5194/acp-12-615-2012](https://doi.org/10.5194/acp-12-615-2012)
65. Kroll JH, Donahue NM, Jimenez JL, Kessler SH, Canagaratna MR, Wilson KR, Altieri KE, Mazzoleni LR, Wozniak AS, Bluhm H, Mysak ER, Smith JD, Kolb CE, Worsnop DR (2011) Carbon oxidation state as a metric for describing the chemistry of atmospheric organic aerosol. *Nat Chem* 3(2):133–139. doi:[10.1038/nchem.948](https://doi.org/10.1038/nchem.948)
66. Heald CL, Kroll JH, Jimenez JL, Docherty KS, DeCarlo PF, Aiken AC, Chen Q, Martin ST, Farmer DK, Artaxo P (2010) A simplified description of the evolution of organic aerosol composition in the atmosphere. *Geophys Res Lett* 37:L08803. doi:[10.1029/2010gl042737](https://doi.org/10.1029/2010gl042737)
67. Aiken AC, Decarlo PF, Kroll JH, Worsnop DR, Huffman JA, Docherty KS, Ulbrich IM, Mohr C, Kimmel JR, Sueper D, Sun Y, Zhang Q, Trimborn A, Northway M, Ziemann PJ, Canagaratna MR, Onasch TB, Alfarra MR, Prevot ASH, Dommen J, Duplissy J, Metzger A, Baltensperger U, Jimenez JL (2008) O/C and OM/OC ratios of primary, secondary, and ambient organic aerosols with high-resolution time-of-flight aerosol mass spectrometry. *Environ Sci Technol* 42(12):4478–4485

68. Epstein SA, Riipinen I, Donahue NM (2010) A semiempirical correlation between enthalpy of vaporization and saturation concentration for organic aerosol. *Environ Sci Technol* 44 (2):743–748. doi:[10.1021/es902497z](https://doi.org/10.1021/es902497z)
69. Cappa CD, Jimenez JL (2010) Quantitative estimates of the volatility of ambient organic aerosol. *Atmos Chem Phys* 10(12):5409–5424
70. Kulmala M, Toivonen A, Makela JM, Laaksonen A (1998) Analysis of the growth of nucleation mode particles observed in boreal forest. *Tellus B Chem Phys Meteorol* 50 (5):449–462
71. Anttila T, Kerminen VM, Kulmala M, Laaksonen A, O’Dowd CD (2004) Modelling the formation of organic particles in the atmosphere. *Atmos Chem Phys* 4:1071–1083
72. Riipinen I, Manninen HE, Yli-Juuti T, Boy M, Sipila M, Ehn M, Junninen H, Petaja T, Kulmala M (2009) Applying the condensation particle counter battery (CPCB) to study the water-affinity of freshly-formed 2–9 nm particles in boreal forest. *Atmos Chem Phys* 9 (10):3317–3330
73. Riipinen I, Pierce JR, Yli-Juuti T, Nieminen T, Hakkinen S, Ehn M, Junninen H, Lehtipalo K, Petaja T, Slowik J, Chang R, Shantz NC, Abbatt J, Leaitch WR, Kerminen VM, Worsnop DR, Pandis SN, Donahue NM, Kulmala M (2011) Organic condensation: a vital link connecting aerosol formation to cloud condensation nuclei (CCN) concentrations. *Atmos Chem Phys* 11 (8):3865–3878. doi:[10.5194/acp-11-3865-2011](https://doi.org/10.5194/acp-11-3865-2011)
74. Pierce JR, Riipinen I, Kulmala M, Ehn M, Petaja T, Junninen H, Worsnop DR, Donahue NM (2011) Quantification of the volatility of secondary organic compounds in ultrafine particles during nucleation events. *Atmos Chem Phys* 11(17):9019–9036
75. Donahue NM, Trump ER, Pierce JR, Riipinen I (2011) Theoretical constraints on pure vapor-pressure driven condensation of organics to ultrafine particles. *Geophys Res Lett* 38:L16801
76. Wexler AS, Lurmann FW, Seinfeld JH (1994) Modeling urban and regional aerosols. 1. Model development. *Atmos Environ* 28(3):531–546
77. Riipinen I, Pierce JR, Donahue NM, Pandis SN (2010) Equilibration time scales of organic aerosol inside thermodenuders: evaporation kinetics versus thermodynamics. *Atmos Environ* 44(5):597–607. doi:[10.1016/j.atmosenv.2009.11.022](https://doi.org/10.1016/j.atmosenv.2009.11.022)
78. Worsnop DR, Zahniser MS, Kolb CE, Gardner JA, Watson LR, Vandoren JM, Jayne JT, Davidovits P (1989) Temperature-dependence of mass accommodation of  $\text{SO}_2$  and  $\text{H}_2\text{O}_2$  on aqueous surfaces. *J Phys Chem* 93(3):1159–1172
79. Ammann M, Pöschl U, Rudich Y (2003) Effects of reversible adsorption and Langmuir-Hinshelwood surface reactions on gas uptake by atmospheric particles. *Phys Chem Chem Phys* 5(2):351–356
80. Davidovits P, Worsnop DR, Jayne JT, Kolb CE, Winkler P, Vrtala A, Wagner PE, Kulmala M, Lehtinen KEJ, Vesala T, Mozurkewich M (2004) Mass accommodation coefficient of water vapor on liquid water. *Geophys Res Lett* 31(22):L22111. doi:[10.1029/2004gl020835](https://doi.org/10.1029/2004gl020835)
81. Smith JD, Cappa CD, Drisdell WS, Cohen RC, Saykally RJ (2006) Raman thermometry measurements of free evaporation from liquid water droplets. *J Am Chem Soc* 128 (39):12892–12898
82. Laaksonen A, Vesala T, Kulmala M, Winkler PM, Wagner PE (2005) Commentary on cloud modelling and the mass accommodation coefficient of water. *Atmos Chem Phys* 5:461–464
83. Winkler PM, Vrtala A, Wagner PE, Kulmala M, Lehtinen KEJ, Vesala T (2004) Mass and thermal accommodation during gas–liquid condensation of water. *Phys Rev Lett* 93(7): 075701
84. Kolb CE, Cox RA, Abbatt JPD, Ammann M, Davis EJ, Donaldson DJ, Garrett BC, George C, Griffiths PT, Hanson DR, Kulmala M, McFiggans G, Pöschl U, Riipinen I, Rossi MJ, Rudich Y, Wagner PE, Winkler PM, Worsnop DR, O’Dowd CD (2010) An overview of current issues in the uptake of atmospheric trace gases by aerosols and clouds. *Atmos Chem Phys* 10(21):10561–10605

85. Nogueira JJ, Vazquez SA, Mazyar OA, Hase WL, Perkins BG, Nesbitt DJ, Martinez-Nunez E (2009) Dynamics of CO<sub>2</sub> scattering off a perfluorinated self-assembled monolayer. Influence of the incident collision energy, mass effects, and use of different surface models. *J Phys Chem A* 113(16):3850–3865
86. Saleh R, Khlystov A, Shihadeh A (2012) Determination of evaporation coefficients of ambient and laboratory-generated semivolatile organic aerosols from phase equilibration kinetics in a thermobalance. *Aerosol Sci Technol* 46(1):22–30
87. Shiraiwa M, Ammann M, Koop T, Poschl U (2011) Gas uptake and chemical aging of semisolid organic aerosol particles. *Proc Natl Acad Sci USA* 108(27):11003–11008
88. Lanz VA, Alfarra MR, Baltensperger U, Buchmann B, Hueglin C, Szidat S, Wehrli MN, Wacker L, Weimer S, Caseiro A, Puxbaum H, Prevot ASH (2008) Source attribution of submicron organic aerosols during wintertime inversions by advanced factor analysis of aerosol mass spectra. *Environ Sci Technol* 42(1):214–220
89. Fraser MP, Cass GR, Simoneit BRT, Rasmussen RA (1997) Air quality model evaluation data for organics .4. C-2-C-36 non-aromatic hydrocarbons. *Environ Sci Technol* 31(8): 2356–2367
90. Robinson AL, Grieshop AP, Donahue NM, Hunt SW (2010) Updating the conceptual model for fine particle mass emissions from combustion systems. *J Air Waste Manag Assoc* 60 (10):1204–1222. doi:10.3155/1047-3289.60.10.1204
91. Williams BJ, Goldstein AH, Kreisberg NM, Hering SV (2006) An in-situ instrument for speciated organic composition of atmospheric aerosols: thermal desorption aerosol GC/MS-FID (TAG). *Aerosol Sci Technol* 40(8):627–638. doi:Doi 10.1080/02786820600754631
92. Lambe AT, Miracolo MA, Hennigan CJ, Robinson AL, Donahue NM (2009) Effective rate constants and uptake coefficients for the reactions of organic molecular markers (n-alkanes, hopanes, and steranes) in motor oil and diesel primary organic aerosols with hydroxyl radicals. *Environ Sci Technol* 43(23):8794–8800. doi:10.1021/es901745h
93. Miracolo MA, Presto AA, Lambe AT, Hennigan CJ, Donahue NM, Kroll JH, Worsnop DR, Robinson AL (2010) Photo-oxidation of low-volatility organics found in motor vehicle emissions: production and chemical evolution of organic aerosol mass. *Environ Sci Technol* 44(5):1638–1643. doi:10.1021/es902635c
94. Shrivastava MK, Lipsky EM, Stanier CO, Robinson AL (2006) Modeling semivolatile organic aerosol mass emissions from combustion systems. *Environ Sci Technol* 40:2671–2677
95. Fraser MP, Cass GR, Simoneit BRT (1998) Gas-phase and particle-phase organic compounds emitted from motor vehicle traffic in a Los Angeles roadway tunnel. *Environ Sci Technol* 32 (14):2051–2060
96. Yokelson RJ, Crouse JD, DeCarlo PF, Karl T, Urbanski S, Atlas E, Campos T, Shinozuka Y, Kapustin V, Clarke AD, Weinheimer A, Knapp DJ, Montzka DD, Holloway J, Weibring P, Flocke F, Zheng W, Toohey D, Wennberg PO, Wiedinmyer C, Mauldin L, Fried A, Richter D, Walega J, Jimenez JL, Adachi K, Buseck PR, Hall SR, Shetter R (2009) Emissions from biomass burning in the Yucatan. *Atmos Chem Phys* 9(15):5785–5812
97. Zhang KM, Wexler AS (2004) Evolution of particle number distribution near roadways - part I: analysis of aerosol dynamics and its implications for engine emission measurement. *Atmos Environ* 38(38):6643–6653
98. Zhang Y, Liu P, Liu XH, Jacobson MZ, McMurry PH, Yu FQ, Yu SC, Schere KL (2010) A comparative study of nucleation parameterizations: 2. Three-dimensional model application and evaluation. *J Geophys Res Atmos* 115:D20213
99. Guenther A, Hewitt CN, Erickson D, Fall R, Geron C, Graedel T, Harley P, Klinger L, Lerdau M, McKay WA, Pierce T, Scholes B, Steinbrecher R, Tallamraju R, Taylor J, Zimmerman P (1995) A global-model of natural volatile organic-compound emissions. *J Geophys Res Atmos* 100(D5):8873–8892. doi:10.1029/94jd02950
100. Jaoui M, Kamens RM (2001) Mass balance of gaseous and particulate products analysis from alpha-pinene/NO<sub>x</sub>/air in the presence of natural sunlight. *J Geophys Res Atmos* 106 (D12):12541–12558

101. Presto AA, Huff Hartz KE, Donahue NM (2005) Secondary organic aerosol production from terpene ozonolysis. 1. Effect of UV radiation. *Environ Sci Technol* 39:7036–7045
102. Isaacman G, Worton DR, Kreisberg NM, Hennigan CJ, Teng AP, Hering SV, Robinson AL, Donahue NM, Goldstein AH (2011) Understanding evolution of product composition and volatility distribution through in-situ GC x GC analysis: a case study of longifolene ozonolysis. *Atmos Chem Phys* 11(11):5335–5346
103. Tolocka MP, Jang M, Ginter JM, Cox FJ, Kamens RM, Johnston MV (2004) Formation of oligomers in secondary organic aerosol. *Environ Sci Technol* 38(5):1428–1434. doi:[Doi 10.1021/Es035030r](https://doi.org/10.1021/Es035030r)
104. Baltensperger U, Kalberer M, Dommen J, Paulsen D, Alfarra MR, Coe H, Fisseha R, Gascho A, Gysel M, Nyeki S, Sax M, Steinbacher M, Prevot ASH, Sjogren S, Weingartner E, Zenobi R (2005) Secondary organic aerosols from anthropogenic and biogenic precursors. *Faraday Discuss* 130:265–278. doi:[Doi 10.1039/B417367h](https://doi.org/10.1039/B417367h)
105. Hall WA, Johnston MV (2011) Oligomer content of alpha-pinene secondary organic aerosol. *Aerosol Sci Technol* 45(1):37–45
106. Surratt JD, Kroll JH, Kleindienst TE, Edney EO, Claeys M, Sorooshian A, Ng NL, Offenberg JH, Lewandowski M, Jaoui M, Flagan RC, Seinfeld JH (2007) Evidence for organosulfates in secondary organic aerosol. *Environ Sci Technol* 41(2):517–527
107. Kroll JH, Seinfeld JH (2005) Representation of secondary organic aerosol laboratory chamber data for the interpretation of mechanisms of particle growth. *Environ Sci Technol* 39(11):4159–4165. doi:[Doi 10.1021/Es048292h](https://doi.org/10.1021/Es048292h)
108. Grieshop AP, Donahue NM, Robinson AL (2007) Is the gas-particle partitioning in alpha-pinene secondary organic aerosol reversible? *Geophys Res Lett* 34(14):L14810. doi:[10.1029/2007gl029987](https://doi.org/10.1029/2007gl029987)
109. An WJ, Pathak RK, Lee BH, Pandis SN (2007) Aerosol volatility measurement using an improved thermodenuder: application to secondary organic aerosol. *J Aerosol Sci* 38(3):305–314. doi:[10.1016/j.jaerosci.2006.12.002](https://doi.org/10.1016/j.jaerosci.2006.12.002)
110. Huffman JA, Ziemann PJ, Jayne JT, Worsnop DR, Jimenez JL (2008) Development and characterization of a fast-stepping/scanning thermodenuder for chemically-resolved aerosol volatility measurements. *Aerosol Sci Technol* 42(5):395–407
111. Lee BH, Pierce JR, Engelhart GJ, Pandis SN (2011) Volatility of secondary organic aerosol from the ozonolysis of monoterpenes. *Atmos Environ* 45(14):2443–2452. doi:[10.1016/j.atmosenv.2011.02.004](https://doi.org/10.1016/j.atmosenv.2011.02.004)
112. Tritscher T, Dommen J, DeCarlo PF, Gysel M, Barmet PB, Praplan AP, Weingartner E, Prévôt ASH, Riipinen I, Donahue NM, Baltensperger U (2011) Volatility and hygroscopicity of aging secondary organic aerosol in a smog chamber. *Atmos Chem Phys* 11(22):11477–11496. doi:[10.5194/acp-11-11477-2011](https://doi.org/10.5194/acp-11-11477-2011)
113. Salo K, Hallquist M, Jonsson AM, Saathoff H, Naumann KH, Spindler C, Tillmann R, Fuchs H, Bohn B, Rubach F, Mentel TF, Muller L, Reinnig M, Hoffmann T, Donahue NM (2011) Volatility of secondary organic aerosol during OH radical induced ageing. *Atmos Chem Phys* 11(21):11055–11067
114. Kostenidou E, Lee BH, Engelhart GJ, Pierce JR, Pandis SN (2009) Mass spectra deconvolution of low, medium, and high volatility biogenic secondary organic aerosol. *Environ Sci Technol* 43(13):4884–4889. doi:[10.1021/es803676g](https://doi.org/10.1021/es803676g)
115. Lee BH, Kostenidou E, Hildebrandt L, Riipinen I, Engelhart GJ, Mohr C, DeCarlo PF, Mihalopoulos N, Prevot ASH, Baltensperger U, Pandis SN (2010) Measurement of the ambient organic aerosol volatility distribution: application during the Finokalia Aerosol Measurement Experiment (FAME-2008). *Atmos Chem Phys* 10(24):12149–12160. doi:[10.5194/acp-10-12149-2010](https://doi.org/10.5194/acp-10-12149-2010)
116. Simoneit BRT (2002) Biomass burning - a review of organic tracers for smoke from incomplete combustion. *Appl Geochem* 17(3):129–162
117. Chan MN, Surratt JD, Claeys M, Edgerton ES, Tanner RL, Shaw SL, Zheng M, Knipping EM, Eddingsaas NC, Wennberg PO, Seinfeld JH (2010) Characterization and quantification of isoprene-derived epoxydiols in ambient aerosol in the southeastern United States. *Environ Sci Technol* 44(12):4590–4596

118. Ervens B, Turpin BJ, Weber RJ (2011) Secondary organic aerosol formation in cloud droplets and aqueous particles (aqSOA): a review of laboratory, field and model studies. *Atmos Chem Phys* 11(21):11069–11102
119. Maria SF, Russell LM, Gilles MK, Myneni SCB (2004) Organic aerosol growth mechanisms and their climate-forcing implications. *Science* 306(5703):1921–1924
120. Seinfeld JH, Pandis SN (2006) *Atmospheric chemistry and physics*, 2nd edn. Wiley, Hoboken
121. Kroll JH, Chan AWH, Ng NL, Flagan RC, Seinfeld JH (2007) Reactions of semivolatile organics and their effects on secondary organic aerosol formation. *Environ Sci Technol* 41(10):3545–3550
122. Pathak R, Donahue NM, Pandis SN (2008) Ozonolysis of beta-pinene: temperature dependence of secondary organic aerosol mass fraction. *Environ Sci Technol* 42(14):5081–5086. doi:[10.1021/es070721z](https://doi.org/10.1021/es070721z)
123. Hildebrandt L, Donahue NM, Pandis SN (2009) High formation of secondary organic aerosol from the photo-oxidation of toluene. *Atmos Chem Phys* 9(9):2973–2986
124. Prisle NL, Engelhart GJ, Bilde M, Donahue NM (2010) Humidity influence on gas-particle phase partitioning of alpha-pinene + O(3) secondary organic aerosol. *Geophys Res Lett* 37:5. doi:[10.1029/2009gl041402](https://doi.org/10.1029/2009gl041402)
125. Bertram AK, Martin ST, Hanna SJ, Smith ML, Bodsworth A, Chen Q, Kuwata M, Liu A, You Y, Zorn SR (2011) Predicting the relative humidities of liquid-liquid phase separation, efflorescence, and deliquescence of mixed particles of ammonium sulfate, organic material, and water using the organic-to-sulfate mass ratio of the particle and the oxygen-to-carbon elemental ratio of the organic component. *Atmos Chem Phys* 11(21):10995–11006
126. Zuend A, Marcolli C, Peter T, Seinfeld JH (2010) Computation of liquid-liquid equilibria and phase stabilities: implications for RH-dependent gas/particle partitioning of organic-inorganic aerosols. *Atmos Chem Phys* 10(16):7795–7820
127. Robinson AL, Donahue NM, Shrivastava MK, Weitkamp EA, Sage AM, Grieshop AP, Lane TE, Pierce JR, Pandis SN (2007) Rethinking organic aerosols: semivolatile emissions and photochemical aging. *Science* 315(5816):1259–1262
128. Weitkamp EA, Sage AM, Pierce JR, Donahue NM, Robinson AL (2007) Organic aerosol formation from photochemical oxidation of diesel exhaust in a smog chamber. *Environ Sci Technol* 41(20):6969–6975
129. Sage AM, Weitkamp EA, Robinson AL, Donahue NM (2008) Evolving mass spectra of the oxidized component of organic aerosol: results from aerosol mass spectrometer analyses of aged diesel emissions. *Atmos Chem Phys* 8(5):1139–1152
130. Zhang Q, Alfara MR, Worsnop DR, Allan JD, Coe H, Canagaratna MR, Jimenez JL (2005) Deconvolution and quantification of hydrocarbon-like and oxygenated organic aerosols based on aerosol mass spectrometry. *Environ Sci Technol* 39(13):4938–4952
131. Shilling JE, Chen Q, King SM, Rosenoern T, Kroll JH, Worsnop DR, DeCarlo PF, Aiken AC, Sueper D, Jimenez JL, Martin ST (2009) Loading-dependent elemental composition of alpha-pinene SOA particles. *Atmos Chem Phys* 9(3):771–782
132. Lim YB, Ziemann PJ (2005) Products and mechanism of secondary organic aerosol formation from reactions of n-alkanes with OH radicals in the presence of NO<sub>x</sub>. *Environ Sci Technol* 39(23):9229–9236
133. Presto AA, Miracolo MA, Donahue NM, Robinson AL (2010) Secondary organic aerosol formation from high-NO(x) photo-oxidation of low volatility precursors: n-alkanes. *Environ Sci Technol* 44(6):2029–2034. doi:[10.1021/es903712r](https://doi.org/10.1021/es903712r)
134. Lim YB, Ziemann PJ (2009) Effects of molecular structure on aerosol yields from OH radical-initiated reactions of linear, branched, and cyclic alkanes in the presence of NO<sub>x</sub>. *Environ Sci Technol* 43(7):2328–2334
135. Pitts JN, Vancauwenberghe KA, Grosjean D, Schmid JP, Fitz DR, Belser WL, Knudson GB, Hynds PM (1978) Atmospheric reactions of polycyclic aromatic-hydrocarbons - facile formation of mutagenic nitro-derivatives. *Science* 202(4367):515–519

136. Kamens RM, Fulcher JN, Zhishi G (1986) Effects of temperature on wood soot pah decay in atmospheres with sunlight and low Nox. *Atmos Environ* 20(8):1579–1587
137. Pankow JF, Isabelle LM, Buchholz DA, Luo WT, Reeves BD (1994) Gas-particle partitioning of polycyclic aromatic-hydrocarbons and alkanes to environmental tobacco-smoke. *Environ Sci Technol* 28(2):363
138. Pankow JF (1987) Review and comparative-analysis of the theories on partitioning between the gas and aerosol particulate phases in the atmosphere. *Atmos Environ* 21(11): 2275–2283
139. Pankow JF (1991) Common gamma-intercept and single compound regressions of gas particle partitioning data vs 1/T. *Atmos Environ Part A General Topics* 25(10):2229–2239
140. Pankow JF (1994) An absorption-model of the gas aerosol partitioning involved in the formation of secondary organic aerosol. *Atmos Environ* 28(2):189–193
141. Chan AWH, Kautzman KE, Chhabra PS, Surratt JD, Chan MN, Crouse JD, Kurten A, Wennberg PO, Flagan RC, Seinfeld JH (2009) Secondary organic aerosol formation from photooxidation of naphthalene and alkylnaphthalenes: implications for oxidation of intermediate volatility organic compounds (IVOCs). *Atmos Chem Phys* 9(9):3049–3060
142. Rogge WF, Hildemann LM, Mazurek MA, Cass GR, Simoneit BRT (1996) Mathematical modeling of atmospheric fine particle-associated primary organic compound concentrations. *J Geophys Res Atmos* 101(D14):19379–19394
143. Weitkamp EA, Lambe AT, Donahue NM, Robinson AL (2008) Laboratory measurements of the heterogeneous oxidation of condensed-phase organic molecular markers for motor vehicle exhaust. *Environ Sci Technol* 42(21):7950–7956. doi:10.1021/es800745x
144. Chirico R, DeCarlo PF, Heringa MF, Tritscher T, Richter R, Prevot ASH, Dommen J, Weingartner E, Wehrle G, Gysel M, Laborde M, Baltensperger U (2010) Impact of aftertreatment devices on primary emissions and secondary organic aerosol formation potential from in-use diesel vehicles: results from smog chamber experiments. *Atmos Chem Phys* 10(23):11545–11563
145. Grieshop AP, Donahue NM, Robinson AL (2009) Laboratory investigation of photochemical oxidation of organic aerosol from wood fires 2: analysis of aerosol mass spectrometer data. *Atmos Chem Phys* 9(6):2227–2240
146. Heringa MF, DeCarlo PF, Chirico R, Tritscher T, Dommen J, Weingartner E, Richter R, Wehrle G, Prevot ASH, Baltensperger U (2011) Investigations of primary and secondary particulate matter of different wood combustion appliances with a high-resolution time-of-flight aerosol mass spectrometer. *Atmos Chem Phys* 11(12):5945–5957
147. Miracolo MA, Hennigan CJ, Ranjan M, Nguyen NT, Gordon TD, Lipsky EM, Presto AA, Donahue NM, Robinson AL (2011) Secondary aerosol formation from photochemical aging of aircraft exhaust in a smog chamber. *Atmos Chem Phys* 11(9):4135–4147
148. Hennigan CJ, Sullivan AP, Collett JL, Robinson AL (2010) Levoglucosan stability in biomass burning particles exposed to hydroxyl radicals. *Geophys Res Lett* 37:L09806. doi:10.1029/2010gl043088
149. Ng NL, Kroll JH, Keywood MD, Bahreini R, Varutbangkul V, Flagan RC, Seinfeld JH, Lee A, Goldstein AH (2006) Contribution of first- versus second-generation products to secondary organic aerosols formed in the oxidation of biogenic hydrocarbons. *Environ Sci Technol* 40(7):2283–2297
150. Zhang JY, Hartz KEH, Pandis SN, Donahue NM (2006) Secondary organic aerosol formation from limonene ozonolysis: homogeneous and heterogeneous influences as a function of NOx. *J Phys Chem A* 110(38):11053–11063
151. Leungsakul S, Jaoui M, Kamens RM (2005) Kinetic mechanism for predicting secondary organic aerosol formation from the reaction of d-limonene with ozone. *Environ Sci Technol* 39(24):9583–9594
152. Donahue NM, Tischuk JE, Marquis BJ, Huff Hartz KE (2007) Secondary organic aerosol from limona ketone: insights into terpene ozonolysis via synthesis of key intermediates. *Phys Chem Chem Phys* 9(23):2991–2998

153. Maksymiuk CS, Gayahtri C, Gil RR, Donahue NM (2009) Secondary organic aerosol formation from multiphase oxidation of limonene by ozone: mechanistic constraints via two-dimensional heteronuclear NMR spectroscopy. *Phys Chem Chem Phys* 11(36): 7810–7818. doi:[10.1039/b820005j](https://doi.org/10.1039/b820005j)
154. Claeys M, Szmigielski R, Kourtev I, Van der Veken P, Vermeylen R, Maenhaut W, Jaoui M, Kleindienst TE, Lewandowski M, Offenberg JH, Edney EO (2007) Hydroxydicarboxylic acids: markers for secondary organic aerosol from the photooxidation of alpha-pinene. *Environ Sci Technol* 41(5):1628–1634
155. Mueller L, Reinnig MC, Naumann KH, Saathoff H, Mentel TF, Donahue NM, Hoffmann T (2012) Formation of 3-methyl-1,2,3-butanetricarboxylic acid via gas phase oxidation of pinonic acid - a mass spectrometric study of SOA aging. *Atmos Chem Phys* 12:1483–1496. doi:[10.5194/acp-12-1483-2012](https://doi.org/10.5194/acp-12-1483-2012)
156. Chhabra PS, Ng NL, Canagaratna MR, Corrigan AL, Russell LM, Worsnop DR, Flagan RC, Seinfeld JH (2011) Elemental composition and oxidation of chamber organic aerosol. *Atmos Chem Phys* 11(17):8827–8845
157. Ng NL, Canagaratna MR, Zhang Q, Jimenez JL, Tian J, Ulbrich IM, Kroll JH, Docherty KS, Chhabra PS, Bahreini R, Murphy SM, Seinfeld JH, Hildebrandt L, Donahue NM, DeCarlo PF, Lanz VA, Prevot ASH, Dinar E, Rudich Y, Worsnop DR (2010) Organic aerosol components observed in northern hemispheric datasets from aerosol mass spectrometry. *Atmos Chem Phys* 10(10):4625–4641. doi:[10.5194/acp-10-4625-2010](https://doi.org/10.5194/acp-10-4625-2010)
158. Donahue NM, Henry KM, Mentel TF, Scharr AK, Spindler C, Bohn B, Brauers T, Dorn HP, Fuchs H, Tillmann R, Wahner A, Saathoff H, Naumann KH, Möhler O, Leisner T, Müller L, Reinnig M-C, Hoffmann T, Salow K, Hallquist M, Frosch M, Bilde M, Tritscher T, Barmet P, Praplan AP, DeCarlo PF, Dommen J, Prévôt ASH, Baltensperger U (2012) Aging of biogenic secondary organic aerosol via gas-phase OH radical reactions. *Proc Natl Acad Sci* 109(34): 13503–13508. doi:[10.1073/pnas.1115186109](https://doi.org/10.1073/pnas.1115186109)
159. Frosch M, Bilde M, DeCarlo PF, Juranyi Z, Tritscher T, Dommen J, Donahue NM, Gysel M, Weingartner E, Baltensperger U (2011) Relating cloud condensation nuclei activity and oxidation level of alpha-pinene secondary organic aerosols. *J Geophys Res Atmos* 116: D22212
160. Barmet P, Dommen J, DeCarlo PF, Tritscher T, Praplan AP, Platt SM, Prévôt ASH, Donahue NM, Baltensperger U (2012) OH clock determination by proton transfer reaction mass spectrometry at an environmental chamber. *Atmos Meas Tech* 5:7471–7498. doi:[10.5194/amt-5-647-2012](https://doi.org/10.5194/amt-5-647-2012)
161. Rudich Y, Donahue NM, Mentel TF (2007) Aging of organic aerosol: bridging the gap between laboratory and field studies. *Annu Rev Phys Chem* 58:321–352
162. Massoli P, Lambe AT, Ahern AT, Williams LR, Ehn M, Mikkila J, Canagaratna MR, Brune WH, Onasch TB, Jayne JT, Petaja T, Kulmala M, Laaksonen A, Kolb CE, Davidovits P, Worsnop DR (2011) Relationship between aerosol oxidation level and hygroscopic properties of laboratory generated secondary organic aerosol (SOA) particles (vol 37, L24801, 2010). *Geophys Res Lett* 38:L03805. doi:[10.1029/2011gl046687](https://doi.org/10.1029/2011gl046687)
163. Hearn JD, Lovett AJ, Smith GD (2005) Ozonolysis of oleic acid particles: evidence for a surface reaction and secondary reactions involving Criegee intermediates. *Phys Chem Chem Phys* 7(3):501–511
164. Sage AM, Weitkamp EA, Robinson AL, Donahue NM (2009) Reactivity of oleic acid in organic particles: changes in oxidant uptake and reaction stoichiometry with particle oxidation. *Phys Chem Chem Phys* 11(36):7951–7962. doi:[10.1039/b904285g](https://doi.org/10.1039/b904285g)
165. Donahue NM, Robinson AL, Hartz KEH, Sage AM, Weitkamp EA (2005) Competitive oxidation in atmospheric aerosols: the case for relative kinetics. *Geophys Res Lett* 32:L16805
166. Huff Hartz KE, Weitkamp EA, Sage AM, Donahue NM, Robinson AL (2007) Laboratory measurements of the oxidation kinetics of organic aerosol mixtures using a relative rate constants approach. *J Geophys Res Atmos* 112:D04204

167. Wagstrom KM, Pandis SN (2009) Determination of the age distribution of primary and secondary aerosol species using a chemical transport model. *J Geophys Res Atmos* 114: D14303. doi:10.1029/2009jd011784
168. Worsnop DR, Morris JW, Shi Q, Davidovits P, Kolb CE (2002) A chemical kinetic model for reactive transformations of aerosol particles. *Geophys Res Lett* 29(20):1996
169. Smith JD, Kroll JH, Cappa CD, Che DL, Liu CL, Ahmed M, Leone SR, Worsnop DR, Wilson KR (2009) The heterogeneous reaction of hydroxyl radicals with sub-micron squalane particles: a model system for understanding the oxidative aging of ambient aerosols. *Atmos Chem Phys* 9(9):3209–3222
170. Lim HJ, Carlton AG, Turpin BJ (2005) Isoprene forms secondary organic aerosol through cloud processing: model simulations. *Environ Sci Technol* 39(12):4441–4446
171. Lim YB, Tan Y, Perri MJ, Seitzinger SP, Turpin BJ (2010) Aqueous chemistry and its role in secondary organic aerosol (SOA) formation. *Atmos Chem Phys* 10(21):10521–10539
172. Ervens B, Volkamer R (2010) Glyoxal processing by aerosol multiphase chemistry: towards a kinetic modeling framework of secondary organic aerosol formation in aqueous particles. *Atmos Chem Phys* 10(17):8219–8244
173. Herrmann H, Hoffmann D, Schaefer T, Brauer P, Tilgner A (2010) Tropospheric aqueous-phase free-radical chemistry: radical sources, spectra. Reaction kinetics and prediction tools. *Chemphyschem* 11(18):3796–3822
174. Sander R (1999) Compilation of Henry's law constants for inorganic and organic species of potential importance in environmental chemistry. <http://www.rolf-sander.net/henry/henry.pdf>
175. Griffin RJ, Nguyen K, Dabdub D, Seinfeld JH (2003) A coupled hydrophobic-hydrophilic model for predicting secondary organic aerosol formation. *J Atmos Chem* 44(2):171–190
176. Volkamer R, Ziemann PJ, Molina MJ (2009) Secondary organic aerosol formation from acetylene (C<sub>2</sub>H<sub>2</sub>): seed effect on SOA yields due to organic photochemistry in the aerosol aqueous phase. *Atmos Chem Phys* 9(6):1907–1928
177. Galloway MM, Huisman AJ, Yee LD, Chan AWH, Loza CL, Seinfeld JH, Keutsch FN (2011) Yields of oxidized volatile organic compounds during the OH radical initiated oxidation of isoprene, methyl vinyl ketone, and methacrolein under high-NO(x) conditions. *Atmos Chem Phys* 11(21):10779–10790
178. DeCarlo PF, Dunlea EJ, Kimmel JR, Aiken AC, Sueper D, Crouse J, Wennberg PO, Emmons L, Shinzuka Y, Clarke A, Zhou J, Tomlinson J, Collins DR, Knapp D, Weinheimer AJ, Montzka DD, Campos T, Jimenez JL (2008) Fast airborne aerosol size and chemistry measurements above Mexico City and central Mexico during the MILAGRO campaign. *Atmos Chem Phys* 8(14):4027–4048
179. Hildebrandt L, Kostenidou E, Mihalopoulos N, Worsnop DR, Donahue NM, Pandis SN (2010) Formation of highly oxygenated organic aerosol in the atmosphere: insights from the Finokalia aerosol measurement experiments. *Geophys Res Lett* 37:L23801. doi:10.1029/2010gl045193



# Formation and aging of secondary organic aerosol from toluene: changes in chemical composition, volatility, and hygroscopicity

L. Hildebrandt Ruiz<sup>1,2</sup>, A. L. Paciga<sup>2,a</sup>, K. M. Cerully<sup>3,b</sup>, A. Nenes<sup>3</sup>, N. M. Donahue<sup>2</sup>, and S. N. Pandis<sup>2,4</sup>

<sup>1</sup>The University of Texas at Austin, Austin, Texas, USA

<sup>2</sup>Carnegie Mellon University, Pittsburgh, Pennsylvania, USA

<sup>3</sup>Georgia Institute of Technology, Atlanta, Georgia, USA

<sup>4</sup>University of Patras, Patras, Greece

<sup>a</sup>now at: Phillips66<sup>®</sup>, Bartlesville, Oklahoma, USA

<sup>b</sup>now at: TSI, Inc., Shoreview, Minnesota, USA

Correspondence to: L. Hildebrandt Ruiz (lhr@che.utexas.edu)

Received: 3 November 2014 – Published in Atmos. Chem. Phys. Discuss.: 12 December 2014

Revised: 5 June 2015 – Accepted: 5 July 2015 – Published: 24 July 2015

**Abstract.** Secondary organic aerosol (SOA) is transformed after its initial formation, but this chemical aging of SOA is poorly understood. Experiments were conducted in the Carnegie Mellon environmental chamber to form secondary organic aerosol (SOA) from the photo-oxidation of toluene and other small aromatic volatile organic compounds (VOCs) in the presence of NO<sub>x</sub> under different oxidizing conditions. The effects of the oxidizing condition on organic aerosol (OA) composition, mass yield, volatility, and hygroscopicity were explored. Higher exposure to the hydroxyl radical resulted in different OA composition, average carbon oxidation state (OS<sub>c</sub>), and mass yield. The OA oxidation state generally increased during photo-oxidation, and the final OA OS<sub>c</sub> ranged from −0.29 to 0.16 in the performed experiments. The volatility of OA formed in these different experiments varied by as much as a factor of 30, demonstrating that the OA formed under different oxidizing conditions can have a significantly different saturation concentration. There was no clear correlation between hygroscopicity and oxidation state for this relatively hygroscopic SOA.

organic carbon mass (Hallquist et al., 2009), the influence of SOA on aerosol composition and related properties is important and complex (Donahue et al., 2009; Kanakidou et al., 2005; Kroll and Seinfeld, 2008). Using measurements in urban, suburban, and remote sites, Zhang et al. (2007) showed that as aerosol ages in the atmosphere, it reaches a highly oxidized state and no longer resembles either fresh primary or secondary aerosol.

Although it is clear that the oxidation of gas-phase compounds and continued oxidation of particle-phase compounds play an important role in SOA production and transformation, the underlying chemistry and thermodynamics are poorly understood. Without the correct representation of SOA production and evolution mechanisms, modeling attempts often lead to underestimations of ambient mass loadings (Heald et al., 2005; Volkamer et al., 2006). The large uncertainty in SOA concentrations predicted by chemical transport models (CTMs) demonstrates the need for experimental data on the multi-generation oxidation reactions or “aging” that lead to changes in mass loadings and physicochemical properties of SOA. Several computational studies have highlighted the importance of not only incorporating extended chemical mechanisms but obtaining corresponding relationships between chemical aging and physicochemical properties of the SOA, such as its volatility, in atmospherically relevant systems (Cappa and Wilson, 2012; Shrivastava et al., 2013)

Considering current “state-of-the-science” aerosol analysis techniques, identifying the plethora of SOA components

## 1 Introduction

Secondary organic aerosol (SOA) is produced when gas-phase precursors are oxidized, forming lower volatility products that partition to the condensed phase. As SOA is estimated to account for approximately 70 % of total aerosol or-

and their individual volatilities is not possible. A unified framework to evaluate complex systems in field or laboratory studies and to track changes in volatility as a function of physicochemical processing is the 2-D-volatility basis set (2D-VBS). It uses coordinates of volatility in terms of effective saturation concentration,  $C^*$ , and oxidation state of carbon,  $OS_c$  (or the oxygen to carbon ratio,  $O : C$ ) to provide a space suitable for the description of the chemical transformations and phase partitioning of SOA (Donahue et al., 2012). Chemical species are lumped by  $C^*$  and  $OS_c$  in discretized bins.

The relationship between organic aerosol (OA) hygroscopicity and extent of oxidation, indicated by  $O : C$ , has been the focus of a number of laboratory and field studies (Alfarra et al., 2013; Chang et al., 2010; Frosch et al., 2011; Jimenez et al., 2009; Latham et al., 2013; Massoli et al., 2010). While OA hygroscopicity often increases with  $O : C$ , some other studies have found weak or no correlation between the two properties (Alfarra et al., 2013; Frosch et al., 2011; Latham et al., 2013; Massoli et al., 2010). It has been shown that  $OS_c$  is likely a better indicator of aerosol oxidation than  $O : C$  as the latter can be affected by non-oxidative processes such as hydration and dehydration while  $OS_c$  increases continually with oxidation (Canagaratna et al., 2015; Kroll et al., 2009, 2011); thus,  $O : C$  may not be as well correlated with observed hygroscopicity.

The organic aerosol  $O : C$  has been proposed to be linked with its volatility in addition to its hygroscopicity (Jimenez et al., 2009), and a few chamber studies have investigated the link among all three properties (Poulain et al., 2010; Tritscher et al., 2011). The conventional view is that the most volatile components should be the least hygroscopic; however, several studies have observed the opposite behavior (Asa-Awuku et al., 2009; Cerully et al., 2014; Meyer et al., 2009; Poulain et al., 2010). Tritscher et al. (2011) found that hygroscopicity and  $O : C$  remained constant with decreased volatility for  $\alpha$ -pinene SOA during aging by OH radicals.

We investigated the relationship between oxidation, volatility and hygroscopicity of SOA formed from the photo-oxidation of toluene (methylbenzene) and other small aromatic volatile organic compounds (VOCs) under a variety of oxidation conditions. Small aromatics are important anthropogenic SOA precursors (Pandis et al., 1992; Vutukuru et al., 2006), and toluene serves as a model system to study the formation of SOA from these compounds. A main objective of our work is to connect the extent of oxidation and the changes in volatility of these experiments within the 2-D-VBS framework.

## 2 Materials and methods

### 2.1 Environmental chamber experiments

Organic aerosol was formed from the photo-oxidation of toluene and other small aromatic VOCs in the Carnegie Mellon Center for Atmospheric Particle Studies (CAPS) environmental chamber. The basic sequence of the experiments was to fill the chamber with clean air, inject the VOC and nitrous acid (HONO), and turn on the UV lights to start formation of OH (from the photolysis of HONO), which oxidizes the VOC and forms secondary organic aerosol (SOA). The number of UV lights used, the initial VOC concentrations, and the number of HONO injections was varied between experiments in order to create different oxidizing environments, as summarized in Table 1. The amount of SOA formed, the SOA oxidation state, its volatility, and its hygroscopicity were measured, as explained in more detail below.

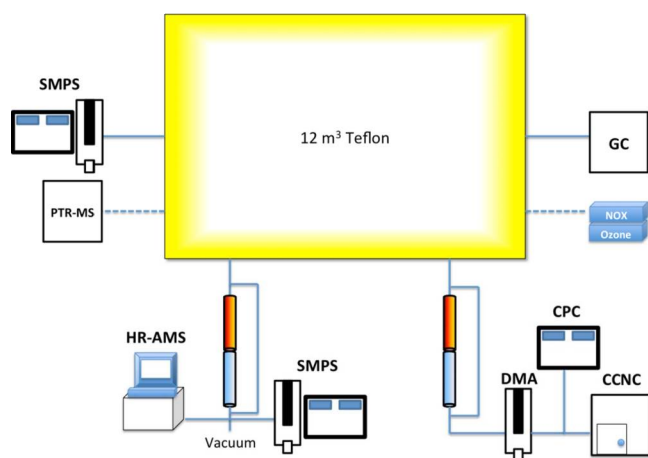
Nitrous acid was produced immediately before injection by drop-wise addition of 12 mL 0.1 M sodium nitrite solution to 24 mL 0.05 M sulfuric acid solution. Ammonium sulfate ( $(NH_4)_2SO_4$ , Sigma Aldrich, 99.99 %) seed particles were used in some experiments (Table 1) to provide surface area onto which organics would condense as SOA. In the unseeded experiments, nucleation of the organic vapors was observed. With the exception of Experiment 7 (Table 1), isotopically labeled toluene was used ( $^{13}C$ -toluene, Cambridge Isotope Laboratories, 99 %) as in a previous study (Hildebrandt et al., 2011). All six ring carbons in the labeled toluene are  $^{13}C$ -substituted, leaving the methyl carbon unsubstituted. In two experiments (Expts. 6 and 8) other small aromatic compounds were injected in addition to toluene as detailed in Table 1 in order to test whether these VOCs behave similarly as toluene. Concentrations of the VOCs were monitored using a proton-transfer reaction mass spectrometer (PTR-MS, Ionicon Analytik GmbH) when available. PTR-MS measurements were corrected for ion-source intensity and humidity as suggested by de Gouw et al. (2003). The sensitivity of the PTR-MS to the VOCs was measured before each experiment using a calibration gas mixture.

Figure 1 illustrates the experimental setup. Particle number and volume of the chamber aerosol were measured using a scanning mobility particle sizer (SMPS), comprised of a TSI model 3080 classifier and a TSI model 3772 condensation particle counter (CPC). Particle mass and chemical composition were measured using a high-resolution time-of-flight aerosol mass spectrometer (AMS) from Aerodyne, Inc. (DeCarlo et al., 2006). The AMS has two ion optical modes named by the shape of the ion flight paths: a single-reflection mode (V mode) with a shorter flight path and hence higher sensitivity but lower resolution, and a double-reflection mode (W mode) with longer flight path and hence higher resolution but lower sensitivity. In this study the AMS was operated according to common protocol with the vaporizer temperature at 600 °C, alternating between V and W modes to collect

**Table 1.** Experimental conditions.

Expt. #	Seeds <sup>a</sup>	[Toluene] <sub>0</sub> <sup>b</sup> (ppb)	[Toluene] <sub>f</sub> <sup>c</sup> (ppb)	HONO injections	Lights (%)	[OH] exposure <sup>d</sup> (cm <sup>-3</sup> s)
1	Yes	~ 300	NA	1	33	NA
2	No	~ 200	NA	1+1	100	NA
3	Yes	~ 300	NA	1+1	100	NA
4	No	~ 200	NA	2	100	NA
5	Yes	~ 100	NA	2+1	100	NA
6	No	~ 100 <sup>e</sup>	NA	2	100	NA
7	Yes	1320	1130	1	33	3.1 × 10 <sup>10</sup>
8	Yes	91 <sup>g</sup>	51 <sup>h</sup>	1	100	10 × 10 <sup>10</sup>
9	Yes	115	28	3+3	100	24 × 10 <sup>10</sup>

<sup>a</sup> (NH<sub>4</sub>)<sub>2</sub>SO<sub>4</sub> seed particles were used in some experiments. <sup>b</sup> Initial toluene concentrations estimated based on volume of VOC injected for Expts. 1–6 and measured by PTR-MS for Expts. 7–9. <sup>c</sup> Final toluene concentration after OH exposure. <sup>d</sup> Total OH exposure over the course of the experiment, estimated from exponential fits to the decay of toluene. Data not available for experiments 1–6 due to lack of PTR-MS data. <sup>e</sup> 5 μL of benzene, o-xylene, and 1,2,4-trimethylbenzene also injected. <sup>f</sup> 16 ppb ethylbenzene, 12 ppb benzene, and 23 ppb 1,2,4-trimethylbenzene also injected. <sup>g</sup> Final concentrations of ethylbenzene, benzene, and 1,2,4-trimethylbenzene: 9, 7, and 13 ppb, respectively.

**Figure 1.** Schematic of experimental setup. Dotted lines indicate that the equipment was used in selected experiments.

mass spectra, and collecting particle time-of-flight (pToF) measurements in V mode.

Air from the chamber was split into two separate streams for analysis of OA concentrations and properties. In the first stream, OA volatility was probed using a thermodenuder (TD) system, similar to the system used in Lee et al. (2010). Aerosol was passed alternately through the TD, heated to a predefined temperature, or a bypass line and then to the SMPS and the AMS for measurements of the particle size distributions and chemical composition. Properties of thermally treated OA were determined by comparing the residual aerosol after heating in the TD to the aerosol which was passed through the bypass line. The standard operating sample flow rate for the TD was 1 liter per minute (L min<sup>-1</sup>),

corresponding to a centerline residence time of ~ 15 s. In the TD followed by the AMS, the flow rate was also sometimes set to 0.6 L min<sup>-1</sup>, corresponding to a centerline residence time of ~ 25 s, to evaluate the effects of a longer residence time on OA evaporation, though these data were not used for thermally denuded CCN comparisons.

In the second stream, aerosol was again passed alternately through the TD or bypass line, then size-selected (approximately 100 to 140 nm) using a differential mobility analyzer (DMA, TSI model 3080) operated with a sheath to aerosol ratio of 10 : 1. Aerosol flow was then split to a CPC (TSI model 3010) and a cloud condensation nuclei counter (CCNc, Droplet Measurement Technologies). The CCNc was operated in Scanning Flow CCN Analysis (SFCA) mode (Moore et al., 2010), allowing for fast measurements of CCN by scanning the flow rate through the CCNc column, which measured the OA hygroscopicity. The thermodenuder positioned before the CCNc operated under the same temperature conditions as the AMS-TD and had a sample flowrate of 1 L min<sup>-1</sup>, which allows for analysis of volatility and hygroscopicity of the complete OA and the thermally denuded OA. Dilution air of 1.1 L min<sup>-1</sup> was introduced after the DMA before splitting to the CCNc and CPC. Flow to the CCNc was held constant at 1.1 L min<sup>-1</sup> using a laminar flow element, while flow in the CCNc was linearly ramped between 0.1 and 0.9 L min<sup>-1</sup> over 60 s. The top to bottom column temperature difference was 6 °C for all experiments.

## 2.2 AMS data analysis

The AMS data were processed in Igor Pro 6.12 (Wavemetrics, Inc.) using the standard AMS data analysis toolkits “Squirrel” version 1.51C for unit mass resolution (UMR) analysis and “Pika” version 1.10C for high resolution (HR)

**Table 2.** Summary of organic aerosol composition and volatility.

Expt #	(NO+NO <sub>2</sub> )/OA <sup>a</sup>	OS <sub>c</sub> <sup>b</sup>	O : C	NO <sup>+</sup> /NO <sub>2</sub> <sup>+</sup> <sup>c</sup>	H <sub>2</sub> O / (CO <sub>2</sub> + <sup>13</sup> CO <sub>2</sub> )	<sup>13</sup> CO / <sup>13</sup> CO <sub>2</sub> <sup>c</sup>	Volatility reduction (25 s) <sup>e</sup>	Volatility reduction (15 s) <sup>e</sup>
1	0.10	-0.14	0.84	8.2	1.70	1.17	3.5	3.6
2	0.11	0.16	0.83	7.5	0.30	1.09	30.4	30.8
3	0.10	0.00	1.04	8.3	2.35	1.23	3.1	3.6
4	0.12	0.01	0.92	7.9	1.70	1.22	3.5	4.0
5	0.12	-0.14	0.94	8.0	2.10	1.22	1.9	2.2
6	0.10	-0.17	0.89	8.6	1.99	1.36	1.7	2.5
7	0.13	-0.29	0.76	8.2	1.85	n/a <sup>d</sup>	1.0	1.0
8	0.10	-0.05	0.94	7.3	1.67	1.13	4.3	4.9
9	0.12	-0.04	1.02	7.0	2.40	1.13	6.2	8.2

<sup>a</sup> After first period of “lights on”. OA includes NO<sup>+</sup> and NO<sub>2</sub><sup>+</sup>. <sup>b</sup> After first period of “lights on”, OS<sub>c</sub> approximated as  $2 \times \text{O} : \text{C} - \text{H} : \text{C}$ . <sup>c</sup> From linear regressions throughout the experiment (when OA present). <sup>d</sup> Not applicable (no isotopically labeled VOC used in Experiment 7). <sup>e</sup> Volatility reduction estimated for data collected at residence times of 15 and 25 s. Values are calculated relative to Experiment 7 which featured the highest volatility.

analysis. HR analysis was performed using the W-mode data since highest resolution is preferred to distinguish between isotopically labeled and unlabeled ions. The lists of ions integrated in the HR analysis is similar to the list used previously (Hildebrandt et al., 2011). Ion masses were fitted up to an  $m/z$  ratio of 105; above this the signal was too noisy and/or the mass spectra were too crowded for reliable identification of ion atomic composition. According to the UMR analysis more than 95% of the organic signal was below  $m/z$  105, and the total organic mass was corrected based on this fraction calculated for each experiment (Table S1 in the Supplement).

### 2.2.1 Modification of standard fragmentation table

Several adjustments were made to the standard fragmentation table (Allan et al., 2004) for the analysis of HR and UMR data as explained in detail in the supplementary material; only the most important adjustments are summarized here. First, the fragmentation table was adjusted to account for hydrogen atoms ( $m/z = 1$ ) formed in the fragmentation of H<sub>2</sub>O (Canagaratna et al., 2015). Second, the amount of H<sub>2</sub>O<sup>+</sup> attributed to organics was chosen so that the mass of water does not correlate with the mass of organics ( $R < 0.01$ ) as expected for these low relative humidity experiments. The ratios of organic H<sub>2</sub>O<sup>+</sup> to (<sup>13</sup>CO<sub>2</sub><sup>+</sup> + CO<sub>2</sub><sup>+</sup>) are provided in Table 2 and ranged from 0.3 to 2.4, higher than the ratio of 0.225 in the default fragmentation table but consistent with recent calibration experiments (Canagaratna et al., 2015). Third, ions assigned to the nitrate family in the HR analysis (NO<sup>+</sup>, NO<sub>2</sub><sup>+</sup>) were added to the total organic aerosol mass in the HR batch table because they appear to be due to organic nitrates: The ratio of NO<sup>+</sup> to NO<sub>2</sub><sup>+</sup> measured in these experiments (Table 2) is around 8, much higher than the ratio of 2.4 measured in calibration experiments using ammonium nitrate. Furthermore, no inorganic nitrate was added in these experiments. Nitric acid is expected to form in the gas phase but does not appear to partition appreciably to the par-

ticle phase, consistent with its high vapor pressure (Fry et al., 2009). Nitrate fragments were not included in the calculation of O : C and H : C since elemental analysis examines the oxidation state of the carbon atoms.

### 2.2.2 Quantification of organic aerosol production

Data were corrected for changes in the instrument air beam (AB) over the course of an experiment. The ionization efficiency (IE) for each experiment was adjusted based on the ratio of the AB during the experiment to the AB during the ionization efficiency calibration conducted before this set of experiments was started (calibration IE/AB =  $4.65 \times 10^{-13}$ ). Additional details on quantification of AMS data are provided in the supplementary material. The AMS collection efficiency (CE) for these data was estimated by matching AMS mass distributions and SMPS volume distributions using the OA density ( $\rho_{\text{org}}$ ) and AMS CE as fitting parameters, with the algorithm developed by Kostenidou et al. (2007).

The amount of organic aerosol formed was quantified as the fractional aerosol mass yield (mass of OA formed divided by mass of toluene reacted). The mass of OA formed was corrected for the depositional loss of particles onto the chamber walls and for the condensational loss of organic vapors to wall-deposited particles. The assumption was made that condensation of organic vapors is not slowed by mass-transfer resistances, and that the wall-deposited particles are in equilibrium with the organic vapors in suspension. Therefore, the total (corrected) concentration of OA can be calculated by multiplying the OA/seed ratio by the initial seed concentration, as discussed in more detail in Hildebrandt et al. (2009). This correction does not account for condensation of organic vapors onto the “clean” Teflon walls. While these losses have been shown to occur (e.g., Matsunaga and Ziemann, 2010), quantification of their magnitude is an area of active research and remains challenging.

In all of the experiments described here, the condensation sink after particle formation was approximately  $1 \text{ min}^{-1}$ ,

while the initial condensation sink to ammonium sulfate seeds in seeded experiments ranged between 0.6 and  $1 \text{ min}^{-1}$ . The timescale for sulfuric acid vapor wall loss in the Carnegie Mellon chamber is approximately  $0.1 \text{ min}^{-1}$ , as determined by the chemical ionization mass spectrometer measurement of sulfuric acid loss (V. Hofbauer, personal communication, 2015). Thus, in all of the seeded experiments, condensing vapors encountered the seeds approximately 10 times before encountering the walls, while in nucleation experiments the suspended aerosol population quickly grew to a size where this was also true. Thus, while wall losses of semi-volatile vapors are a source of uncertainty, we have attempted to ensure that vapor–particle interactions at least dominate over vapor–wall interactions. It is therefore reasonable to expect that observed differences between experiments are not driven by interactions with the walls but instead by chemical processing of the organic aerosol.

## 2.3 Analysis of organic aerosol volatility

### 2.3.1 Data preparation

Volatility data were collected for each experiment after the SOA had formed. During some experiments, measurements were also made during the irradiation period (with the UV lights on) to examine the volatility changes during photooxidation. TD data are analyzed in terms of the volume fraction remaining (VFR) or mass fraction remaining (MFR). Using the total organic mass concentration from the AMS, the MFR was calculated by dividing the mass concentration of the denuded OA by the mass concentration of the OA that had passed through the bypass. These data are presented in the form of a thermogram, which shows the MFR as a function of temperature in the TD.

Particle concentrations decline in the smog chamber after SOA formation chemistry ceases due to losses to the chamber walls. This can lead to biases in the estimated MFR when bypass concentrations before or after the TD sampling period are used. A more accurate MFR was obtained by interpolation of the bypass OA concentrations corresponding to the TD sampling times. Each experiment was analyzed individually for a best fit, usually resulting in an exponential decay function. Graphs of the interpolated bypass data are shown in Fig. S2.

Particle losses in the TD were also taken into account. These losses occur due to diffusion (primarily of small particles), sedimentation (primarily of large particles), and thermophoresis; the losses are therefore a function of sample flow rate, temperature, and particle size (Burtscher et al., 2001). To estimate the losses within the TD setup, size-dependent loss functions were developed using NaCl particles under various TD temperatures and sample flow rates (Lee and Pandis, 2010). The number losses for each TD temperature–residence time combination are calculated by determining the losses over the size distribution measured by

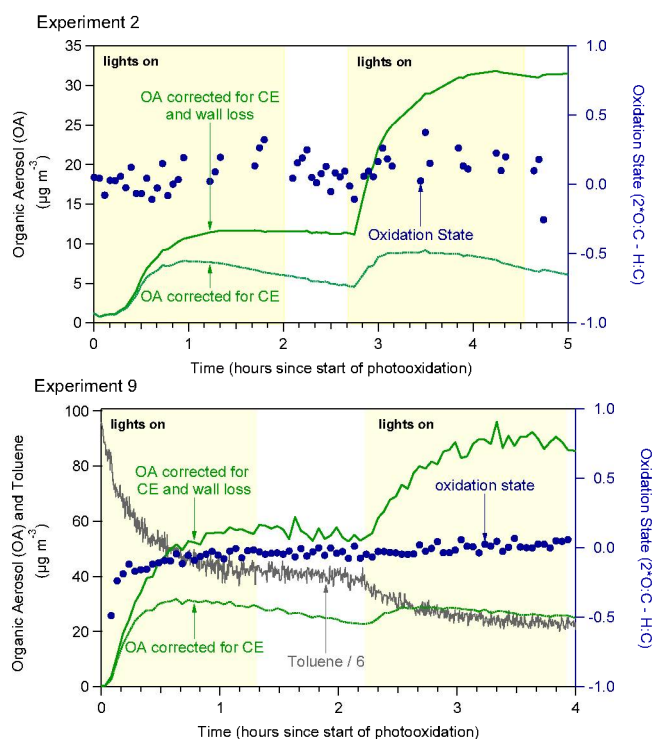


**Figure 2.** Time series of OA concentration (corrected for CE and corrected for CE and wall loss) from an unseeded experiment (2, top) and a seeded experiment (9, bottom), both with two photooxidation periods (“lights on”) before which HONO was injected. The periods during which the reactor was dark are shown with white background while the periods with UV lights are shaded yellow. Also shown is the OA oxidation state (right axis) and concentrations of toluene during Expt. 9 (toluene concentrations have been divided by 6 on the figure for easier readability).

the SMPS. The number losses for each size bin are then converted to a volume-based correction using the particle diameter of each bin. This correction factor is applied to the calculated MFR values. The organic MFR was calculated from AMS bypass and thermodenuder mass concentrations averaged over 6–9 min for a given TD temperature and residence time. It is assumed that there are no significant changes to composition and volatility over these averaging periods.

### 2.3.2 Evaporation model

Due to the non-equilibrium conditions in the TD, a dynamic mass transfer model developed by Riipinen et al. (2010) was used to estimate the relative volatility of the OA formed in the experiments outlined in Table 1. Briefly, aerosol evaporation is simulated using experimental inputs including TD temperature, residence time, particle mode diameter, mass concentration, and OA density. This method utilizes the volatility basis set approach (Donahue et al., 2006) to account for the component complexity in the SOA formed. Assuming the particles are in equilibrium with the vapor phase as they en-

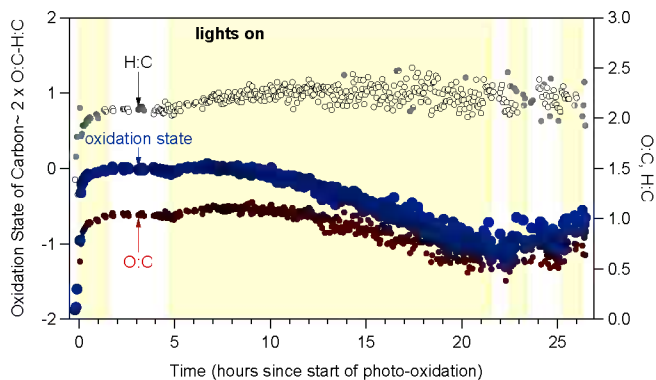


**Figure 3.** Time series of carbon oxidation state (left axis) and elemental ratios of O : C and H : C (right axis) for Expt. 3. The periods during which the reactor was dark are shown in with white background while the periods with UV lights are shaded yellow.

ter the TD, the effective saturation concentration is estimated from a least-squares fit to the experimental thermograms. An important caveat to this approach is that physical properties including mass accommodation coefficient and enthalpy of vaporization, which are usually unknown, can substantially affect the volatility estimated (Lee et al., 2010). The primary goal of these experiments was to observe changes in OA volatility with different levels of oxidation. Thus, relative volatility changes were calculated as described below, thus reducing uncertainties arising from the choice of accommodation coefficient and enthalpy of vaporization.

The volatility of SOA formed in each experiment was determined assuming a fixed volatility distribution shape using four saturation concentrations, 1, 10, 100, and 1000  $\mu\text{g m}^{-3}$ . During the analysis the saturation concentrations are multiplied by a shifting factor,  $s$ . This practically shifts the volatility distribution to lower or higher values, assuming that the shape of the distribution does not change. Differences in shifting factors can then be interpreted as differences in the saturation vapor pressure of the OA formed in these experiments: for example, OA with shifting factor 10 is 10 times more volatile than the OA with shifting factor 1. The volatility distribution used is the fresh toluene SOA distribution estimated by Hildebrandt et al. (2009) for their high  $\text{NO}_x$  experiments: 0.025 for  $C^* = 1$ , 0.51 for  $C^* = 10$ , 0.38 for  $C^* = 100$ , and 0.085 for  $C^* = 1000 \mu\text{g m}^{-3}$  (An organic aerosol concentration of  $50 \mu\text{g m}^{-3}$  was used to convert the product yields reported in Hildebrandt et al., 2009 to normalized mass fractions used here). The shifting factor is estimated for each of the experiments presented here by using the mass transfer model and least-squares fitting to the MFRs. In the last step relative shifting factors are calculated by normalizing them by the shifting factor of the OA formed in Expt. 7, in which SOA had the lowest  $\text{OS}_c$ . In this way, the relative volatility reduction ( $1/s$ ) for each experiment is estimated while accounting for the experiment specifics in-

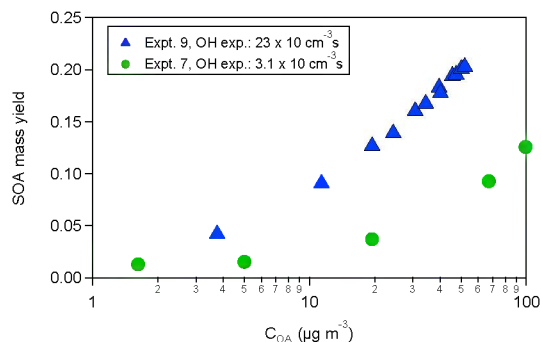


**Figure 4.** Organic aerosol mass yields for Expts. 7 and 9.

cluding residence time, TD temperature, mass concentration, and particle size. Fixed values are used for the enthalpy of vaporization ( $80 \text{ kJ mol}^{-1}$ ) and the mass accommodation coefficient (1.0). The sensitivity of results to these choices is discussed in Sect. 3.2.

## 2.4 Analysis of CCN activity

### 2.4.1 CCNc calibration

The CCNc instrument calibration is used to determine the relationship between instantaneous instrument flow rate and supersaturation as described in Moore et al. (2010). Ammonium sulfate solution is atomized, dried using a silica gel diffusion dryer, charge-neutralized using Po-210, and classified by a DMA. The flow is then introduced into both a CPC and a CCNc. The activation ratio, or the ratio of CCN to total particles, is then plotted against the instantaneous flow rate to yield data that are fit to a sigmoidal activation ratio function. The critical flow rate,  $Q^*$ , is determined, corresponding to where half of the total particles are activated and to a level of supersaturation,  $s^*$ , equal to the critical supersaturation of the classified aerosol (Sect. 2.4.2). The  $Q^*$  and  $s^*$  are determined for a range of aerosol sizes, yielding, for the flow rate range ( $0.1\text{--}0.9 \text{ L min}^{-1}$ ) and temperature gradient ( $\Delta T = 6^\circ\text{C}$ ) in the CCNc column, supersaturations ranging from approximately 0.1 to 0.5%.

### 2.4.2 Calculating aerosol hygroscopicity of size-selected aerosol

Using the method outlined in Sect. 2.4.1,  $s^*$  was determined for each flow rate upscan and downscan. All CCNc data subject to poor counting statistics (where the maximum CCN concentrations were lower than approximately 15 to 20 counts  $\text{cm}^{-3}$ ) were excluded from analysis (Moore et al., 2010). The characteristic hygroscopicity parameter,  $\kappa$  (Petters and Kreidenweis, 2007), of the monodisperse CCN is then determined by

$$\kappa = \frac{4A^3}{27d_p^3s^{*2}}, \quad (1)$$

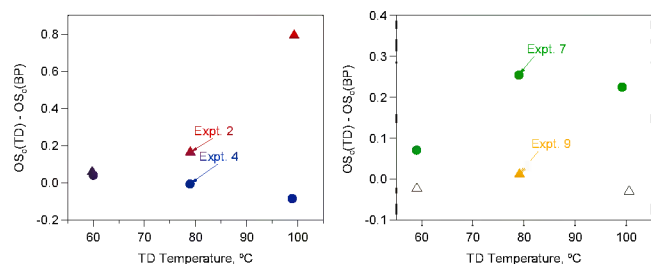


**Figure 5.** Comparison of the difference in oxidation state of denuded and total OA versus TD temperature for two unseeded experiments (2 and 4, left panel) and two seeded experiments (7 and 9, right panel). For OA of intermediate oxidation state (around 0, Expts. 4 and 9), oxidation state of the denuded OA is similar to the oxidation state of the full OA, implying that oxidation state does not correlate significantly with volatility. For OA of higher or lower oxidation state (Expts. 2 and 7, respectively) oxidation state anticorrelates with volatility, shown here as an increase in oxidation state difference with TD temperature.

where  $A = (4M_w\sigma_w)/(RT\rho_w)$ ;  $M_w$ ,  $\sigma_w$ , and  $\rho_w$  are the molar mass, surface tension, and density of water, respectively.  $R$  is the universal gas constant,  $T$  is CCNc mid-column temperature, and  $d_p$  is the dry particle diameter selected by the DMA prior to the CCNc.

### 3 Results and discussion

#### 3.1 Organic aerosol concentration, composition and mass yield

Figure 2 shows the time series of OA concentrations and oxidation state for an unseeded experiment (2, top panel) and a seeded experiment (9, bottom panel). The time series of toluene concentrations are also shown for Expt. 9; these data were not available for Expt. 2. There were two photo-oxidation periods (“lights on”) during each experiment, and HONO was injected every time before lights were turned on. During Experiment 2, the OA was alternatively passed through the bypass and the TD throughout the experiment (only the bypass data are shown in Fig. 2). The TD was held at the same temperature during the photo-oxidation periods to observe changes in volatility during this period, and the temperature in the TD was varied during the dark period to obtain a thermogram. During Experiment 9, the OA was passed only through the bypass during photo-oxidation, and it was alternated between bypass and TD (at different temperatures) during the dark period. The OA concentrations increased during the oxidation periods (“lights on”) as toluene was oxidized to form SOA. Toluene concentrations decreased by approximately 50 % during the first photo-oxidation period in Expt. 9 and decreased an additional 20 % during the second photo-oxidation period. Thus, gas-phase toluene is always present in the system and fresh toluene

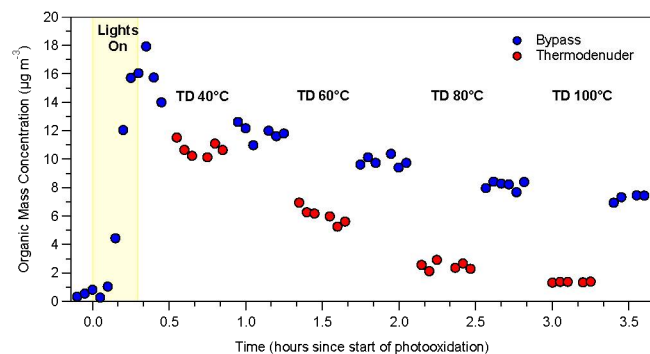
SOA is expected to form at the same time as the previously formed toluene SOA is aged photochemically.

A moderate increase in the OA oxidation state was observed during the “lights on” period in both experiments. Two competing effects can influence the OA oxidation state: First, according to partitioning theory, species of increasingly higher volatility will partition to the particle phase as the OA loading in the system increases. If oxidation state is anticorrelated with volatility this effect would decrease oxidation state when OA concentration increases. Second, the existing OA can be oxidized further (aged), increasing the OA oxidation state as long as the molecules composing the OA do not fragment. The OA oxidation state of the OA formed increased for several hours in the experiments shown in Fig. 2 and all other experiments conducted as part of this work, suggesting that the aging effect dominated.

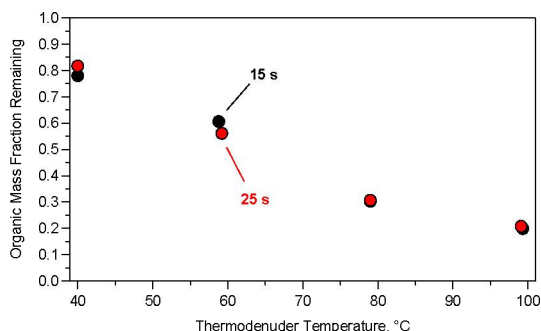
In an attempt to produce highly oxidized OA, photo-oxidation of the OA was continued for over 24 h during experiments 3 and 5. Figure 3 shows the time series of oxidation state and elemental ratios (O : C and H : C) for Expt. 3. As before, HONO was injected before every irradiation period. The OA oxidation state increased during the first few hours of irradiation but significantly decreased after longer irradiation. Plausible explanations for this decrease in oxidation state (which was also observed after long irradiation in Experiment 5) include the condensation of less oxidized vapors, photolysis of OA components and their fragmentation after continued oxidation with OH. Fragmented products may have a high oxidation state but high volatility (due to their smaller size) and evaporate from the OA, decreasing the OA average oxidation state. Photolysis of organic compounds is expected to occur throughout the experiment (e.g., Surratt et al., 2006), but as long as OH reactions dominate, the oxidation state of the bulk OA increases. Future experiments should aim to isolate OH from photolysis reactions by, for example, using a dark OH source. This would help to constrain these effects and eventually represent them in chemical transport models.

Table 2 provides a summary of the OA composition for all experiments investigated here. The observed oxidation state of the OA formed ranged from  $-0.29$  to  $0.16$ . At least 10 % of the OA mass was due to the sum of  $\text{NO}^+$  and  $\text{NO}_2^+$  ions. The observed ratio of  $\text{NO}^+$  to  $\text{NO}_2^+$  (Table 2) was between 7.0 and 8.6, much higher than the ratio of 2.4 measured in calibration experiments using ammonium nitrate, suggesting that the  $\text{NO}^+$  and  $\text{NO}_2^+$  ions originate from organic nitrogen (ON) compounds. Estimating that the ON compounds have an average molecular weight of about  $200 \text{ g mol}^{-1}$ , approximately half of the OA is due to ON. Thus, organic nitrogen compounds are a major constituent in the OA formed in these high- $\text{NO}_x$  photo-oxidation experiments.

In Experiments 6 and 8, other small aromatic VOCs were injected in addition to toluene. The OA formed in these experiments did not stand out in terms of its composition,



**Figure 6.** Bypass (blue) and thermodenuder (red) organic mass concentration time series for Expt. 7. The yellow shaded region denotes time when the UV lights were on. Temperatures represent the TD setpoint temperature. The bypass data have not been corrected for losses to the walls of the chamber. The TD measurements have not been corrected for losses in the TD.



**Figure 7.** Organic mass fraction remaining as a function of thermodenuder temperature at a residence time of 15 s (black) and 25 s (red) for Expt. 7. Thermograms have been corrected for TD losses.

volatility (Sect. 3.3) or hygroscopicity (Sect. 3.4). This suggests that other small aromatic VOCs behave similarly as toluene and that toluene can be used as a model system to study small aromatic VOCs.

### 3.2 High and low oxidation experiments – a case study

This section compares two seeded experiments (number 7 and 9, Table 1) and two unseeded experiments (number 2 and 4). The aim in the design of these experiments was to create different photochemical conditions. Therefore, fewer HONO injections were performed, more toluene was injected, fewer lights were used (resulting in lower UV intensity), and the irradiation period was shorter in Expt. 7 compared to Expt. 9 (10 min and 3 h, respectively). The decay of toluene, monitored by the PTR-MS, was used to estimate the OH exposure of the OA during irradiation. Total OH exposure during Expt. 7 was 7–8 times lower than during Expt. 9. Figure 4 shows the OA mass yields for experiments 7 and 9 as a function of the corrected OA concentration in the system; only the first irradiation period was used for Expt. 9 as uncertainties due

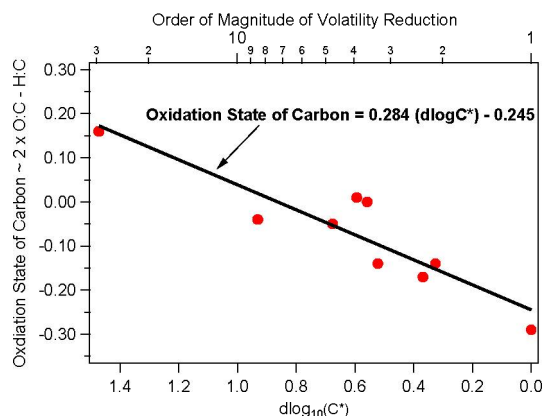


**Figure 8.** Oxidation state and volatility reduction in terms of change of  $\log C^*$  for the toluene SOA system. Red circles represent a single experiment and a single best-fit (black) line shows the trend.

to wall losses increase over the course of an experiment. The OA yields are higher for Expt. 9, which exhibited higher OH exposure. Considering only the first irradiation period, OH exposure in Expt. 9 was 5 times higher than in Expt. 7. The OA formed in Expt. 9 also exhibited significantly higher oxidation state ( $\sim 0$ , Table 2) than the OA formed in Expt. 7 ( $\sim -0.3$ ), and its volatility was approximately a factor of 7 lower than the volatility of the OA formed in Expt. 7 (Table 2).

Previous work has suggested that higher OH exposures help to reduce wall losses (Kroll et al., 2007); therefore, different oxidizing conditions could result in different wall-loss rates of semi-volatile vapors. As mentioned in Sect. 2.2.2 above, the changes observed in these experiments seem to be driven by chemical processes, not by the interactions with chamber walls. Thus, the higher oxidation state and lower volatility observed during Expt. 9 were likely a result of higher OH exposure.

The OA mass yields shown in Fig. 4 are lower than high- $\text{NO}_x$  OA mass yield measured in our previous study (Hildebrandt et al., 2009), likely due to different initial and oxidizing conditions. In the previous study the source of OH and  $\text{NO}_x$  was HOOH and NO, and all NO converted to  $\text{NO}_2$  within a few minutes of the start of photo-oxidation. In the present study the source of OH and  $\text{NO}_x$  was HONO, and both NO and  $\text{NO}_2$  were present throughout the experiments. Gas-phase chemistry is primarily affected by the level of NO, not total  $\text{NO}_x$ , and lower OA mass yields are expected under high NO, high  $\text{NO}_x$  conditions (present study) compared to high  $\text{NO}_x$ , low NO conditions (Hildebrandt et al., 2009).

Differences in the OA composition are also apparent when comparing the total OA to the denuded OA from these two experiments. Figure 5 (right panel) shows the difference in oxidation state of the denuded and the total OA at the different TD temperatures for Expt. 7 and 9. For the less oxidized, more volatile OA formed in Expt. 7, the oxidation state of

the denuded OA is higher than the oxidation state of the total OA, as expected when volatility correlates with oxidation state. The difference is larger at the higher TD temperatures when a larger fraction of the total OA has evaporated. However, for the more oxidized, less volatile OA formed in Expt. 9, the denuded OA has essentially the same oxidation state as the total OA at all TD temperatures. This is consistent with the OA being composed of molecules that have a similar oxidation state but different chain length, resulting in different volatilities. A similar observation was made when sampling highly oxygenated OA during ambient measurements in Finokalia, Greece, where the fraction of OA due to fragments of  $m/z$  44 was not significantly different for denuded and total OA (Hildebrandt et al., 2010).

A similar comparison can be made for two non-seeded experiments (number 2 and 4), which resulted in OA of different oxidation state and volatility (Table 2). Data from the PTR-MS were not available for this experiment; hence, OH exposure could not be estimated and OA mass yields could not be calculated, but it is likely that higher OH concentrations as well as lower OA concentrations in Expt. 2 resulted in the more oxidized, less volatile OA. The OA formed in Expt. 4 had similar oxidation state as the OA formed in Expt. 9 mentioned above ( $\sim 0$ ). The OA formed in Expt. 2 had the highest oxidation state of all OA analyzed here ( $\sim 0.16$ ), and its volatility was about a factor of 7 lower than the volatility of the OA formed in Expt. 4. The left panel of Fig. 5 shows the difference in oxidation state (denuded vs. total) as a function of TD temperature for Expts. 2 and 4. The OA formed in Expt. 4 exhibits similar behavior as the OA formed in Expt. 9, with very little difference between the oxidation state of denuded and total OA. The OA in Expt. 2 shows a higher oxidation state for denuded OA than for non-denuded OA. Thus, it appears that for OA of lower and higher bulk oxidation state, the oxidation state anti-correlates with volatility, shown here as a higher oxidation state of the denuded OA. For OA of intermediate oxidation state (around zero), the volatility of the OA does not correlate significantly with bulk oxidation state. The volatility and oxidation state of OA formed in all experiments is analyzed further below.

### 3.3 Volatility

Figure 6 shows mass concentration time series measured during Experiment 7 including both the bypass and TD measurements. This experiment produced the least oxidized and most volatile SOA and serves as the baseline for comparison of OA volatility in the other experiments. HONO was injected into the chamber and, at  $t = 0$ , the UV lights in the chamber (30 % of them) were turned on. The hydroxyl radical formed during the HONO photolysis began to react with toluene and the organic mass concentration increased due to the formation of SOA. The lights remained on for approximately 15 min and at that point the HONO photolysis was stopped by turning off the UV lights. The AMS then alter-

nated between the bypass line and thermodenuder (operating at different temperatures and residence times) to obtain the thermogram shown in Fig. 7. Half of the organic aerosol mass evaporated at 70 °C ( $T_{50}$  temperature). For this and all other experiments, the MFR was nearly the same after 15 and 25 s residence time in the thermodenuder.

The 15 and 25 s residence time data sets were independently modeled, resulting in two estimates of volatility reduction for each experiment. These were quite similar (Table 2) for all cases, suggesting that these measurements are consistent with the choice of a unity accommodation coefficient. The estimated relative volatility reductions relative to Experiment 7 for all experiments are presented in Table 2, and the experiment-specific model inputs (OA loading, particle mode diameter, and OA density) are presented in Table S2. Volatility was lower in other experiments by as much as a factor of 30, demonstrating that the OA formed under different oxidation conditions can have significantly different vapor pressure. A comparison of the modeled versus the measured MFRs is shown in Fig. S3.

Sensitivity runs were performed in order to examine the effects of the accommodation coefficient and enthalpy of vaporization parameters. In summary, the analysis revealed that changing the mass accommodation coefficients between 0.01, 0.1, and 1 for Expts. 7 and 9, which exhibited quite different experimental conditions, changes neither the relative volatility reduction nor the goodness of fit (represented by the sum of squared residuals, SSR) by more than 15 %. In addition, better least-squares fits are obtained for enthalpy of vaporization of 80 kJ mol<sup>-1</sup> (average SSR for all nine experiments,  $SSR_{\text{avg}} = 0.04$ ) than for enthalpy of vaporizations of 20 or 120 kJ mol<sup>-1</sup> ( $SSR_{\text{avg}} = 0.11$  and 0.09, respectively). Changing the enthalpy of vaporization does not change the trends in volatility reduction between experiments. More detailed results of the sensitivity study are presented in the supplementary material.

### Dependence of volatility on oxidation state

Differences in volatility of the toluene SOA in these experiments can be compared to its carbon oxidation state (Fig. 8). The change in volatility is expressed as the logarithm of the volatility reduction. This is consistent with the assumption of a constant volatility distribution shape shifting. Each data point represents a single experiment in terms of volatility reduction or the change in  $\log C^*$  and the corresponding  $OS_c$ . In general, the more oxidized organic aerosol is, the less volatile it is. This is consistent with functionalization reactions decreasing the volatility of the OA as it is oxidized. Using a least-squares fit, a straight line is fit to the data set giving a relation of  $(OS_c) = 0.284 (\Delta \log_{10} C^*) - 0.245$ . This suggests that an increase of the oxidation state by approximately 0.3 units corresponds to a reduction of the average volatility by an order of magnitude for the toluene SOA system examined here. However, as discussed in Sect. 3.2, the

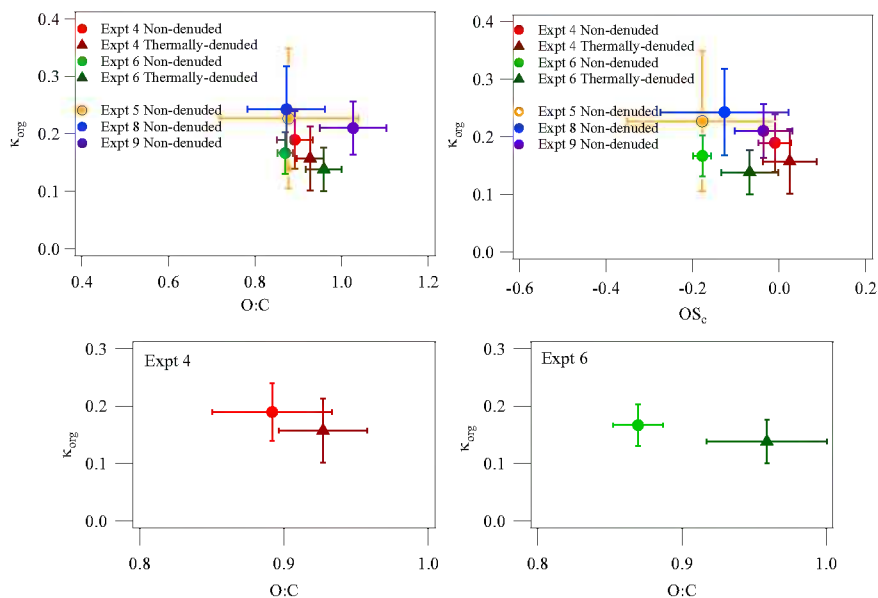


**Figure 9.**  $\kappa_{\text{org}}$  versus O : C (top, left) and  $\text{OS}_{\text{c}}$  (top, right) for all experiments as listed in Table 1. Also shown are magnified hygroscopicity and O : C for unseeded experiments with non-denuded and thermally denuded measurements (bottom). Vertical and horizontal error bars represent the standard deviation in  $\kappa_{\text{org}}$  and O : C or  $\text{OS}_{\text{c}}$ , respectively.

volatility of individual species composing the OA is not always correlated to their oxidation state.

### 3.4 Hygroscopicity

CCNc-derived organic hygroscopicity,  $\kappa_{\text{org}}$ , expressed as the average hygroscopicity of all measured sizes, versus the bulk O : C ratio and  $\text{OS}_{\text{c}}$  is shown in Fig. 9 for each experiment where CCNc data were available. Throughout all experiments,  $\kappa_{\text{org}}$  ranges from 0.10 to 0.25 while bulk O : C ranges from approximately 0.85 to 1.05. For each experiment, after the initial period of photo-oxidation,  $\kappa_{\text{org}}$  remains fairly constant, as does O : C. There is no clear correlation between  $\kappa_{\text{org}}$  and O : C (Fig. 9, top, left) or between  $\kappa_{\text{org}}$  and  $\text{OS}_{\text{c}}$  (Fig. 9, top, right) across all experimental conditions. This is counter to the conventional view that oxidative aging of aerosol generally increases its hygroscopicity (Jimenez et al., 2009).

When investigating  $\kappa_{\text{org}}$  for Expts. 4 and 6 where both non-denuded and thermally denuded measurements were collected, it appears that thermally denuded aerosol (combined measurements from 60, 80, and 100 °C) may show a slight decrease in  $\kappa_{\text{org}}$  with increased O : C (and  $\text{OS}_{\text{c}}$ ) (Fig. 9 bottom). While the change in  $\kappa_{\text{org}}$  as well as O : C and  $\text{OS}_{\text{c}}$  cannot be concluded with confidence due to the relatively large variation in  $\kappa_{\text{org}}$ , it is possible that this relationship between hygroscopicity and oxidation suggests that there may be another process, aside from bulk oxidation changes, causing changes in the measured hygroscopicity. Sareen et al. (2013) showed that gas-phase compounds such as methylglyoxal can act as surfactants, which depress surface tension and enhance CCN activity (and hygroscopicity). As methylglyoxal

as well as other gas-phase surface-active compounds such as benzaldehyde and glyoxal are known products of toluene oxidation by OH (Baltaretu et al., 2009), it is likely that gas-phase surfactants are present in these experiments. If surfactant films are present on the non-denuded aerosol, enhancing their hygroscopicity, then desorption of the surfactants later upon heating may increase surface tension and depress apparent hygroscopicity. A monolayer of surfactant adsorbed from the gas phase would induce a negligible impact on bulk O : C or  $\text{OS}_{\text{c}}$ . Thus, the volatility of OA would not necessarily correlate with its oxidation state if surfactants are present. Another potential explanation for the lack of a clear correlation between  $\kappa_{\text{org}}$  and  $\text{OS}_{\text{c}}$  is that the OA composition is dominated by compounds with similar  $\text{OS}_{\text{c}}$  but different size (e.g., oligomers), as the size of molecules affects their solubility and therefore their hygroscopicity.

## 4 Conclusions

Photochemical aging clearly influences anthropogenic SOA, and the general trend toward increased SOA mass and reduced volatility is consistent with progressive oxidation driving organic aerosol toward the highly oxidized, low-volatility endpoint observed around the world. There is a strong relationship between exposure to OH and physicochemical properties for SOA formed from the oxidation of toluene and other small aromatic VOCs. Organic nitrogen compounds are a major constituent in the SOA formed. An experiment with higher OH exposure showed higher SOA mass yields, more oxidized SOA, and reduced SOA volatility but only

modest differences in hygroscopicity. Volatility varied by a factor of 30 for different OH exposure, and a 10-fold decrease in volatility was associated with a 0.3 increase in carbon oxidation state. The SOA was relatively hygroscopic for organic material, with  $0.1 < \kappa < 0.2$  and if anything, a slightly negative relationship between kappa and oxidation state was observed, suggesting a possible role for surfactants or oligomeric compounds. The relationship between hygroscopicity, oxidation state, and volatility may be modulated by gas-phase compounds.

While individual experiments with different OH exposure showed clear aging effects as different oxidation states and OA volatility, these effects were not evident within every single experiment. This suggests that a complex interplay exists between gas-phase processes, including oxidation reactions that both functionalize and fragment condensable organic species as well as photolysis of some species. The composition, hygroscopicity, and volatility of organic aerosol do not always follow a prescribed relationship, highlighting the need for future laboratory experiments and ambient measurements which evaluate all of these properties.

**The Supplement related to this article is available online at doi:10.5194/acp-15-8301-2015-supplement.**

*Acknowledgements.* This work was supported by the EPA STAR program (grant RD-835405) and the Department of Energy Atmospheric Science Research Program (ASR grant DESC0007075). The high-resolution AMS was purchased with funds from NSF Major Research Instrumentation (CBET0922643) and the Wallace Research Foundation.

Edited by: A. Laskin

## References

- Alfarra, M. R., Good, N., Wyche, K. P., Hamilton, J. F., Monks, P. S., Lewis, A. C., and McFiggans, G.: Water uptake is independent of the inferred composition of secondary aerosols derived from multiple biogenic VOCs, *Atmos. Chem. Phys.*, 13, 11769–11789, doi:10.5194/acp-13-11769-2013, 2013.
- Allan, J. D., Delia, A. E., Coe, H., Bower, K. N., Alfarra, M. R., Jimenez, J. L., Middlebrook, A. M., Drewnick, F., Onasch, T. B., Canagaratna, M. R., Jayne, J. T., and Worsnop, D. R.: A generalised method for the extraction of chemically resolved mass spectra from Aerodyne aerosol mass spectrometer data, *J. Aerosol Sci.*, 35, 909–922, doi:10.1016/j.jaerosci.2004.02.007, 2004.
- Asa-Awuku, A., Engelhart, G. J., Lee, B. H., Pandis, S. N., and Nenes, A.: Relating CCN activity, volatility, and droplet growth kinetics of  $\beta$ -caryophyllene secondary organic aerosol, *Atmos. Chem. Phys.*, 9, 795–812, doi:10.5194/acp-9-795-2009, 2009.
- Baltaretu, C. O., Lichtman, E. I., Hadler, A. B., and Elrod, M. J.: Primary atmospheric oxidation mechanism for toluene., *J. Phys. Chem. A*, 113, 221–30, doi:10.1021/jp806841t, 2009.
- Burtscher, H., Baltensperger, U., Bukowiecki, N., Cohn, P., Hüglin, C., Mohr, M., Matter, U., Nyeki, S., Schmatloch, V., Streit, N., and Weingartner, E.: Separation of volatile and non-volatile aerosol fractions by thermodesorption: Instrumental development and applications, *J. Aerosol Sci.*, 32, 427–442, doi:10.1016/S0021-8502(00)00089-6, 2001.
- Canagaratna, M. R., Jimenez, J. L., Kroll, J. H., Chen, Q., Kessler, S. H., Massoli, P., Hildebrandt Ruiz, L., Fortner, E., Williams, L. R., Wilson, K. R., Surratt, J. D., Donahue, N. M., Jayne, J. T., and Worsnop, D. R.: Elemental ratio measurements of organic compounds using aerosol mass spectrometry: characterization, improved calibration, and implications, *Atmos. Chem. Phys.*, 15, 253–272, doi:10.5194/acp-15-253-2015, 2015.
- Cappa, C. D. and Wilson, K. R.: Multi-generation gas-phase oxidation, equilibrium partitioning, and the formation and evolution of secondary organic aerosol, *Atmos. Chem. Phys.*, 12, 9505–9528, doi:10.5194/acp-12-9505-2012, 2012.
- Cerully, K. M., Bougiatioti, A., Hite Jr., J. R., Guo, H., Xu, L., Ng, N. L., Weber, R., and Nenes, A.: On the link between hygroscopicity, volatility, and oxidation state of ambient and water-soluble aerosol in the Southeastern United States, *Atmos. Chem. Phys. Discuss.*, 14, 30835–30877, doi:10.5194/acpd-14-30835-2014, 2014.
- Chang, R. Y.-W., Slowik, J. G., Shantz, N. C., Vlasenko, A., Liggio, J., Sjostedt, S. J., Leaitch, W. R., and Abbatt, J. P. D.: The hygroscopicity parameter ( $\kappa$ ) of ambient organic aerosol at a field site subject to biogenic and anthropogenic influences: relationship to degree of aerosol oxidation, *Atmos. Chem. Phys.*, 10, 5047–5064, doi:10.5194/acp-10-5047-2010, 2010.
- DeCarlo, P. F., Kimmel, J. R., Trimborn, A. M., Northway, M. J., Jayne, J. T., Aiken, A. C., Gonin, M., Fuhrer, K., Horvath, T., Docherty, K. S., Worsnop, D. R., and Jimenez, J. L.: Field-Deployable, High-Resolution, Time-of-Flight Aerosol Mass Spectrometer, *Anal. Chem.*, 78, 8281–8289, 2006.
- De Gouw, J. A., Goldan, P. D., Warneke, C., Kuster, W. C., Roberts, J. M., Marchewka, M., Bertman, S. B., Pszenny, A. A. P., and Keene, W. C.: Validation of proton transfer reaction-mass spectrometry (PTR-MS) measurements of gas-phase organic compounds in the atmosphere during the New England Air Quality Study (NEAQS) in 2002, *J. Geophys. Res.*, 108, 4682, doi:10.1029/2003JD003863, 2003.
- Donahue, N. M., Robinson, A. L., Stanier, C. O., and Pandis, S. N.: Coupled Partitioning, Dilution, and Chemical Aging of Semivolatile Organics, *Environ. Sci. Technol.*, 40, 2635–2643, doi:10.1021/es052297c, 2006.
- Donahue, N. M., Robinson, A. L., and Pandis, S. N.: Atmospheric organic particulate matter: From smoke to secondary organic aerosol, *Atmos. Environ.*, 43, 94–106, 2009.
- Donahue, N. M., Kroll, J. H., Pandis, S. N., and Robinson, A. L.: A two-dimensional volatility basis set – Part 2: Diagnostics of organic-aerosol evolution, *Atmos. Chem. Phys.*, 12, 615–634, doi:10.5194/acp-12-615-2012, 2012.
- Frosch, M., Bilde, M., DeCarlo, P. F., Juranyi, Z., Tritscher, T., Dommen, J., Donahue, N. M., Gysel, M., Weingartner, E., and Baltensperger, U.: Relating cloud condensation nuclei activity

- and oxidation level of  $\alpha$ -pinene secondary organic aerosols, *J. Geophys. Res.*, 116, D22212, doi:10.1029/2011JD016401, 2011.
- Fry, J. L., Kiendler-Scharr, A., Rollins, A. W., Wooldridge, P. J., Brown, S. S., Fuchs, H., Dubé, W., Mensah, A., dal Maso, M., Tillmann, R., Dorn, H.-P., Brauers, T., and Cohen, R. C.: Organic nitrate and secondary organic aerosol yield from  $\text{NO}_3$  oxidation of  $\beta$ -pinene evaluated using a gas-phase kinetics/aerosol partitioning model, *Atmos. Chem. Phys.*, 9, 1431–1449, doi:10.5194/acp-9-1431-2009, 2009.
- Hallquist, M., Wenger, J. C., Baltensperger, U., Rudich, Y., Simpson, D., Claeys, M., Dommen, J., Donahue, N. M., George, C., Goldstein, A. H., Hamilton, J. F., Herrmann, H., Hoffmann, T., Iinuma, Y., Jang, M., Jenkin, M. E., Jimenez, J. L., Kiendler-Scharr, A., Maenhaut, W., McFiggans, G., Mentel, Th. F., Monod, A., Prévôt, A. S. H., Seinfeld, J. H., Surratt, J. D., Szmigielski, R., and Wildt, J.: The formation, properties and impact of secondary organic aerosol: current and emerging issues, *Atmos. Chem. Phys.*, 9, 5155–5236, doi:10.5194/acp-9-5155-2009, 2009.
- Heald, C. L., Jacob, D. J., Park, R. J., Russell, L. M., Huebert, B. J., Seinfeld, J. H., Liao, H., and Weber, R. J.: A large organic aerosol source in the free troposphere missing from current models, *Geophys. Res. Lett.*, 3, L18809, doi:10.1029/2005GL023831, 2005.
- Hildebrandt, L., Donahue, N. M., and Pandis, S. N.: High formation of secondary organic aerosol from the photo-oxidation of toluene, *Atmos. Chem. Phys.*, 9, 2973–2986, doi:10.5194/acp-9-2973-2009, 2009.
- Hildebrandt, L., Kostenidou, E., Mihalopoulos, N., Worsnop, D. R., Donahue, N. M., and Pandis, S. N.: Formation of highly oxygenated organic aerosol in the atmosphere: Insights from the Finokalia Aerosol Measurement Experiments, *Geophys. Res. Lett.*, 37, L23801, doi:10.1029/2010GL045193, 2010.
- Hildebrandt, L., Henry, K., Kroll, J. H., Pandis, S. N., and Donahue, N. M.: Evaluating the Mixing of Organic Aerosol Components using High-Resolution Aerosol Mass Spectrometry, *Environ. Sci. Technol.*, 45, 6329–6335, doi:10.1021/es200825g, 2011.
- Jimenez, J. L., Canagaratna, M. R., Donahue, N. M., Prevot, A. S. H., Zhang, Q., Kroll, J. H., DeCarlo, P. F., Allan, J. D., Coe, H., Ng, N. L., Aiken, A. C., Docherty, K. S., Ulbrich, I. M., Grieshop, P., Robinson, A. L., Duplissy, J., Smith, J. D., Wilson, K. R., Lanz, V. a, Hueglin, C., Sun, Y. L., Tian, J., Laaksonen, A., Raatikainen, T., Rautiainen, J., Vaattovaara, P., Ehn, M., Kulmala, M., Tomlinson, J. M., Collins, D. R., Cubison, M. J., Dunlea, E. J., Huffman, J. A., Onasch, T. B., Alfarra, M. R., Williams, P. I., Bower, K., Kondo, Y., Schneider, J., Drewnick, F., Borrmann, S., Weimer, S., Demerjian, K., Salcedo, D., Cottrell, L., Griffin, R., Takami, A., Miyoshi, T., Hatakeyama, S., Shimono, a, Sun, J. Y., Zhang, Y. M., Dzepina, K., Kimmel, J. R., Sueper, D., Jayne, J. T., Herndon, S. C., Trimborn, A. M., Williams, L. R., Wood, E. C., Middlebrook, A. M., Kolb, C. E., Baltensperger, U., and Worsnop, D. R.: Evolution of organic aerosols in the atmosphere., *Science*, 326, 1525–1529, doi:10.1126/science.1180353, 2009.
- Kanakidou, M., Seinfeld, J. H., Pandis, S. N., Barnes, I., Dentener, F. J., Facchini, M. C., Van Dingenen, R., Ervens, B., Nenes, A., Nielsen, C. J., Swietlicki, E., Putaud, J. P., Balkanski, Y., Fuzzi, S., Horth, J., Moortgat, G. K., Winterhalter, R., Myhre, C. E. L., Tsigaridis, K., Vignati, E., Stephanou, E. G., and Wilson, J.: Organic aerosol and global climate modelling: a review, *Atmos. Chem. Phys.*, 5, 1053–1123, doi:10.5194/acp-5-1053-2005, 2005.
- Kostenidou, E., Pathak, R. K., and Pandis, S. N.: An Algorithm for the Calculation of Secondary Organic Aerosol Density Combining AMS and SMPS Data, *Aerosol Sci. Technol.*, 41, 1002–1010, doi:10.1080/02786820701666270, 2007.
- Kroll, J. H., Chan, A. W. H., Ng, N. L., Flagan, R. C., and Seinfeld, J. H.: Reactions of Semivolatile Organics and their effects on Secondary Organic Aerosol Formation, *Environ. Sci. Technol.*, 41, 3545–3550, doi:10.1021/es062059x, 2007.
- Kroll, J. H. and Seinfeld, J. H.: Chemistry of secondary organic aerosol: Formation and evolution of low-volatility organics in the atmosphere, *Atmos. Environ.*, 42, 3593–3624, doi:10.1016/j.atmosenv.2008.01.003, 2008.
- Kroll, J. H., Smith, J. D., Che, D. L., Kessler, S. H., Worsnop, D. R., and Wilson, K. R.: Measurement of fragmentation and functionalization pathways in the heterogeneous oxidation of oxidized organic aerosol, *Phys. Chem. Chem. Phys.*, 11, 8005–8014, 2009.
- Kroll, J. H., Donahue, N. M., Jimenez, J. L., Kessler, S. H., Canagaratna, M. R., Wilson, K. R., Altieri, K. E., Mazzoleni, L. R., Wozniak, A. S., Bluhm, H., Mysak, E. R., Smith, J. D., Kolb, C. E., and Worsnop, D. R.: Carbon oxidation state as a metric for describing the chemistry of atmospheric organic aerosol, *Nat. Chem.*, 3, 133–139, doi:10.1038/nchem.948, 2011.
- Latham, T. L., Beyersdorf, A. J., Thornhill, K. L., Winstead, E. L., Cubison, M. J., Hecobian, A., Jimenez, J. L., Weber, R. J., Anderson, B. E., and Nenes, A.: Analysis of CCN activity of Arctic aerosol and Canadian biomass burning during summer 2008, *Atmos. Chem. Phys.*, 13, 2735–2756, doi:10.5194/acp-13-2735-2013, 2013.
- Lee, B.-H. and Pandis, S. N.: Volatility of atmospheric organic aerosol, Carnegie Mellon University, Pittsburgh, 2010.
- Lee, B. H., Kostenidou, E., Hildebrandt, L., Riipinen, I., Engelhart, G. J., Mohr, C., DeCarlo, P. F., Mihalopoulos, N., Prevot, A. S. H., Baltensperger, U., and Pandis, S. N.: Measurement of the ambient organic aerosol volatility distribution: application during the Finokalia Aerosol Measurement Experiment (FAME-2008), *Atmos. Chem. Phys.*, 10, 12149–12160, doi:10.5194/acp-10-12149-2010, 2010.
- Massoli, P., Lambe, A. T., Ahern, A. T., Williams, L. R., Ehn, M., Mikkilä, J., Canagaratna, M. R., Brune, W. H., Onasch, T. B., Jayne, J. T., Petäjä, T., Kulmala, M., Laaksonen, A., Kolb, C. E., Davidovits, P., and Worsnop, D. R.: Relationship between aerosol oxidation level and hygroscopic properties of laboratory generated secondary organic aerosol (SOA) particles, *Geophys. Res. Lett.*, 37, L24801, doi:10.1029/2010GL045258, 2010.
- Matsunaga, A. and Ziemann, P. J.: Gas-Wall Partitioning of Organic Compounds in a Teflon Film Chamber and Potential Effects on Reaction Product and Aerosol Yield Measurements, *Aerosol Sci. Technol.*, 44, 881–892, doi:10.1080/02786826.2010.501044, 2010.
- Meyer, N. K., Duplissy, J., Gysel, M., Metzger, A., Dommen, J., Weingartner, E., Alfarra, M. R., Prevot, A. S. H., Fletcher, C., Good, N., McFiggans, G., Jonsson, Å. M., Hallquist, M., Baltensperger, U., and Ristovski, Z. D.: Analysis of the hygroscopic and volatile properties of ammonium sulphate seeded and unseeded SOA particles, *Atmos. Chem. Phys.*, 9, 721–732, doi:10.5194/acp-9-721-2009, 2009.

- Moore, R. H., Nenes, A., and Medina, J.: Scanning Mobility CCN Analysis – A Method for Fast Measurements of Size-Resolved CCN Distributions and Activation Kinetics, *Aerosol Sci. Technol.*, 44, 861–871, doi:10.1080/02786826.2010.498715, 2010.
- Pandis, S. N., Harley, R. A., Cass, G. R., and Seinfeld, J. H.: Secondary Organic Aerosol Formation And Transport, *Atmos. Environ. Pt. A*, 26, 2269–2282, doi:10.1016/0960-1686(92)90358-R, 1992.
- Petters, M. D. and Kreidenweis, S. M.: A single parameter representation of hygroscopic growth and cloud condensation nucleus activity, *Atmos. Chem. Phys.*, 7, 1961–1971, doi:10.5194/acp-7-1961-2007, 2007.
- Poulain, L., Wu, Z., Petters, M. D., Wex, H., Hallbauer, E., Wehner, B., Massling, A., Kreidenweis, S. M., and Stratmann, F.: Towards closing the gap between hygroscopic growth and CCN activation for secondary organic aerosols – Part 3: Influence of the chemical composition on the hygroscopic properties and volatile fractions of aerosols, *Atmos. Chem. Phys.*, 10, 3775–3785, doi:10.5194/acp-10-3775-2010, 2010.
- Riipinen, I., Pierce, J. R., Donahue, N. M., and Pandis, S. N.: Equilibration time scales of organic aerosol inside thermodenuders: Evaporation kinetics versus thermodynamics, *Atmos. Environ.*, 44, 597–607, doi:10.1016/j.atmosenv.2009.11.022, 2010.
- Sareen, N., Schwier, A. N., Latham, T. L., Nenes, A., and McNeill, V. F.: Surfactants from the gas phase may promote cloud droplet formation., *Proc. Natl. Acad. Sci. USA*, 110, 2723–2728, doi:10.1073/pnas.1204838110, 2013.
- Shrivastava, M. K., Zelenyuk, A., Imre, D., Easter, R. C., Beranek, J., Zaveri, R. A., and Fast, J. D.: Implications of low volatility SOA and gas-phase fragmentation reactions on SOA loadings and their spatial and temporal evolution in the atmosphere, *J. Geophys. Res. Atmos.*, 118, 3328–3342, doi:10.1002/jgrd.50160, 2013.
- Surratt, J. D., Murphy, S. M., Kroll, J. H., Ng, N. L., Hildebrandt, L., Sorooshian, A., Szmigielski, R., Vermeylen, R., Maenhaut, W., Claeys, M., Flagan, R. C., and Seinfeld, J. H.: Chemical Composition of Secondary Organic Aerosol Formed from the Photooxidation of Isoprene, *J. Phys. Chem. A*, 110, 9665–9690, 2006.
- Tritscher, T., Dommen, J., DeCarlo, P. F., Gysel, M., Barmet, P. B., Praplan, A. P., Weingartner, E., Prévôt, A. S. H., Riipinen, I., Donahue, N. M., and Baltensperger, U.: Volatility and hygroscopicity of aging secondary organic aerosol in a smog chamber, *Atmos. Chem. Phys.*, 11, 11477–11496, doi:10.5194/acp-11-11477-2011, 2011.
- Volkamer, R., Jimenez, J. L., San Martini, F., Dzepina, K., Zhang, Q., Salcedo, D., Molina, L. T., Worsnop, D. R., and Molina, M. J.: Secondary organic aerosol formation from anthropogenic air pollution: Rapid and higher than expected, *Geophys. Res. Lett.*, 33, L17811, doi:10.1029/2006GL026899, 2006.
- Vutukuru, S., Griffin, R. J., and Dabdub, D.: Simulation and analysis of secondary organic aerosol dynamics in the South Coast Air Basin of California, *J. Geophys. Res.*, 111, D10S12, doi:10.1029/2005JD006139, 2006.
- Zhang, Q., Jimenez, J. L., Canagaratna, M. R., Allan, J. D., Coe, H., Ulbrich, I., Alfarra, M. R., Takami, A., Middlebrook, A. M., Sun, Y. L., Dzepina, K., Dunlea, E., Docherty, K., DeCarlo, P. F., Salcedo, D., Onasch, T., Jayne, J. T., Miyoshi, T., Shimojo, A., Hatakeyama, S., Takegawa, N., Kondo, Y., Schneider, J., Drewnick, F., Borrmann, S., Weimer, S., Demerjian, K., Williams, P., Bower, K., Bahreini, R., Cottrell, L., Griffin, R. J., Rautiainen, J., Sun, J. Y., Zhang, Y. M., and Worsnop, D. R.: Ubiquity and dominance of oxygenated species in organic aerosols in anthropogenically-influenced Northern Hemisphere midlatitudes, *Geophys. Res. Lett.*, 34, L13801, doi:10.1029/2007gl029979, 2007.

# Brownness of organics in aerosols from biomass burning linked to their black carbon content

Rawad Saleh<sup>1</sup>, Ellis S. Robinson<sup>1</sup>, Daniel S. Tkacik<sup>1</sup>, Adam T. Ahern<sup>1</sup>, Shang Liu<sup>2</sup>, Allison C. Aiken<sup>2</sup>, Ryan C. Sullivan<sup>1</sup>, Albert A. Presto<sup>1</sup>, Manvendra K. Dubey<sup>2</sup>, Robert J. Yokelson<sup>3</sup>, Neil M. Donahue<sup>1</sup> and Allen L. Robinson<sup>1\*</sup>

**Atmospheric particulate matter plays an important role in the Earth's radiative balance. Over the past two decades, it has been established that a portion of particulate matter, black carbon, absorbs significant amounts of light and exerts a warming effect rivaling that of anthropogenic carbon dioxide<sup>1,2</sup>. Most climate models treat black carbon as the sole light-absorbing carbonaceous particulate. However, some organic aerosols, dubbed brown carbon and mainly associated with biomass burning emissions<sup>3–6</sup>, also absorb light<sup>7</sup>. Unlike black carbon, whose light absorption properties are well understood<sup>8</sup>, brown carbon comprises a wide range of poorly characterized compounds that exhibit highly variable absorptivities, with reported values spanning two orders of magnitude<sup>3–6,9,10</sup>. Here we present smog chamber experiments to characterize the effective absorptivity of organic aerosol from biomass burning under a range of conditions. We show that brown carbon in emissions from biomass burning is associated mostly with organic compounds of extremely low volatility<sup>11</sup>. In addition, we find that the effective absorptivity of organic aerosol in biomass burning emissions can be parameterized as a function of the ratio of black carbon to organic aerosol, indicating that aerosol absorptivity depends largely on burn conditions, not fuel type. We conclude that brown carbon from biomass burning can be an important factor in aerosol radiative forcing.**

Black carbon (BC) in atmospheric particulate matter is an important global warming agent (potentially second only to CO<sub>2</sub>) with estimates of its direct radiative forcing (DRF) ranging between 0.17 and 1.48 W m<sup>-2</sup> (ref. 2). The large uncertainty in BC DRF stems partly from the mismatch between BC light absorption (hence its DRF) estimated by climate models and that retrieved using remote sensing, with models usually reporting smaller values<sup>2</sup>. Open biomass burning contributes one-third of the global BC budget. Biomass burning is also a major source of organic aerosol (OA), contributing two-thirds of the global primary OA budget<sup>2,12</sup>, which most climate models treat as purely scattering. The cooling due to this scattering offsets the warming by BC from biomass burning, resulting in negative net DRF for biomass burning emissions<sup>13</sup>. However, there is a growing body of evidence that biomass burning OA contains substantial amounts of light-absorbing brown carbon<sup>3–6</sup> (BrC), which can shift the net biomass burning DRF to positive values<sup>14</sup>. Neglecting absorption by biomass burning OA might lead to misattribution of observed atmospheric particulate matter absorption to BC, contributing to the discrepancy between models and observations. There are

substantial uncertainties in quantifying the effect of BrC. A major obstacle is the very high variability in reported light absorption properties of biomass burning OA, often attributed to fuel type and burn conditions<sup>4,6</sup>, which complicates their treatment in climate models.

In this study, we show that the least volatile fraction (extremely low-volatility organic compounds, ELVOC, defined in the volatility basis set<sup>11</sup> to have saturation concentration  $<3 \times 10^{-4} \mu\text{g m}^{-3}$ ) of biomass burning OA emitted during the Fire Laboratory at Missoula Campaign (FLAME 4) exhibits substantially larger light absorption efficiency than the low-volatility (LVOC) and semi-volatile (SVOC) organic fractions. We parameterize the effective OA absorptivity (the imaginary part of the refractive index  $k_{\text{OA}}$ ) across a diverse set of fuel types and burn conditions using the BC-to-OA ratio of the emissions, which is a measure of the combustion conditions. The  $k_{\text{OA}}$  values derived here can be used in Mie theory calculations to quantify light absorption by biomass burning OA. As the BC-to-OA ratio is tracked in emission inventories<sup>2,15</sup>, our parameterization for biomass  $k_{\text{OA}}$  can be implemented in current large-scale chemical transport and climate models, provided our findings extend to open burning in general beyond FLAME 4.

We conducted experiments to characterize the effective  $k_{\text{OA}}$  in emissions of globally important fuels (Supplementary Section 1). The experiments spanned a broad range of burn conditions, OA loadings and chemical ageing processes (Supplementary Table 1). Dilute emissions were characterized and chemically aged in a smog chamber, replicating plume- and ambient-like conditions.

We performed optical closure, which combines real-time observations of size distributions and optical properties with Mie theory calculations, to retrieve the effective  $k_{\text{OA}}$  (ref. 6). Mie theory is widely used to model light absorption/scattering by atmospheric aerosols<sup>16</sup>, and analyse experimental data and field measurements<sup>5,17</sup>. These calculations often assume a spherical core-shell morphology, which is clearly an approximation given the complex mixing state (fraction of OA internally mixed with BC, that is, exists with BC in the same particles) and morphology of BC and OA particles, which is under debate<sup>5,17–19</sup>. If the OA exist as a coating over the BC, it can enhance BC absorption by refracting light into the BC core (lensing<sup>20,21</sup>). In this study, we retrieve  $k_{\text{OA}}$  using two limiting cases: (1) BC and OA are completely externally mixed (they exist in different particles); and (2) a fraction of the OA is internally mixed with and exists as a coating over the BC, with maximum possible coating thickness (Supplementary Section 2). We note that from a light-absorption perspective, case (1) also corresponds to

<sup>1</sup>Center for Atmospheric Particle Studies, Carnegie Mellon University, Pittsburgh, Pennsylvania 15213, USA, <sup>2</sup>Earth and Environmental Sciences, Los Alamos National Laboratory, Los Alamos, New Mexico 87545, USA, <sup>3</sup>Department of Chemistry, University of Montana, Missoula, Montana 59812, USA. \*e-mail: alr@andrew.cmu.edu

BC and OA being internally mixed, but BC residing on the edge of the particle rather than being coated by OA (ref. 18). For the conditions of our experiments, and biomass burning emissions in general, we expect case (2) to better approximate the mixing state and morphology of BC and OA. BC particles form initially during combustion, and as the emissions temperature drops, organic vapours hit supersaturation and are forced by the second law of thermodynamics to condense (form OA). The BC particles provide surface area that facilitates condensation; thus, whenever condensable organic molecules encounter BC particles, they would prefer to condense on them rather than form new (externally mixed) particles by nucleation. Given the large OA loadings in most of the experiments (Supplementary Table 1), we expect OA to form relatively thick coatings over BC.

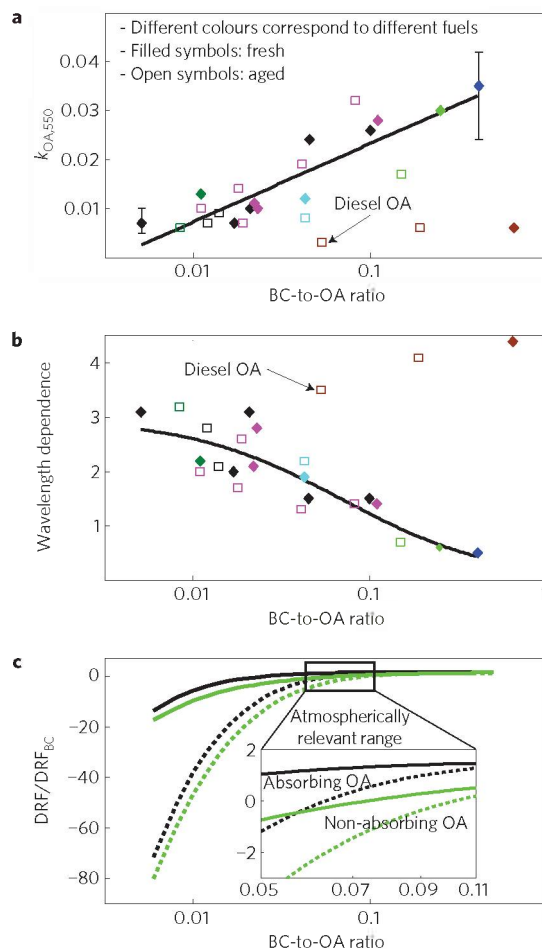
As described in Supplementary Section 3, the internally mixed case (case 2) yields smaller  $k_{\text{OA}}$  values than the externally mixed case (case 1). However, the main conclusions of this work (summarized in Figs 1 and 2 for the internally mixed case and Supplementary Figs 1 and 2 for the externally mixed case), discussed below, hold for both cases. Furthermore, owing to uncertainty in BC mass concentration measurements, the analysis presented here is based on the limiting case of maximum possible BC concentration, which corresponds to a lower limit on the derived  $k_{\text{OA}}$  values (see Supplementary Section 3 for details). Thus,  $k_{\text{OA}}$  values presented in this study should be viewed as lower bound values.

Figure 1a,b shows the effective absorptivity at wavelength ( $\lambda$ ) of 550 nm ( $k_{\text{OA},550}$ ) and the wavelength dependence of  $k_{\text{OA}}$  ( $w$ ; where  $k_{\text{OA}} = k_{\text{OA},550} \times (550/\lambda)^w$ ) as a function of BC-to-OA ratio of the emissions. The wavelength dependence of absorption is often described using the absorption Ångström exponent (AAE). For small particles ( $<50$  nm) in the visible spectrum  $\text{AAE} = w + 1$ . For example, the imaginary part of the refractive index of BC is wavelength independent in the visible spectrum<sup>8</sup> ( $w = 0$ ), and  $\text{AAE} \cong 1$ . The  $k_{\text{OA}}$  values reported here are the absorptivity of OA alone, excluding the contribution from BC.

Figure 1a,b indicates that, regardless of fuel type,  $k_{\text{OA},550}$  increases with the BC-to-OA ratio, whereas  $w$  is inversely proportional to BC-to-OA ratio. Therefore,  $k_{\text{OA}}$  depends strongly on burn conditions, which, to a large extent, dictate the BC-to-OA ratio. As evident from the multiple experiments for black spruce and ponderosa pine, the OA emitted by the same fuel had different  $k_{\text{OA}}$  when the BC-to-OA ratios were different. Thus, biomass fuel type had no discernible effect on  $k_{\text{OA}}$  beyond the BC-to-OA ratio. We note that although  $k_{\text{OA}}$  depends on BC-to-OA ratio and not fuel type, certain fuels often exhibit characteristic BC-to-OA ratios. For example, grass fires, which tended to be flaming, had larger BC-to-OA ratios than boreal fires, which tended to be more smoldering<sup>22</sup>.

The BC-to-OA ratio also depends, although to a lesser extent, on OA loading and secondary OA (SOA) formation. Both phenomena affect  $k_{\text{OA}}$  in a fashion consistent with the trend shown in Fig. 1. As the OA loading increases, the BC-to-OA ratio decreases because more SVOCs partition to the condensed phase<sup>23</sup>, thus reducing the effective  $k_{\text{OA},550}$  (Supplementary Fig. 3). SOA formation has a similar effect because it reduces the BC-to-OA ratio. SOA is less absorptive than primary OA, but has a stronger wavelength dependence<sup>6</sup>, potentially decreasing  $k_{\text{OA},550}$  and increasing  $w$ . This is not clearly observed in some of the experiments because the effect of SOA addition is comparable to measurement uncertainties, but the aged aerosol still falls on the same trend as the fresh aerosol, as shown in Fig. 1a,b.

The observed dependence of  $k_{\text{OA}}$  on BC-to-OA ratio seems to apply solely to biomass burning OA. In Fig. 1a,b, we also plot data for diesel engine emissions. For similar BC-to-OA ratios, diesel  $k_{\text{OA}}$  values are several-fold smaller than biomass burning values. There is no relationship between the diesel  $k_{\text{OA}}$  and the BC-to-OA ratio. This demonstrates that the dependence of  $k_{\text{OA}}$  on BC-to-OA



**Figure 1 | Dependence of  $k_{\text{OA}}$  and DRF on BC-to-OA ratio.** a, b, Filled diamonds and open squares correspond to fresh and chemically aged emissions, respectively. Colours correspond to different fuels: black, black spruce; magenta, ponderosa pine; cyan, rice straw; forest green, organic hay; light green, saw grass; blue, wire grass; and brown, diesel. Whiskers represent upper and lower bounds (Supplementary Section 3). Black lines are least-squares fits to the biomass burning data:  $y = 0.016x + 0.03925$ ,  $R$ -square = 0.734, for  $k_{\text{OA},550\text{nm}}$  versus  $\log_{10}(\text{BC-to-OA ratio})$ , a and  $y = 0.2081/(x + 0.0699)$ ,  $R$ -square = 0.738, for  $w$  versus BC-to-OA ratio, b. c, Ratio of DRF of biomass burning emissions to DRF of biomass burning BC alone. Black lines use  $k_{\text{OA}}$  values obtained in this study. Green lines assume non-absorbing OA ( $k_{\text{OA}} = 0$ ). Solid lines: coating thickness was held constant, and the concentration of externally mixed OA varied in the BC-to-OA ratio space; dotted lines: the fractions of internally and externally mixed OA were held constant at 50%, while the coating thickness varied (see Supplementary Section 7 for details).

ratio for biomass burning emissions is not an artefact of the optical closure analysis.

We performed thermodenuder measurements in a subset of the experiments (Supplementary Table 2) to characterize  $k_{\text{OA}}$  as a function of volatility. Heating at 250 °C stripped LVOCs and SVOCs (77–91% of original particulate matter mass) from the particles, leaving BC (1–10% of original particulate matter mass) and ELVOCs (7–14% of original particulate matter mass). As shown in Fig. 2b,  $k_{\text{OA}}$  values of the ELVOCs (retrieved from the heated measurements) are an order of magnitude larger than the  $k_{\text{OA}}$  values of the total OA (retrieved from the non-heated measurements). This indicates that almost all of the OA absorption was associated with ELVOCs.

The dependence of  $k_{\text{OA}}$  on BC-to-OA ratio supports the conclusion that ELVOCs are an order of magnitude more absorptive

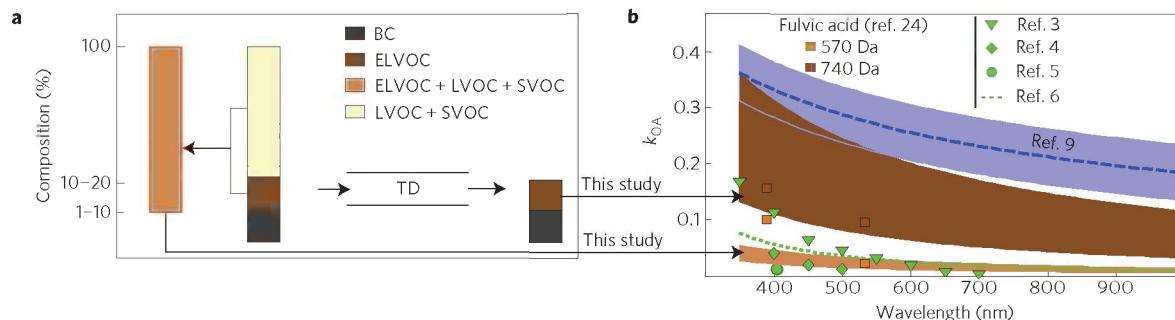


**Figure 2 | Contribution of different OA components to light absorption.** **a**, Composition of the condensed-phase emissions in the experiments that involved heating in the thermodenuder (TD). **b**, The range of  $k_{OA}$  as a function of wavelength for the total OA (light brown shade) and ELVOCs (dark brown shade). Green dotted line and symbols correspond to  $k_{OA}$  values reported in the literature for biomass burning emissions excluding those of ref. 9 (dashed blue line; the blue shaded area is the uncertainty bound). Light and dark brown squares correspond to bulk (nominal molecular mass of 570 Da) and the fraction with largest molecular mass (740 Da) of fulvic acid<sup>24</sup>.

than the total OA (ELVOCs + LVOCs + SVOCs). We propose a mechanism in which the conditions leading to BC formation (an oxygen-deprived, fuel-rich flame) are also conducive to formation of large organic compounds that have very low volatility and are highly absorbing. Consequently, the higher the BC content of the emissions, the larger is the effective OA absorptivity. As this dependence is not observed in diesel emissions (Fig. 1), clearly, fuel composition (a mixture of liquid hydrocarbons in diesel versus large polymers in biomass) and combustion conditions (high pressure in diesel engine versus heat breaking down the solid fuel at atmospheric pressure in biomass burning) are important factors. The dependence of absorptivity on volatility observed here is consistent with the work of a previous study<sup>24</sup>, which found that the absorptivity of fulvic acid components increased with increasing molecular weight, hence decreasing volatility (Fig. 2b).

ELVOCs having  $k_{OA}$  an order of magnitude larger than the total OA explains the seemingly discordant very large  $k_{OA}$  reported in ref. 9 for aged biomass burning particles. That study used transmission electron microscopy, where particles were exposed to vacuum and bombarded with a high-energy electron beam. In such an environment, as in the thermodenuder, LVOCs and SVOCs are expected to evaporate (Supplementary Fig 4), leaving only the highly absorptive ELVOCs in the condensed phase. As shown in Fig. 2b, our  $k_{OA}$  values for ELVOCs are in close agreement with those of ref. 9, and  $k_{OA}$  values for our total OA are in good agreement with data collected using ambient pressure techniques<sup>3–6</sup>.

To illustrate the potential climate forcing implications of our findings, we performed simplified calculations (Supplementary Section 7) to estimate the contribution of biomass burning OA to DRF. Results are shown in Fig. 1c. BC-to-OA ratios between 0.05 and 0.1 are most relevant as they are representative of the mean global values for biomass burning<sup>2</sup>. Under these conditions, if the OA were non-absorbing, the DRF would be negative. This is in concordance with predictions of current climate models that do not treat BrC absorption<sup>13</sup>. BrC absorption, on the other hand, shifts DRF of biomass burning emissions to positive values. Although these are idealized calculations, they suggest that BrC in biomass burning emissions can be a major player alongside BC to govern DRF.

## Methods

Experiments were conducted during FLAME 4 using globally important fuels from boreal forests, grasslands and croplands (Supplementary Table 1). Emissions were diluted to plume- and ambient-like concentrations and injected into two smog chambers<sup>25</sup>. In one of the chambers, the emissions were chemically aged by photo-oxidation or dark ozonolysis, whereas the second chamber served as a control (no oxidation). The ageing time in the chambers was of the order of 1–3 h (Supplementary Fig. 7). For the photo-oxidation experiments, the OH

concentration was similar to atmospheric conditions ( $\sim 2 \times 10^6$  molecules  $\text{cm}^{-3}$ ), whereas for ozonolysis, the ozone concentrations ( $\sim 1$  ppm) were 2 orders of magnitude larger than typical atmospheric and biomass burning plume ozone concentrations ( $\sim 10$ – $50$  ppb). Thus, the ageing time in the ozonolysis experiments was equivalent to a few days of atmospheric ageing. The experiments featured a wide range of burn conditions, which was reflected in the wide range of BC-to-OA ratios in the diluted emissions (Supplementary Table 1).

Effective absorptivity of OA, namely the imaginary part of the refractive index ( $k_{OA}$ ), was retrieved using optical closure, which combines measurement of absorption coefficients, as well as BC and OA size distributions and mixing states, with Mie theory calculations<sup>6</sup> (Supplementary Section 2 and Fig. 4). The Mie theory absorption calculations were based on the formulation in ref. 26 for coated spheres. Optical closure was performed on both fresh and aged emissions. To investigate the volatility of BrC, some experiments also involved heating the emissions in a thermodenuder to 250 °C for an average residence time of 5.8 s. Heating stripped almost 90% of the OA, corresponding to the LVOC and SVOC fraction, from the condensed phase. The remaining ELVOC fraction has effective saturation concentration ( $C^*$ ) less than  $10^{-4}$   $\mu\text{g m}^{-3}$  (Supplementary Fig. 8).

Further details of experimental set-up, instrumentation, data and uncertainty analysis are provided in the Supplementary Methods.

Received 23 February 2014; accepted 10 July 2014;  
published online 3 August 2014

## References

- Ramanathan, V. & Carmichael, G. Global and regional climate changes due to black carbon. *Nature Geosci.* **1**, 221–227 (2008).
- Bond, T. C. *et al.* Bounding the role of black carbon in the climate system: A scientific assessment. *J. Geophys. Res. Atmos.* **118**, 5380–5552 (2013).
- Kirchstetter, T. W. & Novakov, T. Evidence that the spectral dependence of light absorption by aerosols is affected by organic carbon. *J. Geophys. Res.* **109**, 1–12 (2004).
- Chen, Y. & Bond, T. C. Light absorption by organic carbon from wood combustion. *Atmos. Chem. Phys.* **10**, 1773–1787 (2010).
- Lack, D. A., Langridge, J. M., Bahreini, R., Cappa, C. D. & Middlebrook, A. M. Brown carbon and internal mixing in biomass burning particles. *Proc. Natl Acad. Sci. USA* **109**, 14802–14807 (2012).
- Saleh, R. *et al.* Absorptivity of brown carbon in fresh and photo-chemically aged biomass-burning emissions. *Atmos. Chem. Phys.* **13**, 7683–7693 (2013).
- Andreae, M. O., Gelencs, A., Box, P. O. & Veszpr, H. Black carbon or brown carbon? The nature of light-absorbing carbonaceous aerosols. *Atmos. Chem. Phys.* **6**, 3131–3148 (2006).
- Bond, T. C. & Bergstrom, R. W. Light absorption by carbonaceous particles: An investigative review. *Aerosol Sci. Technol.* **39**, 1–41 (2005).
- Alexander, D. T. L., Crozier, P. A. & Anderson, J. R. Brown carbon spheres in East Asian outflow and their optical properties. *Science* **321**, 833–836 (2008).
- Chakrabarty, R. K. *et al.* Brown carbon in tar balls from smoldering biomass combustion. *Atmos. Chem. Phys.* **10**, 6363–6370 (2010).
- Donahue, N. M., Kroll, J. H., Pandis, S. N. & Robinson, A. L. A two-dimensional volatility basis set—Part 2: Diagnostics of organic-aerosol evolution. *Atmos. Chem. Phys.* **12**, 615–634 (2012).
- Bond, T. C. A technology-based global inventory of black and organic carbon emissions from combustion. *J. Geophys. Res.* **109**, 1–43 (2004).

13. Myhre, G. *et al.* Radiative forcing of the direct aerosol effect from AeroCom Phase II simulations. *Atmos. Chem. Phys.* **13**, 1853–1877 (2013).
14. Feng, Y., Ramanathan, V. & Kotamarthi, V. R. Brown carbon: A significant atmospheric absorber of solar radiation? *Atmos. Chem. Phys.* **13**, 8607–8621 (2013).
15. Wiedinmyer, C. *et al.* The Fire INventory from NCAR (FINN): A high resolution global model to estimate the emissions from open burning. *Geosci. Model Dev.* **4**, 625–641 (2011).
16. Jacobson, M. Z. Investigating cloud absorption effects: Global absorption properties of black carbon, tar balls, and soil dust in clouds and aerosols. *J. Geophys. Res.* **117**, D06205 (2012).
17. Cappa, C. D. *et al.* Radiative absorption enhancements due to the mixing state of atmospheric black carbon. *Science* **337**, 1078–1081 (2012).
18. Adachi, K., Chung, S. H. & Buseck, P. R. Shapes of soot aerosol particles and implications for their effects on climate. *J. Geophys. Res.* **115**, 1–9 (2010).
19. China, S., Mazzoleni, C., Gorkowski, K., Aiken, A. C. & Dubey, M. K. Morphology and mixing state of individual freshly emitted wildfire carbonaceous particles. *Nature Commun.* **4**, 2122 (2013).
20. Bond, T. C., Habib, G. & Bergstrom, R. W. Limitations in the enhancement of visible light absorption due to mixing state. *J. Geophys. Res.* **111**, 1–13 (2006).
21. Lack, D. A. & Cappa, C. D. Impact of brown and clear carbon on light absorption enhancement, single scatter albedo and absorption wavelength dependence of black carbon. *Atmos. Chem. Phys.* **10**, 4207–4220 (2010).
22. Akagi, S. K. *et al.* Emission factors for open and domestic biomass burning for use in atmospheric models. *Atmos. Chem. Phys.* **11**, 4039–4072 (2011).
23. May, A. A. *et al.* Gas-particle partitioning of primary organic aerosol emissions: (3) Biomass burning. *J. Geophys. Res.* **118**, 11327–11338 (2013).
24. Dinar, E. *et al.* The complex refractive index of atmospheric and model humic-like substances (HULIS) retrieved by a cavity ring down aerosol spectrometer (CRD-AS). *Faraday Discuss.* **137**, 279–295 (2008).
25. Hennigan, C. J. *et al.* Chemical and physical transformations of organic aerosol from the photo-oxidation of open biomass burning emissions in an environmental chamber. *Atmos. Chem. Phys.* **11**, 7669–7686 (2011).
26. Bohren, C. F. & Huffman, D. R. *Absorption and Scattering of Light by Small Particles* (Wiley, 1983).

### Acknowledgements

FLAME 4 and R.J.Y. were supported by NSF grant ATM-0936321. S.L., A.C.A. and M.K.D. thank DOE's ASR programme F265 for financial support. Carnegie Mellon University team thanks DOE's ASR programme (ER65296) and NSF (AGS-1256042) for financial support. The authors also thank the Fire Science Laboratory Staff and other FLAME 4 team members.

### Author contributions

R.S. performed the data analysis and wrote the manuscript. R.S., A.L.R., N.M.D., R.C.S. and A.A.P. designed the experiments. E.S.R., A.T.A., D.S.T. and R.S. performed smog chamber experiments. A.L.R., A.A.P., R.C.S., A.T.A., D.S.T., E.S.R. and R.S. built the smog chamber experimental set-up. E.S.R. analysed SP2 and HR-AMS data. S.L. and A.C.A. collected and analysed PASS-3 data. R.J.Y. organized FLAME 4. All authors discussed the data and commented on the manuscript.

### Additional information

Supplementary information is available in the online version of the paper. Reprints and permissions information is available online at [www.nature.com/reprints](http://www.nature.com/reprints). Correspondence and requests for materials should be addressed to A.L.R.

### Competing financial interests

The authors declare no competing financial interests.